

Modeling of microalgal metabolism

Thesis committee

Thesis supervisor

Prof. dr. R.H. Wijffels

Professor of Bioprocess Engineering,
Wageningen University

Thesis co-supervisors

Dr. ir. M.G.J. Janssen

Assistant professor Bioprocess Engineering,
Wageningen University

Dr. ir. D.E. Martens

Assistant professor Bioprocess Engineering,
Wageningen University

Other members

Prof. dr. V.A.P. Martins dos Santos

Wageningen University

Prof. dr. K.J. Hellingwerf

University of Amsterdam

Prof. dr. O. Kruse

Bielefeld University, Germany

Dr. B.G. Temmink

Wageningen University

This research has been conducted under the auspices of the Graduate School VLAG

Modeling of microalgal metabolism

Anna Margu rita Jeanetta Kliphuis

Submitted in fulfillment of the requirement for the degree of doctor
at Wageningen University
by the authority of the Rector Magnificus
Prof. dr. M.J. Kropff,
in the presence of the
Thesis Committee appointed by the Academic Board
to be defended in public
on Wednesday 15 December 2010
at 4 p.m. in the Aula

A.M.J. Kliphuis
Modeling of microalgal metabolism
200 pages

PhD Thesis, Wageningen University, Wageningen, NL (2010)
With references, with summaries in Dutch and English

ISBN 978-90-8585-833-1

Twijfel niet.

Voor opi en omi



Contents

Chapter 1	9
Introduction and thesis outline	
Chapter 2	17
Photosynthetic efficiency of <i>Chlorella sorokiniana</i> in a turbulently mixed short light-path photobioreactor	
Chapter 3	43
Light respiration in <i>Chlorella sorokiniana</i>	
Chapter 4	69
Metabolic modeling of <i>Chlamydomonas reinhardtii</i> : energy requirements for photoautotrophic growth and maintenance	
Chapter 5	107
Effect of O ₂ : CO ₂ ratio on the primary metabolism of <i>Chlamydomonas reinhardtii</i>	
Chapter 6	139
Towards high biomass yields - a better understanding of microalgal metabolism	
References	161
Summary	177
Samenvatting	182
Dankwoord	189
Curriculum Vitae	195
Training activities	199



CHAPTER 1

Introduction and thesis outline

Introduction

Microalgae and photoautotrophic growth

Microalgae are a potential source for a wide range of products, such as carotenoids, lipids, hydrogen, protein and starch, which are of interest for food, feed and biofuel applications. However, to produce these compounds the microalgae themselves need to be cultivated first.

Microalgae are unicellular eukaryotic organisms capable of using (sun) light as an energy source through photosynthesis. This process takes place in the chloroplast: a simplified scheme is shown in Figure 1.1. During photoautotrophic growth the photosystems absorb light and water is split, yielding oxygen (O_2) and energy-rich compounds (ATP and NADPH). These energy-rich compounds are subsequently used to fix carbon dioxide (CO_2) and convert it into C3-sugars, the building blocks for biomass (and product) formation. Thus, during photoautotrophic growth microalgae consume CO_2 and produce O_2 . In addition, O_2 is taken up in a number of processes such as mitochondrial respiration and photorespiration.

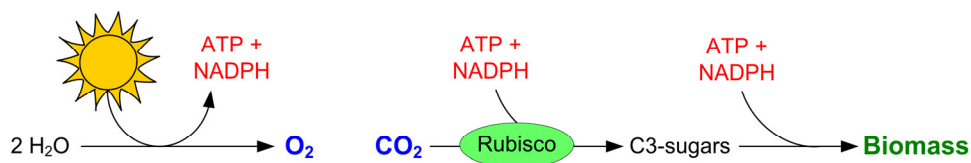


Figure 1.1 Simplified scheme of photoautotrophic metabolism. In the light reaction of photosynthesis photons are absorbed by the photosystems and water is split into O_2 , yielding ATP and NADPH. These are used in the dark reaction to fix CO_2 and produce C3-sugars, the building blocks for biomass formation.

Large-scale cultivation

For the commercial production of microalgal products high productivities are needed, preferably using freely available sunlight as the energy source. Different photobioreactors and culturing techniques for photoautotrophic growth have been investigated, as reviewed by many authors (Eriksen 2008; Grobbelaar 2000; Janssen et al. 2003; Pulz 2001). Current photobioreactors are capable of reaching high photosynthetic efficiencies, but these efficiencies drop when using light intensities as high as those occurring outdoors and when scaling-up photobioreactors. In addition, the net evolved O_2 by photosynthesis can easily build up to high concentrations in closed photobioreactors. This

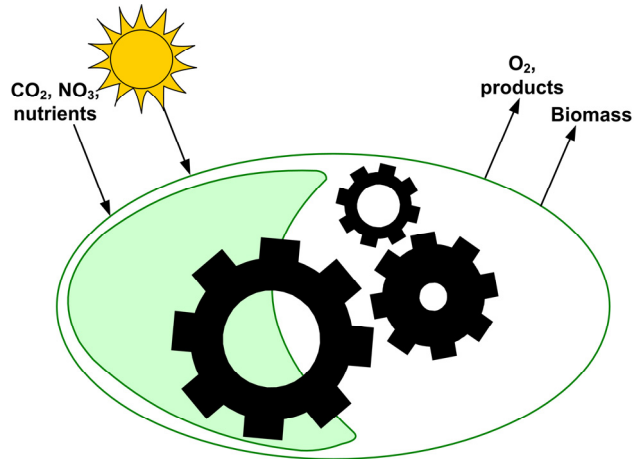


Figure 1.2 Photosynthetic cell factory. Sunlight, CO₂, NO₃ and nutrients are taken up by the cell and metabolized to O₂, biomass and products. This figure shows the metabolism inside the cell as a 'black box', an unknown set of processes. With a metabolic network and subsequent Flux Balance Analysis (FBA) insight in these processes can be gained.

can inhibit growth of the microalgae and have a negative effect on productivity (Carvalho et al. 2006; Miron et al. 1999; Wijffels et al. 2010). Oxygen build-up can only be prevented by gassing the cultures with air, a major energy input and an important economic factor limiting the large-scale cultivation of microalgae. A very important objective of applied algae research is to maximize biomass (or product) yield and at the same time minimize the energy input and cultivation costs. Both have to be balanced in the end. To achieve this, insight in the metabolism of the microalgae is a valuable tool to optimize cultivation parameters accordingly.

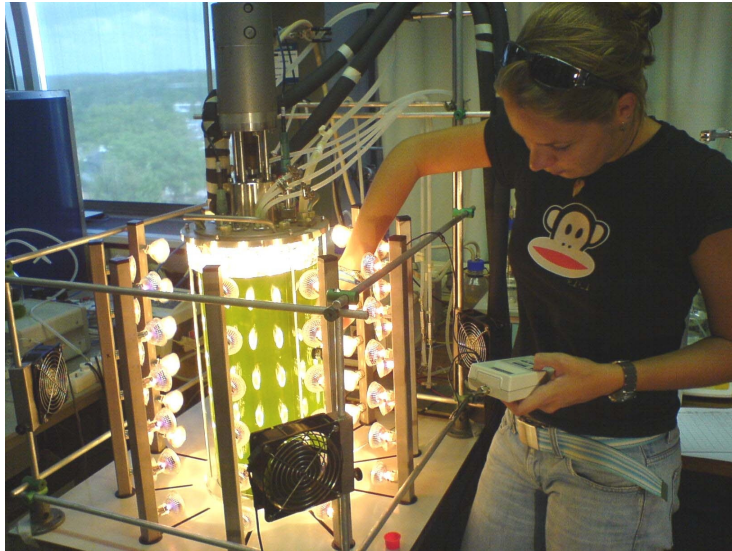


Figure 1.3 Short light-path (SLP) photobioreactor setup.

Flux Balance Analysis as a tool

To obtain the desired insight in the metabolism (more specifically O₂ metabolism) and understand the mechanisms behind the allocation of light energy for microalgal growth, we constructed a metabolic model describing the metabolism of the green microalga *Chlamydomonas reinhardtii*. With this model Flux Balance Analysis (FBA) can be performed to study the effect of cultivation parameters on the metabolism and the biomass yield. FBA is a powerful tool to study the fluxes through metabolic pathways of any organism of interest (Stephanopoulos et al. 1998). It provides information on how nutrients and energy are utilized to form biomass and other components. Information on metabolic fluxes and pathways leads to a better understanding of metabolism and the identification of targets for process optimization.

However, to be able to study the effect of O₂ on the metabolism of *C. reinhardtii*, the energy requirements for growth and maintenance need to be incorporated in the model to accurately describe the metabolism. To estimate these energy requirements and to assess the effect of O₂ on the metabolism, experiments under controlled conditions are necessary. Additionally, inputs and outputs of the metabolism need to be measured accurately to serve as input parameters for FBA.

Controlled lab-scale cultivation and growth monitoring

To be able to perform experiments under controlled conditions and accurately measure the inputs and outputs of the metabolism (CO₂, O₂, biomass, nitrogen, light) on-line during cultivation, a novel cultivation and on-line measurement system is needed. Therefore we designed a lab-scale photobioreactor which combines a short light path of 12 mm with controlled mixing and aeration (Figure 1.3). In this SLP photobioreactor mixing is provided by rotating an inner tube in the cylindrical cultivation vessel. The algae are cultivated in the annular gap between this rotating cylinder and the outer glass cylinder. By uncoupling the mixing from aeration the effect of mixing on the biomass yield can be studied and the gas-exchange can be measured on-line. The on-line measured CO₂ uptake rate (CUR) and O₂ production rate (OPR) can be used as inputs for the metabolic model and give insight in the biomass yield on light. In addition, frequent analyses of reactor samples off-line give information on growth rate, biomass concentration and composition, which can also be used as inputs for the model.

Thesis outline

The aim of this thesis is to obtain insight in the biomass yield on light and the metabolism of microalgae and more specifically the O₂ metabolism because this has a large impact on the energy efficiency. To be able to accurately measure the inputs and outputs of the metabolism (CO₂, O₂, biomass, nitrogen, light) on-line during cultivation, we developed a lab-scale short light-path (SLP) photobioreactor with an on-line measurement system as described in detail in **Chapter 2**. In this photobioreactor mixing was carried out independently from aeration to be able to measure the gas-exchange on-line as well as determine the effect of mixing on the biomass yield of *Chlorella sorokiniana*.

In illuminated microalgal cells several processes in which oxygen is involved occur simultaneously. Under the cultivation conditions in the experiments in **Chapter 3** two processes dominate, photosynthesis and mitochondrial light respiration. The net oxygen exchange rate, which can be directly measured, is the sum of the oxygen production by photosynthesis and oxygen consumption through respiration in the mitochondria. To know the rates of these two processes one of these has to be measured. In **Chapter 3** a method is described to estimate the light respiration rate by measuring the post-illumination oxygen uptake. This method was tested for *Chlorella sorokiniana* at different biomass concentrations and revealed that part of the respiratory activity was coupled to growth and a part was not.

To gain insight in the metabolism and understand the mechanisms behind the allocation of light energy for microalgal growth we constructed a metabolic model. This model describes the primary metabolism for the green microalgae *Chlamydomonas reinhardtii* and is described in **Chapter 4**. This model was based on literature and the sequenced genome of *C. reinhardtii*. In addition to the model, this chapter describes experiments performed to estimate the energy requirements for growth and maintenance and the consequences for the yield of biomass on light energy.

The effect of elevated O₂ concentrations on the yield and metabolism of *C. reinhardtii* is described in **Chapter 5**. By cultivating microalgae under different O₂ : CO₂ ratios in the SLP photobioreactor and measuring the oxygen production rate (OPR) and carbon dioxide uptake rate (CUR) on-line we could assess the effect of elevated O₂ concentrations on the biomass yield of *C. reinhardtii*. The measured rates were used as input for the metabolic model to quantify the effect of higher O₂ : CO₂ ratios and gain insight in the process of photorespiration.

Chapter 1

To thoroughly understand the energy metabolism of microalgal cells and with that the conversion of light energy into biomass, insight into the different processes involved in O₂ production and uptake and CO₂ consumption and production is necessary. In **Chapter 6** an overview is given of the metabolic processes in which O₂ plays a role, as well as how these processes could be measured. Subsequently, ways to improve and expand the metabolic model in order to obtain a better insight in the metabolism are discussed. If a dynamic description of the light reactions of photosynthesis is included it might ultimately be possible to make predictions on biomass and product yield based on the light regime the microalgae are exposed to.





CHAPTER 2

Photosynthetic efficiency of *Chlorella sorokiniana* in a turbulently mixed short light-path photobioreactor

Kliphuis AMJ, de Winter L, Vejrazka C, Martens DE, Janssen M, Wijffels RH (2010)
Photosynthetic efficiency of *Chlorella sorokiniana* in a turbulently mixed
short light-path photobioreactor
Biotechnology Progress 26:687-696

Abstract

To be able to study the effect of mixing as well as any other parameter on productivity of algal cultures we designed a lab-scale photobioreactor in which a short light path (SLP) of (12 mm) is combined with controlled mixing and aeration. Mixing is provided by rotating an inner tube in the cylindrical cultivation vessel creating Taylor vortex flow and as such mixing can be uncoupled from aeration. Gas exchange is monitored online to gain insight in growth and productivity. The maximal productivity, hence photosynthetic efficiency, of *Chlorella sorokiniana* cultures at high light intensities ($1500 \mu\text{mol m}^{-1} \text{s}^{-1}$) was investigated in this Taylor vortex flow SLP photobioreactor. We performed duplicate batch experiments at three different mixing rates: 70, 110 and 140 rpm, all in the turbulent Taylor vortex flow regime. For the mixing rate of 140 rpm we calculated a quantum requirement for oxygen evolution of 21.2 mol PAR photons per mol O_2 and a yield of biomass on light energy of 0.8 g biomass per mol PAR photons. The maximal photosynthetic efficiency was found at relatively low biomass densities (2.3 g L^{-1}) at which light was just attenuated before reaching the rear of the culture. When increasing the mixing rate two-fold we only found a small increase in productivity. Based on these results we conclude that the maximal productivity and photosynthetic efficiency for *Chlorella sorokiniana* can be found at that biomass concentration where no significant dark zone can develop and that the influence of mixing-induced light/dark fluctuations is marginal.

Keywords: Microalgae, *Chlorella sorokiniana*, Productivity, Photosynthetic efficiency, Short light-path photobioreactor, Mixing

Introduction

Microalgal products such as carotenoids and lipids for food, feed and biofuels are of big interest. To produce these compounds the microalgae themselves need to be cultivated first. Different photobioreactors and culturing techniques for photoautotrophic growth have been investigated, as reviewed by many authors (Eriksen 2008; Grobbelaar 2000; Janssen et al. 2003; Pulz 2001). Current photobioreactors are capable of reaching high photosynthetic efficiencies, but these efficiencies drop when using high light intensities as occur outdoors and when scaling-up photobioreactors. Maximization of biomass productivity in (large-scale) outdoor photobioreactors is important. To achieve this, we need more knowledge of the growth characteristics of microalgae and optimize cultivation parameters such as the light regime.

Faster mixing of dense *Spirulina* (*Arthrospira*) cultures in short light path (SLP) panel photobioreactors, for example, can increase the biomass productivity at high light intensities (Qiang et al. 1996; Qiang and Richmond 1996). Under such conditions these cyanobacteria are only shortly exposed to over-saturating light intensities at the bioreactor surface before travelling to darker regions of the photobioreactor and it was hypothesized that this light regime lead to higher photosynthetic efficiencies by preventing over-saturation and inducing light integration (Richmond 2000). However, the photosynthetic efficiencies found for microalgae were considerably lower than for *Spirulina* and the question remains whether the same strategy could be applied for microalgae.

In flat panel photobioreactors mixing is provided by aeration and enhanced by increasing the airflow. To create turbulence, 2.8 to 4.2 L min⁻¹ of air per liter reactor volume must be provided (Qiang et al. 1996; Qiang and Richmond 1996; Qiang et al. 1998). However, in order to be able to accurately measure photosynthetic activity through the on-line monitoring of oxygen production rates and carbon dioxide consumption rates, the airflow needs to be lower to have larger differences in O₂ and CO₂ mass fractions in the ingoing and outgoing gas. In addition, Barbosa et al. (2003) found that high gas flow velocities entering the photobioreactor can cause high shear rates and cell death. Therefore to be able to measure algal productivity accurately we need to uncouple mixing from the gas flow, whilst maintaining a short light path.

To be able to study the effect of mixing as well as any other parameter on productivity of algal cultures we designed a lab-scale photobioreactor which combines a short light path of 12 mm with controlled mixing and aeration (Figure 2.1). In this SLP photobioreactor, all cultivation conditions can be controlled and varied to study the productivity of micro-

algal cultures as a function of different design parameters, e.g. temperature, light intensity, oxygen and carbon dioxide partial pressure, and mixing rate. Mixing is provided by rotating an inner tube in the cylindrical cultivation vessel, inducing Taylor vortex flow. The algae were cultivated in the annular gap between this rotating cylinder and the outer glass cylinder. This system is similar to the device used by Miller et al. (1964) but our system was improved considerably so that algae could be grown for a period of days within the photobioreactor under fully controlled conditions, and microalgae growth could be accurately monitored and quantified during this period.

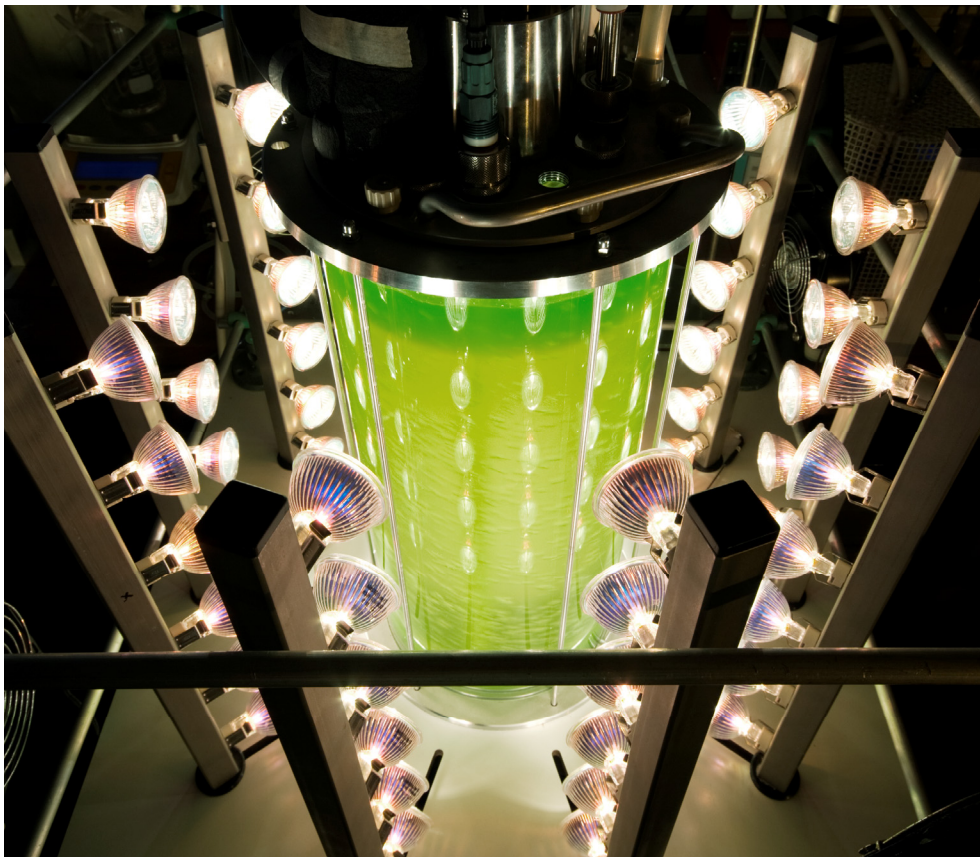


Figure 2.1 Taylor vortex flow SLP photobioreactor containing *Chlorella sorokiniana* at the start of a batch cultivation. The inner rotating cylinder and gas bubbles are still visible at this low initial biomass density.

In this study we determined the maximal productivity of *Chlorella sorokiniana* cultures at high light intensities in the Taylor vortex flow SLP photobioreactor. We worked in the turbulent Taylor vortex flow regime ($Re_{\theta} = 6660 - 13320$) which was shown to give the highest photosynthetic activity for very dense algal cultures (Miller et al. 1964). In our experiments, on the other hand, we started at very low initial biomass concentrations and allowed the microalgae to grow inside the photobioreactor. By continuously monitoring the carbon dioxide consumption rate (CUR) and oxygen production rate (OPR) we were able to assess the maximal productivity and hence the maximal photosynthetic efficiency of microalgae growth. Frequent analysis of reactor samples off-line allowed us to assess at which biomass concentration this optimum was reached. Moreover, the mixing rate was increased with a factor 2 to check whether a further increase in mixing rate led to an increase in productivity.

Theory - Liquid flow in a Couette apparatus

The flow pattern occurring in a Couette apparatus with rotating inner cylinder and fixed outer cylinder is described by Taylor (1923). Taylor vortices will appear when the angular speed of the inner cylinder reaches a critical value, as shown in Figure 2.2. This secondary flow pattern, singly periodic flow, is stable above this critical angular speed. However, when the angular speed of the inner cylinder increases, the centers of the vortices become vertically oscillating waves. This flow pattern is described as wavy vortex flow, or doubly periodic flow. When the angular speed of the inner cylinder increases even more, the flow becomes turbulent (Bird et al. 1960). This turbulent flow is still characterized by a secondary vortex flow, for an example see Yang et al. (2006), and is usually referred to as turbulent Taylor vortex flow.

The transition of these flow patterns largely depends on the radius ratio of the inner and outer cylinder and on the fluid viscosity. Many different ways of analyzing and quantifying the corresponding flow patterns are described in literature (Conway et al. 2004; Curran and Black 2005; Giordano and Giordano 2006; Hondzo et al. 1998; Lathrop et al. 1992; Miller et al. 1964; Resende et al. 2001). However, the problems with these flow instabilities and transitions between flow patterns are complex and cannot be solved by theory alone (Bird et al. 1960). In our system we have a two-phase flow due to the necessity to gas the culture to supply carbon dioxide and remove oxygen. The presence of gas bubbles still allows vortex flow (Murai et al. 2005) but it will further complicate the accurate quantitative evaluation of the liquid flow. In our biotechnological study the flow

patterns in the photobioreactor were therefore only characterized by calculating the corresponding rotational Reynolds (Re_θ) numbers and visually observing the liquid flow. When injecting acid or base into the annular gap filled with the pH indicator phenolphthalein in water, the resulting coloring or de-coloring of the vortices visualized the flow pattern.

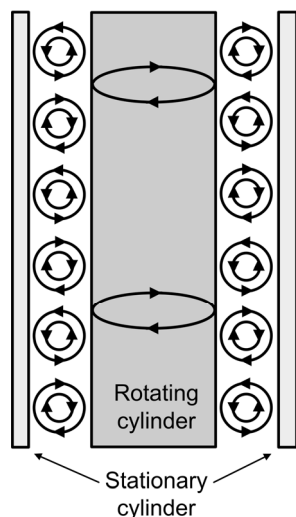


Figure 2.2 Cross section of Taylor vortices occurring in the annular space between two cylinders, an outer stationary and an inner rotating cylinder. These vortices are circular and stacked on top of each other. The centers of the vortices are located exactly in the middle of the annular gap

Materials & Methods

Organism, media and cultivation conditions

Chlorella sorokiniana CCAP 211/8k was obtained from the American Type Culture Collection (ATCC, no. 7516) and cultivated in 250 mL shake flasks containing 100 mL adapted M-8 medium (Mandalam and Palsson 1998), called M-8a (Table 2.1) at pH 6.7. The cultures were grown in a culture chamber at a temperature of 25°C, a light intensity of 20-40 $\mu\text{mol m}^{-2} \text{s}^{-1}$ and a 16/8h day/night cycle. To reach inoculation cell density the cultures were placed in a shake-incubator for two days at a continuous light intensity of 280 $\mu\text{mol m}^{-2} \text{s}^{-1}$ and a head space enriched with 5% carbon dioxide.

For the experiments in the photobioreactor three times concentrated M-8a medium was used to be able to reach high cell densities. The concentration KNO_3 was decreased to 5 mmol L^{-1} .

Reactor set-up and experiments

Chlorella sorokiniana was grown in batch mode in the SLP photobioreactor, depicted

Table 2.1 Composition of M-8a medium.

Compound	Concentration ($\mu\text{mol L}^{-1}$)
KNO ₃	$29.67 \cdot 10^3$
KH ₂ PO ₄	$5.44 \cdot 10^3$
Na ₂ HPO ₄ · 2 H ₂ O	$1.46 \cdot 10^3$
MgSO ₄ · 7 H ₂ O	$1.62 \cdot 10^3$
CaCl ₂ · 2 H ₂ O	88.43
EDTA ferric sodium salt	315.86
Na ₂ EDTA · 2 H ₂ O	100.00
H ₃ BO ₃	1.00
MnCl ₂ · 4 H ₂ O	65.59
ZnSO ₄ · 7 H ₂ O	11.13
CuSO ₄ · 5 H ₂ O	7.33

schematically in Figure 2.3. The photobioreactor had a working volume of 3.4 L, an annular gap width of 12 mm and an illuminated area ($A_{\text{bioreactor}}$) of 0.24 m². The radius of the rotating inner cylinder (r_i) was 0.076 m and the radius of the stationary outer cylinder (r_o) was 0.088 m. Therefore the radius ratio ($\eta = r_i / r_o$) of the photobioreactor was 0.076 m / 0.088 m = 0.86. The inner cylinder was rotating at a different rate in each batch experiment to accomplish different mixing intensities. Three mixing rates were used: 70, 110 and 140 rpm. Every batch experiment was performed in duplicate.

To enable vertical back-mixing four down comers were drilled into the inner cylinder. Without down comers in the inner cylinder no vertical back mixing occurred and the algae accumulated in the top part of the photobioreactor. By adding the down comers, the algae were mixed over the whole annular gap.

The light was provided continuously by 60 tungsten halogen lamps (Philips Masterline ES 45W) surrounding the reactor. The photon flux density (PFD, $\mu\text{mol m}^{-2} \text{s}^{-1}$) was measured with a LI-COR 190-SA 2 π sensor (PAR-range: 400–700 nm) at 80 fixed points inside the reactor before each experiment. The measured light intensities at all 80 points were averaged into a PFD for that particular experiment. An average light intensity of 1500 $\mu\text{mol m}^{-2} \text{s}^{-1}$ could be reached with this set-up. The used light intensity in these experiments ($\sim 1500 \mu\text{mol m}^{-2} \text{s}^{-1}$) is comparable to horizontal solar irradiance in the Netherlands at the peak of summer.

During the experiments light penetration through the culture ($\mu\text{mol m}^{-2} \text{s}^{-1}$) was measured by a spherical light sensor (US-SQS Spherical Micro Quantum Sensor, Heinz Walz GmbH, Germany) placed inside the culture broth at the depth of the annular gap, 12 mm from the internal reactor wall, as illustrated in Figure 2.3.

Using mass flow controllers (Brooks, Smart TMF 5850S), carbon dioxide was supplied by sparging nitrogen (1.55 L min^{-1}) enriched with 2% carbon dioxide through a silicone ring-

sparger at the bottom of the reactor. This gas flow also served to remove excess oxygen from the culture broth. The pH was controlled at $\text{pH } 6.7 \pm 0.1$ by pumping nitric acid (1.7 M), serving also as nitrogen source. The acid, antifoam and overflow were placed on balances and weighed on-line. The reactor was kept at 37°C by a water jacket connected to a temperature-controlled water bath. To prevent water from evaporating into the off-gas the reactor was equipped with a condenser connected to a cryostat set at 2°C . Biomass samples were taken from the bottom of the reactor and weighed off-line.

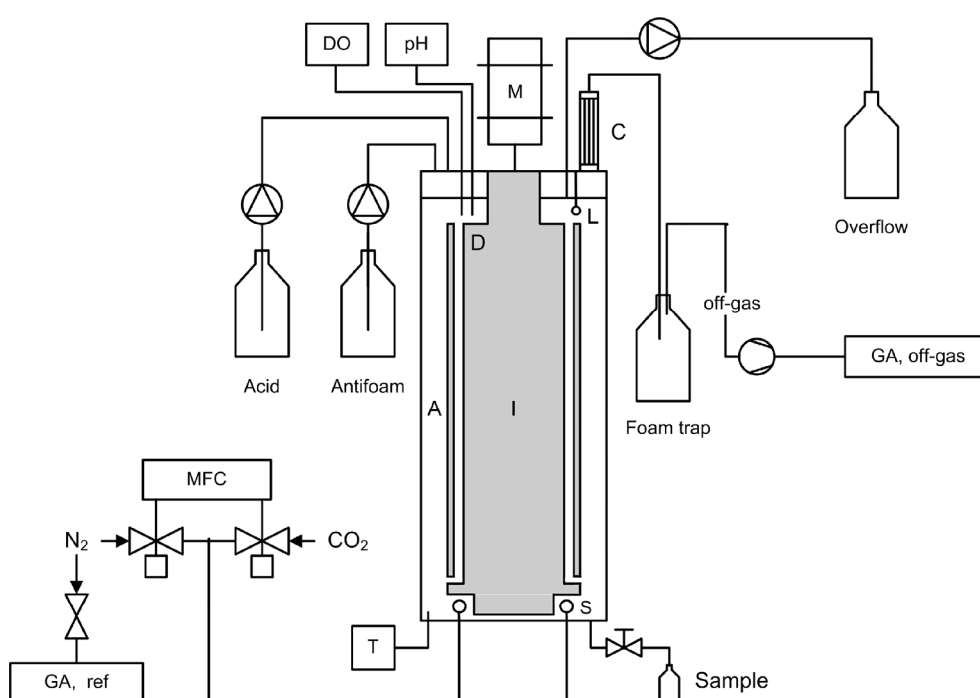


Figure 2.3 Schematic overview (not on scale) of the SLP photobioreactor. A = annular gap, C = condenser, D = internal down comer, DO = dissolved oxygen sensor, GA = gas analyzer, I = inner cylinder, M = motor, MFC = Mass flow controllers for both N_2 and CO_2 , pH = pH control connected to acid pump, S = sparger, T = temperature control connected to cryostat and cooling jacket (not shown).

On-line gas analysis and calculations

The off-gas was analyzed by leading it over a gas analyzer (Servomex, 4100) fitted with two different gas sensor modules, a paramagnetic purity transducer to measure oxygen and an infrared 1500 transducer to measure carbon dioxide.

Before each experiment, a dry and a wet baseline were measured to correct the experimental gas data for moisture content according to equation 1. The dry baseline was measured by leading 1.55 L min^{-1} nitrogen enriched with 2% carbon dioxide over the gas analyzers. For the wet baseline the nitrogen enriched with carbon dioxide was first sparged through the reactor, containing medium at the same temperature and pH as during the batch experiment, and through the condenser before being analyzed.

$$n_{\text{gas,out}} = n_{\text{gas,in}} \cdot \frac{x_{\text{CO}_2,\text{db}}}{x_{\text{CO}_2,\text{wb}}} \quad (1)$$

The total molar gas flow going in ($n_{\text{gas,in}}$, mmol h^{-1}) is corrected for the molar fraction of carbon dioxide in both the dry ($x_{\text{CO}_2,\text{db}}$) and wet baseline ($x_{\text{CO}_2,\text{wb}}$). With this corrected molar gas flow $n_{\text{gas,out}}$ (mmol h^{-1}) and the molar fraction of oxygen ($x_{\text{O}_2,\text{exp}}$) and carbon dioxide ($x_{\text{CO}_2,\text{exp}}$) measured during the experiments, the oxygen production rate (OPR, mmol h^{-1}) and carbon dioxide uptake rate (CUR, mmol h^{-1}) are calculated according to equations 2 and 3.

$$\text{OPR} = \frac{n_{\text{gas,out}} \cdot (x_{\text{O}_2,\text{exp}} - x_{\text{O}_2,\text{wb}})}{100} \quad (2)$$

$$\text{CUR} = \frac{n_{\text{gas,out}} \cdot (x_{\text{CO}_2,\text{exp}} - x_{\text{CO}_2,\text{wb}})}{100} \quad (3)$$

The ratio between the OPR and CUR is the photosynthetic quotient PQ. The PQ can be calculated according to equation 4:

$$\text{PQ} = \frac{\text{OPR}}{\text{CUR}} \quad (4)$$

The quantum requirement for oxygen (QR_{O_2} , $\text{mol photons mol O}_2^{-1}$) and carbon dioxide (QR_{CO_2} , $\text{mol photons mol CO}_2^{-1}$) are calculated according to equations 5 and 6. The photon flux (PF, mmol h^{-1}) is calculated using the measured average photon flux density (PFD, $\mu\text{mol m}^{-2} \text{ s}^{-1}$) and the illuminated photobioreactor area $A_{\text{bioreactor}}$ (m^2) described earlier.

$$\text{QR}_{\text{O}_2} = \frac{\text{PF}}{\text{OPR}} \quad (5)$$

$$QR_{CO_2} = \frac{PF}{CUR} \quad (6)$$

These QR values are a measure for productivity and are expressed as the quanta of light (mol photons) that are needed to produce one mol of oxygen (QR_{O_2}) or to fix one mol of carbon dioxide into biomass (QR_{CO_2}). All incident photons are assumed to be absorbed by the algae.

The biomass yield on light energy ($Y_{x,E}$, $g \text{ mol}^{-1}$) is defined as gram dry biomass formed per mol incident photons on the photobioreactor surface according to equation 7. We assumed that all consumed carbon is converted into biomass. The dry biomass C-molar mass (m_{biomass} , $g \text{ mol}^{-1}$) was determined as described in the next paragraph.

$$Y_{x,E} = \frac{CUR \cdot m_{\text{biomass}}}{PF} \quad (7)$$

With the theoretical $QR_{\text{min}O_2}$ of 10 and the dry biomass C-molar mass (m_{biomass} , $g \text{ mol}^{-1}$) we can calculate the theoretical maximal yield of biomass on light energy for photoautotrophic growth on nitrate, $Y_{x,E\text{max}}$ ($g \text{ mol}^{-1}$) according to equation 8. According to the growth equation, equation 11, 1.42 moles of oxygen are produced per C-mol biomass produced (Y_{O_2x}). The $QR_{\text{min}CO_2}$ follows from this value and is 14.

$$Y_{x,E\text{max}} = \frac{m_{\text{biomass}}}{QR_{\text{min}O_2} \cdot Y_{O_2x}} \quad (8)$$

This gives a theoretical maximal biomass yield ($Y_{x,E\text{max}}$) for growth on nitrate of 1.57 gram dry weight per mol of photons (quanta).

Mixing

The flow patterns in the SLP photobioreactor at different mixing rates were observed by staining with a pH indicator (phenolphthalein). When injecting acid or base into the annular gap filled with a phenolphthalein in water solution, the resulting coloring or decoloring of the vortices visualized the flow pattern. Next to visual observations of the flow patterns, corresponding rotational Reynolds numbers (Re_θ) were calculated. Mixing rates in rpm can be converted into Reynolds numbers using equation 9 and 10, in which r_i is the diameter of the inner cylinder (m), r_o is the diameter of the outer cylinder (m), v

is the kinematic viscosity ($\text{m}^2 \text{s}^{-1}$) and Ω is the angular speed of the inner cylinder (rad s^{-1}). Ω is calculated by multiplying the rotation rate of the inner cylinder, N (s^{-1}) with 2π .

$$\text{Re}_\theta = \frac{\Omega \cdot r_i \cdot (r_o - r_i)}{\nu} \quad (9)$$

$$\Omega = 2 \cdot \pi \cdot N \quad (10)$$

Statistical analyses

The quantum requirement for O_2 and CO_2 (QR_{O_2} and QR_{CO_2}) and the biomass yield ($Y_{x/E}$) values (dependent variables) for the optima in the batches with three mixing rates (independent variables) were analyzed with the ANOVA PostHoc Tukey HSD test to test whether they differed significantly from each other ($P < 0.05$).

Biomass Determinations

Optical Density

The optical densities (OD) at 530 nm (OD_{530}) and 680 nm (OD_{680}) were measured on a spectrophotometer (Spectronic R20, Genesys, Spectronic Instruments, UK) against M-8a medium as a blank. At 530 nm the algae hardly absorb any light and cellular light scattering is determining the optical density. At 680 nm the optical density is determined by both scattering and light absorption by chlorophyll-a. The ratio between the OD_{680} and OD_{530} is therefore a relative measure of the amount of chlorophyll per cell (Bosma et al. 2008) and can be used as an indication of bleaching of cells due to photo inhibition. This ratio should stay above 1.0 for healthy cells.

Cell number and cell size

Cell number and cell size were determined with a Beckman Coulter Multisizer 3 (Beckman Coulter Inc., Fullerton USA, 50 μm orifice). The samples were diluted with filtered (0.2 μm) Coulter® Isoton® II dilution buffer to a cell concentration between $1 \cdot 10^5$ and $3 \cdot 10^5$ cells mL^{-1} . The cell number and cell size were used to calculate the total biovolume.

Dry Weight Determination

Whatman glass microfiber filters (\varnothing 55 mm, pore size 0.7 μm) were dried at 95°C overnight and placed in a desiccator to cool to room temperature. The empty filters were

weighed and pre-wet with de-mineralized water. Two grams of sample was diluted with de-mineralized water and filtrated under mild vacuum (0.67 bar). The filter was rinsed twice with de-mineralized water to remove adhering inorganic salts. The wet filters containing the samples were again dried at 95°C overnight, allowed to cool to room temperature in a desiccator and weighed. The difference in weight between the dry filters containing the samples and the empty weight was the dry weight of the samples.

Nitrate Determination

Samples were prepared by centrifuging 2 mL of biomass sample from the reactor at 6000 rpm for five minutes in an Eppendorf centrifuge. The supernatant was filtered through a 0.2 µm filter to remove remaining cell debris. The supernatant was then analyzed by Ion Chromatography on a Dionex AS17 analytical column.

Elemental Composition

Biomass samples were centrifuged for 10 min at 4500 rpm and the resulting pellets were washed three times with de-mineralized water by re-suspending and centrifuging and stored at -20°C. Algae pellets stored at -20°C were freeze dried and ground to a fine powder. This freeze dried algal powder was combusted at 925°C in the oven of an elemental analyzer (EA 1110, ThermoQuest CE Instruments). C, H and N content were measured. Ash content was determined by burning the freeze-dried algae samples in an oven at 550°C. From these determinations the O content and subsequently the dry biomass molar mass ($m_{\text{biomass}}, \text{g mol}^{-1}$) could be calculated (C, H, O, N and ash) (Duboc et al. 1999; Gurakan et al. 1990).

Results

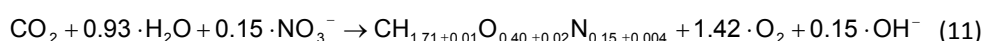
Batch growth of C. sorokiniana in the Taylor vortex flow SLP photobioreactor

To assess the maximal productivity and photosynthetic efficiency of *Chlorella sorokiniana* in a SLP photobioreactor, batch experiments at different turbulent mixing rates were performed. The mixing in the Taylor vortex flow photobioreactor was accomplished by rotating the inner tube at three different rates: 70, 110 and 140 rpm. A typical result of such a batch experiment can be seen in Figure 2.4a. This graph shows the oxygen production rate (OPR) and carbon dioxide uptake rate (CUR) obtained by duplicate batch cultivations (a and b) at a mixing rate of 70 rpm. Also the biomass dry weight in g L^{-1} is plotted for both experiments. The results for the other two mixing rates are similar and

therefore only the results at 70 rpm are shown in Figure 2.4 (following page).

After inoculating with a very low biomass density the algae were grown at a light intensity of $200 \mu\text{mol m}^{-2} \text{s}^{-1}$. When the biomass concentration increased to around 0.1 g L^{-1} dry weight the light was increased to $600 \mu\text{mol m}^{-2} \text{s}^{-1}$ as indicated by the first closed arrow in Figure 2.4a. The OPR and CUR increased due to this sudden increase in available photons, which means that the algae were light limited before. When the biomass concentration reached 1.2 g L^{-1} dry weight the light was increased to $1500 \mu\text{mol m}^{-2} \text{s}^{-1}$, which is the light intensity of interest (indicated by the second closed arrow in Figure 2.4a). After this second increase in light supply, the OPR and CUR increased dramatically and continued to increase until an optimum was reached, indicated by the open arrows. This sudden increase indicates again that the algae were light limited. After reaching the optimum at a biomass density of 2.3 g L^{-1} dry weight the OPR and CUR decreased again until the batch was ended.

With the on-line gas analysis the experiments can be monitored and the quantum requirement (QR) can be determined during the batch at any given time point. This gives insight into the photoautotrophic growth during the whole experiment, not just at sample points. By monitoring the most important substrate (carbon dioxide) and product (oxygen) on-line, the ratio between these, the photosynthetic quotient (PQ), can be calculated (equation 4). For autotrophic growth on nitrate the PQ should be around 1.4 as can be seen from the net growth equation (equation 11).



The biomass composition (CHON) for *Chlorella sorokiniana* was determined at the end of the described experiments and the values in equation 11 represent the average values \pm 95% confidence interval.

The PQ value shows if the composition of the produced biomass changes (Eriksen et al. 2007), different substrates are used or other products are formed, thus serving as a control parameter for photoautotrophic growth according to equation 11. The PQ values for the batch experiments at 70 rpm are shown in Figure 2.4b. Initially the error on the on-line gas data causes a large fluctuation in the PQ but when the OPR and CUR increase, the PQ value stabilizes around 1.4. When the light intensity is increased the second time, the PQ shifts shortly, due to a sudden increase in OPR and CUR, but quickly returns to its previous value around 1.4. For all experiments the PQ was around 1.4, indicating that the algae were growing according to equation 11.

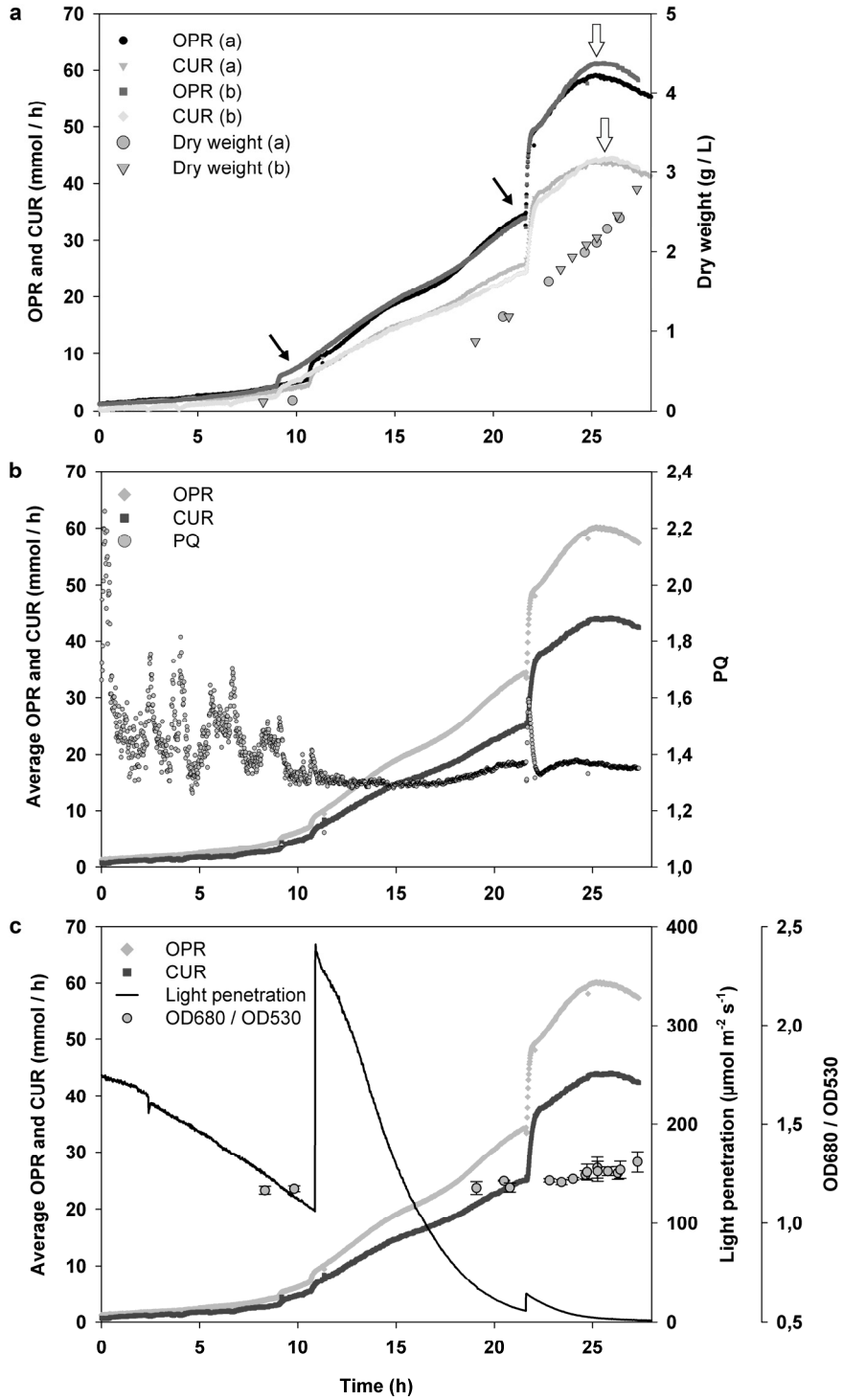


Figure 2.4 Detailed overview of duplicate batch experiments at a mixing rate of 70 rpm. a) Oxygen production rates (OPR), carbon dioxide uptake rates (CUR) (in mmol h^{-1}) and dry weight concentrations (in g L^{-1}) for duplicate batch experiments a and b. All data are normalized for the time point of light increase to $1500 \mu\text{mol m}^{-2} \text{s}^{-1}$. Closed arrows indicate the time points of stepwise light increase. Open arrows indicate the time points with the maximal productivity and minimal quantum requirement for oxygen evolution and carbon dioxide fixation. b) Average oxygen production rate (OPR), carbon dioxide consumption rate (CUR) (in mmol h^{-1}) and photosynthetic quotient (PQ) for both experiments. c) Average oxygen production rate (OPR), carbon dioxide consumption rate (CUR) (in mmol h^{-1}), OD 680 / OD 530 ratio as indication of photo inhibition and the light penetration through the culture (in $\mu\text{mol m}^{-2} \text{s}^{-1}$).

The $\text{OD}_{680}/\text{OD}_{530}$ ratio for the experiments at 70 rpm is shown in Figure 2.4c. This ratio between the optical density measured at 680 nm (OD_{680}) and 530 nm (OD_{530}) is a relative measure of the amount of chlorophyll per cell (Bosma et al. 2008) and can be used as an indication and control parameter for bleaching of cells due to photo inhibition. This ratio stays around 1.2 for all experiments and seems to be unaffected by the step-wise increase of available photons.

During the experiments, the light penetrating the culture (shown in Figure 2.4c) was measured by a spherical PAR sensor hanging inside the culture at the depth of the annular gap. The step wise light increase can be clearly seen as well as the fast decrease of light penetrating the culture when the biomass increased. At the optimum OPR and CUR all the light was absorbed in the annular gap.

Productivity and photosynthetic efficiency

The batch experiments at 110 and 140 rpm gave similar results as the results described for 70 rpm. The only difference was the height of the optimum, which was slightly higher with increasing mixing rate. At this optimum, the quantum requirement for oxygen (QR_{O_2}) and carbon dioxide (QR_{CO_2}) as well as the biomass yield on light energy (Y_{xE}) were calculated and compared for the different mixing rates. Both the QR_{O_2} and QR_{CO_2} decreased, and the Y_{xE} increased with increasing mixing rate (Table 2.2). However, the increase in productivity was very small. Only the increase in productivity between 70 and 140 rpm was significant ($P < 0.05$). Table 2.3 shows the P-values of QR_{O_2} , QR_{CO_2} and Y_{xE} for multiple comparisons of mixing rates obtained with the PostHoc Tukey HSD test. Significance is indicated with asterisks.

Table 2.2 Mixing rates in rpm and corresponding rotational Reynolds numbers calculated according to equations 9 and 10. Also the quantum requirement for oxygen production (QR_{O_2}), carbon dioxide consumption (QR_{CO_2}) (in mol photons / mol oxygen or carbon dioxide) and the biomass yield on light energy ($Y_{x/E}$ in gram dry biomass / mol photons) at three different mixing rates (70, 110 and 140 rpm) are given. Experiments were done at a high light intensity ($\sim 1500 \mu\text{mol m}^{-2} \text{s}^{-1}$). The values are \pm the standard deviation of the duplicate experiments.

Mixing rate (rpm)	Reynolds number	QR_{O_2} (mol mol ⁻¹)	QR_{CO_2} (mol mol ⁻¹)	$Y_{x/E}$ (g mol ⁻¹)
70	6660	22.7 \pm 0.56	30.98 \pm 0.32	0.76 \pm 0.008
110	10466	21.8 \pm 0.27	29.97 \pm 0.16	0.79 \pm 0.004
140	13320	21.2 \pm 0.001	29.44 \pm 0.25	0.80 \pm 0.007

Table 2.3 PostHoc Tukey HSD table: P-values of QR_{O_2} , QR_{CO_2} and $Y_{x/E}$ for multiple comparisons of mixing rates. Significance is indicated by asterisks.

Mixing rates compared (rpm)	QR_{O_2} (mol mol ⁻¹)	QR_{CO_2} (mol mol ⁻¹)	$Y_{x/E}$ (g mol ⁻¹)
70 – 110	0.163	0.056	0.060
110 – 140	0.336	0.239	0.229
140 – 70	0.048 *	0.018 *	0.019 *

Mixing effects

At a mixing rate of 70 rpm we observed Taylor vortex flow: bands of revolving liquid were clearly visible. At both 110 and 140 rpm vortex flow was still clearly visible. The same bands of revolving liquid were observed, but at these higher mixing rates they were oscillating vertically (forming waves) around the inner cylinder. The rising gas bubbles caused by sparging did not disrupt the flow pattern as was also found by Miller et al. (1964) and Murai et al. (2005), but increased the mass transfer between the vortices as described below. The down comers did not disturb the observed flow patterns either, but largely increased the mixing efficiency. When injecting base into the top of the photobioreactor, the coloring spread quickly through the down comers to the bottom of the photobioreactor.

The rotational Reynolds numbers (Re_{θ}) corresponding to the different mixing rates were 6660 (70 rpm), 10466 (110 rpm) and 13320 (140 rpm). The critical rotational Reynolds number ($Re_{\theta,c}$) gives the flow condition where Couette flow becomes unstable and Taylor vortices appear. This critical number can be predicted using equation 12, derived by Esser and Grossman (1996).

$$Re_{\theta,c} = \frac{1}{0.1556^2} \cdot \frac{(1+\eta)}{2 \cdot \eta \cdot \sqrt{(1-\eta)} \cdot (3+\eta)} \quad (12)$$

$$\text{In which } \eta = \frac{r_i}{r_o}$$

For our photobioreactor set-up $Re_{\theta,c}$ is 58. Fully turbulent Taylor vortex flow develops at Re_{θ} values above $25 \cdot Re_{\theta,c}$, which is 1455 for our system. This approximation is based on the review of Di Prima and Swinney (1979) and is based on a radius ratio (η) of 0.875 which is very close to the one of our system which is 0.86.

Based on these numbers the flow regime in our study should be turbulent Taylor vortex flow. This is not in contradiction with our visual observation since in turbulent Taylor vortex flow the vortex structure is also present; there is a macroscopic degree of order while the local flow is random. Because of the down comers inside the rotating cylinder (Figure 2.3) also an axial flow develops. Our visual observation of the liquid flow clearly showed that the vortex flow was not affected by this axial flow. Nevertheless, the presence of axial flow and the influence of the second, gaseous phase will lead to a deviation of the Re_{θ} number at which turbulent Taylor vortex flow is fully developed. Considering we worked in the Re_{θ} range of 6660 to 13320, which is considerably higher than the predicted transition at 1455 in a single phase system without axial flow, it is safe to conclude that we performed our study in the turbulent Taylor vortex flow regime.

Mass transfer

Table 2.4 shows the concentrations of dissolved oxygen and carbon dioxide in the culture broth at the points of maximum productivity for the three mixing rates. The measured dissolved oxygen concentrations were in the range of 120 - 140% air saturation (269 - 314 $\mu\text{mol L}^{-1}$). Ugwu et al. (2007) observed a strong decrease in biomass productivity for *C. sorokiniana* when dissolved oxygen concentrations exceeded 200% air saturation (448 $\mu\text{mol L}^{-1}$). Because of the much lower oxygen concentrations in our experiments, we as-

sume that oxygen was not inhibiting the productivity.

The concentrations of dissolved carbon dioxide were in the range 110 - 130 $\mu\text{mol L}^{-1}$ (Table 2.4) as calculated with the method described by Royce and Thornhill (1991). This method is based on the measured OPR and dissolved oxygen concentration to calculate the mass transfer coefficient for O_2 and subsequently CO_2 , followed by the calculation of the dissolved carbon dioxide concentration. The affinity constant K_m for carbon dioxide was found to be in the range of 15 - 65 $\mu\text{mol L}^{-1}$ for different species of *Chlorella* and for Rubisco itself (Bozzo et al. 2000; Jensen and Bahr 1977; Moroney and Somanchi 1999; Shelp and Calvin 1980). This K_m value indicates the concentration of carbon dioxide at which photosynthesis works at half its capacity. The concentration of dissolved carbon dioxide in our experiments (Table 2.4) was much higher than the K_m , showing that carbon was not limiting for growth.

Mixing rate (rpm)	DO (%)	DO ($\mu\text{mol L}^{-1}$)	$[\text{CO}_2]_{\text{oi}}$ ($\mu\text{mol L}^{-1}$)
70	133	298	117
110	133	298	112
140	126	282	130

Table 2.4 Dissolved oxygen (DO) and dissolved carbon dioxide concentrations ($[\text{CO}_2]_{\text{oi}}$) at the point of optimal productivity for the three different mixing rates.

Discussion

The observed optimum in OPR and CUR at a biomass density of 2.3 g L^{-1} is the point where the QR reaches its minimal value and the $Y_{x\epsilon}$ its maximal value for the batch experiments and therefore this is the point of maximum productivity. To find this optimum at such low biomass densities was unexpected since Qiang and Richmond (1996) demonstrated that the optimal culture density was proportional to the used light intensity. At high light intensities such as we used in these experiments, they found optimal culture densities from 8 to 13 g L^{-1} for cultures of *Spirulina platensis* in flat panel photobioreactors with a short light path.

The decrease in OPR and CUR after having reached an optimum was also remarkable. When increasing the light intensity to the maximum value, we did expect to see an increase in OPR and CUR and this was indeed observed (Figure 2.4). More light is available per cell so the algae can fix more carbon dioxide, produce more oxygen and grow faster.

While the algae keep growing further, the available light per cell decreases due to mutual shading and the OPR and CUR reach an optimum. It was expected, however, that the optimum could be maintained over a wider and higher range of biomass densities. Such a wide optimum was not reached and a clear optimum was observed for the OPR and CUR between 2 and 3 g L⁻¹ after which the productivity decreased again.

The existence of such a distinct optimum could be explained by taking into account a significant maintenance requirement of the microalgae. Maintenance in this context is defined as energy consumption for purposes other than growth (Pirt 1965). Thus, a portion of the available light per cell is used to generate energy for maintenance and the remainder is used for growth. The amount of light energy needed for maintenance is proportional to the total amount of cells inside the photobioreactor. Before reaching the optimum productivity, the increase in maintenance requirement must be offset by the increase of the total amount of light energy absorbed by the increasing amount of microalgal cells in the photobioreactor. After reaching the optimum productivity, the cell density is such that all light is absorbed in the system. When the cell density increases further, the amount of light energy available for growth will continuously decrease because of the continuous increase of energy needed for maintenance processes.

The amount of available light per cell continuously decreases, which is also visualized by the light intensity measured inside the culture broth. In Figure 2.4c the light intensity is shown during the course of an experiment. At the point where productivity was optimal all light was attenuated just before reaching the sensor at the end of the annular gap. After reaching the optimum productivity a dark zone developed in the algal suspension and we conclude that this dark zone must have led to the decrease in productivity and photosynthetic efficiency. In the dark zone there will be only respiration and no net photosynthesis. This respiratory activity can be considered a way for microalgae to derive the energy needed for maintenance purposes.

Our observations are in agreement with the findings of Lee and Palsson (1995) and Janssen et al. (2007), who did batch experiments with *Chlorella kessleri* and *Chlorella sorokiniana* and observed similar optima in OPR and CUR at low biomass densities (around 1.8 g L⁻¹ for both references). Moreover, the maximal productivity of photoautotrophic cyanobacteria in a wide range of photobioreactors has recently been accurately predicted by Cornet and Dussap (2009) based on a simple analytical analysis. This analysis was implicitly based on the fact that maximal productivity was reached at that cell density where the light intensity at the rear of the microalgae suspension was equal to

the compensation light intensity. The compensation light intensity is defined as the light intensity where net photosynthesis is zero and gross photosynthesis matches respiration. Consequently this analysis also holds for our experiments with *Chlorella sorokiniana*.

Working at a high mixing rate ($Re_0 = 6660$) a further increase in mixing only resulted in a marginal increase in productivity and photosynthetic efficiency. The experiments at 110 and 140 rpm gave similar results as the one described for 70 rpm. The height of the optimum only increased slightly with increasing mixing rate. This means that with higher mixing rates a little more carbon dioxide was consumed and oxygen produced with the same amount of available photons per surface area. This resulted in a small decrease in the quantum requirement for oxygen evolution (QR_{O_2}) and carbon dioxide fixation (QR_{CO_2}) and a small increase in the biomass yield on light energy ($Y_{x/E}$) (Table 2.2). However, only the increase in photosynthetic efficiency between 70 and 140 rpm was significant ($P < 0.05$) (Table 2.3).

Apparently we were working at those mixing rates which resulted in the highest productivity and a further increase in turbulence or mixing rate did not lead to a significant improvement of photosynthetic efficiency. It has to be stressed that cell death due to high shear forces inside the culture broth did not occur. No cell rupture or cell lysis was observed during frequent microscopic analysis of the microalgal suspension. Our observations correspond partly to the data reported by Miller et al. (1964), who found that the photosynthetic activity was highest in the turbulent flow regime which was also used in our study. A re-examination of Miller's data, on the other hand, shows that the quantum requirement for oxygen evolution (QR_{O_2}) was still 29 under maximal mixing (see appendix for calculations). In our study we observed a QR_{O_2} of 21 to 23 indicating that photosynthetic efficiency was considerably higher. Considering the fact that Miller et al. only performed short term experiments with much denser algal cultures it is very difficult to bring our work in line with the much older work of Miller et al.

The minimal value we found for QR_{O_2} was 21.2 mol photons per mol of oxygen produced, at a mixing rate of 140 rpm. Although this is a good efficiency at over-saturating light intensities, it is still two times higher than the theoretical QR_{minO_2} which lies around 10 for photoautotrophic growth at very low light intensities. For example, Emerson and Lewis (1943) found a QR_{minO_2} of 11 for *Chlorella pyrenoidosa* and Ley and Mauzerall (1986) found an average QR_{minO_2} of 10.4 ± 1.8 for *Chlorella vulgaris*. Bjorkman and Dem-

mig (1987) determined an average $QR_{\min O_2}$ of 9.43 ± 0.09 for 37 species of C3-plants. This theoretical minimal quantum requirement can be combined with the stoichiometry of the growth reaction (equation 11) to calculate the theoretical maximum biomass yield $Y_{xE_{\max}}$ on light energy (i.e. photons). For growth on nitrate this gives a maximum yield of 1.57 g mol^{-1} and, as mentioned, this yield can only be reached under low, sub-saturating, light levels. This value sets the ultimate target for the biomass yield Y_{xE} in photobioreactors since this determines the productivity.

The maximal value for Y_{xE} found in our experiments was 0.8 g mol^{-1} at a mixing rate of 140 rpm, which is two times lower than the theoretical $Y_{xE_{\max}}$ of 1.57 g mol^{-1} . This is in contrast to what Qiang and Richmond (1996) have found for the cyanobacterium *Spirulina* (*Arthrospira*). For *Spirulina* yields approached 1.5 g mol^{-1} and these record yields were related to the use of short-light path reactors combined with high biomass densities and turbulent mixing, resulting in favorable light-dark cycles (the so-called flashing light effect).

Based on our observations we think that in SLP photobioreactors ($\geq 1 \text{ cm}$) it is not possible to reach the theoretical maximum biomass yield $Y_{xE_{\max}}$ of 1.57 g mol^{-1} for microalgae under over-saturating light. In our work no real dark zone developed at the point of optimal productivity and consequently there was no cycling between light and dark zones. Mixing only lead to movement of the microalgal cells through the light gradient within the light zone. Growth of *Chlorella sorokiniana* appears to be fundamentally different than that described for *Spirulina* (*Arthrospira*) by Richmond and co-workers. Interestingly, our work is in agreement with the analysis of *Spirulina* growth by Cornet and Dusap (2009). In addition, the yields found for microalgae by other researchers are comparable to the yields we observed (Hu et al. 1996; Hu et al. 1998; Meiser et al. 2004; Richmond et al. 2003). Our biomass yields also agree with the findings of Morita et al. (2000), who found a similar efficiency for experiments with *Chlorella sorokiniana* (the same strain as used in our study) using high light intensities ($\sim 1000 \mu\text{mol m}^{-2} \text{ s}^{-1}$).

The fact that we found the optimal productivity at a fairly low biomass concentration could hypothetically be explained by the induction of growth inhibition as biomass density increases. Evidence of this phenomenon was found by Richmond and coworkers for *Spirulina* and also a green microalga, *Nannochloropsis* (Richmond et al. 2003). Removing growth inhibition for *Nannochloropsis* only resulted in a biomass yield of 0.4 g mol^{-1} in a

1 cm light path reactor under over-saturating light, whereas we report 0.8 g mol^{-1} for *Chlorella* in this study. With *Chlorella* growth inhibition is not likely to occur, even at high biomass densities as shown by Mandalam and Palsson (1995). In our experiments a balanced growth medium for *Chlorella* developed by Mandalam and Palsson (1998) was used. This balanced medium can support high biomass densities. Moreover, Lee and Palsson (1995) used medium perfusion in their batch experiments with *Chlorella kessleri*, thus removing any growth inhibiting compounds that could be present at higher biomass densities. With perfusion they also observed an optimum oxygen production rate at a biomass density of 1.8 g L^{-1} , indicating that growth inhibition does not play a role.

In conclusion we found high biomass yields under over-saturating light conditions, comparable or higher than yield values for green microalgae in literature. Surprisingly, these high yields occurred at relatively low biomass densities. We think this is related to the effect of a maintenance related requirement for light energy. The maximal productivity is reached at that biomass density where all light is just attenuated before reaching the rear of the culture. When increasing mixing rates two-fold we only found a small increase in productivity, showing that we worked at the optimal mixing rate yielding maximal photosynthetic efficiency and hence productivity at over-saturating light conditions.

Nomenclature

η	Radius ratio (-)
λ	Wavelength (nm)
ν	Kinematic viscosity ($\text{m}^2 \text{ s}^{-1}$)
Ω	Angular speed (rad s^{-1})
$A_{\text{bioreactor}}$	Illuminated photobioreactor area (m^2)
c	Speed of light (m s^{-1})
$[\text{CO}_2]_{\text{ol}}$	Concentration dissolved carbon dioxide in the medium ($\mu\text{mol L}^{-1}$)
CUR	Carbon uptake rate (mmol h^{-1})
DO	Dissolved oxygen (% air saturation)
E	Energy content of 1 mol of photons at a certain wavelength (kJ mol^{-1})
h	Planck's constant (J s)
K_m	Affinity constant for carbon dioxide ($\mu\text{mol L}^{-1}$)
m_{biomass}	Molar mass of dry biomass (g mol^{-1})
N	Rotation rate (s^{-1})

N_A	Avogadro constant (mol^{-1})
$n_{\text{gas,in}}$	Total molar gas flow going into the reactor (mmol h^{-1})
$n_{\text{gas,out}}$	Total molar gas flow going out of the reactor corrected for moisture content (mmol h^{-1})
OPR	Oxygen production rate (mmol h^{-1})
PAR	Photosynthetic active radiation, all photons between 400 and 700 nm
PF	Photon flux (mmol h^{-1})
PFD	Photon flux density ($\mu\text{mol m}^{-2} \text{s}^{-1}$)
PQ	Photosynthetic quotient (-)
QR	Quantum requirement, mol photons needed per mol of oxygen produced or carbon dioxide fixated (mol mol^{-1})
QR_{CO_2}	Quantum requirement for CO_2 fixation (mol mol^{-1})
QR_{min}	Minimal quantum requirement either for CO_2 fixation, QR_{minCO_2} , or for O_2 production, QR_{minO_2} (mol mol^{-1})
QR_{O_2}	Quantum requirement for O_2 production (mol mol^{-1})
Re_θ	Rotational Reynolds number (-)
$Re_{\theta,c}$	Critical rotational Reynolds number (-)
r_i	Radius of inner (rotating) cylinder (m)
r_o	Radius of outer (stationary) cylinder (m)
$x_{\text{CO}_2,\text{db}}$	Molar fraction of CO_2 in dry baseline (-)
$x_{\text{CO}_2,\text{exp}}$	Molar fraction of CO_2 in experimental gas data (-)
$x_{\text{CO}_2,\text{wb}}$	Molar fraction of CO_2 in wet baseline (-)
$x_{\text{O}_2,\text{exp}}$	Molar fraction of O_2 in experimental gas data (-)
$x_{\text{O}_2,\text{wb}}$	Molar fraction of O_2 in dry baseline (-)
$Y_{\text{O}_2,x}$	Oxygen produced per C-mol biomass produced (mol C-mol^{-1})
$Y_{x,E}$	Biomass yield on light energy (g mol^{-1})
$Y_{x,E\text{max}}$	Maximal yield of biomass on light energy (g mol^{-1})

Acknowledgements

This research project is financially supported by Technology Foundation STW-VICI (WLM.6622). The authors declare that they have no conflict of interest.

We want to thank Fred van den End for setting up the on-line data acquisition and the Ontwikkelwerkplaats AFSG for manufacturing the Taylor vortex flow SLP photobioreactor.

Appendix

To be able to compare the QR_{O_2} for *Chlorella sorokiniana* found by Miller et al. (1964) and our study, their maximal efficiency of 0.115 mol O_2 per kWh was re-calculated to mol O_2 per mol photons (QR_{O_2}). For this the equivalent amount of mol photons for 1 kWh needs to be calculated. This can be calculated by applying Planck's law (equation 13).

$$E = \frac{h \cdot c}{\lambda} \cdot N_A \quad (13)$$

In this equation Planck's constant (h , in J s) and the speed of light (c , in $m s^{-1}$) are multiplied and divided by the wavelength (λ , in nm). This is the energy content of one particle, which can be re-calculated to 1 mol by multiplying with the Avogadro constant (N_A , in mol^{-1}). Since Miller et al. used halogen light a wavelength of 600 nm is taken since this represents the spectrum in the visible range.

The resulting number is the energy content of 1 mol of photons at a wavelength of 600 nm (E , in $J mol^{-1}$). Miller et al. used an infrared filter to filter the light. A fraction of 0.185 was passing the filter and illuminating the surface of their photobioreactor. Therefore we have to multiply by 0.185 to correct for this.

With this we can calculate that 1 kWh of energy represents 3.35 mol photons. The maximal efficiency found by Miller et al. was 0.115 mol O_2 per 1 kWh or per 3.35 mol photons. This results in a QR_{O_2} of 29 $mol mol^{-1}$.





CHAPTER 3

Light respiration in *Chlorella sorokiniana*

Kliphuis AMJ, Janssen M, van den End EJ, Martens DE, Wijffels RH (2010)

Light respiration in *Chlorella sorokiniana*

Accepted for publication in Journal of Applied Phycology

Abstract

Respiration and photosynthesis are two important processes in microalgal growth that occur simultaneously in the light. To know the rates of both processes at least one of them has to be measured. To be able to measure the rate of light respiration of *Chlorella sorokiniana* the measurement of oxygen uptake must be fast, preferably in the order of minutes. We measured the immediate post-illumination respiratory O₂ uptake rate (OUR) *in-situ*, using fiber-optic oxygen micro-sensors, and a small and simple extension of the cultivation system. This method enables rapid and frequent measurements without disturbing the cultivation and growth of the microalgae. Two batch experiments were performed with *Chlorella sorokiniana* in a short light-path photobioreactor and the OUR was measured at different time points. The net oxygen production rate (net OPR) was measured on-line. Adding the OUR and net OPR gives the gross oxygen production rate (gross OPR), which is a measure for the oxygen evolution by photosynthesis. The gross OPR was 35-40% higher than the net OPR for both experiments. The respiration rate is known to be related to the growth rate and it is suggested that faster algal growth leads to a higher energy (ATP) requirement and, as such, respiratory activity increases. This hypothesis is supported by our results, as the specific OUR is highest in the beginning of the batch culture when the specific growth rate is highest. In addition, the specific OUR decreases towards the end of the experiments until it reaches a stable value of around 0.3 mmol O₂ h⁻¹ g⁻¹. This value for the specific OUR is equal to the maintenance requirement of *Chlorella sorokiniana* as determined in an independent study of Zijffers et al. (2010). This suggests that respiration could fulfill the maintenance requirements of the microalgal cells.

Keywords: Microalgae, *Chlorella sorokiniana*, Respiration, Maintenance, Photosynthetic efficiency, Short light-path photobioreactor

Introduction

Respiration and photosynthesis are two important processes in microalgal growth that occur simultaneously in the light. These two processes and their relationship are extensively studied in plant science as reviewed by many authors (Badger et al. 1998; Geider and Osborne 1989; Graham 1980; Hoefnagel et al. 1998; Hunt 2003; Raghavendra et al. 1994; Turpin et al. 1988), because the balance between them determines, to a large extent, the growth and yield of most plants. (Hunt 2003)

In illuminated microalgal cells three processes in which oxygen is involved occur simultaneously. These processes are schematically shown in Figure 3.1. The first process is photosynthesis in which oxygen is released and ATP and NADPH are produced to be able to fix CO₂ into glyceraldehyde 3-phosphate (GAP). This can then be converted into biomass building-blocks. The second process is respiration. This process mainly takes place in the mitochondria where NADH is oxidized to generate extra energy in the form of ATP to support biomass formation and maintenance processes. In this process oxygen is consumed. (Geider and Osborne 1989; Graham 1980; Hoefnagel et al. 1998; Turpin et al. 1988) The third process that can occur in the light is photorespiration. The oxygenase activity of Rubisco can also fix oxygen instead of carbon dioxide, forming glycolate. (Tural and Moroney 2005) To convert glycolate into glyceraldehyde 3-phosphate, so it can be re-used in biosynthesis, energy is needed. This process occurs at high extracellular oxygen concentrations or at low carbon dioxide concentrations and can be neglected when this is not the case (Peltier and Thibault 1985).

To understand the energy metabolism of algal cells and with that the conversion of light energy into biomass, insight into the rates of these three processes is necessary. In this paper we work under conditions where photorespiration can be neglected. In this situation the net oxygen exchange rate, which can be directly measured, is the sum of the oxygen production by photosynthesis and oxygen consumption through respiration in the mitochondria. To know the rates of these two processes one of these has to be measured. In this paper we estimate the light respiration rate by measuring the post-illumination oxygen uptake. The rate of post-illumination O₂ uptake has been shown to provide a good measure for respiratory O₂ uptake in the light (Grande et al. 1989; Weger et al. 1989; Xue et al. 1996). In *Chlorella pyrenoidosa* respiration rates decreased from an initially high rate immediately after transfer to darkness to a much lower rate after 12-24 hours in darkness (Geider and Osborne 1989). Bate et al. (1988) found a decline of respiration to the basal rate of steady state dark respiration within an hour upon transfer to

darkness for *Dunaliella tertiolecta*. This suggests that to be able to measure the rate of light respiration of *Chlorella sorokiniana* the measurement of post-illumination oxygen uptake must be performed immediately upon transfer to darkness. In addition, at higher biomass concentrations the oxygen uptake rate will be high and therefore the oxygen concentration will decrease to zero in the order of a few minutes. Therefore an oxygen probe with a short response time is needed.

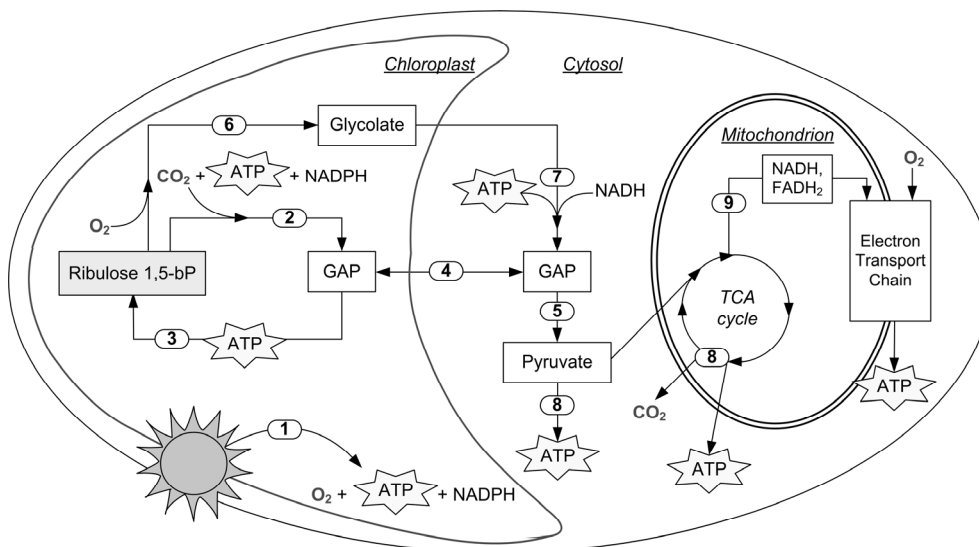


Figure 3.1 Simplified overview of an algal cell in the light, showing the processes in which oxygen and energy in the form of ATP are either consumed or produced. In the chloroplast light is fixed (1), yielding O₂, NADPH and ATP. These are needed by Rubisco to fix carbon dioxide into glyceraldehyde 3-phosphate (GAP) (2). GAP can be regenerated into Ribulose 1,5-bisphosphate using ATP (3) or can be transported to the cytosol (4) to be converted into building blocks for biomass (5). The oxygenase activity of Rubisco can also fix O₂, forming glycolate (6). This process is called photorespiration. Energy is consumed to convert glycolate into GAP so it can enter the central carbon metabolism (7). Energy in the form of ATP is yielded through the glycolysis and TCA cycle (8). Electrons are carried via NADH and FADH₂ to the electron transport chain located in the membrane of the mitochondria (9), yielding more ATP by taking up O₂.

Widely used methods to determine respiratory O₂ uptake in the light are gas analysis, Mass Spectrometry using oxygen isotopes and Clark type oxygen electrodes. The advantages and disadvantages of these methods for O₂ measurements are reviewed by Hunt (2003), Suresh et al. (2009) and Millan-Almaraz et al. (2009). The main drawbacks of

these methods are the time scale in which measurements are possible and the fact that for some of the methods the algae need to be transferred from the cultivation vessel to a measurement chamber. This can cause changes in growth rate and thus in respiration rate. Fast and *in-situ* measurements of oxygen uptake are preferred and these can be done using luminescence-based O₂ sensors. These fiber-optic sensors offer advantages over electrochemical devices such as lack of oxygen consumption, insensitivity to interfering agents and, most important, a faster response time. (López-Gejo et al. 2009) In addition, Tyystjarvi et al. (1998) found the same oxygen uptake data with fiber-optic sensors as with leaf disk O₂ electrodes, indicating that measuring OUR with fiber-optic sensors is a reliable method.

This paper describes a new method to measure the rate of respiration of *Chlorella sorokiniana* in the light, *in-situ* inside a short light-path (SLP) photobioreactor during cultivation, by means of a simple extension of the cultivation system. This is done by measuring the immediate post-illumination O₂ uptake using two types of commercially available fiber-optic oxygen micro-sensors. This method enables rapid and frequent measurements without disturbing the cultivation and growth of the microalgae. In the photobioreactor set-up used the net oxygen production rate (OPR) is measured on-line using a gas analysis system. This net OPR represents the oxygen that is produced as a sum of all processes in the cell that either produce or consume oxygen. By measuring the oxygen uptake rate (OUR) by respiration and adding the amount of consumed oxygen to the amount of net produced oxygen the gross OPR can be calculated giving the total rate of photosynthesis. Consequently, the method described in this paper gives insight into the different processes in which oxygen is involved in the light inside a microalgal cell, and more specifically it gives insight into the energy requirements for biomass formation and maintenance.

Materials & Methods

Organism, media and cultivation conditions

Chlorella sorokiniana CCAP 211/8k was obtained from the American Type Culture Collection (ATCC, no. 7516) and cultivated in 250 mL shake flasks containing 100 mL adapted M-8 medium (Mandalam and Palsson 1998), called M-8a (Table 3.1) at pH 6.7. The cultures were grown in a culture chamber at a temperature of 25°C, a light intensity of 20-40 μmol m⁻² s⁻¹ and a 16/8h day/night cycle. To reach inoculation cell density the cultures were placed in a shake-incubator for two days at a continuous light intensity of 280 μmol

$\text{m}^{-2} \text{s}^{-1}$ and a head space enriched with 5% carbon dioxide. For the experiments in the photobioreactor three times concentrated M-8a medium was used to be able to reach high cell densities. The concentration KNO_3 was decreased to 5 mmol L^{-1} , since HNO_3 was added on-demand via the pH control.

Reactor set-up

Chlorella sorokiniana was grown in batch mode in a short light-path (SLP) photobioreactor, depicted schematically in Figure 3.2. This photobioreactor design is described in more detail in Kliphuis et al. (2010a). The photobioreactor had a working volume of 3.4 L, an annular gap width of 12 mm and an illuminated area

(A_{pbr}) of 0.24 m^2 . The radius of the rotating inner cylinder (r_i) was 0.076 m and the radius of the stationary outer cylinder (r_o) was 0.088 m. Therefore the radius ratio ($\eta = r_i / r_o$) of the photobioreactor was $0.076 \text{ m} / 0.088 \text{ m} = 0.86$.

The inner cylinder was rotating at a speed of 70 rpm during the batch cultivations. To enable vertical back-mixing four down comers were drilled into the inner cylinder. Without down comers in the inner cylinder no vertical back mixing occurred and the algae accumulated in the top part of the photobioreactor. By adding the down comers, the algae were mixed over the whole annular gap.

The light was provided continuously by 60 tungsten-halogen lamps (Philips Masterline ES 45W) surrounding the reactor. The photon flux density (PFD, $\mu\text{mol m}^{-2} \text{s}^{-1}$) was measured with a LI-COR 190-SA 2 π sensor (PAR-range: 400–700 nm) at 80 fixed points inside the reactor before each experiment. The measured light intensities at all 80 points were averaged into a PFD for that particular experiment. An average light intensity of $1500 \mu\text{mol m}^{-2} \text{s}^{-1}$ could be reached with this set-up. The light intensity applied in these experiments ($\sim 1500 \mu\text{mol m}^{-2} \text{s}^{-1}$) is comparable to horizontal solar irradiance in the Netherlands at the peak of summer.

Table 3.1 Composition of M-8a medium

Compound	Concentration ($\mu\text{mol L}^{-1}$)
KNO_3	$29.67 \cdot 10^3$
KH_2PO_4	$5.44 \cdot 10^3$
$\text{Na}_2\text{HPO}_4 \cdot 2 \text{H}_2\text{O}$	$1.46 \cdot 10^3$
$\text{MgSO}_4 \cdot 7 \text{H}_2\text{O}$	$1.62 \cdot 10^3$
$\text{CaCl}_2 \cdot 2 \text{H}_2\text{O}$	88.43
EDTA ferric sodium salt	315.86
$\text{Na}_2\text{EDTA} \cdot 2 \text{H}_2\text{O}$	100.00
H_3BO_3	1.00
$\text{MnCl}_2 \cdot 4 \text{H}_2\text{O}$	65.59
$\text{ZnSO}_4 \cdot 7 \text{H}_2\text{O}$	11.13
$\text{CuSO}_4 \cdot 5 \text{H}_2\text{O}$	7.33

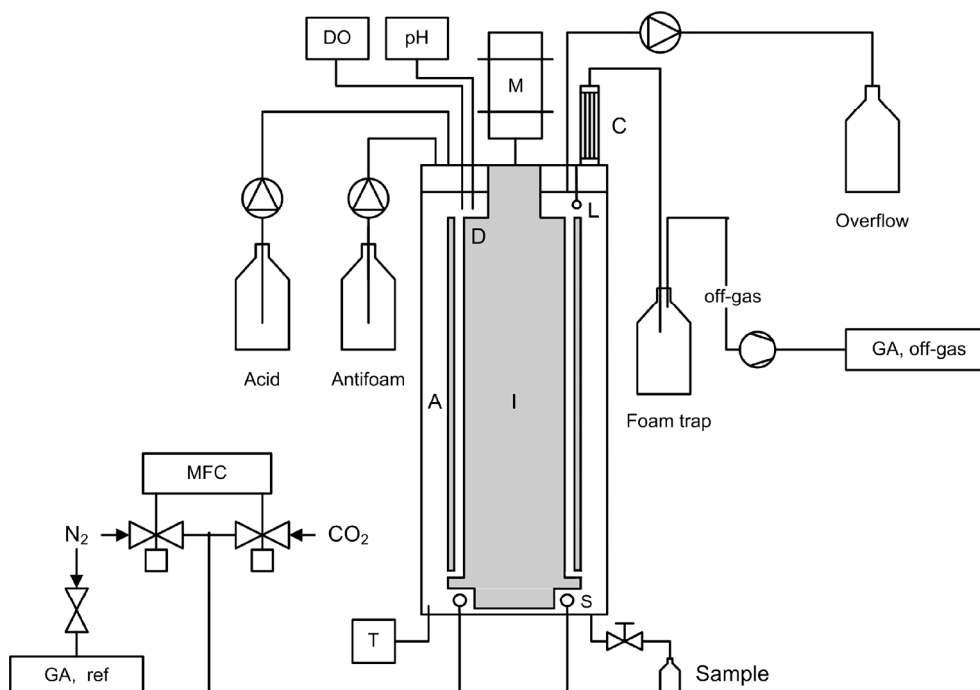


Figure 3.2 Schematic overview (not on scale) of the SLP photobioreactor. A = annular gap, C = condenser, D = internal down comer, DO = dissolved oxygen sensor, GA = gas analyzer, I = inner cylinder, L = spherical light sensor, M = motor, MFC = Mass flow controllers for both N_2 and CO_2 , pH = pH control connected to acid pump, S = sparger, T = temperature control connected to cryostat and cooling jacket (not shown)

During the experiments the transmitted irradiance through the culture ($\mu\text{mol m}^{-2} \text{s}^{-1}$) was measured by a spherical light sensor (US-SQS Spherical Micro Quantum Sensor, Heinz Walz GmbH, Germany) placed inside the culture broth at the depth of the annular gap, 12 mm from the internal reactor wall, as illustrated in Figure 3.2.

Using mass flow controllers (Brooks, Smart TMF 5850S), carbon dioxide was supplied by sparging nitrogen (1.55 L min^{-1}) enriched with 2% carbon dioxide through a silicone ring-sparger at the bottom of the reactor. This gas flow also served to remove excess oxygen from the culture broth. The pH was controlled at $\text{pH } 6.7 \pm 0.1$ by pumping nitric acid (1.7 M), serving also as nitrogen source. The acid bottle, antifoam bottle, and overflow bottle were placed on balances and weighed on-line. The reactor was kept at 37°C , the optimal temperature for *Chlorella sorokiniana* (Sorokin and Myers 1953), by a water jacket con-

nected to a temperature-controlled water bath. To prevent water from evaporating into the off-gas the reactor was equipped with a condenser connected to a cryostat set at 2°C. Biomass samples were taken from the bottom of the reactor and weighed off-line.

On-line gas analysis and calculations

The off-gas was analyzed by leading it over a gas analyzer (Servomex, 4100) fitted with two different gas sensor modules, a paramagnetic purity transducer to measure oxygen and an infrared 1500 transducer to measure carbon dioxide.

Before each experiment, a dry and a wet baseline were measured to correct the experimental gas data for moisture content according to equation 1. The dry baseline was measured by leading 1.55 L min⁻¹ nitrogen enriched with 2% carbon dioxide over the gas analyzers. For the wet baseline the nitrogen enriched with carbon dioxide was first sparged through the reactor, containing medium at the same temperature and pH as during the batch experiment, and through the condenser before being analyzed.

$$n_{\text{gas,out}} = n_{\text{gas,in}} \cdot \frac{x_{\text{CO}_2,\text{db}}}{x_{\text{CO}_2,\text{wb}}} \quad (1)$$

The total molar gas flow going in ($n_{\text{gas,in}}$, mmol h⁻¹) is corrected for the molar fraction of carbon dioxide in both the dry ($x_{\text{CO}_2,\text{db}}$) and wet baseline ($x_{\text{CO}_2,\text{wb}}$). With this corrected molar gas flow $n_{\text{gas,out}}$ (mmol h⁻¹) and the molar fraction of oxygen ($x_{\text{O}_2,\text{exp}}$) and carbon dioxide ($x_{\text{CO}_2,\text{exp}}$) measured during the experiments, the oxygen production rate (OPR, mmol h⁻¹) and carbon dioxide uptake rate (CUR, mmol h⁻¹) are calculated according to equations 2 and 3.

$$\text{OPR} = \frac{n_{\text{gas,out}} \cdot (x_{\text{O}_2,\text{exp}} - x_{\text{O}_2,\text{wb}})}{100} \quad (2)$$

$$\text{CUR} = \frac{n_{\text{gas,out}} \cdot (x_{\text{CO}_2,\text{exp}} - x_{\text{CO}_2,\text{wb}})}{100} \quad (3)$$

The ratio between the OPR and CUR is the photosynthetic quotient PQ. The PQ can be calculated according to equation 4:

$$\text{PQ} = \frac{\text{OPR}}{\text{CUR}} \quad (4)$$

The observed biomass yield on light energy ($Y_{x,E(\text{obs})}$, g mol^{-1}) is defined as gram dry biomass formed per mol incident photons on the photobioreactor surface according to equation 5. The photon flux (PF_{in} , mmol h^{-1}) is calculated using the measured average photon flux density (PFD_{in} , $\mu\text{mol m}^{-2} \text{s}^{-1}$) and the illuminated photobioreactor area A_{pbr} (m^2) described earlier. We assumed that all consumed carbon is converted into biomass. The dry biomass C-molar mass (M_{biomass} , g mol^{-1}) was determined as described in the next paragraph.

$$Y_{x,E(\text{obs})} = \frac{\text{CUR} \cdot M_{\text{biomass}}}{\text{PF}_{\text{in}}} \quad (5)$$

The theoretical maximal biomass yield ($Y_{x,E(\text{max})}$) for growth on nitrate is estimated to be 1.57 gram dry weight per mol of photons (quanta) (calculation in Kliphuis et al. (2010a)).

Respiration measurements

Oxygen uptake through respiration (OUR) was measured using two different fiber-optic oxygen micro-sensors as shown in Table 3.2. In experiment I the OceanOptics (OO) micro-sensor was used and in experiment II the PreSens (PS) micro-sensor was used.

The measurement principle of both oxygen micro-sensors is based on the effect of dynamic fluorescence quenching by molecular oxygen. Light pulses by a LED (475nm) are sent to the tip of the micro-sensor coated by a Ru(II) complex, which is excited by the light. The excited complex fluoresces at 600 nm. If the excited complex encounters an oxygen molecule, the excess energy is transferred to the oxygen molecule, quenching the fluorescence signal. So when more oxygen is present, more of the fluorescence will be quenched, resulting in lower fluorescence. The fluorescence light is collected by the probe, transported through the optical fiber to the detector and translated into an oxygen concentration. The OceanOptics micro-sensor translates the fluorescence intensity (or phase shift) to an oxygen concentration. The PreSens micro-sensor translates the

Table 3.2 Two types of fiber-optic oxygen micro-sensors used in this study.

Type of micro-sensor	Measuring method	Response time	Exp.
AL-300 FOXY (Ocean Optics)	Fluorescence intensity	< 1s (no optical isolation)	I
NTH-PSt1-L2.5-TS-NS40/0.4-YOP (PreSens)	Fluorescence decay time	< 1s (optical isolation)	II

fluorescence decay time to an oxygen concentration. This decay time is the phase angle between the exciting and the emitted signal and is shifted as a function of the oxygen concentration. The PreSens micro-sensor was equipped with an optically isolated sensor tip to exclude intrinsic chlorophyll fluorescence from the microalgae cells.

To be able to measure the oxygen uptake rate of *Chlorella sorokiniana* inside the photobioreactor, the fiber-optic micro-sensors needed to be calibrated in M-8a medium at 37° C. The Ocean Optics micro-sensor was calibrated using a second order polynomial algorithm (non-linear Stern-Volmer relationship) for which three standards with known O₂ concentration were needed. M-8a medium at 37°C saturated with N₂ was used as 0% air saturation, with pressurized air as 100% air saturation and with pure O₂ as 476.2% air saturation. The PreSens micro-sensor was calibrated using the linear Stern-Volmer algorithm for which two standards with known O₂ concentration were needed. Therefore M-

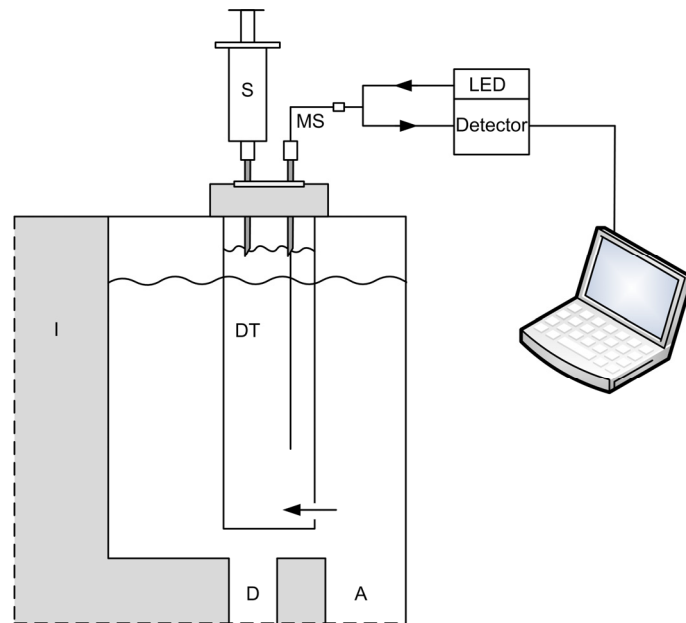


Figure 3.3 Schematic overview of the OUR measurement setup (not on scale). The algae are sucked into the dark tube using a syringe. The OUR of the algae is measured by a fiber-optic micro-sensor connected to a light source (LED) and a detector to detect the fluorescence quenching by oxygen at the sensor tip. The detector in turn is connected to a pc with the designated software to log the oxygen uptake in time. A = annular gap, D = internal down comer, DT = dark tube, I = inner cylinder, MS = micro-sensor, S = syringe.

8a medium at 37°C saturated with N₂ as 0% air saturation and with pressurized air as 100% air saturation were used. The output of the fiber-optic micro-sensors was O₂ concentration in percentages air saturation. The concentration dissolved O₂ in mmol L⁻¹ M-8a medium could be calculated from the percentages air saturation by correcting for the temperature and salinity of the M-8a medium according to Quicker et al. (1981).

A dark tube with a volume of 8 mL, closed with a septum was placed in the top of the photobioreactor, hanging in the culture broth as shown schematically in Figure 3.3. The fiber-optic oxygen micro-sensor was inserted into the dark tube through the septum with help of a needle. Algae were sucked into the dark tube through a small hole (Ø 1 mm) in the bottom of the tube using a needle and a syringe. As soon as the algae are in the dark they will immediately stop photosynthesizing and oxygen uptake through respiration can be measured by logging the decrease in oxygen concentration in time. The micro-sensors were connected to the corresponding detectors which were in turn connected to a pc logging the data using the corresponding software supplied with the micro-sensors. Before and after each measurement the tube was flushed with air.

Oxygen uptake rate calculation

The slope of the decrease in oxygen concentration (mmol kg⁻¹ h⁻¹) is multiplied by the reactor volume (V_{pbr} , kg) to give the oxygen uptake rate (OUR) in mmol h⁻¹, according to equation 6:

$$\text{OUR (t)} = \text{Slope} \cdot V_{pbr} \quad (6)$$

In previous experiments with *Chlorella sorokiniana* we observed the formation of a biofilm when the batch experiment was kept running for longer than 60 hours and biomass densities increased to more than 10 g L⁻¹. The cells forming this biofilm were not detectable with dry weight measurements but were most probably still alive and actively contributing to oxygen production and consumption in the photobioreactor. The total accumulation of biomass, so the cells in suspension and the live cells in biofilm, at each time point during the cultivation ($C_{x,tot}(t)$, g) can be calculated from the CUR (CUR(t), mol). For this we assume that every mol of CO₂ which is taken up is converted into one C-mol of dry biomass with a known molecular weight ($M_{biomass}$, g mol⁻¹), according to equation 7.

$$C_{x,tot}(t) = C_x(0) + \int_0^t CUR(t) \cdot M_{biomass} dt \quad (7)$$

To calculate the cumulative CUR, the amount of inoculum had to be added to the CUR at $t=0$ ($C_x(0)$, g). The elemental composition and molecular weight of *Chlorella sorokiniana* biomass was $CH_{1.71 \pm 0.01}O_{0.40 \pm 0.02}N_{0.15 \pm 0.004}$ with a $M_{biomass}$ of $23.682 \text{ g mol}^{-1}$ (including ash), as determined by Kliphuis et al. (2010a). This total biomass can be compared with the measured dry weight of the cells in suspension to assess whether there was biofilm formation during the experiment. If biofilm formation takes place in the photobioreactor it is not possible to determine if that is also the case inside the dark measuring tube. Therefore we can calculate two values for the OUR. If we assume that inside the dark tube the same biofilm is built up as in the rest of the photobioreactor and that this biofilm actively contributes to the OUR, the measured OUR in mmol h^{-1} represents the OUR for the whole reactor. If however there is no biofilm build-up inside the dark tube or the biofilm would be inactive due to the darkness in the tube, the measured OUR is only caused by the cells in suspension which are sucked into the tube. This measured OUR in mmol h^{-1} then only represents the cells in suspension. To be able to calculate the OUR for the whole reactor, we then need to correct for the cells that are present in the form of biofilm in the photobioreactor, hence OUR_{corr} .

With the measured dry weight we first calculate the specific OUR per biomass ($OUR_{spec}(t)$, $\text{mmol h}^{-1} \text{ g}^{-1}$) by dividing the OUR at time t (mmol h^{-1}) with the measured dry weight at that time ($C_x(t)$, g) according to equation 8:

$$OUR_{spec}(t) = \frac{OUR(t)}{C_x(t)} \quad (8)$$

By multiplying with the total biomass present in the reactor ($C_{x,tot}(t)$, g) calculated from the CUR (equation 7), the OUR_{corr} (mmol h^{-1}) can be calculated with equation 9:

$$OUR_{corr}(t) = OUR_{spec}(t) \cdot C_{x,tot}(t) \quad (9)$$

The resulting OUR, whether corrected or not, can be added up to the Net OPR at time t (OPR, mmol h^{-1}) as measured with gas analysis at that time point, according to Equation 10. This gives the gross OPR (OPR_{gross}) at time t (mmol h^{-1}), which shows the total oxygen evolution at that time point.

$$\text{OPR}_{\text{gross}}(t) = \text{OPR}(t) + \text{OUR}_{(\text{corr})}(t) \quad (10)$$

Biomass Determinations

Cell number and cell size

Cell number and cell size were determined with a Beckman Coulter Multisizer 3 (Beckman Coulter Inc., Fullerton USA, 50 μm orifice). The samples were diluted with filtered (0.2 μm) Coulter® Isoton® II dilution buffer to a cell concentration between $1 \cdot 10^5$ and $3 \cdot 10^5$ cells mL^{-1} . The cell number and cell size were used to calculate the total biovolume.

Dry Weight Determination

Whatman GF/F glass microfiber filters (\varnothing 55 mm, pore size 0.7 μm) were dried at 95°C overnight and placed in a desiccator to cool to room temperature. The dry, empty filters were weighed and pre-wet with de-mineralized water. Two grams of sample were diluted with de-mineralized water and filtrated under mild vacuum (0.67 bar absolute). The filter was rinsed twice with de-mineralized water to remove adhering inorganic salts. The wet filters containing the samples were dried again at 95°C overnight, allowed to cool to room temperature in a desiccator and weighed. The difference in weight between the dry filters containing the samples and the empty weight was the dry weight of the samples.

Results

Two batch experiments were performed with *Chlorella sorokiniana* in a SLP photobioreactor. The mixing in the SLP photobioreactor was accomplished by rotating the inner tube at 70 rpm. The results of these batch experiments can be seen in Figure 3.4. Figure 3.4a shows the net oxygen production rate (OPR) and carbon dioxide uptake rate (CUR) obtained by duplicate batch cultivations (I and II). After inoculating with a very low biomass density the algae were grown at a light intensity of 200 $\mu\text{mol m}^{-2} \text{s}^{-1}$. When the biomass concentration increased to 0.1 g L^{-1} dry weight the light was increased to 600 $\mu\text{mol m}^{-2} \text{s}^{-1}$. When the biomass concentration reached 1.2 g L^{-1} dry weight the light was increased to 1500 $\mu\text{mol m}^{-2} \text{s}^{-1}$, which is the light intensity of interest. After this increase in light supply to 1500 $\mu\text{mol m}^{-2} \text{s}^{-1}$ at 23 hours, the OPR and CUR increased dramatically and continued to increase until an optimum was reached at 27 hours. After reaching this

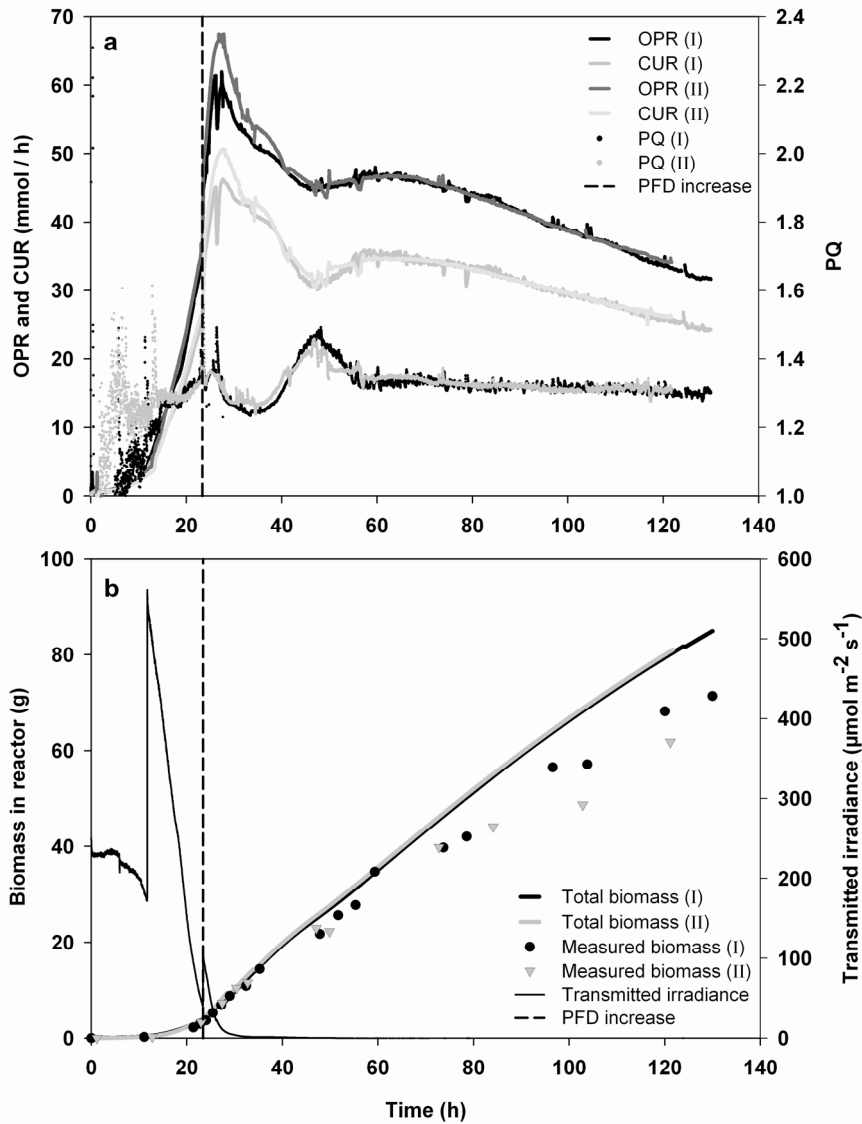


Figure 3.4 Detailed overview of duplicate batch experiments I and II at a mixing rate of 70 rpm. a) Oxygen production rates (OPR), carbon dioxide uptake rates (CUR) (in mmol h^{-1}) and photosynthetic quotient (PQ) for both experiments. All data are normalized for the time point of light increase to $1500 \mu\text{mol m}^{-2} \text{s}^{-1}$, which is indicated with a dotted line. b) Total biomass present in the reactor (in g) as calculated from the CUR as well as the measured dry weight present in the reactor (in g) for duplicate batch experiments I and II. Also plotted is the transmitted irradiance through the culture during the batch experiment. The two peaks indicate the step-wise light increase, the first time to $600 \mu\text{mol m}^{-2} \text{s}^{-1}$ when the biomass is still relatively low and the second time to $1500 \mu\text{mol m}^{-2} \text{s}^{-1}$. This second light increase is indicated with a dotted line.

optimum at a biomass density of 2.3 g L^{-1} dry weight the OPR and CUR decreased again until the batch was ended.

The PQ values for the duplicate experiments are also shown in Figure 3.4a. When the light was increased to $1500 \mu\text{mol m}^{-2} \text{ s}^{-1}$ the PQ fluctuated and finally stabilized at a value of 1.34 for both duplicate experiments. The PQ value shows if the composition of the produced biomass changes (Eriksen et al. 2007), different substrates are used or other products are formed, thus serving as a control parameter for photoautotrophic growth. In this case the PQ for both experiments shows the same trend and the same values, indicating that the growth of both cultures was comparable. The fluctuation of the PQ observed after the light increase to $1500 \mu\text{mol m}^{-2} \text{ s}^{-1}$ is probably related to changes in biomass composition as for example a change in the amount of stored carbohydrates.

During the experiments the light penetrating the culture was measured by a spherical PAR sensor hanging inside the culture at the depth of the annular gap as shown in Figure 3.4b. The step wise light increase can be clearly seen as well as the fast decrease of light penetrating the culture when the biomass increased. At the optimum OPR and CUR all the light was absorbed in the annular gap.

The biomass dry weight present in the reactor (in grams) is plotted in Figure 3.4b for both experiments. Both the measured biomass, representing the biomass in suspension as determined by dry weight measurements, and the calculated total biomass, representing all the biomass present in the reactor calculated with equation 7, are given. In the beginning of the batch experiments the measured and the calculated total biomass were equal but during the experiment, as the biomass density increased above 10 g L^{-1} , these values started to deviate. This deviation was due to the formation of a biofilm. During the experiments, especially experiment II, a thin biofilm formed on the reactor wall which contributed to the OPR and CUR but could not be measured by taking samples and measuring dry weight because these only represented the cells present in suspension.

Respiration measurements

During the batch experiments respiration was quantified by measuring the oxygen uptake rate (OUR) of the microalgae inside the dark tube. Figure 3.5 shows such a duplicate measurement. When the algae were sucked into the dark tube the starting oxygen concentration was the same as in the photobioreactor at that time point. Then the oxygen concentration started to decrease due to oxygen uptake by respiration. All oxygen was

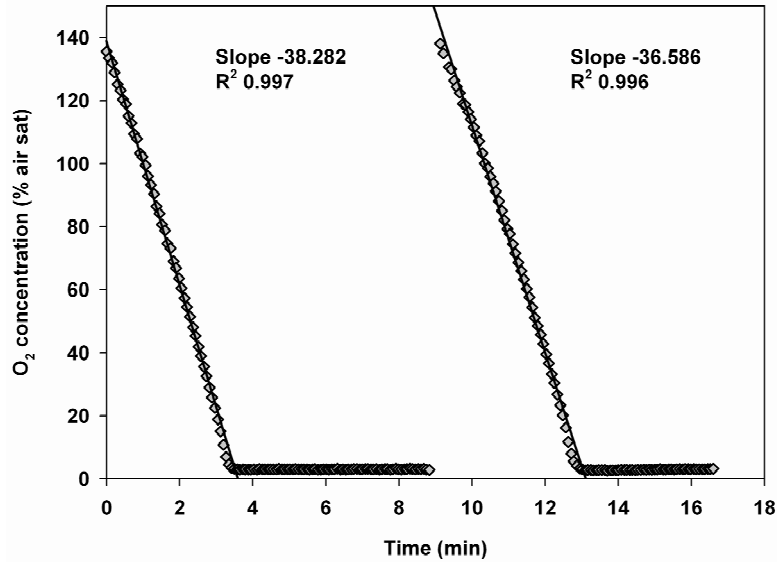


Figure 3.5 Duplicate OUR measurement. Upon transfer to the dark the microalgae consumed the oxygen present in the liquid. The starting oxygen concentration was equal to the DO in the photobioreactor. When all oxygen was consumed the tube was flushed and the process was repeated for a duplicate measurement at that time point. At the same time one biomass sample was taken. The oxygen concentration was measured in % air saturation. The slope represents the OUR and was converted to mmol h^{-1} using equation 6.

consumed after about 4 minutes and after a while the tube was flushed and new algae were sucked into the dark for a duplicate measurement. The oxygen concentration in % air saturation was converted to mmol L^{-1} as described before, and the slope thus gave the OUR (t) in mmol h^{-1} (equation 6). This measurement was performed at different time points during the batch (either in duplicate or triplicate) and a biomass sample was taken from the bottom of the photobioreactor simultaneously. Figure 3.4b shows a deviation between the measured and calculated biomass content of the bioreactor at higher biomass concentrations and we observed the formation of a thin biofilm. This biofilm formation starts at high biomass concentrations of over 10 g L^{-1} and becomes more pronounced at even higher concentrations of around 20 g L^{-1} dry weight. These biomass concentrations are very high for microalgal cultivations. The algae are probably very light limited at that point and likely react to this by forming a thin biofilm. To be able to also judge respiration and gross OPR at these high biomass concentrations the OUR was also corrected according to equation 9. This correction was performed assuming no biofilm build up in the dark tube and only in the photobioreactor. This correction also reflects

the situation if a possible biofilm inside the dark tube would be inactive due to the darkness in the tube. The uncorrected OUR gives the values for the assumption that there was a biofilm in the dark tube and the build-up was equal to that in the whole bioreactor. Both values will be given in all figures to show the two most extreme scenarios and the margin of error that can be due to biofilm formation at (very) high biomass densities.

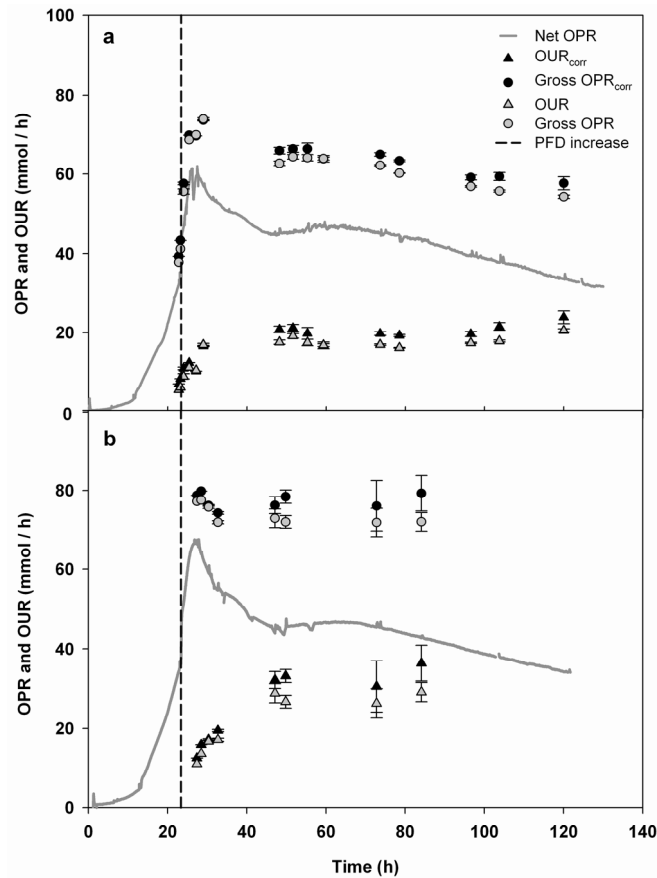


Figure 3.6 Oxygen uptake rates and gross oxygen production rates (OPR) for duplicate batch experiments I (Figure a) and II (Figure b) at 70 rpm. The net oxygen production rate (Net OPR) was measured on-line during the batch cultivations. The oxygen uptake rate (OUR) was measured with the oxygen micro-sensors at different time points as indicated with triangles. The error bars represent the standard deviation of duplicate or triplicate OUR measurements at that time point. Adding up the OUR and the net OPR at these time points gives the gross OPR, indicated with circles. The closed symbols give the corrected values for OUR (OUR_{corr}), assuming no biofilm build up in the dark tube and only in the photobioreactor. The open symbols give the values for OUR for the assumption that there was a biofilm in the dark tube and the build-up was equal to that in the whole bioreactor. The light increase to $1500 \mu\text{mol m}^{-2} \text{s}^{-1}$ is indicated by a dotted line.

Figure 3.6a shows the OUR data for experiment I and Figure 3.6b shows the OUR data for experiment II. Both graphs show the net OPR as measured on-line and the OUR measured with the oxygen micro-sensors, indicated with triangles. The values for both OUR and OUR_{corr} are equal in the beginning of the experiment and start to deviate in time, due to the biofilm increasing in size. Both OUR and OUR_{corr} follow the same pattern for both experiments. Figure 3.6 also shows the gross OPR for both experiments, indicated with circles. The net OPR is measured on-line based on the gas analysis and represents the oxygen that is produced as a sum of all processes in the cell that either produce or consume oxygen. In photosynthesis oxygen is produced but in mitochondrial respiration oxygen is consumed again. This is not reflected in the net OPR but by measuring the OUR and adding the amount of consumed oxygen to the amount of net produced oxygen the gross OPR can be calculated. The OUR and gross OPR increase with increasing net OPR

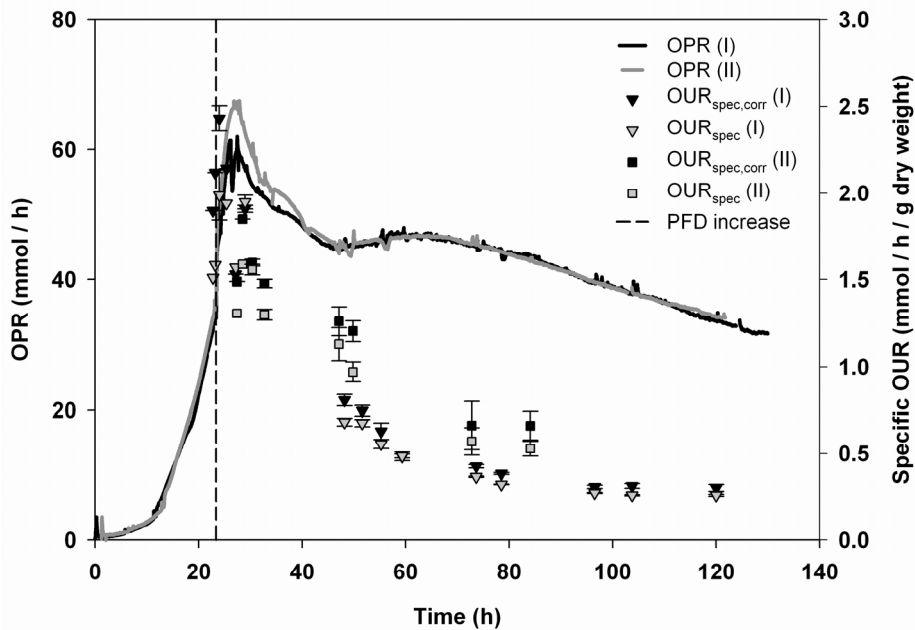


Figure 3.7 Specific OUR ($\text{mmol h}^{-1} \text{g Dw}^{-1}$) for duplicate experiments I and II. The OPR was measured on-line. The OUR was measured at different time points at which the biomass concentration was also measured. The closed symbols give the corrected values for OUR_{spec} ($OUR_{spec,corr}$), assuming no biofilm build up in the dark tube and only in the photobioreactor. The open symbols give the values for OUR_{spec} for the assumption that there was a biofilm in the dark tube and the build-up was equal to that in the whole bioreactor. The error bars represent the standard deviation of duplicate or triplicate OUR measurements at that time point. The light increase to $1500 \mu\text{mol m}^{-2} \text{s}^{-1}$ is indicated by a dotted line.

and stabilize after the optimum OPR is reached. The gross OPR is 30-45% higher than the net OPR.

From the OUR and the simultaneous biomass measurements the specific OUR could be calculated according to equation 8. To obtain the corrected specific OUR, the measured OUR was divided by the total biomass $C_{x,tot}$ calculated according to equation 7. These data are shown in Figure 3.7 for both experiment I and II. The on-line measured OPR for both experiments is shown and the dotted line represents the light increase to $1500 \mu\text{mol m}^{-2} \text{s}^{-1}$. The specific OUR is highest at the optimum OPR and decreases with the decreasing OPR until it reaches a stable value at the end of the experiments.

Discussion

To be able to gain insight in microalgal respiration during photosynthesis in the light we measured the oxygen uptake of the algae immediately upon transfer into darkness during different time points in the batch experiments. The post-illumination oxygen uptake rates were thus measured at different biomass concentrations and therefore at different light supply rates. Immediately upon transfer to darkness photosynthesis stopped and the oxygen present in the dark tube was taken up by the algae within minutes. Both optical micro-sensors were able to measure this uptake since the response time of both sensors was in the order of seconds. The measured decrease of oxygen is shown in Figure 3.5. This measurement was very similar to all other measurements we performed. On each measurement output we performed linear regression and we always found a R^2 of 0.95 or higher and a P value well below 0.05, indicating that the decrease of oxygen was linear. From these measurements a slope could be calculated, indicating the volumetric OUR in $\text{mmol h}^{-1} \text{kg}^{-1}$. It is also interesting to note that during this measurement no change in the slope could be detected. On the timescale of these measurements the oxygen uptake rate did not decrease towards the lower respiration rate of dark adapted algae. This lower dark rate would be reached on a timescale of hours according to literature (Bate et al. 1988; Geider and Osborne 1989) and with this fast measurement we were not able to see this lower respiration rate of dark adapted algae. Therefore the measured OUR must have been predominantly caused by mitochondrial (light) respiration.

Another process that could cause oxygen uptake in the light is photorespiration, but we estimated that photorespiration only could take place at a low rate. Ogren (1984) described an equation to calculate the relative rate of photosynthesis versus photorespira-

tion v_c/v_o for isolated Rubisco, equation 11. It is important to note that this equation was derived for free Rubisco enzymes and that several transport processes play a role in the functioning of Rubisco in whole cells. Currently it is not possible to calculate the intracellular CO_2 and O_2 concentration at the site of Rubisco and the selectivity of the free enzyme is the only way to estimate whether photorespiration takes place at the concentrations of O_2 and CO_2 present in the cultivation medium. The specificity factor S_{rel} was determined experimentally to be 61 for *Chlamydomonas reinhardtii* (Ogren 1984).

$$\frac{v_c}{v_o} = S_{\text{rel}} \cdot \frac{[\text{CO}_2]}{[\text{O}_2]} \quad (11)$$

At the point of maximum productivity in experiment II, which was higher than for experiment I, the dissolved oxygen reached 122% air saturation corresponding to an oxygen concentration in the medium of $260 \mu\text{mol L}^{-1}$. At this point the concentration dissolved CO_2 was $102 \mu\text{mol L}^{-1}$ as calculated by the method described by Royce and Thornhill (1991). This method is based on the measured OPR and dissolved oxygen concentration to calculate the mass transfer coefficient for O_2 and subsequently CO_2 , followed by the calculation of the dissolved carbon dioxide concentration.

The ratio of photosynthesis and photorespiration v_c/v_o then becomes 23.93. This means that the rate of photorespiration is indeed very low, 4% of photosynthesis, at that point. During the rest of the experiment the ratio of CO_2 to O_2 increased again so the rate of photorespiration will have been less than 4% of gross photosynthesis. This is much smaller than the difference between net and gross OPR and this difference therefore must have been predominantly caused by mitochondrial respiration.

To show the total oxygen evolution by photosynthesis (the gross OPR), the on-line measured net OPR and the OUR were added up. This is shown in Figure 3.6. The graphs for both experiments generally show the same pattern, although the values for experiment II are slightly higher. This could be due to the use of different micro-sensors. It is known that the respiration rate is related to the growth rate (Falkowski et al. 1985). So when the algae are growing faster, more energy for growth is needed and the OUR will be higher and, consequently, the gross OPR will be higher too as can be seen from our results. The OUR increases with increasing biomass and when the PQ (as shown in Figure 3.4) stabilizes the OUR values also become relatively constant. Near the end of both experiments the OUR starts to increase. When looking at the rates of oxygen uptake where

the PQ is constant the gross OPR was 35-40% higher than the Net OPR for both experiments. This is in agreement with the 33% found by Weger et al. (1989) for *Thalassiosira* as measured by Mass Spectrometry, and the 17-43% found for cyanobacterial biofilms as measured with a Clark type micro-sensor (Kühl et al. 1996). Bate et al. (1988) found a difference of 15.6% for the green alga *Dunaliella tertiolecta*.

Compared to specific studies using *Chlorella sorokiniana*, our values are high. In two studies Vona et al. determined the difference between gross OPR and Net OPR to be 5% for *C. sorokiniana* (Vona et al. 2004; Vona et al. 1999). However, they used different culture conditions and more importantly they used a different, *ex-situ*, method to measure the oxygen uptake rate. In the aforementioned study, the respiratory oxygen uptake was measured by transferring the cells to a biological oxygen meter (BOM) equipped with an oxygen electrode. Transferring the cells from the cultivation vessel to a BOM might result in a lower growth rate and a lower oxygen uptake of the cells.

Similar to a previous study (Kliphuis et al. 2010a), we observed an optimum OPR and CUR at a biomass concentration of around 2.3 g L^{-1} for both batch experiments with *Chlorella sorokiniana*, Figure 3.4a. This point is the moment where the biomass yield on light energy ($Y_{x,E(\text{obs})}$) reaches its maximum value, 0.82 g mol^{-1} for experiment I and 0.87 g mol^{-1} for experiment II. At first, more light was available per cell. Because of this the algae could fix more CO_2 , produce more O_2 and grow faster. While the biomass concentration in the photobioreactor keeps increasing, as can be seen in Figure 3.4b, the available light per cell decreases due to mutual shading, and the OPR and CUR reach an optimum. After this point the OPR and CUR decrease again and keep on doing so until the end of the batch experiment.

This decrease in net OPR and CUR after having reached the optimum can now be related to the specific oxygen uptake rate (OUR) which is shown in Figure 3.7. The specific OUR is highest at the optimum of the net OPR and decreases together with the net OPR until it reaches a stable value towards the end of the experiments. This trend can be explained by taking into account that part of the respiratory activity is coupled to growth, as discussed before, but that another part is related to the maintenance requirements of the microalgae. Maintenance in this context is defined as energy consumption for purposes other than growth (Pirt 1965). When there is sufficient light available per cell the algae grow fast and need energy (ATP) to support growth. This energy is supplied by respiration of a part of the carbohydrates produced in photosynthesis and thus the specific OUR will be high. A portion of the available light per cell, on the other hand, is needed to gen-

erate energy for maintenance, possibly also via respiration of carbohydrates produced in photosynthesis. Thus, after having reached the optimum productivity, the cell density is such that all light is absorbed in the system. When the cell density increases further, the energy extracted from this light (via photosynthesis and respiration) will decrease from a maximal value during the optimum, consisting of a large growth-associated fraction and a smaller but constant maintenance-associated fraction, to a low value, composed of predominantly the constant maintenance-associated fraction.

This analysis is supported by the maintenance requirement of *Chlorella sorokiniana* which was determined in an independent study of Zijffers et al. (2010). The specific OUR decreases towards the end of the experiments until it reaches a stable value of around $0.3 \text{ mmol O}_2 \text{ h}^{-1} \text{ g}^{-1}$. This low value for the specific OUR is in the same order as the value for maintenance requirement determined experimentally by Zijffers et al. (2010). Zijffers et al. determined a maintenance constant of $6.8 \text{ mmol photons g}^{-1} \text{ h}^{-1}$ for *Chlorella sorokiniana* based on the maintenance/growth model by Pirt (1986). The corresponding yield $Y_{x,E}$ was $0.75 \text{ g mol photons}^{-1}$ for growth on urea. The $Y_{x,E_{\max}}$ for photoautotrophic growth on urea is estimated to be 1.8 g mol^{-1} . The maintenance constant therefore needs to be corrected for this growth inefficiency by multiplying with a factor $0.75/1.8$, yielding a corrected maintenance constant of $2.84 \text{ mmol photons g}^{-1} \text{ h}^{-1}$. In the light reaction of photosynthesis, 8 photons are used to produce one mol of O_2 . The formed ATP is used to fix one mol of CO_2 into one C-mol biomass. When this biomass is respired again, one mol of O_2 is taken up. When we assume that all oxygen uptake is due to maintenance, one mol of oxygen is taken up per 8 photons, giving $2.84 * 1/8 = 0.36 \text{ mmol O}_2 \text{ g}^{-1} \text{ h}^{-1}$. This value represents the OUR for maintenance only and corresponds well with the value found in our experiments.

In short, Zijffers et al. determined the maintenance light requirements of *C. sorokiniana* based on the corresponding light use. In this study we measured the specific oxygen consumption rate which converged to a low and constant value at the end of the batch cultivation. Recalculating the data from Zijffers et al. to a specific respiratory oxygen consumption shows that both values are almost the same. This shows that respiration could fulfill the maintenance requirements of the microalgal cells.

To conclude, the method described in this paper for measuring the respiration rates of microalgae proved to be a good technique for determining the oxygen uptake *in situ* during cultivation in a photobioreactor. Only a small and simple extension of the system

was necessary to be able to measure respiration rates. This method enables rapid and frequent measurements without disturbing the cultivation and growth of the microalgae. The rate of oxygen uptake in the light gives insight in the gross oxygen evolution by photosynthesis which is 30-45% higher than net oxygen evolution rate. Respiration rates in the light are very high and consequently photosynthesis rates are very high to produce sugars which can be respired to produce extra ATP for growth. Measuring respiration rates during a batch cultivation showed the relationship between growth and respiration as an energy supporting mechanism. It also provided strong evidence that respiration could fulfill the maintenance requirement of the microalgal cells.

Nomenclature

η	Radius ratio of the photobioreactor (-)
μ_t	Specific growth rate at time t (h^{-1})
A_{pbr}	Illuminated photobioreactor area (m^2)
CUR	Carbon dioxide uptake rate (mmol h^{-1})
CUR_{cum}	Cumulative carbon dioxide uptake rate (mol)
C_x	Biomass present in the photobioreactor as measured with dry weight measurement (g)
$C_{x,\text{tot}}$	Total biomass present in the photobioreactor, including biofilm, calculated from CO_2 uptake (g)
K_m	affinity constant for carbon dioxide ($\mu\text{mol L}^{-1}$)
M_{biomass}	Molar mass of dry biomass (g mol^{-1})
$m_{E,x}$	Maintenance coefficient ($\text{mol g}^{-1} \text{h}^{-1}$)
$n_{\text{gas,in}}$	Total molar gas flow going into the reactor (mmol h^{-1})
$n_{\text{gas,out}}$	Total molar gas flow going out of the reactor corrected for moisture content (mmol h^{-1})
OPR	Oxygen production rate (mmol h^{-1})
$\text{OPR}_{\text{gross}}$	Gross oxygen production rate (mmol h^{-1})
OUR	Oxygen uptake rate (mmol h^{-1})
OUR_{corr}	Oxygen uptake rate corrected for biofilm in the photobioreactor (mmol h^{-1})
OUR_{spec}	Oxygen uptake rate per unit biomass ($\text{mmol h}^{-1} \text{g}^{-1}$)
PAR	Photosynthetic active radiation, all photons between 400 and 700 nm (-)
PF_{in}	Photon flux on the surface of the photobioreactor (mmol h^{-1})
PFD_{in}	Photon flux density on the surface of the photobioreactor ($\mu\text{mol m}^{-2} \text{s}^{-1}$)

PQ	Photosynthetic quotient (-)
$r_{E,x}$	Light supply rate ($\mu\text{mol g}^{-1} \text{s}^{-1}$)
r_i	Radius of inner (rotating) cylinder (m)
r_o	Radius of outer (stationary) cylinder (m)
V_{pbr}	Photobioreactor volume (kg)
$x_{\text{CO}_2,\text{db}}$	Molar fraction of CO_2 in dry baseline (-)
$x_{\text{CO}_2,\text{exp}}$	Molar fraction of CO_2 in experimental gas data (-)
$x_{\text{CO}_2,\text{wb}}$	Molar fraction of CO_2 in wet baseline (-)
$x_{\text{O}_2,\text{exp}}$	Molar fraction of O_2 in experimental gas data (-)
$x_{\text{O}_2,\text{wb}}$	Molar fraction of O_2 in dry baseline (-)
$Y_{x,E}$	Biomass yield on light energy (g mol^{-1})
$Y_{x,E\text{max}}$	Maximal yield of biomass on light energy (g mol^{-1})
$Y_{x,E(\text{obs})}$	Observed biomass yield on light energy (g mol^{-1})

Acknowledgements

This research project is financially supported by Technology Foundation STW-VICI (WLM.6622). The authors declare that they have no conflict of interest.





CHAPTER 4

Metabolic modeling of *Chlamydomonas reinhardtii*:
energy requirements for photoautotrophic growth
and maintenance

Kliphuis AMJ, Klok AJ, Martens DE, Lamers PP, Janssen M, Wijffels RH (2010)
Metabolic modeling of *Chlamydomonas reinhardtii*: energy requirements
for photoautotrophic growth and maintenance
Submitted for publication

Abstract

In this study a metabolic network describing the primary metabolism of *Chlamydomonas reinhardtii* was constructed. By performing chemostat experiments at different growth rates energy parameters for maintenance and biomass formation were determined. The chemostats were run at low light intensities resulting in a high biomass yield on light of 1.25 g mol^{-1} . The ATP requirement for biomass formation from biopolymers (K_x) was determined to be 109 mmol g^{-1} ($18.9 \text{ mol mol}^{-1}$) and the maintenance requirement (m_{ATP}) was determined to be $2.85 \text{ mmol g}^{-1} \text{ h}^{-1}$. With these energy requirements included in the metabolic network, the network accurately describes the primary metabolism of *C. reinhardtii* and can be used for modeling of *C. reinhardtii* growth and metabolism. Simulations showed that cultivating microalgae at low growth rates is unfavorable because of the high maintenance requirements which result in low biomass yields. At high light supply rates biomass yields will decrease due to light saturation effects. Thus, to optimize biomass yield on light energy in photobioreactors, an optimum between low and high light supply rates should be found. These simulations show that flux balance analysis can be used as a tool to gain insight into the metabolism of algae and ultimately can be used for the maximization of algal biomass and product yield.

Keywords: *Chlamydomonas reinhardtii*, Energy requirements, Flux Balance Analysis (FBA), Yield, Maintenance, Respiration

Introduction

Microalgae are interesting organisms because of their ability to produce a wide range of compounds, such as carotenoids (Ben-Amotz et al. 1982; Kleinegris et al. 2010; Lamers et al. 2008), lipids (Chisti 2007; Griffiths and Harrison 2009; Hu et al. 2008), hydrogen (Ghirardi et al. 2000; Melis et al. 2000), protein (Becker 2007; Boyd 1968) and starch (Delrue et al. 1992). These algal compounds have numerous applications, varying from fine chemicals to biofuels to food additives. To make commercial bulk production of these compounds economically feasible, maximization of algal biomass production and optimization of biomass composition is necessary. Understanding of how compounds are produced in the algal metabolism will help to fully exploit the potential of microalgae and their products.

Flux Balance Analysis (FBA) is a powerful tool to study the fluxes through metabolic pathways of any organism of interest. It provides information on how nutrients and energy are utilized to form biomass and other components. Using information on metabolic fluxes and pathways a better understanding of metabolism is obtained and targets for process optimization or genetic modification can be identified. Several metabolic network models have been published for common production organisms, such as *E. coli* (Carlson and Srienc 2004; Kayser et al. 2005), *Saccharomyces cerevisiae* (Forster et al. 2003) and *Corynebacterium glutamicum* (Kieldsen and Nielsen 2009). Due to the increasing interest in microalgae as production organisms, metabolic networks for photoautotrophic organisms such as *Chlorella vulgaris* (Yang et al. 2000) and *Arthrospira platensis* (*Spirulina*) (Cogne et al. 2003) have been developed as well. Flux balance analysis will improve understanding of algal metabolism and ultimately can be used for the maximization of algal biomass and product yield (Schmidt et al. 2010).

Chlamydomonas reinhardtii has been studied extensively in the past decades. It is regarded as a model organism for green microalgae because of its diverse metabolism and its ability to grow photoautotrophically as well as heterotrophically on acetate (Gfeller and Gibbs 1984; Heifetz et al. 2000). In addition, *C. reinhardtii* is able to accumulate starch (Ball et al. 1990) and produce hydrogen when grown anaerobically (Melis et al. 2000). The *Chlamydomonas* genome has been sequenced (Merchant et al. 2007) and the availability of this genetic information provides a sound basis for the development of metabolic network models. Recently, Boyle and Morgan (2009) and Manichaikul et al. (2009) developed two extensive genome-scale models describing the primary metabolism of *C. reinhardtii* divided over several cellular compartments and as such both models

have a high degree of compartmentalization. They qualitatively and up to a limited extent quantitatively predict algal metabolism and are well suited to get a better insight in algal metabolism. However, quantitative validation is very limited and there are some difficulties in developing such detailed models. For a number of reactions the localization is not known and has to be assumed. Also information on the exchange of metabolites between compartments is limited. Finally, to reduce the number of fluxes that cannot be calculated, many, often complex, measurements are needed. When developing a metabolic model the practical applicability should be considered. Extensive, fully compartmentalized models are excellent tools for the qualitative study of cellular reaction networks and their regulation, but are generally not suited for quantitative studies because of their underdetermined characteristics. A model for finding specific engineering bottlenecks and solutions would call for simple, easy to handle networks, which require less input parameters and optimization commands but still represent the important characteristics of metabolism (Burgard et al. 2001). Therefore, we developed a more condensed metabolic model describing the primary metabolism of *C. reinhardtii*, in which reactions are less extensively compartmentalized and which is thus less underdetermined.

Apart from the above mentioned uncertainties on compartmentalization and transport steps, the stoichiometry of the energy metabolism is not fixed in these models. The amount of energy in the form of adenosine triphosphate (ATP) required for biomass formation and maintenance is difficult to determine and varies between different microorganisms and growth conditions (Pirt 1965). These parameters are essential in metabolic modeling because they largely influence the growth dynamics and biomass or product yields calculated by the model. It is known from previous studies that theoretical estimates of the amount of ATP used for the production of biomass based solely on the required energy for the formation of biopolymers is much lower than the experimentally determined value (Baart et al. 2008; Kayser et al. 2005; Roels 1983). Additional energy is required for the assembly of biopolymers into growing biomass. In order to obtain a correct metabolic network model these parameters have to be determined experimentally. In this paper we describe the construction of a metabolic model for *Chlamydomonas reinhardtii* and the subsequent experimental determination of the energy requirements for maintenance and biomass formation. In this model photosynthesis and the Calvin cycle are the only processes that are compartmentalized in order to separate these processes from the pentose phosphate pathway in the cytosol and energy generation in the

mitochondria. Furthermore, reactions in linear pathways are lumped. The energy parameters are estimated from a series of chemostats operated at different dilution rates, a commonly used method for heterotrophic micro-organisms (Kayser et al. 2005; Taymaz-Nikerel et al. 2010). To our best knowledge this has not been applied to photoautotrophically grown microalgae, most probably because light is a challenging energy source to measure accurately. This study shows how this method can be applied to determine energy parameters for photoautotrophic organisms. The final model including the determined energy parameters was used to calculate the respiration rate at different specific growth rates, which enabled prediction of optimal growth rates for efficient light use.

Materials & methods

Organism, medium and cultivation conditions

Chlamydomonas reinhardtii CC1690 (Chlamydomonas Genetics Centre, Duke University) was cultivated in 250 mL shake flasks containing 100 mL defined medium (Table 4.1) at pH 7.0. The medium was based on the Sueoka high salts (HS) medium, enriched for magnesium and calcium (Sueoka et al. 1967). Additional EDTA was added to prevent precipitation of salts. Nitrate was used as a nitrogen source and enough nitrogen was added to support 4.5 g L^{-1} biomass. Finally, 1 mL of trace element solution was added to the medium. This trace element solution was based on Hutner's trace element solution (Hutner et al. 1950). The medium was sterilized by filtering through a Whatman liquid filter (pore size $0.2 \text{ }\mu\text{m}$) into a pre-sterilized medium vessel. The medium for the photobioreactor experiments was enriched with $5.00 \text{ mmol L}^{-1} \text{ NaHCO}_3$ to ensure sufficient dissolved CO_2 supply to the algae. *C. reinhardtii* cultures were maintained in a culture chamber at a temperature of 25°C , a light intensity of $20\text{-}40 \text{ }\mu\text{mol m}^{-2} \text{ s}^{-1}$ and a 16/8h day/night cycle. To reach inoculation cell density the cultures were placed in a shake-incubator for three days at a continuous light intensity of $280 \text{ }\mu\text{mol m}^{-2} \text{ s}^{-1}$ and a headspace enriched with 5% carbon dioxide.

Reactor set-up and experiments

C. reinhardtii was cultivated in chemostat mode in a pre-sterilized flat panel photobioreactor. Dilution rates in a range of 0.018 h^{-1} to 0.064 h^{-1} were used. Figure 4.1 shows a schematic overview of the experimental setup. The photobioreactor consisted of two transparent polycarbonate sheets held together by a stainless steel frame. The reactor had a working volume (V_{pbr}) of 0.4 L, a light path of 25 mm and an illuminated area (A_{pbr})

Table 4.1 Composition of *Chlamydomonas reinhardtii* medium, designed to reach 5 g L^{-1} biomass dry weight. 1 mL of trace element stock was added per liter medium. NaHCO_3 was added to the medium for experiments in the photobioreactor.

Medium		Trace element stock	
Compound	Concentration (mmol L^{-1})	Compound	Concentration (mmol L^{-1})
KNO_3	24.73	$\text{FeSO}_4 \cdot 7 \text{ H}_2\text{O}$	17.96
KH_2PO_4	5.29	$\text{Na}_2\text{EDTA} \cdot \text{H}_2\text{O}$	148.69
K_2HPO_4	8.28	$\text{ZnSO}_4 \cdot 7 \text{ H}_2\text{O}$	7 6.51
$\text{MgSO}_4 \cdot 7 \text{ H}_2\text{O}$	1.14	H_3BO_3	184.38
$\text{CaCl}_2 \cdot 2 \text{ H}_2\text{O}$	0.39	$\text{MnCl}_2 \cdot 4 \text{ H}_2\text{O}$	25.57
$\text{Na}_2\text{EDTA} \cdot 2 \text{ H}_2\text{O}$	0.18	$\text{CoCl}_2 \cdot 6 \text{ H}_2\text{O}$	6.77
NaHCO_3	5.00	$\text{CuSO}_4 \cdot 5 \text{ H}_2\text{O}$	6.29
		$(\text{NH}_4)_6\text{Mo}_7\text{O}_{24} \cdot 4 \text{ H}_2\text{O}$	0.89

of 195 cm^2 ($10 \times 19.5 \text{ cm}$).

Using mass flow controllers (Brooks, Smart TMF SLA5850) the system was aerated with pressurized air at an airflow of 0.2 L min^{-1} . The pH was controlled at 7.0 ± 0.2 by the automatic addition of CO_2 to the airflow. The temperature was maintained at 25°C by an external water bath.

Continuous illumination was provided by a red LED panel of $20 \times 20 \text{ cm}$ (LED Light Source SL 3500, 627nm, Photon System Instruments, Czech Republic) placed on one side of the photobioreactor. An average light intensity of $<100 \mu\text{mol m}^{-2} \text{ s}^{-1}$ was used. The photon flux density (PFD, $\mu\text{mol m}^{-2} \text{ s}^{-1}$) was measured with a LI-COR 190-SA 2π sensor (PAR range: 400–700nm) at 15 fixed points behind the reactor. The measured light intensities at all 15 points were averaged into a PFD for that particular experiment. During the experiments the light falling through the culture was measured in the same way. The average photon flux density absorbed by the algal culture (PFD_{abs} , $\mu\text{mol m}^{-2} \text{ s}^{-1}$) could be calculated by subtracting the light falling through the culture at steady state from the amount of light falling through the reactor filled with medium only. The resulting value was corrected for the loss of light due to backscattering of light on the algal cells, for which a fixed loss of 2% was assumed (Pottier et al. 2005).

After inoculation at an optical density at 530nm (OD_{530}) of 0.05, the culture was grown in batch mode until a sufficient optical density was reached. Then the medium supply was started at a constant dilution rate until steady state was reached. In these experiments steady state was defined as a constant optical density, biovolume and cell density (C_x , g L^{-1}) in the photobioreactor for at least 5 residence times. Biomass samples were taken from the middle of the reactor or from the overflow, which was collected on ice. Both sample methods gave the same results. Due to the small reactor volume it was necessary to take the larger samples for dry weight determination and biomass composition from the overflow in order to prevent disturbances of the steady state equilibrium.

Biomass determinations

Cell number and cell size

Cell number and cell size were determined in duplicate with a Beckman Coulter Mul-

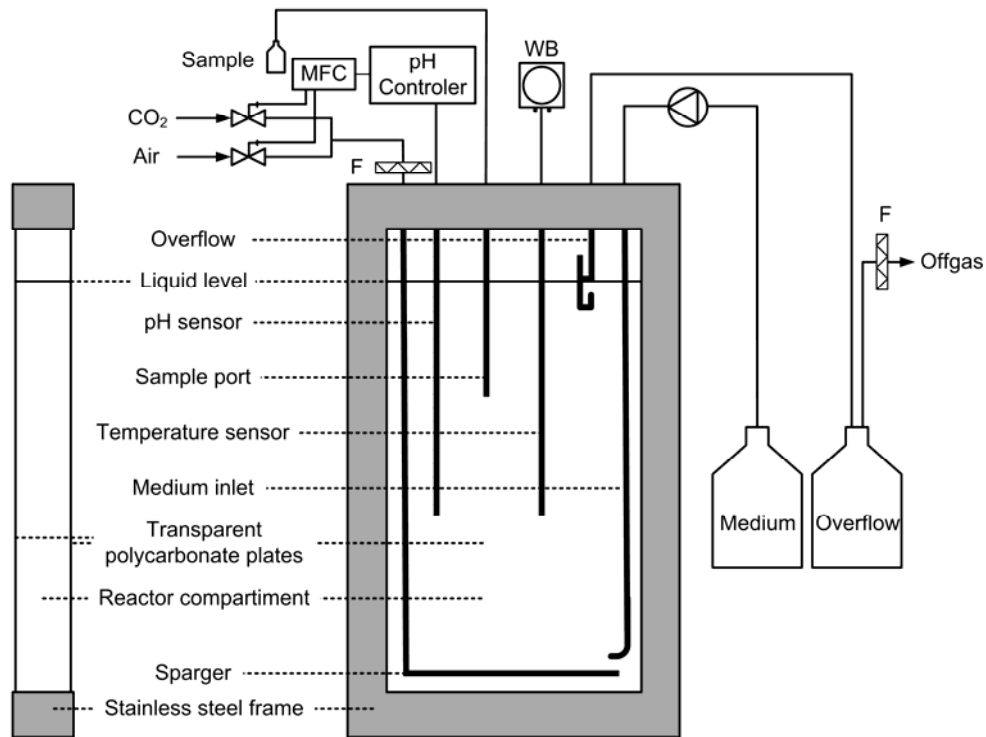


Figure 4.1 Schematic front and side view of the photobioreactor set-up (not on scale) for the chemostat experiments. MFC = mass flow controller for both air and CO₂, WB = water bath, F = air filter.

tisizer 3 (Beckman Coulter Inc., Fullerton USA, 50 μm orifice). The samples were diluted with filtered (0.2 μm) Coulter® Isoton® II dilution buffer to a cell concentration between $1 \cdot 10^5$ and $3 \cdot 10^5$ cells mL^{-1} . The cell number and cell size were used to calculate the total biovolume.

Dry Weight Determination

Whatman glass microfiber filters (\varnothing 55 mm, pore size 0.7 μm) were dried at 95°C overnight and placed in a desiccator to cool to room temperature. The empty filters were weighed and pre-wet with de-mineralized water. Two grams of sample were diluted with de-mineralized water and filtrated under mild vacuum. The filter was rinsed twice with de-mineralized water to remove adhering inorganic salts. The wet filters containing the samples were dried at 95°C overnight, allowed to cool to room temperature in a desiccator and weighed. The microalgal dry weight of the samples was then calculated from the difference in weight between the dry filters with and without biomass.

Biomass composition

Liquid samples were centrifuged for 10 min at 1750 rcf and the resulting pellets were washed three times with de-mineralized water by re-suspending and centrifuging and stored at -20°C. Algae pellets stored at -20°C were freeze dried and ground to a fine powder. The freeze dried algae powder was used for all further biomass composition analyses. Ash content was determined by burning the freeze-dried algae samples in an oven at 550°C, so that all organic material was oxidized and the ash residue remained.

Lipids and pigments

Lipid content was determined gravimetrically after extraction of the freeze dried algal powder with a 5:4 methanol:chloroform mixture. This extraction was described by Lamers et al. (2010). The resulting total lipid extract contained all lipid-like compounds present in the algal cells, including pigments. Therefore the weight of the total lipid extract had to be corrected for the amount of pigments present. Pigments were determined spectrophotometrically after dissolving the lipid residue in methanol. The total pigment content was calculated using absorption equations for chlorophyll in methanol (Porra 2002). The relative fatty acid composition was determined by GC-analysis according to the method described by Bosma et al. (2008).

Carbohydrates

Carbohydrates were measured by treating the freeze dried algae powder with a phenol solution and concentrated sulphuric acid, according to Dubois et al. (1956) and Herbert et al. (1971). The absorbance of the resulting solution was measured at 483 nm. Pure glucose was used as a standard.

Protein content and amino acid composition

The nitrogen content of the biomass was determined on a Flash EA 1112 Protein Analyzer (Thermo Scientific, Waltham USA). To calculate the amount of protein from the nitrogen content a N to protein conversion factor of 4.58 ± 0.11 was used (Lourenço et al. 1998). This factor was determined specifically for several microalgal species at different growth phases.

The relative amino acid composition was determined by Ansynth Service BV (Berkel en Roodenrijs, The Netherlands), using classical ion-exchange liquid chromatography with post-column ninhydrin derivatisation and photometric detection. Proteins were hydrolyzed by acid hydrolysis prior to column injection. Cysteine, methionine and tryptophan were determined separately. Cysteine and methionine were measured by oxidation followed by acid hydrolysis, and tryptophan by alkaline hydrolysis followed by reverse phase HPLC.

Nucleic Acids

The nucleic acids DNA and RNA were not measured directly, but were calculated from cell number data. From the amount of different nucleotides in *Chlamydomonas reinhardtii* (Merchant et al. 2007) it could be calculated that each cell contains $1.3 \cdot 10^{-13}$ g DNA per cell. RNA was assumed to be present in a 28 fold higher concentration than DNA. Valle et al. (1981) determined this ratio RNA:DNA for *Chlamydomonas reinhardtii* by measuring DNA and RNA contents at various cell concentrations, by means of a fluorometric determination.

Flux balancing

The metabolism of an organism can be described by a set of reaction equations defining the stoichiometric conversion of substrates into products (Stephanopoulos et al. 1998). The stoichiometry matrix *S* contains the stoichiometric coefficients of the substrates and products for the different reactions in the metabolic network, which also includes the

transport reactions over the membranes. To be able to calculate fluxes, mass balances are written for all the intracellular metabolites present in the network. Assuming steady state and neglecting the accumulation of intermediates, this results in the next set of linear equations:

$$A \cdot x = 0 \quad (1)$$

In which A is the transpose of the stoichiometry matrix S and x is the vector which contains the reaction rates. The solution space of equation 1 was studied to find possible dead ends in the model, which were subsequently removed. Because part of the rates in x is usually measured, equation 1 can be converted to:

$$A_c \cdot x_c = -A_m \cdot x_m \quad (2)$$

Where x_c contains the unknown and x_m contains the measured rates. A_c and A_m are the corresponding parts of the matrix A. By studying the null space of A_c it was revealed that our system was underdetermined and therefore no unique solution of equation 2 exists. Underdeterminancies were solved by setting constraints to some of the fluxes in the underdetermined part of the metabolism and using optimization of an objective function. Thus, linear programming/optimization was used according to equation 3:

$$\begin{aligned} \text{Objective function : } & \max(c \cdot x) \\ \text{Constraints : } & A \cdot x = 0 \\ & LB \leq x \leq UB \end{aligned} \quad (3)$$

In which c contains the objective function and LB and UB are the lower and upper boundary of reaction rate x. In this study we used the objective functions 'maximize biomass yield' and 'maximize ATP yield'. Constraints were set on transport fluxes depending on whether a compound was consumed or produced. In case a rate was measured, the transport rate was constrained to the measured value. Reactions that are irreversible were constrained to one direction. To solve the underdetermined parts constraints were set in such a way that flux distributions that are thermodynamically impossible were excluded. Mathcad 14.0 (M020, Parametric Technology Corporation, USA) was used for network analysis and Matlab (version 6.0.0.88, release 12, The MathWorks Inc., USA) was used for *in silico* simulations.

Theoretical Aspects - Energy parameters

The ATP balance for complete metabolic network models can be written as equation 4:

$$q_{\text{ATP,ox}} + q_{\text{ATP,light}} + \sum q_i^{\text{ATP}} - K_x \cdot \mu - m_{\text{ATP}} = 0 \quad (4)$$

In this balance the first term, $q_{\text{ATP,ox}}$ ($\text{mmol g}^{-1} \text{h}^{-1}$), is the specific ATP production rate in oxidative phosphorylation in the mitochondria. The second term, $q_{\text{ATP,light}}$ ($\text{mmol g}^{-1} \text{h}^{-1}$), represents sum of the specific ATP production rate in the light reaction in the chloroplast. The third term, $\sum q_i^{\text{ATP}}$ ($\text{mmol g}^{-1} \text{h}^{-1}$), is the specific ATP production and consumption in the part of the metabolism that has a known ATP stoichiometry. Notably, the synthesis reactions of the biopolymers that make up biomass have a known ATP stoichiometry and are therefore included in this term. The energy requirements for the formation of protein, DNA, RNA and chlorophyll were assumed to be 4.306, 1.372, 0.4 and 2.0 mol ATP per mol of the respective macromolecule (Berg et al. (2003); <http://www.kegg.com>). The specific ATP consumption rate required to assemble these biopolymers into functional growing biomass does not have a fixed stoichiometry and is represented by the fourth term in the ATP balance equation. In this term μ (h^{-1}) is the specific growth rate and K_x (mmol g^{-1}) is a constant, which represents the additional amount of ATP needed to make biomass from biopolymers, by others defined as the 'growth associated maintenance' (Kayser et al. 2005; Taymaz-Nikerel et al. 2010). Finally, the fifth term represents the maintenance ATP requirement, m_{ATP} ($\text{mmol g}^{-1} \text{h}^{-1}$), which vary with the type of organism and the culture conditions.

The specific ATP production rate in the mitochondria depends on the P/O ratio, which represents the amount of ATP formed per oxygen atom that is reduced. Here we assume a constant P/O ratio of 2.5 for NADH and 1.5 for FADH₂. The stoichiometry of the light reaction also depends on environmental conditions. Here we assume a fixed stoichiometry of 8 photons resulting in the generation of 2 NADPH and 3 ATP. With these two assumptions all reactions contained in the first three terms have a fixed stoichiometry. The ATP balance (equation 4) thus shows that the sum of these three terms (hereafter ' q_{ATP} ') must be equal to the amount of ATP required for maintenance and for biomass formation from biopolymers.

The parameters K_x and m_{ATP} can be determined from experiments by determining q_{ATP} at different growth rates. For this purpose a series of chemostat cultures operated at different dilution rates were performed. By definition, the growth rate during steady state is

equal to the dilution rate and thus by setting different dilution rates different growth rates can be studied. At steady state the biomass density (C_x , g L⁻¹) and the photon flux density absorbed by the algae (PFD_{abs}, μmol m⁻² s⁻¹) were measured. With these values a light supply rate per amount of biomass (r_{Ex} , mmol g⁻¹ h⁻¹) can be calculated for each growth rate μ (h⁻¹) according to equation 5:

$$r_{Ex} = \frac{\text{PFD}_{\text{abs}} \cdot A_{\text{pbr}}}{C_x \cdot V_{\text{pbr}}} \quad (5)$$

In which PFD_{abs} is the absorbed photon flux density (in mmol m⁻² h⁻¹ in this equation), A_{pbr} is the illuminated surface of the photobioreactor (m²) and V_{pbr} the working volume of the photobioreactor (L).

At high light intensities light saturation occurs and light energy is dissipated as heat and fluorescence, causing a decrease in the efficiency of the photosystems (Krause and Weis 1991; van der Tol et al. 2009). Consequently, the actual rate with which photons are used in algal metabolism is not known. Moreover, elevated light intensities also induce damage to the algal cells (Kok 1955), possibly increasing the energy consumption for maintenance purposes. *Chlamydomonas reinhardtii* becomes light saturated at light intensities of 300 μmol m⁻² s⁻¹ (Janssen et al. 2000). At light intensities below 100 μmol m⁻² s⁻¹ light energy is limiting and is used at maximal efficiency as can be deduced from the fact that the growth curve increases linearly with light intensities below this level (Janssen et al. 2000). Hence the chemostat experiments to estimate the energy parameters for the metabolic model were performed at low light intensities (<100 μmol m⁻² s⁻¹), to ensure that the photosystems were working at maximum efficiency and to prevent any light damage to the algal cells. However, even at low light intensities not all light is taken up by the photosystem and therefore the calculated light supply rate r_{Ex} should be corrected for the maximum efficiency (Φ_{Pmax}) of the photosystems. Φ_{Pmax} was assumed to be 0.8, which corresponds to a quantum requirement of oxygen evolution of 10 (instead of 8 according to the Z-scheme). This is in accordance with measurements of the quantum requirement under ideal low-light conditions for a variety of organisms using a variety of experimental techniques (Bjorkman and Demmig 1987; Dubinsky et al. 1986; Emerson and Lewis 1943; Evans 1987; Ley and Mauzerall 1982; Malkin and Fork 1996; Tanada 1951). The specific light utilization rate ($r_{Ex,u}$ in mmol g⁻¹ h⁻¹), which is the rate with which light is used to generate ATP and NADPH, can now be calculated according to equation 6:

$$r_{Ex,u} = \Phi_{\text{Pmax}} \cdot r_{Ex} \quad (6)$$

With the specific light utilization rate r_{Ex} and the specific growth rate μ as input for the metabolic model, q_{ATP} can be calculated for each different growth rate. Since the composition of the biomass can have a significant effect on the flux distribution in the model (Pramanik and Keasling 1998) and thus on q_{ATP} , the biomass composition was measured for each steady state and also used as input for the model. The q_{ATP} was calculated by setting K_x to zero in the overall biomass formation reaction (reaction 147). From equation 4 it can be seen that q_{ATP} is now equal to the maintenance term. In the metabolic model maintenance is represented as the hydrolysis of ATP in reaction 57 of the model. Thus by maximizing the flux through this reaction, using the specific light utilization rate, the specific growth rate and the biomass composition as input, the amount of ATP that is produced in the part of the network which has a known stoichiometry, q_{ATP} , can be calculated for each steady state. Subsequently, we can determine K_x and m_{ATP} by plotting q_{ATP} as a function of the specific growth rate μ . The slope of this line, obtained by linear regression, represents K_x and the intercept represents m_{ATP} , according to equation 4. Note that setting K_x to zero and maximizing the flux through the ATP hydrolysis reaction is just a method to calculate the ATP production rate. To complete the metabolic model with the correct energy requirements for biomass formation and maintenance, the value for K_x has to be incorporated in the biomass synthesis reaction (reaction 147) after conversion to the appropriate units (mol mol^{-1}). The maintenance ATP requirement is incorporated by constraining the ATP hydrolysis reaction to the value of m_{ATP} .

Results and discussion

Metabolic network construction

A metabolic network describing the primary metabolism of *Chlamydomonas reinhardtii* was constructed based on literature (Berg et al. 2003; Boyle and Morgan 2009; Cogne et al. 2003; Harris 2009; Yang et al. 2000) and the KEGG database (Kanehisa and Goto (2000), <http://www.kegg.com>). We cross checked the model with the genome of *Chlamydomonas reinhardtii* (Merchant et al. 2007) to ensure the presence of the enzymes catalyzing the modeled reactions. In this model we described two cell compartments, the chloroplast and the cytosol, to be able to uncouple the Calvin cycle, the PPP and the production and consumption of NADPH. For the light reaction only linear electron transport was modeled.

A large network with over 300 enzymatic reactions was obtained. This extensive model was reduced to a smaller, more practical network. This was done by lumping linear path-

ways into one reaction equation. The resulting network contains 160 reactions and 164 compounds and is listed in Appendix A. A simplified overview of this metabolic network is shown in Figure 4.2.

We found that several enzymatic steps which were necessary in the network were not annotated in the KEGG database. Therefore we performed protein BLAST (Basic local alignment search tool, Altschul et al. (1990)) searches against the *Chlamydomonas reinhardtii* genome, using amino acid sequences from green (micro) organisms for the 'missing' enzymes. Table 4.2 (pages 84-85) shows the enzymes, the E.C. numbers and the corresponding geneIDs that were found in this way. The reactions in the network (partly)

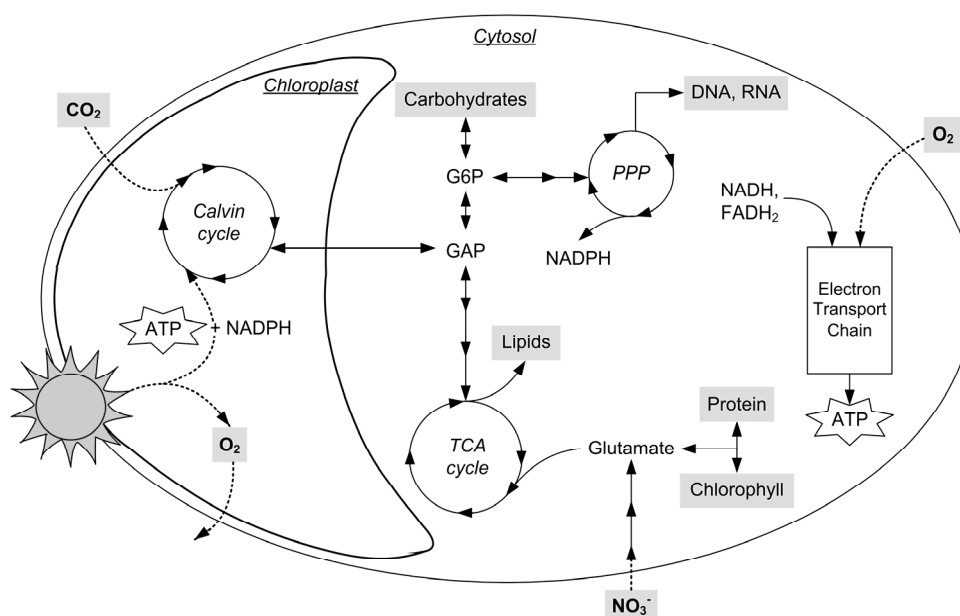


Figure 4.2 Simple overview of an algal cell in the light, showing the main metabolic processes. The model contains two compartments. The light reaction and Calvin cycle are placed in the chloroplast compartment and all other processes are located in the cytosol compartment. Light energy is harvested in the chloroplast, yielding O_2 , ATP and NADPH. These are needed to fix carbon dioxide in the Calvin cycle into glyceraldehyde 3-phosphate (GAP). GAP can be transported to the cytosol to be converted into building blocks for biomass. Lipids are formed through glycolysis and the tri-carboxylic acid (TCA) cycle. Nitrate is taken up by the cell and converted into glutamate which in turn can be converted to protein and chlorophyll. GAP can be converted to glucose 6-phosphate (G6P) from which carbohydrates are formed. G6P can also enter the pentose phosphate pathway (PPP) which yields NADPH, DNA and RNA. Electrons are carried by NADH and $FADH_2$ to the mitochondrial electron transport chain, yielding ATP by taking up O_2 .

catalyzed by these enzymes are also given. In total 41 enzymes were found not to be annotated in the KEGG database, of which 39 were retrieved by BLAST searches. Of these 39 enzymes, several have a geneID and are annotated but are not taken up in the KEGG database yet. Other enzymes have a draft geneID and still need to be annotated.

Only two enzymes could not be found in this way. The first one is ATP phosphoribosyltransferase (E.C. 2.4.2.17). This enzyme is essential in histidine formation and is described in the Chlamydomonas sourcebook (Harris 2009). The second enzyme is homoserine acetyltransferase (E.C. 2.3.1.31), which is necessary in cysteine formation. This enzyme is present in other green microalgae (*Ostreococcus lucimarinus*), cyanobacteria (*Synechococcus elongates*, *Anabaena variabilis*) and diatoms (*Phaeodactylum tricoratum*, *Thalassiosira pseudonana*). BLAST searches with the amino acid sequences from these organisms did not give a result. Therefore we assume this reaction is performed by another but similar enzyme, because this step is essential in the formation of cysteine. Because both histidine and cysteine were measured in the amino acid composition and not added to the medium, they had to be formed within the metabolism. Thus both reactions were taken up in the model.

By studying the null space of matrix A_c (equation 2), twelve underdetermined parts were revealed in the model. This means that there is no unique solution for equation 2. By measuring and setting constraints to some of the fluxes in the underdetermined parts of the metabolism and using optimization of objective functions, unique solutions could be obtained. Reactions that are irreversible were constrained to one direction and thermodynamically impossible combinations of reactions were also constrained in the correct direction. In the appendix the arrows indicate whether a reaction is reversible or irreversible and if so, in which direction it is set. By choosing the objective functions 'maximize biomass yield' and 'maximize ATP yield' unique values could be calculated for the fluxes in all but two underdetermined parts. The first remaining underdeterminancy involved the anaplerotic routes between phosphoenolpyruvate (PEP), pyruvate (PYR) and oxaloacetate (OXA). This was solved by setting the upper and lower boundaries of the flux through reaction 35 to zero. The second underdetermined part involved the coupling of the pentose phosphate pathway (PPP), the glycolysis and the tricarboxylic acid cycle (TCA). The aerobic degradation of sugars can occur through both the PPP as well as the TCA if NADPH and NADH are freely exchangeable through reaction 54, a transhydrogenase reaction. We restricted this by setting this reaction forward so NADPH can only be converted to NADH. In this way the fluxes through the PPP will only be dictated by the demand of NADPH and PPP intermediates.

Table 4.2 'Missing' reactions in the *Chlamydomonas reinhardtii* database which were found by blasting the sequences from other green (micro)organisms against the genome.

Nr.	Reaction	E.C. nr.	Name	GenelID
43	DHAP + H ₂ O ⇌ DHA + Pi	3.1.3.1	Alkaline phosphatase	5723324 PHOD
44	DHA + H ⁺ + NADPH ⇌ GLYC + NADP	1.1.1.56	Dihydroxyacetone reductase	5720300 LC128
47	H ⁺ + NADH + NO ₃ ⇌ H ₂ O + NAD + NO ₂	1.7.1.1	Nitrate reductase	5722285 NIT1
50	APS + NADH → AMP + NAD + SO ₃	1.8.99.2	Adenylyl sulfate reductase	5722644 MET16
54	NAD + NADPH → NADH + NADP	1.6.1.2	NAD(P) transhydrogenase	5725773 CHLREDRAFT_139758
70	2 PEP + ATP + E4P + NADPH → ADP + CHO + NAD P + 4 Pi	1.1.1.25 2.7.1.71	Shikimate dehydrogenase Shikimate kinase	5719875 SHKD1 5716011 SHKF1
71	CHO ⇌ PRE	5.4.99.5	Chorismate mutase	5723071 CHM1
72	GLU + H ⁺ + PRE ⇌ AKG + CO ₂ + H ₂ O + PHE	4.2.1.51	Prephenate dehydratase	5722023 PRD1
73	GLU + NAD + PRE ⇌ AKG + CO ₂ + NADH + TYR	1.3.1.43	Prephanate dehydrogenase	5720883 AGD1
76	3 H ₂ O + 2 NAD + ATP + GLN + PRPP → AICAR + AKG + HIS + Pi + 2 NADH + 2 PPI + 5 H ⁺	2.4.2.17 2.4.2.- 3.1.3.15	ATP phosphoribosyltransferase Glutamine amidotransferase Histidinolphosphatase	<i>not found</i> , HIS1 (Harris 2009) 5722944 HIS7 5720418 HIS2
81	3 H ⁺ + 2 NADH + GLU ⇌ PRO + 2 H ₂ O + 2 NAD	1.5.1.2	Pyroline-5-carboxylate reductase	5723082 PCR1
82	AKG + O ₂ + PRO ⇌ CO ₂ + HydPro + SUC	1.14.1.2	Prolyl 4-hydroxylase	5721719 PHX1
84	2 H ⁺ + ASA + GLU + NADH + PYR ⇌ AKG + DAP + H ₂ O + NAD	1.3.1.26 2.6.1.83	Dihydrodipicolinate reductase LL-diaminopimelate aminotransferase	5723456 DPR1 5718617 DPA1
88	AcCoA + CYS + H ₂ O + HSER ⇌ Ace + CoA + HCYS + H ⁺ + NH ₄ ⁺ + PYR	2.3.1.31	Homoserine acetyltransferase	<i>not found</i>
91	H ₂ O + NAD + O ₂ + cRu15DP → H ⁺ + NADH + Pi + cG3P + glyoxylate	3.1.3.18	Phosphoglycolate phosphatase	5728979 PGP1, 5716118 PGP2, 5721833 PGP3
96	H ⁺ + HydPyr + NADH ⇌ Glycerate + NAD	1.1.1.81	Glycolate dehydrogenase Hydroxypyruvate reductase	5721055 GYD1 5717070 HPR1

97	ATP + Glycerate → ADP + 2 H ⁺ + 3PG	2.7.1.31	Glycerate kinase	5719520 GLYK
100	H ₂ O + MYLTHF ↔ H ⁺ + N10FTHF	3.5.4.9	Methenyl-THF cyclohydrolase	5728457 CHLREDRAFT 194856
101	ATP + FORM + THF → ADP + N10FTHF + Pi	3.5.4.9	Methenyl-THF cyclohydrolase	5728457 CHLREDRAFT 194856
102	MYLTHF + NADPH ↔ METHF + NADP	1.5.1.5	Methylene-THF dehydrogenase	5728457 CHLREDRAFT 194856
103	H ⁺ + METHF + NADPH ↔ MTHF + NADP	1.5.1.20	Methylene-THF reductase	5728030 CHLREDRAFT 111330
104	5FTHF + ATP + H ₂ O → ADP + H ⁺ + N10FTHF + Pi	6.3.3.2	5-formyl-THF cycloligase	5723199 FLC1
105	FORM + H ⁺ + THF ↔ H ₂ O + N10FTHF	3.5.1.10	Formyl-THF deformylase	5728093 CHLREDRAFT 111421
106	DHF + H ⁺ + NADPH ↔ NADP + THF	1.5.1.3	Dihydrofolate reductase	5725986 CHLREDRAFT 139742
113	C160ACP + H ⁺ + NADH + O ₂ ↔ C16:1ACP + NAD + 2 H ₂ O	1.14.19.2	Stearyl-ACP desaturase	5717289 FAB2
115	C162ACP + H ⁺ + NADH + O ₂ ↔ C16:3ACP + NAD + 2 H ₂ O	1.14.19.-	Oxidoreductase (fatty acid desaturase)	5715517 FAD7
117	C180ACP + H ⁺ + NADH + O ₂ ↔ C18:1ACP + NAD + 2 H ₂ O	1.14.19.2	Stearyl-ACP desaturase	5717289 FAB2
119	C182ACP + H ⁺ + NADH + O ₂ ↔ C18:3ACP + NAD + 2 H ₂ O	1.14.19.-	Oxidoreductase (fatty acid desaturase)	5715517 FAD7
121	4 ATP + 2 GLN + 2 H ₂ O + ASP + CO ₂ + GLY + N10FTHF + PRPP → AICAR + FUM + PPI + THF + 2 GLU + 4 ADP + 4 Pi + 7 H ⁺	2.1.2.2	Phosphoribosylglycinamide formyltransferase	5719655 CHLREDRAFT 117678
132	ASP + GTP + IMP ↔ AMP + FUM + GDP + Pi + 2 H ⁺	4.3.2.2	Adenylosuccinate lyase	5719041 CHLREDRAFT 99287
133	ATP + H ⁺ + METHF + NADPH + UDP → ADP + DHF + H ₂ O + NADP + dTTP	4.3.2.2	Adenylosuccinate lyase	5719041 CHLREDRAFT 99287
140	18 H ⁺ + 15 NADPH + 8 ATP + 4 GAP + 4 PYR → Phytol-PP + 4 ADP + 4 AMP + 4 CO ₂ + 7 PPI + 8 H ₂ O + 15 NADP	2.1.1.45	Thymidylate synthase	5725986 CHLREDRAFT 139742
144	4 NADPH + 2.5 O ₂ + 2 ATP + AdMET + Mg ²⁺ + Pporphyrin + Phytol-PP → AdHCYS + Chlorophyll + PPI + 2 ADP + 2 H ₂ O + 2 Pi + 3 H ⁺ + 4 NADP	2.5.1.29	Geranylgeranyl-diphosphate synthase	5728730 GGPS
		2.1.1.11	Magnesium protoporphyrin IX methyltransferase	5727888 CHLM
		1.14.13.81	Mg-protoporphyrin IX monomethyl ester (oxidative) cyclase	5716556 CTH1
		1.3.1.75	Divinyl chlorophyllide a 8-vinyl-reductase	5715602 DVR1

Chemostat experiments

To estimate the energy parameters for maintenance and the formation of biomass, we performed seven chemostat experiments at low light intensities and low dilution rates ranging from 0.018 h^{-1} to 0.064 h^{-1} . The experiments were performed at low light intensities, to make sure the photosystems were working at maximum efficiency (Baker et al. 2007) and to prevent light damage to the algal cells. When steady state was reached the biomass density C_x (g L^{-1}) and the photon flux density absorbed by the algae (PFD_{abs} , $\mu\text{mol m}^{-2} \text{ s}^{-1}$) were measured for each dilution rate. In Table 4.3 the biomass density and the absorbed photon flux density at the different growth rates are given. With these values a light supply rate per amount of biomass (r_{Ex} , $\text{mmol g}^{-1} \text{ h}^{-1}$) could be calculated for each growth rate μ (h^{-1}) according to equation 5. The relationship between the specific light supply rate r_{Ex} ($\text{mmol g}^{-1} \text{ h}^{-1}$) and the growth rate μ (h^{-1}) can be described using the model of Pirt (1965) as used by Zijffers et al. (2010) according to equation 7:

$$r_{\text{Ex}} = \frac{\mu}{Y_{\text{xE}}} + m_{\text{E}} \quad (7)$$

In which m_{E} is the maintenance requirement ($\text{mmol photons g}^{-1} \text{ h}^{-1}$) and Y_{xE} the yield of biomass on light ($\text{g biomass mmol photons}^{-1}$). The amount of light used by the algae increases proportionally to the growth rate, while a fixed amount of maintenance light

Table 4.3 Biomass density (C_x , g L^{-1}), absorbed photon flux density (PFD_{abs} , $\mu\text{mol m}^{-2} \text{ s}^{-1}$) and growth rates (μ , h^{-1}) determined for each chemostat experiment. The specific light utilization rate ($r_{\text{Ex,u}}$, $\text{mol g}^{-1} \text{ h}^{-1}$) is calculated from these data using equations 6 and 8.

Growth rate μ (h^{-1})	Biomass density C_x (g L^{-1})	Photon flux density absorbed PFD_{abs} ($\mu\text{mol m}^{-2} \text{ s}^{-1}$)	Specific light utilization rate $r_{\text{Ex,u}}$ ($\text{mmol g}^{-1} \text{ h}^{-1}$)
0.018 ± 0.000	0.78 ± 0.04	88	15.8 ± 1.5
0.019 ± 0.000	0.84 ± 0.08	87	16.7 ± 0.8
0.031 ± 0.001	0.41 ± 0.02	80	25.7 ± 1.4
0.034 ± 0.001	0.39 ± 0.02	73	26.8 ± 1.6
0.052 ± 0.001	0.21 ± 0.01	51	36.1 ± 1.7
0.061 ± 0.003	0.11 ± 0.01	36	45.5 ± 3.7
0.064 ± 0.001	0.10 ± 0.01	31	44.8 ± 3.7

Table 4.4 Comparison of biomass yields on light energy and the used light intensities for different microalgae from literature.

Organism	$Y_{x/E}$ or $Y_{x/E}^{obs}$ (g mol ⁻¹)	Light intensity ($\mu\text{mol m}^{-2} \text{s}^{-1}$)	Reference
<i>Chlamydomonas reinhardtii</i>	1.25 ^a	80	This paper
<i>Dunaliella tertiolecta</i>	0.78 ^a	930	Zijffers et al. (2010)
<i>Chlorella sorokiniana</i>	0.75 ^a	930	Zijffers et al. (2010)
<i>Chlorella sorokiniana</i>	0.80 ^b	1500	Kliphuis et al. (2010a)
<i>Chlorella sorokiniana</i>	1.00 ^b	2100	Cuaresma et al. (2009)
<i>Chlamydomonas reinhardtii</i>	1.11 ^{b,c}	110	Takache et al. (2010)
<i>Chlamydomonas reinhardtii</i>	0.73 ^{b,c}	500	Takache et al. (2010)
<i>Chlamydomonas reinhardtii</i>	0.51 ^{b,c}	1000	Takache et al. (2010)

^a $Y_{x/E} = \mu / (r_{Ex} + m_E)$, according to equation 7.

^b $Y_{x/E}^{obs} = \mu / r_{Ex}$ (the observed yield was not corrected for maintenance requirements)

^c recalculated from data obtained in flat Torus photobioreactor by Takache et al. (2010)

energy is necessary to keep the algae in a healthy state. Regression on the specific growth rates μ and specific light supply rates r_{Ex} for all chemostat experiments yields a straight line with a R^2 of 0.988. According to equation 7, the offset of this line gives a m_E of 5.99 mmol g h⁻¹ and the inverse of the slope gives a $Y_{x/E}$ of 1.25 g mol⁻¹. This $Y_{x/E}$ is high compared to biomass yields found for other green microalgae as can be seen from Table 4.4. Cuaresma et al. (2009), Kliphuis et al. (2010a) and Zijffers et al. (2010) found yields ranging from 0.5 g mol⁻¹ to 1.0 g mol⁻¹ for several green microalgae. These yields were all obtained at high light intensities of 1000 $\mu\text{mol m}^{-2} \text{s}^{-1}$ or more. At low light intensities we expect a higher yield than at high light intensities because at high light intensities the antenna complexes in the algal photosystems become saturated. The remainder of the absorbed light will be dissipated as heat or fluorescence (Krause and Weis 1991; van der Tol et al. 2009). In addition, elevated light intensities also induce damage to the algal cells (Kok 1955), possibly increasing the energy consumption for maintenance purposes. Therefore, high light intensities will lead to low photosynthetic efficiencies as can also be seen from the yields for *Chlamydomonas reinhardtii* obtained by Takache et al. (2010). The difference between the yields at high and low light intensities in these experiments

reflects the fact that a large part of the light is 'wasted' at higher light intensities. The high biomass yield found in our experiments supports the hypothesis that the efficiency of the algal photosystems was indeed high at a light intensity of $80 \mu\text{mol m}^{-2} \text{s}^{-1}$. Moreover, it seems that we were working at maximal efficiency because the relation between specific light utilization and specific growth rate is linear ($R^2 = 0.988$). This shows that the biomass yield is constant and not influenced by the change in light regime (Table 4.3), indicating we reached the maximal value of this yield parameter.

It needs to be stressed that even at these low light intensities not all absorbed light can be converted in the photosystems. Therefore the light supply rate r_{Ex} was corrected for the maximum efficiency ($\Phi_{\text{Pmax}} = 0.8$) of the photosystems to obtain the specific light utilization rate $r_{\text{Ex,u}}$ (equation 6), which is also shown in Table 4.3. This specific light utilization rate $r_{\text{Ex,u}}$ should be used for energy parameter estimation, since this rate represents the actual amount of photons that enter the algal metabolism. As expected, regression on the specific growth rates μ and specific light utilization rates $r_{\text{Ex,u}}$ also yields a straight line according to equation 7. The offset of this line gives a m_{E} of $4.79 \text{ mmol g}^{-1} \text{ h}^{-1}$ and the inverse of the slope gives a $Y_{\text{x/E}}$ of 1.57 g mol^{-1} . These values represent the yield and maintenance requirements corrected for the inefficiency of light use, Φ_{Pmax} .

Biomass composition

The composition of the biomass can have a significant effect on the flux distribution in the model and thus on the estimation of energy parameters (Pramanik and Keasling 1998). Therefore, the macromolecular biomass composition (%w/w) was determined for six of the steady states as shown in Table 4.5. In addition, the average biomass composition for all growth rates is given here. These compositions, along with the corresponding growth rates μ and light utilization rates $r_{\text{Ex,u}}$, were used for the model simulation of each steady state. The macromolecular biomass composition was not measured for $\mu = 0.019 \text{ h}^{-1}$ and therefore the composition of $\mu = 0.018 \text{ h}^{-1}$ was used to perform model simulations for this growth rate.

The biomass composition did not show much variation as a function of growth rate, although the carbohydrate content seemed to increase at increasing growth rates. The pigment content, on the other hand, decreased at increasing growth rate, which can be explained by the fact that the amount of light per cell increased at increasing growth rate, because the culture became more diluted. Such a response of microalgae to decrease the amount of photosynthetic pigments upon an increase in irradiance, is known

Table 4.5 Measured biomass composition (% w/w) normalized to 100% and average biomass composition of *C. reinhardtii* at different specific growth rates μ (h^{-1}) including the standard deviations. The sum of the individual biomass components including ash was comparable to the measured dry weights within 10%.

	μ (h^{-1})						Average ^c
	0.018	0.031	0.034	0.052	0.061	0.064	
Protein ^a	42.48 ± 0.55	39.34 ± 0.77	40.17 ± 1.10	41.63 ± 0.67	40.16 ± 0.40	37.61 ± 0.88	40.23 ± 1.71
Carbohydrate ^a	24.09 ± 2.00	21.70 ± 0.73	24.62 ± 2.15	27.29 ± 4.08	26.26 ± 1.59	28.87 ± 1.11	25.47 ± 2.54
Lipids ^a	14.13 ± 0.28	22.16 ± 2.24	17.72 ± 0.88	14.25 ± 0.47	16.78 ± 3.85	18.65 ± 1.84	17.28 ± 3.01
DNA ^b	0.21 ± 0.008	0.20 ± 0.004	0.23 ± 0.006	0.22 ± 0.002	0.23 ± 0.002	0.19 ± 0.002	0.21 ± 0.02
RNA ^b	5.99 ± 0.23	5.57 ± 0.12	6.48 ± 0.16	6.04 ± 0.06	6.57 ± 0.06	5.27 ± 0.05	5.99 ± 0.50
Chlorophyll ^a	7.06 ± 0.07	5.59 ± 0.03	5.13 ± 0.05	4.73 ± 0.07	4.34 ± 0.20	4.01 ± 0.06	5.14 ± 1.09
Ash ^a	6.05 ± 0.03	5.44 ± 0.40	5.66 ± 0.24	5.84 ± 0.11	5.66 ± 0.24	5.41 ± 0.42	5.68 ± 0.24

^a N = 3

^b Based on literature values (Merchant et al. 2007; Valle et al. 1981) and the measured dry weight and cell numbers. N = 3, 6, 5, 4, 8 respectively.

^c Average biomass composition for all growth rates with the standard deviation for all six growth rates.

as photoacclimation (Dubinsky and Stambler 2009). Protein, nucleic acids and ash content did not vary significantly. Since the composition of the biomass did not change very much in this range of growth rates, the average biomass composition was used in the final model. In Appendix C the elemental composition of all macromolecules and of the *Chlamydomonas reinhardtii* biomass itself is given. The amino acid composition and the average fatty acid composition can be found in Appendix D and E.

Energy requirements for growth and maintenance

Using the specific growth rate μ , the specific light utilization rate $r_{Ex,u}$ (Table 4.3) and the biomass composition as determined for each steady state (Table 4.5) as input for the model, q_{ATP} can be calculated as described in the Theoretical aspects section. Figure 4.3 shows the plot of q_{ATP} against the specific growth rate, μ . Linear regression through these points yields a straight line ($P < 0.05$). According to equation 4, the offset of this line gives the ATP required for maintenance (m_{ATP}), being $2.85 \text{ mmol g}^{-1} \text{ h}^{-1}$. The slope represents K_x , the amount of ATP needed to make biomass from biopolymers and has a value of 109

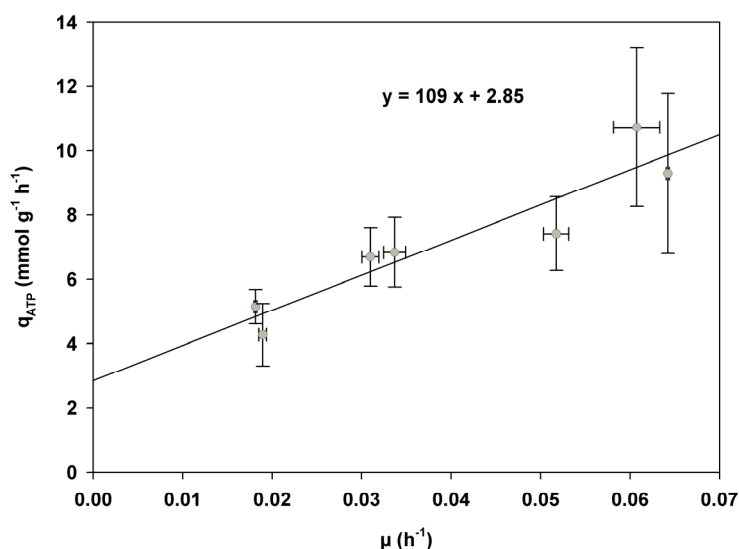


Figure 4.3 Plot of the calculated specific overall ATP production rate q_{ATP} ($\text{mmol g}^{-1} \text{ h}^{-1}$) against the experimentally determined growth rate (μ , h^{-1}). q_{ATP} was calculated with the model for each growth rate. Regression through these points yields a straight line of which the offset gives the ATP required for maintenance m_{ATP} , $2.85 \text{ mmol g}^{-1} \text{ h}^{-1}$. The slope gives the constant which represents the additional amount of ATP needed to make biomass from the biopolymers (K_x), 109 mmol g^{-1} , according to equation 4. The error bars represent the minimum and maximum values for q_{ATP} and the growth rate μ , which follow from the relative errors of biomass measurements.

mmol g⁻¹. From this number it could be calculated that 18.9 mol ATP is required to transport and assemble one mol biomass. This amount was added to the biomass synthesis reaction (mol ATP per mol biomass, reaction 147) of the final model. The ATP hydrolysis flux (reaction 57) was set to the value for m_{ATP} to fix the maintenance requirements of the final metabolic model.

An overview of values for K_x and m_{ATP} for several micro-organisms is presented in Table 4.6. The value for K_x depends on the characteristics of the model, for example the degree of compartmentalization and the ATP stoichiometry for biopolymer formation and thus the value for K_x differs per model. To make a good comparison of the total ATP use in several species $1/Y_{\text{xATP}}$ (mol ATP g⁻¹) is also given, which is the total amount of ATP required to make 1 gram of biomass. As can be seen from Table 4.6 there is considerable variation in the values for $1/Y_{\text{xATP}}$, K_x and m_{ATP} for different micro-organisms. This can be due to the type of micro-organism, the culture conditions and the assumptions made in the models. Firstly, these parameters depend on the assumed P/O ratio, the relationship between ATP synthesis and oxygen consumption. We assumed that NADH yields 2.5 ATP and FADH₂ yields 1.5 ATP upon respiration. However, lower values for these ratios would result in lower values for K_x and m_{ATP} . Secondly, we assumed a ratio between NADPH and ATP production during linear electron transport in chloroplast of 3:2 (ATP:NADPH) which exactly fits the requirements of the Calvin cycle. Studies on Spinach chloroplasts, how-

Table 4.6 Comparison of yields and maintenance coefficients of different micro-organisms from literature.

Organism	$1/Y_{\text{xATP}}$ (mol g ⁻¹)	K_x (mol g ⁻¹)	m_{ATP} (mmol g ⁻¹ h ⁻¹)	Reference
<i>Chlamydomonas reinhardtii</i> ^a	0.43	0.11	2.85	This paper
<i>Petunia hybrida</i> (cell culture) ^b	0.44	0.15	1.41	de Gucht and van der Plas (1995)
<i>Saccharomyces cerevisiae</i> ^b	0.35	0.07	1.00	Forster et al. (2003)
<i>Escherichia coli</i> ^b	0.31	0.09	2.81	Kayser et al. (2005)
<i>Escherichia coli</i> ^b	0.40	0.10	4.70	Carlson and Srienç (2004)
<i>Streptomyces coelicolor</i> ^b	-	0.08	3.69	Borodina et al. (2005)
<i>Neisseria meningitides</i> ^b	0.40	0.05	1.61	Baart et al. (2008)
<i>Corynebacterium glutamicum</i> ^b	0.29	0.03	-	Kieldsen and Nielsen (2009)

^a photoautotrophic growth on light and CO₂

^b heterotrophic growth on glucose. Glucose yields 32 ATP (Berg et al. 2003)

ever, show that linear electron transport only can deliver 2.57 ATP per every 2 NADPH and that cyclic photosynthetic electron transport (i.e. cyclic photophosphorylation) is needed to generate additional ATP (Allen 2003). This cyclic pathway was not included in our model because the additional ATP requirement is small and it would make our model underdetermined. Its necessity, however, could partly explain the fact that the experimentally determined minimal quantum requirement of oxygen evolution is 10 instead of 8 as discussed before (equivalent to $\Phi_{pmax} = 0.8$) and as such it is implicitly present in our model. Besides the balance of ATP and NADPH in the chloroplast, the microalgal cells as a whole require substantial ATP as is extensively discussed in this study. According to our model ATP must be generated by the complete conversion of sugars (GAP) produced in the chloroplast by the combined action of glycolysis, TCA cycle and oxidative phosphorylation in the cytosol and mitochondria (Figure 4.2). It is interesting to note that this pathway ultimately yields 1 mol of ATP per 1.5 mol photons (see 'Simulation of oxygen uptake through respiration' for calculation). Cyclic photophosphorylation on the other hand, would only yield 1 molecule of ATP per 2 photons (Allen 2003). This shows that energy generation through linear photosynthetic electron transport is energetically more favorable than through cyclic electron transport and supports our description of *C. reinhardtii* metabolism.

Thirdly, the parameter K_x accounts for the requirement of ATP for biomass formation which is not accounted for in the part of the network with a known energy stoichiometry. For more complex models involving more compartmentalization, a larger part of the ATP may be accounted for and consequently the value of this parameter would become lower. However, for the two more extensive models described for *Chlamydomonas* the energy parameters were not properly estimated. Manichaikul et al. (2009) used parameters taken from yeast cultivation and not from *C. reinhardtii* itself. Boyle and Morgan (2009) estimated the energy parameters for autotrophic, heterotrophic and mixotrophic growth by fitting their model to one experimentally determined biomass yield, based on experiments performed in shake flasks. The maintenance parameter was taken from literature and not measured. Boyle and Morgan estimated a K_x of 29.89 mmol g⁻¹, which is indeed lower than our value, as would be expected for a more detailed model. However, they used shake flask experiments to estimate this parameter. Shake flasks usually have undefined light regimes, which makes it difficult to properly measure the absorbed light by the culture (PFD_{abs}) and thus the light supply rate (r_{Ex}). Also the efficiency of photosynthesis is unknown under these cultivation conditions. Furthermore, only a single

growth rate was used, making the estimation highly dependent on the assumed value of the maintenance parameter.

Simulation of oxygen uptake through respiration

With the average biomass composition (Table 4.5) for all chemostats and the energy requirements for both maintenance and growth associated processes, a working model was obtained as shown in the appendix. With this model we simulated the mitochondrial respiration rate ($\text{mmol O}_2 \text{ g}^{-1} \text{ h}^{-1}$) at different growth rates (μ, h^{-1}). Figure 4.4 (separate figure sheet) shows the flux distribution through the network at a specific growth rate μ of 0 h^{-1} and 0.062 h^{-1} . The size of the fluxes in $\text{mmol g}^{-1} \text{ h}^{-1}$ are shown in boxes, red boxes for $\mu = 0 \text{ h}^{-1}$ and black boxes for $\mu = 0.062 \text{ h}^{-1}$. Light is taken up in the light reaction of photosynthesis and with the energy that is formed CO_2 is fixed in the Calvin cycle. The carbon is moved to the cytosol in the form of GAP, where it enters the glycolysis and TCA cycle. Part of the GAP is used to synthesize biopolymers and part is used here to generate energy in the form of ATP, NADH and FADH_2 . NADH and FADH_2 are in turn respired in the mitochondria to generate additional ATP to fulfill the energy requirements for growth and maintenance. The flux distribution at $\mu = 0 \text{ h}^{-1}$ shows the maintenance metabolism without biomass formation. It also shows that the minimal light uptake rate is $4.28 \text{ mmol photons g}^{-1} \text{ h}^{-1}$, which is used to provide energy for maintenance ($2.85 \text{ mmol g}^{-1} \text{ h}^{-1}$). Using these fluxes it can be calculated that in this model 1.5 mol photons should be consumed to produce 1 mol ATP.

Figure 4.5 shows the simulated biomass yield on light ($Y_{x/E}$ in g mol^{-1} , closed dots) for several growth rates μ . These simulations give an ideal situation since no light saturation is modeled and consequently the biomass yield $Y_{x/E}$ increases asymptotically to the maximal value of 1.57 g mol^{-1} at very high specific growth rates. In reality light saturation will occur due to the high light intensities necessary to reach maximal growth rates. The photons are absorbed, but the energy is only partly used for growth, causing a decrease in the biomass yield on light energy ($\Phi_P < \Phi_{P_{\max}}$, equation 6). If light saturation (Baker et al. 2007; Krause and Weis 1991; van der Tol et al. 2009) would be taken into account the yield in Figure 4.5 would reach an optimum and decrease as soon as light saturation occurs. The simulated respiration rate (open diamonds), calculated by the sum of the oxygen consumption rates in oxidative phosphorylation (reactions 52 and 53) and the fraction of oxygen used for maintenance (open triangles) are also plotted in Figure 4.5. As expected, respiration is a linear function of the growth rate and regression through these

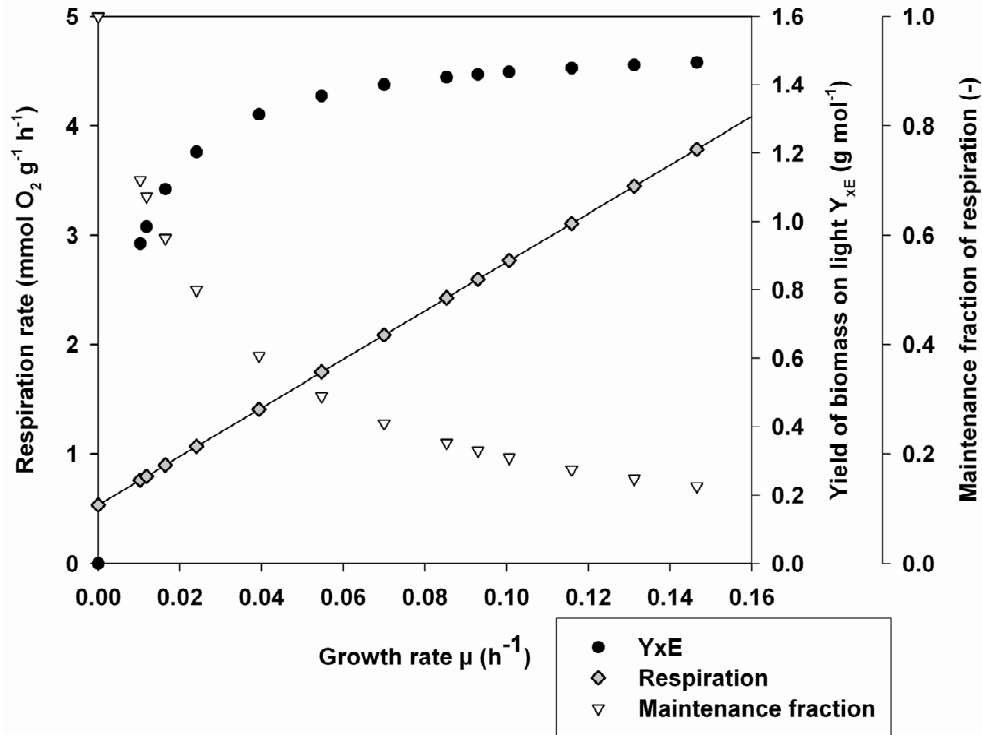


Figure 4.5 Simulated respiration rates ($\text{mmol O}_2 \text{ g}^{-1} \text{ h}^{-1}$) at several growth rates (μ , h^{-1}). Regression through these points yields a straight line with an intercept at $\mu = 0$ of $0.53 \text{ mmol O}_2 \text{ g}^{-1} \text{ h}^{-1}$. This value is the oxygen uptake rate through respiration which is necessary for maintenance purposes. The maintenance fraction of the respiration rate is also plotted and shows which part of respiration is used for maintenance purposes. This graph also shows the simulated biomass yields on light energy ($Y_{x/E}$, g mol^{-1}) for these growth rates. The simulations give an ideal situation since light saturation is not modeled. If light saturation would be taken into account the yield would reach an optimum and decrease as soon as light saturation occurs.

points yields a straight line with an intercept of $0.53 \text{ mmol O}_2 \text{ g}^{-1} \text{ h}^{-1}$ at $\mu = 0 \text{ h}^{-1}$. This value is the oxygen uptake rate through respiration which is necessary for maintenance purposes. In earlier experimental work (Kliphuis et al. 2010b) we measured that the respiration rate required for maintenance for *Chlorella sorokiniana* was $0.3 \text{ mmol O}_2 \text{ g}^{-1} \text{ h}^{-1}$. This is in the same order as the value we now calculated for *Chlamydomonas reinhardtii* but almost twofold lower. As mentioned before, this is likely to be species specific. It can be seen that at low growth rates a relatively large part of respiration is needed for maintenance purposes. At high growth rates the largest part of respiration is needed for energy generation for growth purposes. Consequently, cultivating microalgae at low spe-

cific growth rates results in a low biomass yield $Y_{x/E}$, since a large part of the energy is used for maintenance processes rather than growth. This effect was experimentally confirmed for *Chlorella sorokiniana* and *Dunaliella tertiolecta* by Zijffers et al. (2010).

Conclusions

A metabolic network describing the primary metabolism of *C. reinhardtii* was constructed. By performing chemostat experiments energy parameters for maintenance and biomass formation were obtained. The chemostats were run at low light intensities resulting in a high biomass yield on light of 1.25 g mol^{-1} . The ATP requirement for biomass formation from biopolymers (K_x) was determined to be 109 mmol g^{-1} ($18.9 \text{ mol mol}^{-1}$) and the maintenance requirement (m_{ATP}) was determined to be $2.85 \text{ mmol g}^{-1} \text{ h}^{-1}$. These values are in the same range as literature values. With these energy requirements included in the metabolic network, the network accurately describes the primary metabolism of *C. reinhardtii* and can be used for modeling of *C. reinhardtii* growth and metabolism. Simulations with this metabolic model showed that mitochondrial respiration both provides energy for maintenance and additional energy to support growth. The high maintenance requirements at low growth rates result in low biomass yields and thus cultivating algae at low growth rates is unfavorable. Cultivating algae at high light supply rates is less favorable as well, because the biomass yield will decrease due to light saturation effects. Thus, to optimize biomass yield on light energy in photobioreactors, an optimum between these two situations should be found.

The simulations presented in this paper show that the metabolic model can be used as a tool to gain insight into the metabolism of *Chlamydomonas reinhardtii* and ultimately can be used for the maximization of biomass and product yield.

Nomenclature

μ	Specific growth rate (h^{-1})
Σq_i^{ATP}	Specific ATP production rate in the metabolism with known ATP stoichiometry ($\text{mmol g}^{-1} \text{ h}^{-1}$)
Φ_p	Photochemical quantum yield (-)
$\Phi_{p\text{max}}$	Maximum photochemical quantum yield (-)
A	Transpose of the stoichiometric matrix of the network (-)
A_{pbr}	Illuminated surface of the photobioreactor (m^2)
C_x	Biomass concentration in the photobioreactor (g L^{-1})

K_x	ATP requirement for the formation of biomass from biopolymers (mmol g^{-1} or mol mol^{-1})
m_{ATP}	Maintenance ATP requirements ($\text{mmol ATP g}^{-1} \text{h}^{-1}$)
m_E	Maintenance light energy requirements ($\text{mmol photons g}^{-1} \text{h}^{-1}$)
N	Number of measurements (-)
OD_{530}	Optical density measured at 530nm on a spectrophotometer (-)
PFD	Photon flux density ($\mu\text{mol m}^{-2} \text{s}^{-1}$)
PFD_{abs}	Average photon flux density absorbed by the microalgal culture ($\mu\text{mol m}^{-2} \text{s}^{-1}$)
q_{ATP}	Total specific ATP production rate in the metabolism ($\text{mmol g}^{-1} \text{h}^{-1}$)
$q_{\text{ATP,light}}$	Specific ATP production rate in the chloroplast ($\text{mmol g}^{-1} \text{h}^{-1}$)
$q_{\text{ATP,ox}}$	Specific ATP production rate in oxidative phosphorylation ($\text{mmol g}^{-1} \text{h}^{-1}$)
r_{Ex}	Specific light supply rate ($\text{mol g}^{-1} \text{h}^{-1}$)
$r_{\text{Ex,u}}$	Specific light utilization rate ($\text{mmol g}^{-1} \text{h}^{-1}$)
V_{pbr}	Working photobioreactor volume (L)
Y_{xATP}	Biomass yield on ATP (g mol^{-1})
Y_{xE}	Biomass yield on light energy (g mol^{-1})
$Y_{\text{xE}}^{\text{obs}}$	Observed experimental biomass yield on light energy, not corrected for maintenance requirements (g mol^{-1})

Acknowledgements

This research project is financially supported by Technology Foundation STW-VICI (WLM.6622) and was performed in the TTW-cooperation framework of Wetsus, centre of excellence for sustainable water technology (www.wetsus.nl). Wetsus is funded by the Dutch Ministry of Economic Affairs. The authors like to thank the participants of the research theme 'algae' for their fruitful discussions and their financial support. The authors declare that they have no conflict of interest.

Appendix

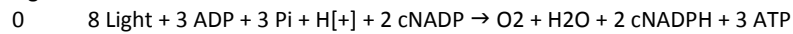
A. Metabolic model of *Chlamydomonas reinhardtii*

Arrows indicate the direction and reversibility of the reactions. The compounds in the chloroplast are notated with a 'c' before the abbreviation. All fluxes are in $\text{mmol g}^{-1} \text{h}^{-1}$.

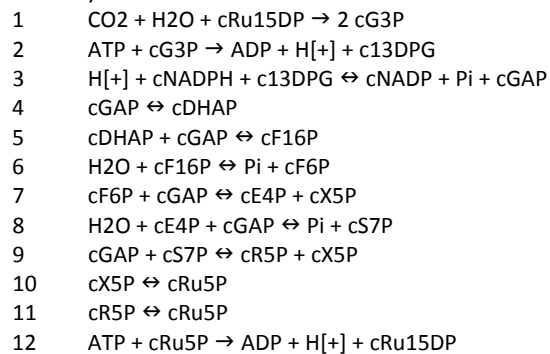
Metabolic modeling of Chlamydomonas reinhardtii

The factor in the biomass export reaction (159) converts the biomass flux through reaction 147 (in $\text{mmol g}^{-1} \text{h}^{-1}$) to $\text{mg g}^{-1} \text{h}^{-1}$, the biomass production rate.

Light reaction



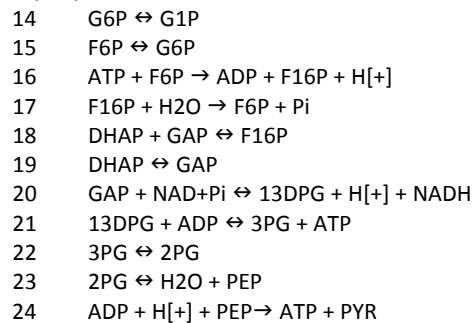
Calvin cycle



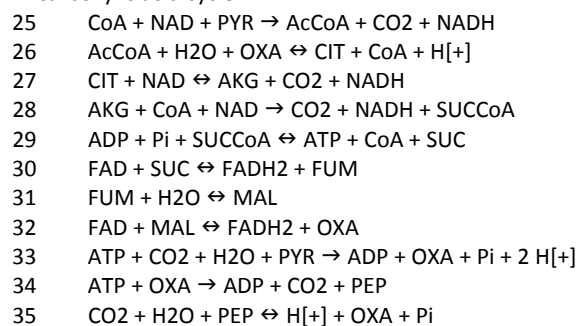
Transport chloroplast to cytosol



Glycolysis



Tricarboxylic acid cycle



Chapter 4

Pentose phosphate pathway

- 36 $G6P + H_2O + NADP \leftrightarrow 6PG + NADPH + 2 H^+$
37 $6PG + NADP \leftrightarrow CO_2 + NADPH + RU5P$
38 $RU5P \leftrightarrow R5P$
39 $RU5P \leftrightarrow X5P$
40 $R5P + X5P \leftrightarrow GAP + S7P$
41 $GAP + S7P \leftrightarrow E4P + F6P$
42 $F6P + GAP \leftrightarrow E4P + X5P$

Glycerol

- 43 $DHAP + H_2O \leftrightarrow DHA + Pi$
44 $DHA + H^+ + NADPH \leftrightarrow GLYC + NADP$
45 $ATP + GLYC \rightarrow ADP + GLYC3P + H^+$
46 $GLYC3P + NAD \leftrightarrow DHAP + H^+ + NADH$

N and S fixation

- 47 $H^+ + NADH + NO_3 \leftrightarrow H_2O + NAD + NO_2$
48 $5 H^+ + 3 NADPH + NO_2 \leftrightarrow NH_4^+ + 2 H_2O + 3 NADP$
49 $ATP + SO_4 \rightarrow APS + PPi$
50 $APS + NADH \rightarrow AMP + NAD + SO_3$
51 $5 H^+ + 3 NADPH + SO_3 \leftrightarrow H_2S + 3 H_2O + 3 NADP$

Oxidative phosphorylation

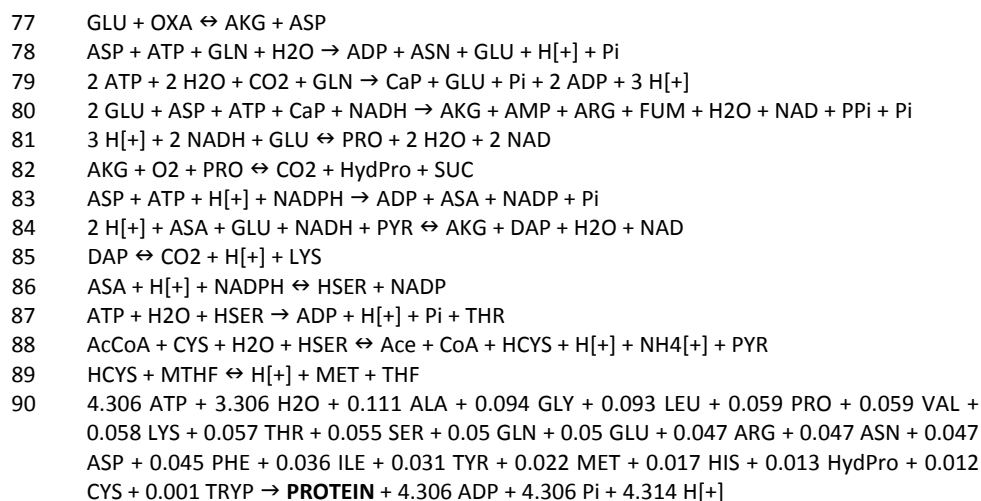
- 52 $1.5 ADP + 1.5 H^+ + 1.5 Pi + FADH_2 + 0.5 O_2 \rightarrow FAD + 1.5 ATP + 2.5 H_2O$
53 $3.5 H^+ + 2.5 ADP + 2.5 Pi + NADH + 0.5 O_2 \rightarrow NAD + 2.5 ATP + 3.5 H_2O$
54 $NAD + NADPH \rightarrow NADH + NADP$
55 $H_2O + PPi \rightarrow H^+ + 2 Pi$
56 $AMP + ATP \rightarrow 2 ADP$
57 $ATP + H_2O \rightarrow ADP + H^+ + Pi$

Amino acids and protein

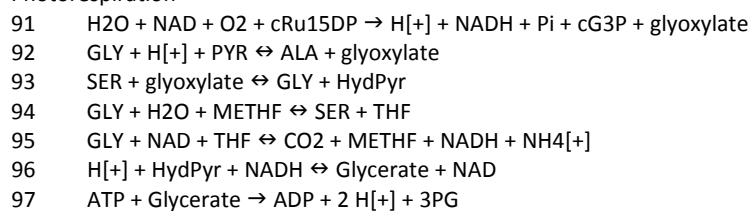
- 58 $AKG + H^+ + NADPH + NH_4^+ \rightarrow GLU + H_2O + NADP$
59 $ATP + GLU + NH_4^+ \rightarrow ADP + GLN + H^+ + Pi$
60 $AKG + GLN + H^+ + NADPH \leftrightarrow NADP + 2 GLU$
61 $3PG + GLU + H_2O + NAD \leftrightarrow AKG + H^+ + NADH + Pi + SER$
62 $SER \rightarrow NH_4^+ + PYR$
63 $AcCoA + H_2S + SER \leftrightarrow Ace + CYS + CoA + H^+$
64 $ATP + Ace + CoA \rightarrow ADP + AcCoA + Pi$
65 $GLU + PYR \rightarrow AKG + ALA$
66 $H^+ + THR \leftrightarrow 2\text{-oxobutan} + NH_4^+$
67 $2\text{-oxobutan} + GLU + H^+ + NADPH + PYR \leftrightarrow AKG + CO_2 + H_2O + ILE + NADP$
68 $2 H^+ + ALA + NADPH + PYR \leftrightarrow CO_2 + H_2O + NADP + VAL$
69 $2 PYR + AcCoA + GLU + H^+ + NAD + NADPH \leftrightarrow AKG + CoA + LEU + NADH + NADP + 2 CO_2$
70 $2 PEP + ATP + E4P + NADPH \rightarrow ADP + CHO + NADP + 4 Pi$
71 $CHO \leftrightarrow PRE$
72 $GLU + H^+ + PRE \leftrightarrow AKG + CO_2 + H_2O + PHE$
73 $GLU + NAD + PRE \leftrightarrow AKG + CO_2 + NADH + TYR$
74 $CHO + GLN \leftrightarrow ANTH + GLU + H^+ + PYR$
75 $ANTH + H^+ + PRPP + SER \leftrightarrow CO_2 + GAP + PPi + TRYP + 2 H_2O$
76 $3 H_2O + 2 NAD + ATP + GLN + PRPP \rightarrow AICAR + AKG + HIS + Pi + 2 NADH + 2 PPi + 5 H^+$

98

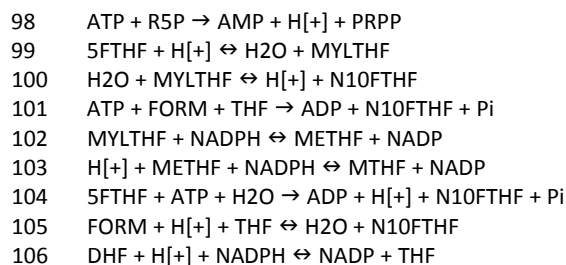
Metabolic modeling of Chlamydomonas reinhardtii



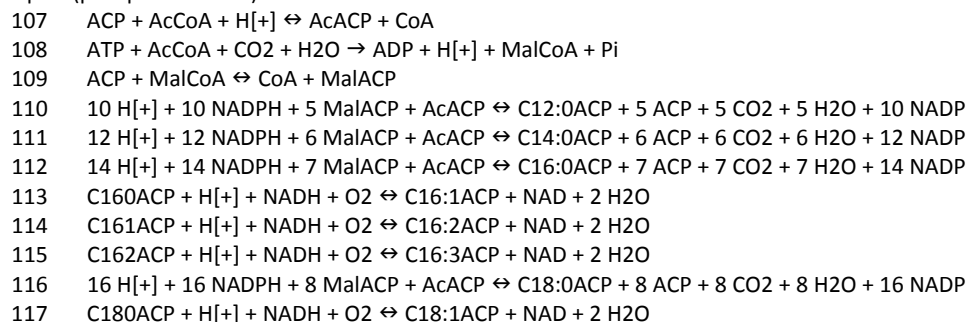
Photorespiration



THF metabolism



Lipids (phosphatidic acid)



Chapter 4

- 118 $C18:1ACP + H[+] + NADH + O_2 \rightleftharpoons C18:2ACP + NAD + 2 H_2O$
119 $C18:2ACP + H[+] + NADH + O_2 \rightleftharpoons C18:3ACP + NAD + 2 H_2O$
120 $GLYC3P + 0.474 C16:0ACP + 0.446 C18:3ACP + 0.276 C18:2ACP + 0.253 C16:3ACP + 0.16 C18:1ACP + 0.148 C16:2ACP + 0.104 C12:0ACP + 0.051 C14:0ACP + 0.048 C18:0ACP + 0.04 C16:1ACP \rightleftharpoons PA + 2 ACP + 2 H[+]$

Nucleic acids

- 121 $4 ATP + 2 GLN + 2 H_2O + ASP + CO_2 + GLY + N10FTHF + PRPP \rightarrow AICAR + FUM + PPi + THF + 2 GLU + 4 ADP + 4 Pi + 7 H[+]$
122 $ASP + CaP + H[+] + O_2 + PRPP \rightleftharpoons CO_2 + H_2O + H_2O_2 + PPi + Pi + UMP$
123 $2 H_2O_2 \rightleftharpoons O_2 + 2 H_2O$
124 $ATP + UMP \rightarrow ADP + UDP$
125 $ATP + UDP \rightleftharpoons ADP + UTP$
126 $ATP + GLN + H_2O + UTP \rightarrow ADP + CTP + GLU + Pi + 2 H[+]$
127 $ATP + CDP \rightleftharpoons ADP + CTP$
128 $AICAR + N10FTHF \rightleftharpoons H_2O + IMP + THF$
129 $ATP + H_2O + IMP + NAD + NH_4[+] \rightarrow AMP + GMP + NADH + PPi + 3 H[+]$
130 $ATP + GMP \rightarrow ADP + GDP$
131 $ATP + GDP \rightleftharpoons ADP + GTP$
132 $ASP + GTP + IMP \rightleftharpoons AMP + FUM + GDP + Pi + 2 H[+]$
133 $ATP + H[+] + METHF + NADPH + UDP \rightarrow ADP + DHF + H_2O + NADP + dTTP$
134 $ATP + CDP + H[+] + NADPH \rightarrow ADP + H_2O + NADP + dCTP$
135 $ATP + GDP + H[+] + NADPH \rightarrow ADP + H_2O + NADP + dGTP$
136 $ATP + H[+] + NADPH \rightleftharpoons H_2O + NADP + dATP$
137 $2.372 H_2O + 1.372 ATP + 0.18 dATP + 0.18 dTTP + 0.32 dCTP + 0.32 dGTP \rightarrow DNA + PPi + 1.372 ADP + 1.372 Pi + 2.372 H[+]$
138 $1.4 H_2O + 0.56 ATP + 0.34 GTP + 0.16 UTP + 0.34 CTP \rightarrow 0.4 ADP + 0.4 H[+] + 0.4 Pi + PPi + RNA$

Chlorophyll

- 139 $12 H[+] + 8 ATP + 8 GLU + 8 NADPH + 2.5 O_2 \rightarrow PPorphyrin + 4 NH_4[+] + 6 CO_2 + 8 AMP + 8 NADP + 8 PPi + 13 H_2O$
140 $18 H[+] + 15 NADPH + 8 ATP + 4 GAP + 4 PYR \rightarrow Phytol-PP + 4 ADP + 4 AMP + 4 CO_2 + 7 PPi + 8 H_2O + 15 NADP$
141 $ATP + H_2O + MET \rightarrow AdMET + H[+] + PPi + Pi$
142 $AdHCYS + H_2O \rightleftharpoons Ad + HCYS$
143 $ATP + Ad \rightarrow ADP + AMP + H[+]$
144 $4 NADPH + 2.5 O_2 + 2 ATP + AdMET + Mg^{2+} + PPorphyrin + Phytol-PP \rightarrow AdHCYS + Chlorophyll + PPi + 2 ADP + 2 H_2O + 2 Pi + 3 H[+] + 4 NADP$

Starch and carbohydrates

- 145 $G1P \rightleftharpoons Pi + STARCH$
146 $G1P \rightleftharpoons CARB + Pi$

Biomass formation

- 147 $18.8996 ATP + 18.8996 H_2O + 0.6417 PROTEIN + 0.2713 CARB + 0.0453 PA + 0.0305 RNA + 0.0102 Chlorophyll + 0.0011 DNA \rightarrow Biomass + 18.7763 H[+] + 18.8996 ADP + 18.8996 Pi$

Transport

148	CO ₂ ← CO ₂ _ex
149	O ₂ → O ₂ _ex
150	H ₂ O ↔ H ₂ O_ex
151	Pi ↔ Pi_ex
152	SO ₄ ↔ SO ₄ _ex
153	NO ₃ ↔ NO ₃ _ex
154	Mg ²⁺ ↔ Mg ²⁺ _ex
155	Light ← Light_ex
156	H ⁺ ↔ H ⁺ _ex
157	GLYC → GLYC_ex
158	STARCH → STARCH_ex
159	Biomass → 172.848 Biomass_ex

B. Compound abbreviations

13DPG	1,3-diPhosphoglycerate	C16:1ACP	Trans-Hexadec-2-enoyl-ACP (Palmitoleic acid)
2-oxobutan	2-Oxobutanoate	C16:2ACP	Hexadecadienoic acid
2PG	2-Phosphoglycerate	C16:3ACP	Hexadecatrienoic acid
3PG	3-Phosphoglycerate	C18:0ACP	Octadecanoyl-ACP (Stearic acid)
5FTHF	5-Formyl-THF	C18:1ACP	Cis-11-ocadecanoate-ACP (Oleic acid)
6PG	6-Phosphogluconate	C18:2ACP	Linoleic acid
AcACP	Acetyl-ACP	C18:3ACP	Alpha-linoleic acid
AcCOA	Acetyl-CoA	CaP	Carbamoyl phosphate
Ace	Acetate	CARB	Carbohydrate
ACP	Acetyl-carrier protein	CDP	Cytidine diphosphate
Ad	Adenosine	Chlorophyll	Chlorophyll
AdHCYS	S-Adenosyl-L-homocysteine	CHO	Chorismate
AdMET	S-Adenosyl-L-methionine	CIT	Citrate
ADP	Adenosine diphosphate	CO ₂	Carbon dioxide
AICAR	5-Aminoimidazole-4-carboxamide ribonucleine	CO ₂ _ex	Carbon dioxide (extracellular)
AKG	2-Oxoglutarate (alpha-ketoglutarate)	CoA	Coenzyme A
ALA	Alanine	CTP	Cytidine triphosphate
AMP	Adenosine monophosphate	CYS	Cysteine
ANTH	Anthranilate	DAP	Diaminopimelate
APS	Adenylyl sulfate	dATP	Deoxy ATP
ARG	Arginine	dCTP	Deoxy CTP
ASA	L-Aspartic semialdehyde	dGTP	Deoxy GTP
ASN	Asparagine	DHA	Dihydroxyacetone (Glycerone)
ASP	Aspartate	DHAP	Dihydroxyacetone-P
ATP	Adenosine triphosphate	DHF	Dihydrofolate
Biomass	Biomass	DNA	Deoxyribonucleic acid
Biomass_ex	Biomass (g)	dTTP	Deoxy TTP
C12:0ACP	Dodecanoyl-ACP (Lauric acid)	E4P	Erythrose 4-phosphate
C14:0ACP	Tetradecanoyl-ACP (Myristic acid)	F16P	Fructose 1,6-bisphosphate
C16:0ACP	Hexadecanoyl-ACP (Palmitic acid)	F6P	Fructose 6-phosphate
		FAD	Flavin adenine dinucleotide

	oxidized	NADH	Nicotinamide reduced
FADH2	Flavin adenine dinucleotide	NADP	Nicotinamidephosphate oxidized
	reduced	NADPH	Nicotinamidephosphate reduced
FORM	Formic acid	NH4[+]	Ammonium
FUM	Fumarate	NH4[+]_ex	Ammonium (extracellular)
G1P	Glucose 1-phosphate	NO2	Nitrite
G6P	Glucose 6-phosphate	NO3	Nitrate
GAP	Glyceraldehyde 3-phosphate	NO3_ex	Nitrate (extracellular)
GDP	Guanosine diphosphate	O2	Oxygen
GLN	Glutamine	O2_ex	Oxygen (extracellular)
GLU	Glutamate	OXA	Oxaloacetate
GLY	Glycine	PA	Phosphatidic acid
GLYC	Glycerol	PEP	Phosphoenolpyruvate
GLYC3P	Glycerol 3-phosphate	PHE	Phenylalanine
Glycerate	Glycerate	Phytly-PP	Phytly-diphosphate
GLYC_ex	Glycerol (extracellular)	Pi	Orthophosphate
glyoxylate	Glyoxylate	Pi_ex	Orthophosphate (extracellular)
GMP	Guanosine monophosphate	PPi	Pyrophosphate
GTP	Guanosine triphosphate	PPorphyrin	Protoporphyrine
H[+]	Proton	PRE	Prephanate
H[+]_ex	Proton (extracellular)	PRO	Proline
H2O	Water	PROTEIN	Protein
H2O2	Hydrogen peroxide	PRPP	Phosphorybosylpyrophosphate
H2O_ex	Water (extracellular)	PYR	Pyruvate
H2S	Hydrogen sulfide	R5P	Ribose 5-phosphate
HCYS	Homocysteine	RNA	Ribonucleic acid
HIS	Histidine	Ru15DP	Ribulose 1,5-bisphosphate
HSER	Homoserine	RU5P	Ribulose 5-phosphate
HydPro	Hydroxyproline	S7P	Sedoheptulose 7-phosphate
HydPyr	3-Hydroxypyruvate	SER	Serine
ILE	Isoleucine	SO3	Sulphite
IMP	Inosine monophosphate	SO4	Sulphate
LEU	Leucine	SO4_ex	Sulphate (extracellular)
Light	Photons	STARCH	Starch
Light_ex	Photons (extracellular)	STARCH_ex	Starch (extracellular)
LYS	Lysine	SUC	Succinate
MAL	Malate	SUCCoA	Succinyl Coenzyme A
MalCoA	Malonyl-CoA	THF	Tetrahydrofolate
MET	Methionine	THR	Threonine
METHF	5,10-Methylene-THF	TRYP	Tryptophan
Mg2[+]	Magnesium	TYR	Tyrosine
Mg2[+]_ex	Magnesium (extracellular)	UDP	Uridine diphosphate
MTHF	Methyl-THF	UMP	Uridine monophosphate
MYLTHF	5,10-Methenyl-THF	UTP	Uridine triphosphate
N10FTHF	10-Formyl-THF	VAL	Valine
NAD	Nicotinamide oxidized	X5P	Xylulose 5-phosphate

C. Elemental composition of macromolecules

	C	H	O	N	P	S	Charge
Protein	4.8	7.6	1.5	1.3	0	0.03	-
Carbohydrates	6.0	10.0	5.0	0	0	0	-
Lipids (PA)	36.3	63.4	8.0	0	1.0	0	-2
DNA	9.7	12.2	7.0	3.8	1.0	0	-2
RNA	9.5	12.8	8.0	3.8	1.0	0	-1
Chlorophyll	55.0	72.0	5.0	4.0	0	0	-
Biomass	7.2	11.7	3.0	1.0	0.08	0.02	-

The average elemental biomass composition thus becomes $\text{CH}_{1.62}\text{O}_{0.41}\text{N}_{0.14}\text{P}_{0.01}\text{S}_{0.003}$.

The biomass contains an ash fraction of 0.057. This yields a molecular weight of $23.97 \text{ g C}\cdot\text{mol}^{-1}$.

D. Protein composition

Amino Acid	% (mol AA/mol protein)
Alanine (Ala)	11.07
Arginine (Arg)	4.67
Asparagine (Asn)	4.68
Aspartate (Asp)	4.68
Cysteine (Cys)	1.17
Glutamate (Glu)	4.96
Glutamine (Gln)	4.96
Glycine (Gly)	9.36
Histidine (His)	1.69
Hydroxyproline (HydPro)	1.30
Isoleucine (Ile)	3.59
Leucine (Leu)	9.25
Lysine (Lys)	5.78
Methionine (Met)	2.22
Phenylalanine (Phe)	4.45
Proline (Pro)	5.92
Serine (Ser)	5.51
Threonine (Thr)	5.71
Tryptophan (Trp)	0.10
Tyrosine (Tyr)	3.08
Valine (Val)	5.86

In the network, proteins were modeled as a coupling of one average amino acid, consuming 4.306 mol ATP. One average amino acid constitutes of the sum of the molar fractions of the various amino acids present in *C. reinhardtii*.

E. Lipid composition

Fatty acid	% (mol FA/mol PA)
12:0	10.42 ± 0.56
14:0	5.14 ± 0.30
16:0	47.35 ± 1.36
16:1	3.96 ± 0.09
16:2	14.78 ± 0.17
16:3	25.30 ± 0.57
18:0	4.78 ± 0.34
18:1	16.01 ± 0.11
18:2	27.63 ± 0.31
18:3	44.62 ± 1.29

In the network, lipids (PA, phosphatidic acid) were modeled as a Glycerol 3-phosphate molecule with two acetyl-ACP tails. The average acetyl-ACP chains constitute of the sum of two times the molar fractions of the various fatty acids present in *C. reinhardtii*.





CHAPTER 5

Effect of O₂ : CO₂ ratio on the primary metabolism of *Chlamydomonas reinhardtii*

Kliphuis AMJ, Janssen M, Martens DE, Wijffels RH (2010)
Effect of O₂ : CO₂ ratio on the primary metabolism of *Chlamydomonas reinhardtii*
Submitted for publication

Abstract

High oxygen : carbon dioxide ratios may have a negative effect on growth and productivity of microalgae. To investigate the effect of O₂ and CO₂ concentrations and the ratio between these on the metabolism of *Chlamydomonas reinhardtii*, we performed turbidostat experiments at different O₂ : CO₂ ratios. These experiments showed that elevated O₂ concentrations and the corresponding increase in the ratio of O₂ : CO₂ common in photobioreactors led to a reduction of growth and biomass yield on light with 20-30%. This is most probably related to the oxygenase activity of Rubisco and the resulting process of photorespiration. Using flux balance analysis with measured rates for each experiment we were able to quantify the ratio of the oxygenase reaction to the carboxylase reaction of Rubisco and could demonstrate that photorespiration indeed can cause the reduction in biomass yield on light. The calculated ratio of the oxygenase reaction to the carboxylase reaction was 16.6% and 20.5% for air with 2% CO₂ and 1% CO₂ respectively. Thus photorespiration has a significant impact on the biomass yield on light already at conditions common in photobioreactors (air with 2% CO₂).

Keywords: *Chlamydomonas reinhardtii*, Oxygen, Photorespiration, Flux balance analysis (FBA), Yield.

Introduction

During photoautotrophic growth microalgae consume carbon dioxide (CO₂) and produce oxygen (O₂). The evolved O₂ can easily build up to high concentrations in closed photobioreactors and this can have a negative effect on productivity and inhibit growth of the microalgae (Carvalho et al. 2006; Miron et al. 1999; Wijffels et al. 2010). Therefore, high O₂ concentrations are generally prevented by increasing the gas flow through the culture and thus removing O₂ faster. However, this requires more energy and thus increases operation costs (Norsker et al. 2010; Wijffels et al. 2010). If inhibitory levels of O₂ could be increased this would thus result in a reduction of the operational costs. Therefore it is important to understand the effect of O₂ concentration and the ratio with CO₂ concentration on algal metabolism.

The main processes that can occur at high O₂ : CO₂ ratios are photorespiration, the Mehler reaction (water-water cycle) and photoinhibition. The Mehler reaction and photoinhibition are thought to occur only at a strong imbalance between light absorption and utilization of the reductants generated in the light reactions (Adir et al. 2003; Cruz et al. 2005; Hideg 1997). The Mehler reaction takes place when the NADP/NADPH pool as well as the other components of the photosynthetic apparatus are reduced. High light intensities, CO₂ limitation and low temperatures can induce this situation (Badger et al. 2000). However, over-reduction of the chloroplast can also be prevented by transporting NADPH out of the chloroplast through a shuttle mechanism, the Malate/Oxaloacetate shuttle. This shuttle is activated by high NADPH levels in the chloroplast. This process seems to be preferred over the Mehler reaction, provided enough Oxaloacetate is present (Hoefnagel et al. 1998). Thus, these processes will occur at high light intensities and/or low growth rates due to nutrient limitations or temperature stress. In this paper we focus on the effect of the O₂ : CO₂ ratio on photorespiration, by avoiding these conditions and thus preventing photoinhibition and the Mehler reaction from occurring. Photorespiration occurs when high concentrations of O₂ and/or low concentrations of CO₂ are present (Foyer et al. 2009; Ogren 1984; Wingler et al. 2000). In this process Ribulose 1,5-bisphosphate carboxylase/oxygenase (Rubisco, EC 4.1.1.39) reacts with O₂ instead of CO₂. When Rubisco fixes CO₂, two molecules of Glycerate 3-phosphate are formed (Figure 5.1a). These can be converted back to Ribulose 1,5-bisphosphate or can be used in the central carbon metabolism to form biomass components. However, if O₂ is fixed only one Glycerate 3-phosphate is formed and one molecule of Glycolate 2-phosphate (Figure 5.1b). This compound is converted into glyoxylate

through glycolate and can subsequently be converted to Glycerate 3-phosphate at the expense of energy in the form of ATP. In addition CO_2 is 'lost' and needs to be re-fixed in the Calvin cycle. Ammonium (NH_4^+) is also 'lost' and needs to be re-fixed into Glutamate. This costs additional ATP and NADPH which are generated in the light reaction (linear electron transport) of photosynthesis and thus this costs additional light. Thus, in case photorespiration occurs less energy is available for growth, which will decrease the yield of microalgal biomass on light. To prevent this, it is important to keep the O_2 : CO_2 ratio low in order to minimize photorespiration and maximize biomass yield on light energy.

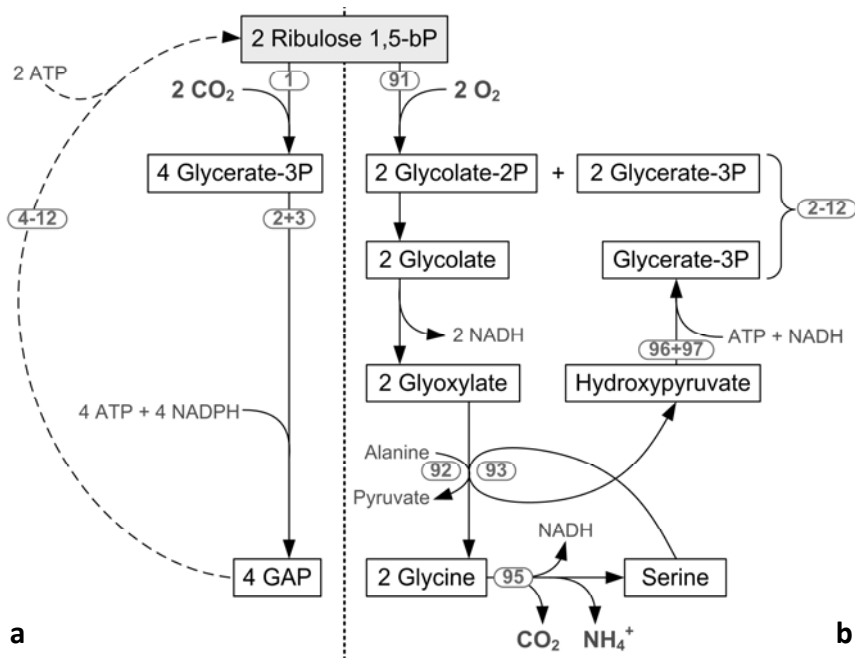


Figure 5.1 Carboxylase and oxygenase reactions of Rubisco, followed by the Calvin cycle (a) and photorespiration (b). The two processes are shown for two Ribulose 1,5-bisphosphate molecules each. The numbers correspond to the reactions in the metabolic model as shown in Appendix A. When Rubisco binds CO_2 (a), per two CO_2 four Glycerate 3-phosphate are formed, which can be converted to Glycerate 3-phosphate (GAP). GAP can be regenerated into Ribulose 1,5-bP at the expense of ATP or be used in the central carbon metabolism to form building blocks for biomass. When Rubisco binds O_2 (b), per two O_2 two Glycerate 3-phosphate and two Glycolate 2-phosphate are formed. To convert these two Glycolate 2-phosphate to one Glycerate 3-phosphate, ATP is consumed, CO_2 and ammonia (NH_4^+) are lost. Re-fixing this lost CO_2 and NH_4^+ costs more ATP and NADPH elsewhere in the metabolism.

The aim of this study is to get insight in the effect of the oxygen to carbon dioxide ratio on photorespiration and the metabolism of *Chlamydomonas reinhardtii* in general. The metabolism at different $O_2 : CO_2$ ratios is analyzed using a previously developed metabolic flux model describing the primary metabolism of *C. reinhardtii* (Kliphuis et al. 2010c). A simplified overview of this metabolic network is shown in Figure 5.2.

To assess the effect of different $O_2 : CO_2$ ratios on the metabolism of *Chlamydomonas reinhardtii* we performed two turbidostat experiments in a SLP photobioreactor. We examined four steady states, two control steady states at a very low $O_2 : CO_2$ ratio and two steady states at higher ratios, which are common in photobioreactors. Since these

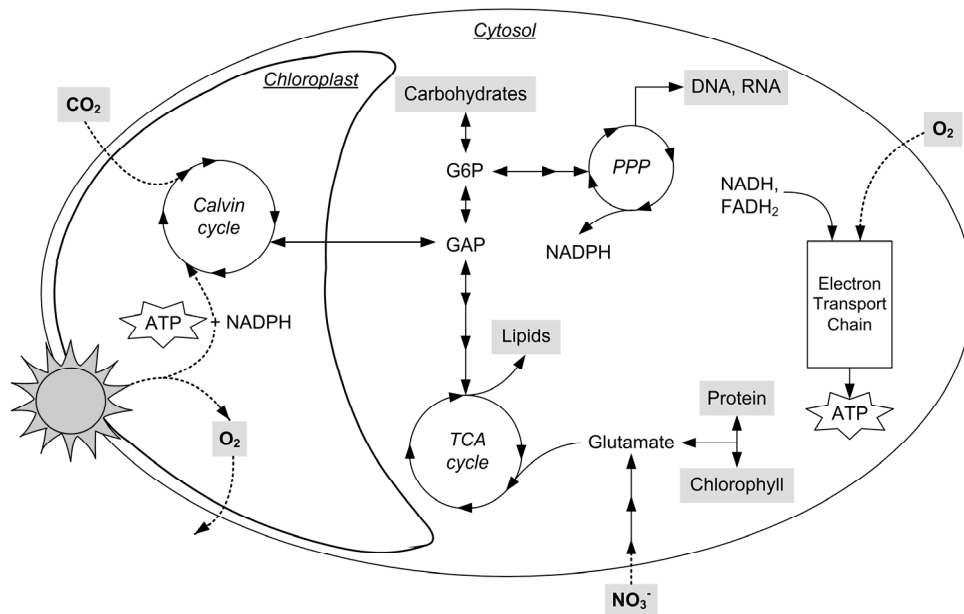


Figure 5.2 Simple overview of an algal cell in the light, showing the main metabolic processes. The model contains two compartments. The light reaction and Calvin cycle are placed in the chloroplast compartment and all other processes are located in the cytosol compartment. Light energy is harvested in the chloroplast, yielding O_2 , ATP and NADPH. These are needed to fix carbon dioxide in the Calvin cycle into glyceraldehyde 3-phosphate (GAP). GAP can be transported to the cytosol to be converted into building blocks for biomass. Lipids are formed through glycolysis and the tricarboxylic acid (TCA) cycle. Nitrate is taken up by the cell and converted into glutamate which in turn can be converted to protein and chlorophyll. GAP can be converted to glucose 6-phosphate (G6P) from which carbohydrates are formed. G6P can also enter the pentose phosphate pathway (PPP) which yields NADPH, DNA and RNA. Electrons are carried by NADH and $FADH_2$ to the mitochondrial electron transport chain, yielding ATP by taking up O_2 .

experiments were performed in turbidostat mode the biomass concentration in the reactor and thus the amount of light supplied per amount of biomass, i.e. the light supply rate r_{Ex} , was the same for each steady state and only the ratio of O_2 to CO_2 varied. Furthermore, the average light intensity experienced by the microalgae was sub-saturating, about $150 \mu\text{mol m}^{-2} \text{s}^{-1}$. Under these conditions we assumed that the main effect of the $O_2 : CO_2$ ratio will be on photorespiration and the Mehler reaction and photoinhibition are negligible.

Materials & Methods

Organism, medium and cultivation conditions

Chlamydomonas reinhardtii CC1690 (Chlamydomonas Genetics Centre, Duke University) was cultivated in 250 mL shake flasks containing 100 mL defined medium (Table 5.1) at pH 6.7. The medium was based on the Sueoka high salts (HS) medium, enriched for magnesium and calcium (Sueoka et al. 1967). The micronutrients were based on Hutner's trace element solution (Hutner et al. 1950). Additional EDTA was added to prevent precipitation of salts. Nitrate was used as a nitrogen source and enough nitrogen was added

Table 5.1 Composition of *Chlamydomonas reinhardtii* medium designed to reach 5 g L^{-1} biomass dry weight. The concentrations were doubled for photobioreactor cultivations, except for the phosphate buffer. The nitrate concentration was lowered to 10 mmol L^{-1} for the photobioreactor experiments.

Medium		Trace element stock	
Compound	Concentration (mmol L^{-1})	Compound	Concentration (mmol L^{-1})
KNO_3	24.73	$\text{FeSO}_4 \cdot 7 \text{ H}_2\text{O}$	17.96
KH_2PO_4	5.29	$\text{Na}_2\text{EDTA} \cdot \text{H}_2\text{O}$	148.69
K_2HPO_4	8.28	$\text{ZnSO}_4 \cdot 7 \text{ H}_2\text{O}$	76.51
$\text{MgSO}_4 \cdot 7 \text{ H}_2\text{O}$	1.14	H_3BO_3	184.38
$\text{CaCl}_2 \cdot 2 \text{ H}_2\text{O}$	0.39	$\text{MnCl}_2 \cdot 4 \text{ H}_2\text{O}$	25.57
$\text{Na}_2\text{EDTA} \cdot 2 \text{ H}_2\text{O}$	0.39	$\text{CoCl}_2 \cdot 6 \text{ H}_2\text{O}$	6.77
		$\text{CuSO}_4 \cdot 5 \text{ H}_2\text{O}$	6.29
NaHCO_3	1.00 ^a	$(\text{NH}_4)_6\text{Mo}_7\text{O}_{24} \cdot 4 \text{ H}_2\text{O}$	0.89

^a NaHCO_3 was only added to the medium for photobioreactor experiments.

to support 5 g L⁻¹ biomass. For the photobioreactor experiments the nitrate concentration in the medium was lowered to 10 mM since nitrate was added on demand via the pH control. The medium for the photobioreactor experiments was enriched with 1 mmol L⁻¹ NaHCO₃ and aerated overnight with either N₂ or pressurized air enriched with 1 or 2% CO₂. *C. reinhardtii* cultures were maintained in a culture chamber at a temperature of 25°C, a light intensity of 20-40 μmol m⁻² s⁻¹ and a 16/8h day/night cycle. To reach inoculation cell density the cultures were placed in a shake-incubator for three days at a continuous light intensity of 280 μmol m⁻² s⁻¹ and a headspace enriched with 5% CO₂.

Reactor set-up and experiments

Chlamydomonas reinhardtii was cultivated in turbidostat mode in a short light-path (SLP) photobioreactor, depicted schematically in Figure 5.3. This photobioreactor design is described in more detail in Kliphuis et al. (2010a). The photobioreactor had a working volume of 3.4 L, an annular gap width of 12 mm and an illuminated area (A_{pbr}) of 0.24 m². The inner cylinder was rotating at a speed of 70 rpm during the turbidostat cultivations, while the outer cylinder was stationary. To enable vertical back-mixing four down comers were drilled into the inner cylinder. Without down comers in the inner cylinder no vertical back mixing occurred and the algae accumulated in the top part of the photobioreactor. By adding the down comers, the algae were mixed over the whole annular gap. The light was provided continuously by 60 tungsten-halogen lamps (Philips Masterline ES 45W) surrounding the reactor. The photon flux density (PFD_{in}, μmol m⁻² s⁻¹) was measured with a LI-COR 190-SA 2π quantum sensor (PAR-range: 400-700 nm) at 80 fixed points inside the reactor before each experiment. The measured light intensities at all 80 points were averaged into a PFD_{in} for that particular experiment. An average incoming light intensity (PFD_{in}) of 600 μmol m⁻² s⁻¹ was used for the experiments.

During the experiments the light transmitted through the culture (μmol m⁻² s⁻¹) was measured by a spherical PAR quantum sensor (US-SQS Spherical Micro Quantum Sensor, Heinz Walz GmbH, Germany) placed inside the culture broth at the depth of the annular gap, 12 mm from the internal reactor wall, as illustrated in Figure 5.3. With this light sensor the turbidity of the culture was controlled by maintaining the photon flux density at this position (PFD_{out}) at 10 μmol m⁻² s⁻¹.

Assuming an exponential decrease of the photon flux density at increasing depth inside the photobioreactor the spatially averaged light intensity (PFD_{avg}) can be calculated

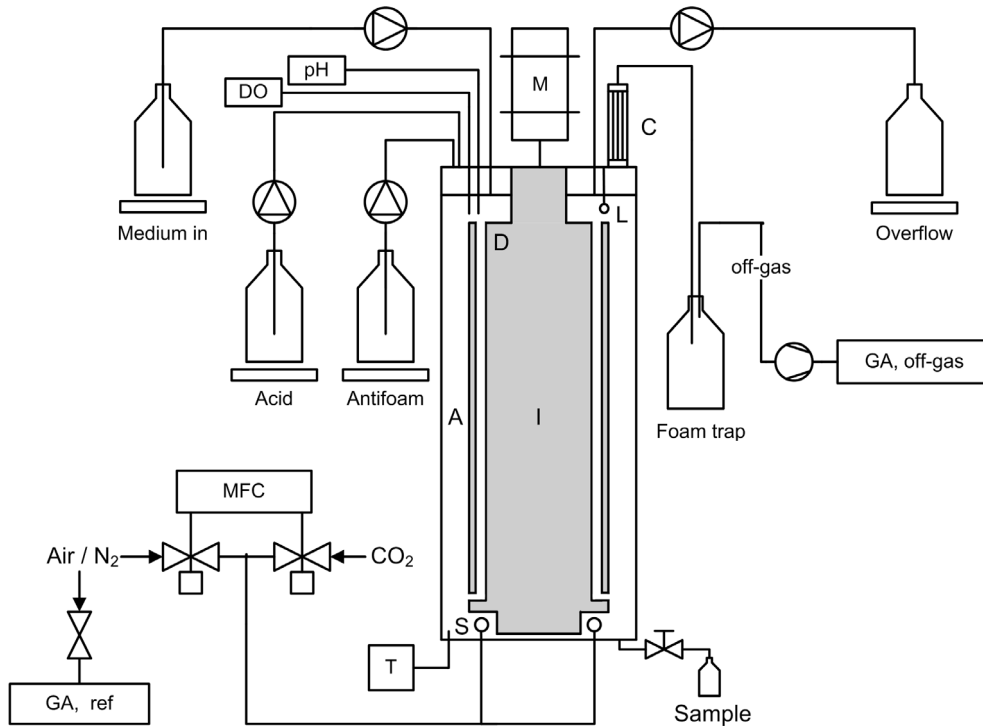


Figure 5.3 Schematic overview (not on scale) of the SLP photobioreactor. A = annular gap, C = condenser, D = internal down comer, DO = dissolved oxygen sensor, GA = gas analyzer, I = inner cylinder, L = spherical quantum sensor, M = motor, MFC = Mass flow controllers for both N_2 or air and CO_2 , pH = pH sensor connected to acid pump via control unit, S = sparger, T = temperature control connected to cryostat and cooling jacket (not shown). The acid bottle, antifoam bottle, medium in and overflow bottle were placed on balances and weighed on-line.

based on equation 1. In which a is the attenuation coefficient of the microalgal broth (in m^{-1}) and d is the optical depth of the system (12 mm). With a PFD_{in} of $600 \mu mol m^{-2} s^{-1}$ and a PFD_{out} of $10 \mu mol m^{-2} s^{-1}$ the result is a PFD_{avg} of $144 \mu mol m^{-2} s^{-1}$.

$$PFD_{avg} = \frac{1}{d} \cdot \left\{ \frac{PFD_{in}}{-a} \cdot (e^{-a \cdot d} - 1) \right\} \quad (1)$$

$$\text{In which: } a = \frac{\ln\left(\frac{PFD_{out}}{PFD_{in}}\right)}{-d}$$

Using mass flow controllers (Brooks, Smart TMF 5850S), carbon dioxide was supplied by sparging nitrogen (N₂) or pressurized air (1.5 L min⁻¹) enriched with 1 or 2% CO₂ through a silicone ring sparger at the bottom of the reactor. This gas flow also served to remove excess oxygen from the culture broth.

Foam formation was prevented by adding antifoam (Antifoam B silicone emulsion, Mallinckrodt Baker B.V.) to the culture when foam formation was detected by a foam sensor. The pH was controlled at pH 6.7 ± 0.1 by pumping nitric acid (1.2 M), serving also as nitrogen source. The acid bottle, antifoam bottle, medium in and overflow bottle were placed on balances and weighed on-line. The reactor was kept at 25°C by a water jacket connected to a temperature-controlled water bath. To prevent water from evaporating into the off-gas the reactor was equipped with a condenser connected to a cryostat set at 2°C.

After inoculation at an optical density at 530 nm (OD₅₃₀) of 0.05, the culture was grown in batch mode until a sufficient optical density was reached. Then the medium supply was started, automatically controlled by the turbidity of the culture. The quantum sensor behind the annular gap measured the light transmitted through the culture and thus the turbidity of the culture. When this transmitted light was less than 10 μmol m⁻² s⁻¹, the culture was automatically diluted until this set-point was restored. The resulting dilution rate *D*, and as such the specific growth rate μ (in steady state $\mu = D$), was continuously monitored. This turbidostat operation was maintained until steady state was reached. In these experiments steady state was defined as a constant specific growth rate (i.e. dilution rate), optical density, biovolume and cell density (*C_x*, g L⁻¹) in the photobioreactor for at least 7 residence times.

Biomass samples were taken from the culture overflow and weighed off-line. When steady state was reached the overflow was collected on ice overnight to have enough biomass material for biomass composition determinations.

On-line gas analysis and calculations

The off-gas was analyzed by leading it over a gas analyzer (Servomex, 4100) fitted with two different gas sensor modules, a paramagnetic purity transducer to measure oxygen and an infrared 1500 transducer to measure carbon dioxide. Before each experiment, a dry and a wet baseline were measured to correct the experimental gas data for the volume change due to the consumption of CO₂ and the production of O₂ and the moisture content. The dry baseline was measured by leading 1.5 L min⁻¹ N₂ or air enriched with 1%

or 2% CO₂ over the gas analyzers. For the wet baseline the N₂ or air enriched with CO₂ was first sparged through the reactor, containing medium at the same temperature and pH as during the turbidostat experiment, and through the condenser before being analyzed. The total molar gas flow going in ($n_{\text{gas,in}}$, mmol h⁻¹) is corrected for the volume change due to the consumption of CO₂ and the production of O₂ and for the moisture content ($x_{\text{H}_2\text{O}}$) according to equations 2 and 3.

$$n_{\text{gas,out,exp}} = n_{\text{gas,in}} \cdot \frac{(1 - x_{\text{O}_2,\text{db}} - x_{\text{CO}_2,\text{db}})}{(1 - x_{\text{O}_2,\text{exp}} - x_{\text{CO}_2,\text{exp}} - x_{\text{H}_2\text{O}})} \quad (2)$$

$$x_{\text{H}_2\text{O}} = 1 - \frac{x_{\text{O}_2,\text{wb}}}{x_{\text{O}_2,\text{db}}} \quad (3)$$

With this corrected molar gas flow $n_{\text{gas,out,exp}}$ (mmol h⁻¹) and the molar fraction of oxygen ($x_{\text{O}_2,\text{exp}}$) and carbon dioxide ($x_{\text{CO}_2,\text{exp}}$) measured during the experiments, the oxygen production rate (OPR, mmol h⁻¹) and carbon dioxide uptake rate (CUR, mmol h⁻¹) are calculated according to equations 4 and 5.

$$\text{OPR} = \frac{n_{\text{gas,out,exp}} \cdot (x_{\text{O}_2,\text{exp}} - x_{\text{O}_2,\text{wb}})}{100} \quad (4)$$

$$\text{CUR} = \frac{n_{\text{gas,out,exp}} \cdot (x_{\text{CO}_2,\text{exp}} - x_{\text{CO}_2,\text{wb}})}{100} \quad (5)$$

The observed biomass yield on light energy ($Y_{\text{xE}}^{\text{obs}}$, g mol⁻¹) is defined as gram dry biomass formed per mol incident photons on the photobioreactor surface according to equation 6. The photon flux (PF_{in} , mmol h⁻¹) is calculated using the measured average photon flux density (PFD_{in} , μmol m⁻² s⁻¹) and the illuminated photobioreactor area A_{pbr} (m²) described earlier. We assumed that all consumed carbon is converted into biomass. The dry biomass C-molar mass (m_{biomass} , g mol⁻¹) was determined as described in the next paragraph.

$$Y_{\text{xE}}^{\text{obs}} = \frac{\text{CUR} \cdot m_{\text{biomass}}}{\text{PF}_{\text{in}}} \quad (6)$$

Biomass determinations

Cell number and cell size

Cell number and cell size were determined in duplicate with a Beckman Coulter Multisizer 3 (Beckman Coulter Inc., Fullerton USA, 50 µm orifice). The samples were diluted with filtered (0.2 µm) Coulter® Isoton® II dilution buffer to a cell concentration between $1 \cdot 10^5$ and $3 \cdot 10^5$ cells mL⁻¹. The cell number and cell size were used to calculate the total biovolume.

Dry Weight Determination

Whatman glass microfiber filters (Ø 55 mm, pore size 0.7 µm) were dried at 95°C overnight and placed in a desiccator to cool to room temperature. The empty filters were weighed and pre-wet with de-mineralized water. Two grams of sample were diluted with de-mineralized water and filtrated under mild vacuum. The filter was rinsed twice with de-mineralized water to remove adhering inorganic salts. The wet filters containing the samples were dried at 95°C overnight, allowed to cool to room temperature in a desiccator and weighed. The microalgal dry weight of the samples was then calculated from the difference in weight between the dry filters with and without biomass. Dry weight determinations were performed in triplicate.

Biomass composition

Liquid samples were centrifuged for 10 min at 1750 rcf and the resulting pellets were washed three times with de-mineralized water by re-suspending and centrifuging and stored at -20°C. Algae pellets stored at -20°C were freeze dried and ground to a fine powder. The freeze dried algae powder was used for all further biomass composition analyses.

Elemental Composition (C, H, O, N, ash)

C, H and N content were measured in duplicate for each steady state by combustion of the freeze dried algal powder at 925°C in the oven of an elemental analyzer (EA 1110, ThermoQuest CE Instruments). Ash content was determined by burning the freeze-dried algae samples in an oven at 550°C, so that all organic material was oxidized and the ash residue remained. From these determinations the O content and subsequently the dry biomass molar mass (m_{biomass} , g C-mol⁻¹) could be calculated (C, H, O, N and ash) (Duboc et al. 1999; Gurakan et al. 1990).

Lipids and pigments

Lipid content was determined gravimetrically after extraction of the freeze dried algal powder with a 5:4 methanol:chloroform mixture. This extraction was described by Lamers et al. (2010). The resulting total lipid extract contained all lipid-like compounds present in the algal cells, including pigments. Therefore the weight of the total lipid extract had to be corrected for the amount of pigments present. Pigments were determined spectrophotometrically after dissolving the lipid residue in methanol. The total pigment content was calculated using absorption equations for chlorophyll in methanol (Porra 2002). The relative fatty acid composition was determined by GC-analysis according to the method described by Bosma et al. (2008).

Carbohydrates

Carbohydrates were measured by treating the freeze dried algae powder with a phenol solution and concentrated sulphuric acid, according to Dubois et al. (1956) and Herbert et al. (1971). The absorbance of the resulting solution was measured at 483 nm. Pure glucose was used as a standard.

Protein content and amino acid composition

The nitrogen content of the biomass was determined on a Flash EA 1112 Protein Analyzer (Thermo Scientific, Waltham USA). To calculate the amount of protein from the nitrogen content a N to protein conversion factor of 4.58 ± 0.11 was used (Lourenço et al. 1998). This factor was determined specifically for several microalgal species at different growth phases.

The relative amino acid composition was determined by Ansynth Service BV (Berkel en Roodenrijs, The Netherlands), using classical ion-exchange liquid chromatography with post-column ninhydrin derivatisation and photometric detection. Proteins were hydrolyzed by acid hydrolysis prior to column injection. Cysteine, methionine and tryptophan were determined separately. Cysteine and methionine were measured by oxidation followed by acid hydrolysis, and tryptophan by alkaline hydrolysis followed by reverse phase HPLC.

Nucleic Acids

The nucleic acids DNA and RNA were not measured directly, but were calculated from cell number data. From the amount of different nucleotides in *Chlamydomonas reinhard-*

tii (Merchant et al. 2007) it could be calculated that each cell contains $1.3 \cdot 10^{-13}$ g DNA per cell. RNA was assumed to be present in a 28 fold higher concentration than DNA. Valle et al. (1981) determined this ratio RNA : DNA for *Chlamydomonas reinhardtii* by measuring DNA and RNA contents at various cell concentrations, by means of a fluorometric determination.

Metabolic model and flux balancing

A metabolic network describing the primary metabolism of *Chlamydomonas reinhardtii* was constructed as described in (Kliphuis et al. 2010c). The metabolism of an organism can be described by a set of reaction equations defining the stoichiometric conversion of substrates into products (Stephanopoulos et al. 1998). The stoichiometry matrix S contains the stoichiometric coefficients of the substrates and products for the different reactions in the metabolic network, which also includes the transport reactions over the membranes. To be able to calculate fluxes, mass balances are written for all the intracellular metabolites present in the network. Assuming steady state and neglecting the accumulation of intermediates, this results in the next set of linear equations:

$$A \cdot x = 0 \tag{7}$$

In which A is the transpose of the stoichiometry matrix S and x is the vector which contains the reaction rates.

The combination of the model with the measured rates resulted in two redundancy relations, a carbon balance and a combined redox/nitrogen balance. Before proceeding with flux calculations, we checked whether the rates were consistent using the redundancy relations and a Chi-square test. Subsequently, when the rates were consistent they were balanced according to van der Heijden et al. (1994). These balanced rates were then used as input for the model.

Linear programming/optimization was used to calculate flux distributions according to equation 8:

$$\begin{aligned} \text{Objective function : } & \max(c \cdot x) \\ \text{Constraints : } & A \cdot x = 0 \\ & LB \leq x \leq UB \end{aligned} \tag{8}$$

In which c contains the objective function and LB and UB are the lower and upper boundary of reaction rate x. In this study we used the objective functions 'minimize light use'

and 'maximize oxygenase reaction rate'. Constraints were set on transport fluxes depending on whether a compound was consumed or produced. In case a rate was measured, the transport rate was constrained to the measured value. Reactions that are irreversible were constrained to one direction. To solve the underdetermined parts constraints were set in such a way that flux distributions that are thermodynamically impossible were excluded. Mathcad 14.0 (M020, Parametric Technology Corporation, USA) was used for network analysis and Matlab (version 6.0.0.88, release 12, The MathWorks Inc., USA) was used for *in silico* simulations.

Results and Discussion

Experiments

To assess the effect of different $O_2 : CO_2$ ratios on the metabolism of *Chlamydomonas reinhardtii* we performed two separate turbidostat experiments in a SLP photobioreactor, in which four steady states were studied. In the first experiment (1) the control steady state in which the culture was sparged with N_2 enriched with 2% CO_2 was studied. In the second experiment (2) the two other steady states in which the culture was sparged with air enriched with either 2% CO_2 or 1% CO_2 were studied. At the end of this second experiment the control steady state was repeated to check the reproducibility of the system.

Figure 5.4 shows the biomass concentration, the oxygen production rate (OPR) and the carbon dioxide uptake rate (CUR) for the steady states during the second experiment. Since the control steady states were comparable, only the results of the second experiment are shown in Figure 5.4. Vertical dotted lines indicate the switch from one condition to the next. The fluctuations in the gas data coincide with the cell cycles of the algae (approx. 24h) and the steady states were therefore taken over multiples of 24 hours (horizontal bars in Figure 5.4). In this experiment we started by sparging the culture with air enriched with 2% CO_2 until steady state was reached, indicated with a horizontal bar. Then the concentration CO_2 was lowered to 1% in the ingoing gas and the OPR and CUR decreased. Finally, as stated, we switched back to N_2 enriched with 2% CO_2 similar to the steady state in experiment 1 to check whether the experiments were reproducible. Upon this decrease in O_2 and increase in CO_2 the OPR and CUR immediately increased. For all steady states the biomass concentration stayed the same as regulated by the turbidity control. At steady state the measured dilution rate D was equal to the specific growth rate μ .

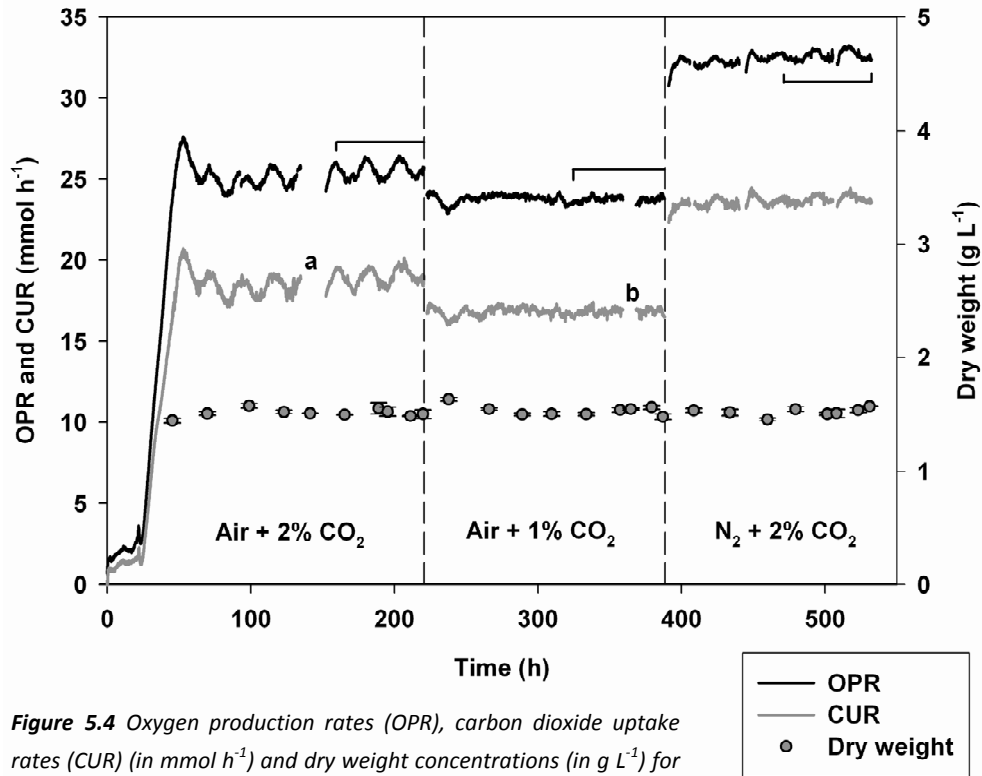


Figure 5.4 Oxygen production rates (OPR), carbon dioxide uptake rates (CUR) (in $mmol h^{-1}$) and dry weight concentrations (in $g L^{-1}$) for a turbidostat experiment with three different steady states. The vertical dotted lines represent the transitions from one condition to the next. The horizontal bars indicate the steady states for each condition. In the OPR and CUR lines some gaps can be seen, indicated by lowercase letters a and b, which are caused by excess addition of antifoam, leading to a disruption in the gas data.

The steady state results are summarized in Table 5.2 in which the measured PFD_{in} and calculated PFD_{avg} for each experiment is given along with the measured specific growth rate μ (i.e. dilution rate D), dry weight concentration C_x and biomass yield on light energy Y_{xE} (calculated with equation 6) for each steady state. The microalgae are exposed to a light gradient in the photobioreactor and thus are not continuously exposed to the incoming PFD_{in} . Therefore the spatially averaged PFD_{avg} (equation 1) gives a better measure of the light intensity that the microalgae experience and photoinhibition is unlikely to occur at these light intensities.

The slightly lower growth rate and CUR for the control steady state in the first experiment (1) compared to the control steady state in the second experiment (2) is due to the

Table 5.2 Overview of the incoming and average light intensity, specific growth rate μ , dry weight concentration C_x , average CUR, and biomass yield on light energy $Y_{x/E}$ for the examined steady states.

Steady state	PFD _{in} ($\mu\text{mol m}^{-2} \text{s}^{-1}$)	PFD _{avg} ^a ($\mu\text{mol m}^{-2} \text{s}^{-1}$)	Growth rate μ (h^{-1})	Dry weight C_x (g L^{-1})	CUR (mmol h^{-1})	Biomass yield $Y_{x/E}$ (g mol^{-1})
N ₂ + 2% CO ₂ (1)	606	145	0.092 ± 0.004	1.58 ± 0.06	22.02 ± 0.60	0.97 ± 0.03
N ₂ + 2% CO ₂ (2)	635	151	0.100 ± 0.004	1.53 ± 0.05	23.76 ± 0.22	1.00 ± 0.01
Air + 2% CO ₂ (2)	635	151	0.081 ± 0.004	1.51 ± 0.07	18.98 ± 0.46	0.79 ± 0.02
Air + 1% CO ₂ (2)	635	151	0.078 ± 0.003	1.52 ± 0.04	16.85 ± 0.17	0.70 ± 0.01

^a PFD_{out} was always maintained at 10 $\mu\text{mol m}^{-2} \text{s}^{-1}$ by means of the turbidostat control

slightly lower PFD_{in} in experiment 1. Apart from this the two control steady states with N₂ and 2% CO₂ were similar, which also proves that the experiments are reproducible.

The $Y_{x/E}$ for the steady states with N₂ was around 1.00 g mol^{-1} . This is high considering that at very low light intensities (around 80 $\mu\text{mol m}^{-2} \text{s}^{-1}$) we determined a biomass yield of 1.25 g mol^{-1} for *C. reinhardtii* (Kliphuis et al. 2010c), which seems to approach the maximal yield for *C. reinhardtii*. This illustrates the high yield that can be reached with microalgae cultures under optimal conditions. These optimal conditions are low O₂ concentrations and high CO₂ concentrations as well as a biomass density at which light can fully penetrate the culture but is almost completely absorbed. In a previous study (Kliphuis et al. 2010a) we determined that the highest productivity of a *Chlorella sorokiniana* culture occurred at the point where all light was almost attenuated when reaching the quantum sensor at the end of the annular gap. No dark zone had developed yet and thus there was still light available for all microalgal cells. For this reason we selected a set-point for the current turbidostat experiments of 10 $\mu\text{mol m}^{-2} \text{s}^{-1}$, the light intensity transmitted through the annular gap, and hence no dark zone could develop.

Changing the ingoing gas composition to air with 2% CO₂ and subsequently to air with 1% CO₂, thus increasing the O₂ : CO₂ ratio in the medium, caused a decrease in the specific growth rate and in the yield of biomass on light. The yield of biomass on light decreased from 1.0 g mol^{-1} for N₂ with 2% CO₂ to respectively 0.79 and 0.71 g mol^{-1} for air with 2% CO₂ and air with 1% CO₂. The $Y_{x/E}$ for the steady states in which air was used are comparable to the yields found by Takache et al. (2010) for *C. reinhardtii*. They found a $Y_{x/E}$ of 0.73 g mol^{-1} at a PFD_{in} of 500 $\mu\text{mol m}^{-2} \text{s}^{-1}$ for a culture sparged with air and CO₂ on demand as

pH control. However, Takache et al. used ammonium (NH₄⁺) as N-source, a more reduced source than nitrate (NO₃⁻) which we used in our cultivations. Using a more reduced N-source higher biomass yields can be obtained and our biomass yield is thus high compared to the yield obtained by Takache et al..

Because the light regime was always the same during the turbidostat experiments and nutrients were supplied in excess, the change in the specific growth rate and the biomass yield on light energy were only dependent on the O₂ : CO₂ ratio in the ingoing gas and thus in the medium.

Modeling

To quantify the effect of the O₂ : CO₂ ratio on the metabolism of *Chlamydomonas reinhardtii* the metabolic flux distribution was calculated for the different steady states. For this purpose a metabolic network describing the primary metabolism of *Chlamydomonas reinhardtii* was used, which was constructed as described in (Kliphuis et al. 2010c) and shown in the Appendix. This model includes the ATP requirements for maintenance and biomass formation for *C. reinhardtii*. The light utilization rate $r_{Ex,U}$, CUR, OPR, biomass formation rate and the biomass composition were used as inputs for the model. Since the biomass composition may be different for the different steady states, the macromolecular biomass composition (%w/w) was determined for each steady state. As shown in Table 5.3 the biomass composition for the different steady states was not significantly different. There seems to be some variation in carbohydrate content between the steady states, but since only a duplicate measurement was done this is statistically not significant. The average dry biomass molar mass $m_{biomass}$ was determined to be $23.08 \pm 0.16 \text{ g mol}^{-1}$.

The biomass compositions were used for the model simulations by filling in the molar biomass composition normalized to 100% in reaction 147 (Appendix A) for each steady state. The elemental composition of the macromolecules and the biomass for each steady state are given in Appendix C and D. Since the protein and lipid composition did not vary significantly between the steady states, both for protein and lipids the average composition was used in all simulations. These average amino acid and fatty acid compositions can be found in Appendix D and E.

For the measured rates there are two balances that need to be closed, being a carbon balance and a combined nitrogen/redox balance. For all steady states these two balances closed. Subsequently the rates were balanced and used as input for the metabolic model. The balanced rates are shown in Table 5.4.

Table 5.3 Measured biomass composition (% w/w) of *C. reinhardtii* at different steady state conditions, including the standard deviations. The sum of the individual biomass components including ash was comparable to the measured dry weights within 10%.

	Steady state			
	N ₂ + 2% CO ₂ (1)	N ₂ + 2% CO ₂ (2)	Air + 2% CO ₂ (2)	Air + 1% CO ₂ (2)
Protein ^a	46.1 ± 0.8	45.2 ± 0.8	46.3 ± 0.79	45.9 ± 0.8
Carbohydrate ^a	26.6 ± 1.1	20.5 ± 1.8	20.8 ± 2.4	22.1 ± 1.8
Lipids ^b	13.5 ± 1.1	11.1 ± 0.6	14.2 ± 0.9	11.8 ± 1.0
DNA ^c	0.11 ± 0.007	0.07 ± 0.003	0.12 ± 0.009	0.11 ± 0.004
RNA ^c	3.0 ± 0.2	2.0 ± 0.1	3.3 ± 0.2	3.0 ± 0.1
Chlorophyll ^a	4.2 ± 0.4	3.8 ± 0.4	4.4 ± 0.3	4.4 ± 0.1
Ash ^d	5.9	6.3	6.6	5.3
Total	99 ± 1.7	90 ± 3.2	96 ± 2.7	93 ± 2.2

^a N = 2

^b N = 3

^c N = 5, Based on literature values (Merchant et al. 2007; Valle et al. 1981) and the measured dry weight and cell numbers.

^d N = 1

Table 5.4 Balanced input parameters for the metabolic model at different steady states. The biomass production was calculated from the measured specific growth rate μ . The light utilization rate $r_{Ex,u}$ for both N₂ steady states was calculated with the model as described in the text.

Steady state	Biomass prod. (mmol g ⁻¹ h ⁻¹)	OPR (mmol g ⁻¹ h ⁻¹)	CUR (mmol g ⁻¹ h ⁻¹)	$r_{Ex,u}$ (mmol g ⁻¹ h ⁻¹)
N ₂ + 2% CO ₂ (1)	0.59 ± 0.02	5.47 ± 0.14	3.89 ± 0.10	67.00 ± 2.62
N ₂ + 2% CO ₂ (2)	0.68 ± 0.01	6.18 ± 0.12	4.33 ± 0.09	75.59 ± 2.38
Air + 2% CO ₂ (2)	0.52 ± 0.02	4.94 ± 0.14	3.46 ± 0.10	75.52 ± 3.71
Air + 1% CO ₂ (2)	0.49 ± 0.01	4.57 ± 0.08	3.21 ± 0.05	74.87 ± 1.90

Even at low light intensities not all light is taken up by the photosystem and the maximum efficiency of the photosystems ($\Phi_{P_{max}}$) is 0.8, which corresponds to a quantum requirement of oxygen evolution of 10 (instead of 8 according to the Z-scheme). This is in accordance with measurements of the quantum requirement under ideal low-light conditions for a variety of organisms using a variety of experimental techniques (Bjorkman and Demmig 1987; Dubinsky et al. 1986; Emerson and Lewis 1943; Evans 1987; Ley and Mauzerall 1982; Malkin and Fork 1996; Tanada 1951). Since the experiments in this study are done at higher light intensities the efficiency with which light is used is probably lower than 0.8. Thus, to calculate the light utilization rate, which is used as an input for the model, first the efficiency factor for these experiments must be calculated. The duplicate control steady states with N₂ and 2% CO₂ were used to determine this efficiency of light use, i.e. the amount of light that was utilized by the photosystem of the algae to form biomass with growth rate μ for that steady state. In the case of these steady states we assume that the O₂ : CO₂ ratio is so low that the rate of the oxygenase reaction approaches zero and photorespiration does not occur. The specific light utilization rate $r_{Ex,u}$ was calculated by constraining all measured rates and minimizing the light reaction (reaction 0 in the Appendix). The obtained light uptake rate (reaction 155) represents the minimal $r_{Ex,u}$ that was necessary to form the measured amount of biomass. This value was less than the light supplied to the microalgal culture per gram dry weight, r_{Ex} , since not all light was used efficiently by the microalgal photosystems. By comparing the specific light utilization rate $r_{Ex,u}$ with the specific light supply rate r_{Ex} the photochemical quantum yield Φ_p could be determined according to equation 9. This photochemical quantum yield Φ_p is a measure for the efficiency of light use of the microalgae in these turbidostat experiments.

$$r_{Ex,u} = \Phi_p \cdot r_{Ex} = \Phi_p \cdot \frac{PFD_{in} \cdot A_{pbr}}{C_x \cdot V_{pbr}} \quad (9)$$

In which PFD_{in} is the measured incoming photon flux density for that experiment (here in $mmol\ m^{-2}\ h^{-1}$), A_{pbr} is the illuminated photobioreactor area (m^2), C_x is the steady state biomass concentration ($g\ L^{-1}$) and V_{pbr} is the working volume of the photobioreactor (L). Table 5.4 shows the $r_{Ex,u}$ as calculated with the model for both control steady states. The difference in these specific values is caused by the differences in PFD_{in} and C_x (Table 5.2) between both steady states but this eventually translates in similar photochemical quantum yields. For the first control steady state (1) the Φ_p was 0.70 and for the second con-

trol steady state (2) the Φ_p was 0.72. This means that on average 71% of the light was used efficiently and the rest was dissipated as heat or fluorescence. This value is quite high considering the maximum value of 80%, which was obtained at much lower light intensities than used here. This confirms that photorespiration, photoinhibition and the Mehler reaction do not, or hardly occur under these conditions, since these would result in a lower efficiency.

Because the experiments were done in turbidostat mode, the biomass concentration was more or less constant for all steady states and thus the amount of light supplied per gram dry weight was constant. Therefore it can be safely assumed that Φ_p is also constant for all steady states and for the calculation of the specific light utilization rate for the other steady states, the average of these two values, 0.71 was used. Furthermore, since only the $O_2 : CO_2$ ratio changes we assume that photorespiration is the main cause for the decrease in the biomass yield on light energy.

With the calculated Φ_p the $r_{Ex,u}$ could be calculated for the other steady states in which air was used (Table 5.4) by multiplying with the specific light supply rate for those steady states. Again the variation in these biomass specific values is due to the small variation in C_x between steady states. To calculate the flux through photorespiration for the steady states with air, the $r_{Ex,u}$ (light uptake rate, reaction 155), specific carbon and oxygen production rate and the biomass production rate (calculated from the growth rate μ , reaction 147) were constrained to their measured, balanced values. Subsequently, the flux through the oxygenase reaction of Rubisco (reaction 91) was maximized. Because the light utilization rate was the same for all steady states the amount of energy (ATP) generated in all conditions was also the same. Since at higher $O_2 : CO_2$ ratios less biomass was formed, less energy was needed for biomass formation and there was an excess of energy in these steady states. By maximizing the flux through the oxygenase reaction all this 'excess' ATP generated from light which was not necessary to form biomass will be consumed in the photorespiratory pathway. Thus, for each steady state the rate through the oxygenase reaction and thus the rate of photorespiration responsible for the observed decrease in biomass yield on light was calculated, as well as the fluxes through the rest of the metabolism.

Figure 5.5 (separate figure sheet) shows the flux distribution through the metabolic network for steady states $N_2 + 2\% CO_2$ (2) (red boxes) and air + 2% CO_2 (2) (black boxes). The flux through the light reaction of photosynthesis (reaction 0) is almost equal for both

situations because the specific light utilization rate is similar for all steady states as explained before. The fluxes through the carboxylase and the oxygenase reaction of Rubisco are shown in the chloroplast for both situations. In the steady state with N₂ the flux through the oxygenase reaction and the subsequent reactions to Glycerate 3-phosphate are zero as assumed. At air with 2% CO₂ the flux through the oxygenase reaction increases to 1.45 mmol g⁻¹ h⁻¹. At the same time the flux through the carboxylase reaction decreases from 9.45 to 8.72 mmol g⁻¹ h⁻¹. Furthermore, the 'lost' NH₄⁺ needs to be re-fixed in the metabolism, causing an increase in the flux to Glutamate (reaction 58) from 0.76 to 1.31 mmol g⁻¹ h⁻¹. Finally, since the growth rate is lower for this steady state fluxes for the biosynthesis of biomass components decrease.

The ratio between the carboxylase reaction and the oxygenase reaction is given in Table 5.5 alongside the O₂ and CO₂ concentrations in the medium for all steady states. These medium concentrations were calculated with the method described by Royce and Thornhill (1991). This method is based on the measured OPR and dissolved oxygen (DO) concentration to calculate the mass transfer coefficient for O₂ and subsequently CO₂, followed by the calculation of the dissolved carbon dioxide concentration. The ratio between the carboxylase reaction and the oxygenase reaction gives the amount of photorespiration for each steady state. When switching from N₂ with 2% CO₂ to air with 2% CO₂ the oxygen concentration increases about threefold and the O₂ : CO₂ ratio increases twofold, coinciding with an increase in photorespiration to 16.5%. When the concentration CO₂ is decreased from 2% to 1% in the ingoing gas the O₂ concentration slightly decreases to 305 mM. Due to the strong decrease in CO₂ concentration the ratio of O₂ : CO₂ again increases twofold. However, this results in only a small additional increase in

Table 5.5 Dissolved oxygen concentrations ([O₂]_{ol}), dissolved carbon dioxide concentrations ([CO₂]_{ol}) and the ratio of dissolved O₂ : CO₂ at each steady state. The amount of photorespiration was calculated with the metabolic model as the ratio of the oxygenase reaction to the carboxylase reaction rate of Rubisco.

Steady state	[O ₂] _{ol} (μmol L ⁻¹)	[CO ₂] _{ol} (μmol L ⁻¹)	Ratio O ₂ : CO ₂	% photorespiration
N ₂ + 2% CO ₂ (1)	141	460	1 : 3.3	-
N ₂ + 2% CO ₂ (2)	142	451	1 : 3.2	-
Air + 2% CO ₂ (2)	329	527	1 : 1.6	16.5 ± 5.5
Air + 1% CO ₂ (2)	305	217	1 : 0.7	20.5 ± 2.9

photorespiration from 16.5% to 20.5%. The fact that this additional increase in photorespiration is so small could be explained from the fact that the concentrations for O₂ and CO₂ are medium concentrations, which very well may not be representative for the concentrations near Rubisco. The carbon concentrating mechanism (CCM) which *C. reinhardtii* possesses could keep the CO₂ concentration near Rubisco high and reduce the oxygenase flux. Although according to Ghoshal and Goyal (2001) and Ogren (1984) the CCM is probably not induced at the CO₂ concentrations used here, their findings were based on the CO₂ concentration in the ingoing gas and not on the dissolved CO₂ concentrations in the culture broth. Therefore, we cannot exclude the presence and activity of a CCM which could explain the smaller effect of decreased CO₂ concentrations compared to increased O₂ concentrations.

The calculated photorespiration rates are realistic values (Hoefnagel et al. (1998) reports 20 - 35% photorespiration under normal conditions), showing that photorespiration can indeed explain the reduction in biomass yield on light. However, this is based on the assumption that the Mehler reaction and photoinhibition do not occur. Although at the used conditions of average light intensities and high growth rates this assumption is justified, knowledge on when these processes occur in *C. reinhardtii* is still limited. Therefore, it remains to be validated that only photorespiration was responsible for the observed decrease in specific growth rate. Despite this remaining uncertainty, this metabolic flux model gives insight in the metabolism of *C. reinhardtii* at higher O₂ : CO₂ ratios and quantifies photorespiration and its implications of on the biomass yield on light energy of the microalgae.

Conclusion

In conclusion, this study shows that elevated oxygen concentrations and the corresponding increase in the ratio of O₂ versus CO₂ common in photobioreactors leads to a reduction of the biomass yield on light of the microalgae *Chlamydomonas reinhardtii*. A reduction in yield of 20% was already observed at conditions common in photobioreactors (air with 2% CO₂). Using metabolic flux modeling with measured rates for each steady state we were able to quantify the ratio of the oxygenase reaction to the carboxylase reaction of Rubisco. This showed that the observed decrease in yield can be explained from an increase in oxygenase activity of Rubisco and the resulting process of photorespiration, up to 20.5% of the carboxylase activity.

Nomenclature

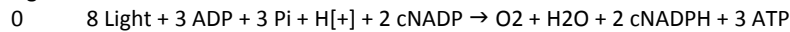
μ	Specific growth rate (h^{-1})
Φ_p	Photochemical quantum yield (-)
$\Phi_{p\max}$	Maximum photochemical quantum yield (-)
A_{pbr}	Illuminated photobioreactor area (m^2)
CUR	Carbon dioxide uptake rate (mmol h^{-1})
C_x	Biomass concentration (dry weight) in the photobioreactor (g L^{-1})
D	Dilution rate (h^{-1})
K_m	affinity constant for carbon dioxide ($\mu\text{mol L}^{-1}$)
m_{biomass}	Measured C-molar mass of dry biomass (C, H, O, N and ash) (g C-mol^{-1})
N	Number of measurements (-)
$n_{\text{gas,in}}$	Total molar gas flow going into the reactor (mmol h^{-1})
$n_{\text{gas,out,exp}}$	Total molar gas flow going out of the reactor corrected for moisture content and volume change (mmol h^{-1})
OD_{530}	Optical density measured at 530 nm on a spectrophotometer (-)
OPR	Oxygen production rate (mmol h^{-1})
PAR	Photosynthetic active radiation, all photons between 400 and 700 nm (-)
PFD_{avg}	Spatially averaged light intensity ($\mu\text{mol m}^{-2} \text{s}^{-1}$)
PFD_{in}	Incoming photon flux density ($\mu\text{mol m}^{-2} \text{s}^{-1}$)
PFD_{out}	Photon flux density falling through the culture ($\mu\text{mol m}^{-2} \text{s}^{-1}$)
PF_{in}	Photon flux on the surface of the photobioreactor (mmol h^{-1})
PQ	Photosynthetic quotient (-)
r_{Ex}	Specific light supply rate ($\text{mmol g}^{-1} \text{h}^{-1}$)
$r_{\text{Ex,u}}$	Specific light utilization rate ($\text{mmol g}^{-1} \text{h}^{-1}$)
V_{pbr}	Photobioreactor volume (L)
$x_{\text{CO}_2,\text{db}}$	Molar fraction of CO ₂ in dry baseline (-)
$x_{\text{CO}_2,\text{exp}}$	Molar fraction of CO ₂ in experimental gas data (-)
$x_{\text{CO}_2,\text{wb}}$	Molar fraction of CO ₂ in wet baseline (-)
$x_{\text{H}_2\text{O}}$	Molar fraction of moisture in the gas (-)
$x_{\text{O}_2,\text{db}}$	Molar fraction of O ₂ in dry baseline (-)
$x_{\text{O}_2,\text{exp}}$	Molar fraction of O ₂ in experimental gas data (-)
$x_{\text{O}_2,\text{wb}}$	Molar fraction of O ₂ in wet baseline (-)
$Y_{\text{xE}}^{\text{obs}}$	Observed experimental biomass yield on light energy (g mol^{-1})

Appendix

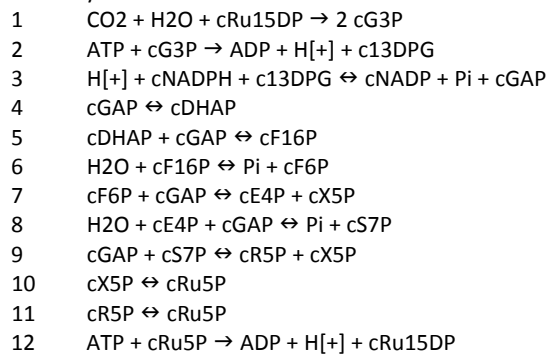
A. Metabolic model of *Chlamydomonas reinhardtii*

Arrows indicate the direction and reversibility of the reactions. The compounds in the chloroplast are notated with a 'c' before the abbreviation. All fluxes are in $\text{mmol g}^{-1} \text{h}^{-1}$. The flux through reaction 57, the ATP requirement for maintenance, was set to 2.582 $\text{mmol g}^{-1} \text{h}^{-1}$ as determined for *C. reinhardtii* in a previous study (Kliphuis et al. 2010c). The factor (given by x) in the biomass export reaction (159) converts the biomass flux through reaction 147 (in $\text{mmol g}^{-1} \text{h}^{-1}$) to $\text{mg g}^{-1} \text{h}^{-1}$, the biomass production rate. The amount of macromolecule (given by lowercase letters) to produce one mol of biomass in reaction 147 depends on the biomass composition for each steady state.

Light reaction



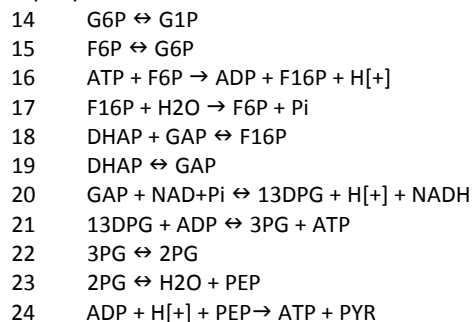
Calvin cycle



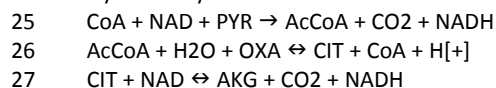
Transport chloroplast to cytosol



Glycolysis



Tricarboxylic acid cycle



Effect of O₂ : CO₂ ratio on the primary metabolism of Chlamydomonas reinhardtii

- 28 AKG + CoA + NAD → CO₂ + NADH + SUCCoA
29 ADP + Pi + SUCCoA ↔ ATP + CoA + SUC
30 FAD + SUC ↔ FADH₂ + FUM
31 FUM + H₂O ↔ MAL
32 FAD + MAL ↔ FADH₂ + OXA
33 ATP + CO₂ + H₂O + PYR → ADP + OXA + Pi + 2 H⁺
34 ATP + OXA → ADP + CO₂ + PEP
35 CO₂ + H₂O + PEP ↔ H⁺ + OXA + Pi

Pentose phosphate pathway

- 36 G6P + H₂O + NADP ↔ 6PG + NADPH + 2 H⁺
37 6PG + NADP ↔ CO₂ + NADPH + RU5P
38 RU5P ↔ R5P
39 RU5P ↔ X5P
40 R5P + X5P ↔ GAP + S7P
41 GAP + S7P ↔ E4P + F6P
42 F6P + GAP ↔ E4P + X5P

Glycerol

- 43 DHAP + H₂O ↔ DHA + Pi
44 DHA + H⁺ + NADPH ↔ GLYC + NADP
45 ATP + GLYC → ADP + GLYC3P + H⁺
46 GLYC3P + NAD ↔ DHAP + H⁺ + NADH

N and S fixation

- 47 H⁺ + NADH + NO₃ ↔ H₂O + NAD + NO₂
48 5 H⁺ + 3 NADPH + NO₂ ↔ NH₄⁺ + 2 H₂O + 3 NADP
49 ATP + SO₄ → APS + PPi
50 APS + NADH → AMP + NAD + SO₃
51 5 H⁺ + 3 NADPH + SO₃ ↔ H₂S + 3 H₂O + 3 NADP

Oxidative phosphorylation

- 52 1.5 ADP + 1.5 H⁺ + 1.5 Pi + FADH₂ + 0.5 O₂ → FAD + 1.5 ATP + 2.5 H₂O
53 3.5 H⁺ + 2.5 ADP + 2.5 Pi + NADH + 0.5 O₂ → NAD + 2.5 ATP + 3.5 H₂O
54 NAD + NADPH → NADH + NADP
55 H₂O + PPi → H⁺ + 2 Pi
56 AMP + ATP → 2 ADP
57 ATP + H₂O → ADP + H⁺ + Pi

Amino acids and protein

- 58 AKG + H⁺ + NADPH + NH₄⁺ → GLU + H₂O + NADP
59 ATP + GLU + NH₄⁺ → ADP + GLN + H⁺ + Pi
60 AKG + GLN + H⁺ + NADPH ↔ NADP + 2 GLU
61 3PG + GLU + H₂O + NAD ↔ AKG + H⁺ + NADH + Pi + SER
62 SER → NH₄⁺ + PYR
63 AcCoA + H₂S + SER ↔ Ace + CYS + CoA + H⁺
64 ATP + Ace + CoA → ADP + AcCoA + Pi
65 GLU + PYR → AKG + ALA
66 H⁺ + THR ↔ 2-oxobutan + NH₄⁺
67 2-oxobutan + GLU + H⁺ + NADPH + PYR ↔ AKG + CO₂ + H₂O + ILE + NADP

Chapter 5

- 68 $2 \text{ H}^{+} + \text{ALA} + \text{NADPH} + \text{PYR} \rightleftharpoons \text{CO}_2 + \text{H}_2\text{O} + \text{NADP} + \text{VAL}$
69 $2 \text{ PYR} + \text{AcCoA} + \text{GLU} + \text{H}^{+} + \text{NAD} + \text{NADPH} \rightleftharpoons \text{AKG} + \text{CoA} + \text{LEU} + \text{NADH} + \text{NADP} + 2 \text{ CO}_2$
70 $2 \text{ PEP} + \text{ATP} + \text{E4P} + \text{NADPH} \rightarrow \text{ADP} + \text{CHO} + \text{NADP} + 4 \text{ Pi}$
71 $\text{CHO} \rightleftharpoons \text{PRE}$
72 $\text{GLU} + \text{H}^{+} + \text{PRE} \rightleftharpoons \text{AKG} + \text{CO}_2 + \text{H}_2\text{O} + \text{PHE}$
73 $\text{GLU} + \text{NAD} + \text{PRE} \rightleftharpoons \text{AKG} + \text{CO}_2 + \text{NADH} + \text{TYR}$
74 $\text{CHO} + \text{GLN} \rightleftharpoons \text{ANTH} + \text{GLU} + \text{H}^{+} + \text{PYR}$
75 $\text{ANTH} + \text{H}^{+} + \text{PRPP} + \text{SER} \rightleftharpoons \text{CO}_2 + \text{GAP} + \text{PPi} + \text{TRYP} + 2 \text{ H}_2\text{O}$
76 $3 \text{ H}_2\text{O} + 2 \text{ NAD} + \text{ATP} + \text{GLN} + \text{PRPP} \rightarrow \text{AICAR} + \text{AKG} + \text{HIS} + \text{Pi} + 2 \text{ NADH} + 2 \text{ PPi} + 5 \text{ H}^{+}$
77 $\text{GLU} + \text{OXA} \rightleftharpoons \text{AKG} + \text{ASP}$
78 $\text{ASP} + \text{ATP} + \text{GLN} + \text{H}_2\text{O} \rightarrow \text{ADP} + \text{ASN} + \text{GLU} + \text{H}^{+} + \text{Pi}$
79 $2 \text{ ATP} + 2 \text{ H}_2\text{O} + \text{CO}_2 + \text{GLN} \rightarrow \text{CaP} + \text{GLU} + \text{Pi} + 2 \text{ ADP} + 3 \text{ H}^{+}$
80 $2 \text{ GLU} + \text{ASP} + \text{ATP} + \text{CaP} + \text{NADH} \rightarrow \text{AKG} + \text{AMP} + \text{ARG} + \text{FUM} + \text{H}_2\text{O} + \text{NAD} + \text{PPi} + \text{Pi}$
81 $3 \text{ H}^{+} + 2 \text{ NADH} + \text{GLU} \rightleftharpoons \text{PRO} + 2 \text{ H}_2\text{O} + 2 \text{ NAD}$
82 $\text{AKG} + \text{O}_2 + \text{PRO} \rightleftharpoons \text{CO}_2 + \text{HydPro} + \text{SUC}$
83 $\text{ASP} + \text{ATP} + \text{H}^{+} + \text{NADPH} \rightarrow \text{ADP} + \text{ASA} + \text{NADP} + \text{Pi}$
84 $2 \text{ H}^{+} + \text{ASA} + \text{GLU} + \text{NADH} + \text{PYR} \rightleftharpoons \text{AKG} + \text{DAP} + \text{H}_2\text{O} + \text{NAD}$
85 $\text{DAP} \rightleftharpoons \text{CO}_2 + \text{H}^{+} + \text{LYS}$
86 $\text{ASA} + \text{H}^{+} + \text{NADPH} \rightleftharpoons \text{HSER} + \text{NADP}$
87 $\text{ATP} + \text{H}_2\text{O} + \text{HSER} \rightarrow \text{ADP} + \text{H}^{+} + \text{Pi} + \text{THR}$
88 $\text{AcCoA} + \text{CYS} + \text{H}_2\text{O} + \text{HSER} \rightleftharpoons \text{Ace} + \text{CoA} + \text{HCYS} + \text{H}^{+} + \text{NH}_4^{+} + \text{PYR}$
89 $\text{HCYS} + \text{MTHF} \rightleftharpoons \text{H}^{+} + \text{MET} + \text{THF}$
90 $4.306 \text{ ATP} + 3.306 \text{ H}_2\text{O} + 0.111 \text{ ALA} + 0.092 \text{ GLY} + 0.09 \text{ LEU} + 0.061 \text{ VAL} + 0.06 \text{ LYS} + 0.056 \text{ PRO} + 0.056 \text{ THR} + 0.054 \text{ SER} + 0.052 \text{ ARG} + 0.052 \text{ GLN} + 0.052 \text{ GLU} + 0.047 \text{ ASN} + 0.047 \text{ ASP} + 0.041 \text{ PHE} + 0.037 \text{ ILE} + 0.03 \text{ TYR} + 0.024 \text{ MET} + 0.017 \text{ HIS} + 0.012 \text{ CYS} + 0.009 \text{ HydPro} + 0.001 \text{ TRYP} \rightarrow \text{PROTEIN} + 4.306 \text{ ADP} + 4.306 \text{ Pi} + 4.319 \text{ H}^{+}$

Photorespiration

- 91 $\text{H}_2\text{O} + \text{NAD} + \text{O}_2 + \text{cRu15DP} \rightarrow \text{H}^{+} + \text{NADH} + \text{Pi} + \text{cG3P} + \text{glyoxylate}$
92 $\text{GLY} + \text{H}^{+} + \text{PYR} \rightleftharpoons \text{ALA} + \text{glyoxylate}$
93 $\text{SER} + \text{glyoxylate} \rightleftharpoons \text{GLY} + \text{HydPyr}$
94 $\text{GLY} + \text{H}_2\text{O} + \text{METHF} \rightleftharpoons \text{SER} + \text{THF}$
95 $\text{GLY} + \text{NAD} + \text{THF} \rightleftharpoons \text{CO}_2 + \text{METHF} + \text{NADH} + \text{NH}_4^{+}$
96 $\text{H}^{+} + \text{HydPyr} + \text{NADH} \rightleftharpoons \text{Glycerate} + \text{NAD}$
97 $\text{ATP} + \text{Glycerate} \rightarrow \text{ADP} + 2 \text{ H}^{+} + 3 \text{ PG}$

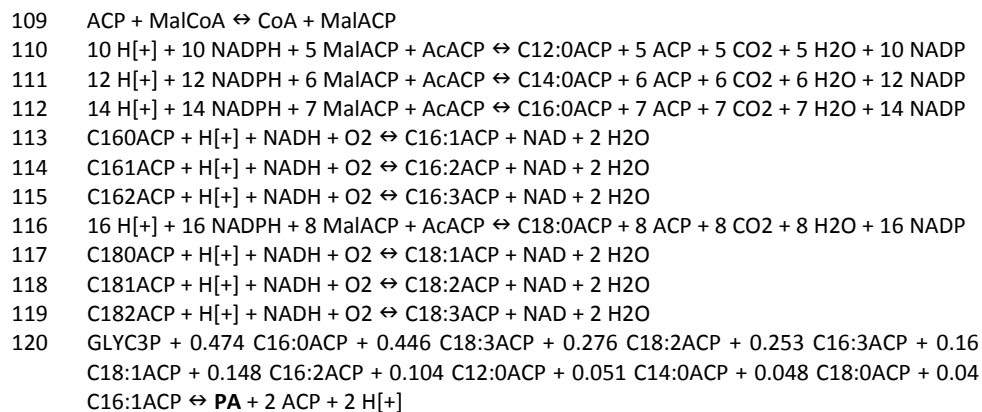
THF metabolism

- 98 $\text{ATP} + \text{R5P} \rightarrow \text{AMP} + \text{H}^{+} + \text{PRPP}$
99 $5\text{FTHF} + \text{H}^{+} \rightleftharpoons \text{H}_2\text{O} + \text{MYLTHF}$
100 $\text{H}_2\text{O} + \text{MYLTHF} \rightleftharpoons \text{H}^{+} + \text{N10FTHF}$
101 $\text{ATP} + \text{FORM} + \text{THF} \rightarrow \text{ADP} + \text{N10FTHF} + \text{Pi}$
102 $\text{MYLTHF} + \text{NADPH} \rightleftharpoons \text{METHF} + \text{NADP}$
103 $\text{H}^{+} + \text{METHF} + \text{NADPH} \rightleftharpoons \text{MTHF} + \text{NADP}$
104 $5\text{FTHF} + \text{ATP} + \text{H}_2\text{O} \rightarrow \text{ADP} + \text{H}^{+} + \text{N10FTHF} + \text{Pi}$
105 $\text{FORM} + \text{H}^{+} + \text{THF} \rightleftharpoons \text{H}_2\text{O} + \text{N10FTHF}$
106 $\text{DHF} + \text{H}^{+} + \text{NADPH} \rightleftharpoons \text{NADP} + \text{THF}$

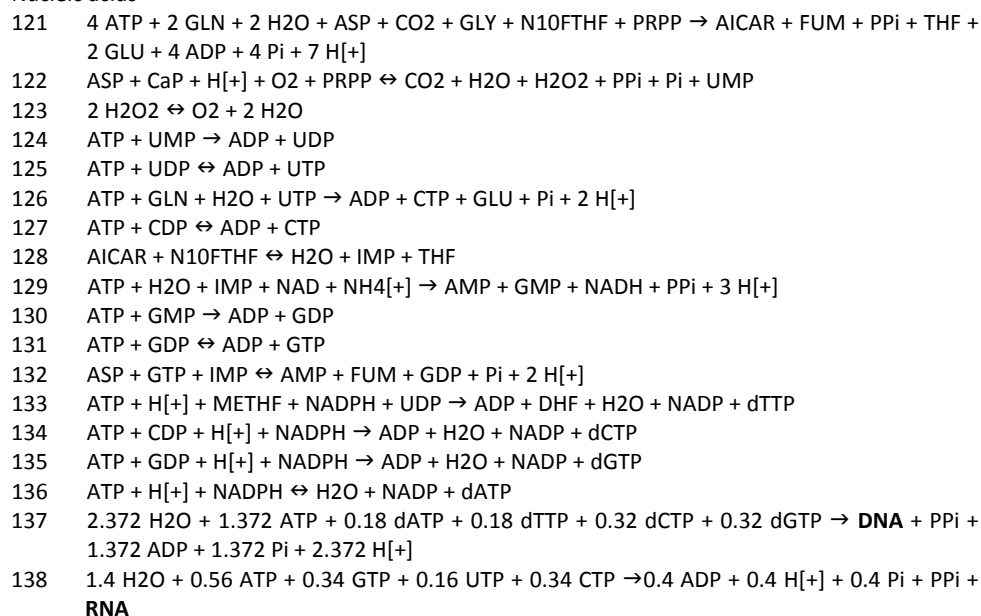
Lipids (phosphatidic acid)

- 107 $\text{ACP} + \text{AcCoA} + \text{H}^{+} \rightleftharpoons \text{AcACP} + \text{CoA}$
108 $\text{ATP} + \text{AcCoA} + \text{CO}_2 + \text{H}_2\text{O} \rightarrow \text{ADP} + \text{H}^{+} + \text{MalCoA} + \text{Pi}$

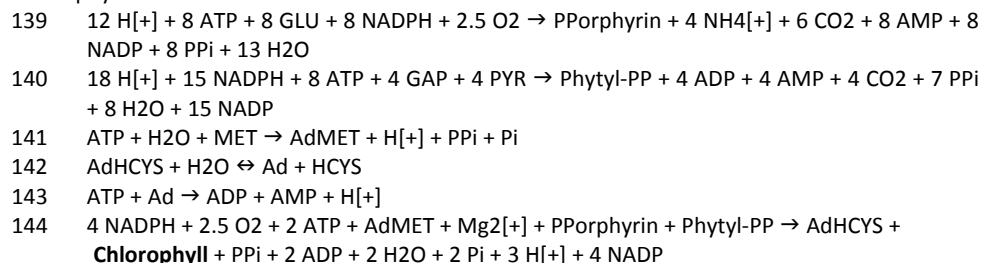
Effect of O₂ : CO₂ ratio on the primary metabolism of Chlamydomonas reinhardtii



Nucleic acids



Chlorophyll



Starch and carbohydrates

- 145 G1P \leftrightarrow Pi + STARCH
 146 G1P \leftrightarrow **CARB** + Pi

Biomass formation

- 147 18.8996 **ATP** + 18.8996 H₂O + **a PROTEIN** + **b CARB** + **c PA** + **d RNA** + **e Chlorophyll** + **f DNA**
 \rightarrow **Biomass** + **g H[+]** + 18.8996 ADP + 18.8996 Pi

Transport

- 148 CO₂ \leftarrow CO_{2_ex}
 149 O₂ \rightarrow O_{2_ex}
 150 H₂O \leftrightarrow H₂O_ex
 151 Pi \leftrightarrow Pi_ex
 152 SO₄ \leftrightarrow SO_{4_ex}
 153 NO₃ \leftrightarrow NO_{3_ex}
 154 Mg²⁺ \leftrightarrow Mg²⁺_ex
 155 Light \leftarrow Light_ex
 156 H⁺ \leftrightarrow H⁺_ex
 157 GLYC \rightarrow GLYC_ex
 158 STARCH \rightarrow STARCH_ex
 159 Biomass \rightarrow **x** Biomass_ex

B. Compound abbreviations

13DPG	1,3-diPhosphoglycerate	ATP	Adenosine triphosphate
2-oxobutan	2-Oxobutanoate	Biomass	Biomass
2PG	2-Phosphoglycerate	Biomass_ex	Biomass (g)
3PG	3-Phosphoglycerate	C12:0ACP	Dodecanoyl-ACP (Lauric acid)
5FTHF	5-Formyl-THF	C14:0ACP	Tetradecanoyl-ACP (Myristic acid)
6PG	6-Phosphogluconate	C16:0ACP	Hexadecanoyl-ACP (Palmitic acid)
AcACP	Acetyl-ACP	C16:1ACP	Trans-Hexadec-2-enoyl-ACP (Palmitoleic acid)
AcCOA	Acetyl-CoA	C16:2ACP	Hexadecadienoic acid
Ace	Acetate	C16:3ACP	Hexadecatrienoic acid
ACP	Acetyl-carrier protein	C18:0ACP	Octadecanoyl-ACP (Stearic acid)
Ad	Adenosine	C18:1ACP	Cis-11-ocadecanoate-ACP (Oleic acid)
AdHCYS	S-Adenosyl-L-homocysteine	C18:2ACP	Linoleic acid
AdMET	S-Adenosyl-L-methionine	C18:3ACP	Alpha-linoleic acid
ADP	Adenosine diphosphate	CaP	Carbamoyl phosphate
AICAR	5-Aminoimidazole-4-carboxamide ribonucleine	CARB	Carbohydrate
AKG	2-Oxoglutarate (alpha-ketoglutarate)	CDP	Cytidine diphosphate
ALA	Alanine	Chlorophyll	Chlorophyll
AMP	Adenosine monophosphate	CHO	Chorismate
ANTH	Anthranilate	CIT	Citrate
APS	Adenylyl sulfate	CO ₂	Carbon dioxide
ARG	Arginine	CO _{2_ex}	Carbon dioxide (extracellular)
ASA	L-Aspartic semialdehyde	CoA	Coenzyme A
ASN	Asparagine		
ASP	Aspartate		

Effect of O₂ : CO₂ ratio on the primary metabolism of Chlamydomonas reinhardtii

CTP	Cytidine triphosphate	LYS	Lysine
CYS	Cysteine	MAL	Malate
DAP	Diaminopimelate	MalCoA	Malonyl-CoA
dATP	Deoxy ATP	MET	Methionine
dCTP	Deoxy CTP	METHF	5,10-Methylene-THF
dGTP	Deoxy GTP	Mg2[+]	Magnesium
DHA	Dihydroxyacetone (Glycerone)	Mg2[+]_ex	Magnesium (extracellular)
DHAP	Dihydroxyacetone-P	MTHF	Methyl-THF
DHF	Dihydrofolate	MYLTHF	5,10-Methenyl-THF
DNA	Deoxyribonucleic acid	N10FTHF	10-Formyl-THF
dTTP	Deoxy TTP	NAD	Nicotinamide oxidized
E4P	Erythrose 4-phosphate	NADH	Nicotinamide reduced
F16P	Fructose 1,6-bisphosphate	NADP	Nicotinamidephosphate oxidized
F6P	Fructose 6-phosphate	NADPH	Nicotinamidephosphate reduced
FAD	Flavin adenine dinucleotide oxidized	NH4[+]	Ammonium
FADH2	Flavin adenine dinucleotide reduced	NH4[+]_ex	Ammonium (extracellular)
FORM	Formic acid	NO2	Nitrite
FUM	Fumarate	NO3	Nitrate
G1P	Glucose 1-phosphate	NO3_ex	Nitrate (extracellular)
G6P	Glucose 6-phosphate	O2	Oxygen
GAP	Glyceraldehyde 3-phosphate	O2_ex	Oxygen (extracellular)
GDP	Guanosine diphosphate	OXA	Oxaloacetate
GLN	Glutamine	PA	Phosphatidic acid
GLU	Glutamate	PEP	Phosphoenolpyruvate
GLY	Glycine	PHE	Phenylalanine
GLYC	Glycerol	Phytyl-PP	Phytyl-diphosphate
GLYC3P	Glycerol 3-phosphate	Pi	Orthophosphate
Glycerate	Glycerate	Pi_ex	Orthophosphate (extracellular)
GLYC_ex	Glycerol (extracellular)	PPi	Pyrophosphate
glyoxylate	Glyoxylate	PPorphyrin	Protoporphyrine
GMP	Guanosine monophosphate	PRE	Prephanate
GTP	Guanosine triphosphate	PRO	Proline
H[+]	Proton	PROTEIN	Protein
H[+]_ex	Proton (extracellular)	PRPP	Phosphorybosylpyrophosphate
H2O	Water	PYR	Pyruvate
H2O2	Hydrogen peroxide	R5P	Ribose 5-phosphate
H2O_ex	Water (extracellular)	RNA	Ribonucleic acid
H2S	Hydrogen sulfide	Ru15DP	Ribulose 1,5-bisphosphate
HCYS	Homocysteine	RU5P	Ribulose 5-phosphate
HIS	Histidine	S7P	Sedoheptulose 7-phosphate
HSER	Homoserine	SER	Serine
HydPro	Hydroxyproline	SO3	Sulphite
HydPyr	3-Hydroxypyruvate	SO4	Sulphate
ILE	Isoleucine	SO4_ex	Sulphate (extracellular)
IMP	Inosine monophosphate	STARCH	Starch
LEU	Leucine	STARCH_ex	Starch (extracellular)
Light	Photons	SUC	Succinate
Light_ex	Photons (extracellular)	SUCCoA	Succinyl Coenzyme A
		THF	Tetrahydrofolate
		THR	Threonine

TRYP	Tryptophan	UTP	Uridine triphosphate
TYR	Tyrosine	VAL	Valine
UDP	Uridine diphosphate	X5P	Xylulose 5-phosphate
UMP	Uridine monophosphate		

C. Elemental composition of macromolecules

	C	H	O	N	P	S	Charge
Protein	4.77	7.58	1.45	1.35	0	0.04	-
Carbohydrates	6	10	5	0	0	0	-
Lipids (PA)	36.34	63.39	8	0	1	0	-2
DNA	9.68	12.18	7	3.82	1	0	-2
RNA	9.50	12.84	8	3.84	1	0	-1
Chlorophyll	55	72	5	4.00	0	0	-

The composition is given for one mol of macromolecule.

D. Protein composition

Amino Acid	% (mol AA/mol protein)
Alanine (Ala)	11.07 ± 0.03
Arginine (Arg)	5.16 ± 0.01
Asparagine (Asn)	4.66 ± 0.02
Aspartate (Asp)	4.66 ± 0.02
Cysteine (Cys)	1.19 ± 0.02
Glutamate (Glu)	5.17 ± 0.03
Glutamine (Gln)	5.17 ± 0.03
Glycine (Gly)	9.23 ± 0.03
Histidine (His)	1.69 ± 0.01
Hydroxyproline (HydPro)	0.94 ± 0.05
Isoleucine (Ile)	3.69 ± 0.02
Leucine (Leu)	8.96 ± 0.02
Lysine (Lys)	6.04 ± 0.05
Methionine (Met)	2.42 ± 0.04
Phenylalanine (Phe)	4.12 ± 0.02
Proline (Pro)	5.62 ± 0.02
Serine (Ser)	5.42 ± 0.02
Threonine (Thr)	5.59 ± 0.02
Tryptophan (Trp)	0.10 ± 0.00
Tyrosine (Tyr)	2.98 ± 0.02
Valine (Val)	6.14 ± 0.03

Effect of O₂ : CO₂ ratio on the primary metabolism of Chlamydomonas reinhardtii

In the network, proteins were modeled as a coupling of one average amino acid, consuming 4.306 mol ATP. One average amino acid constitutes of the sum of the molar fractions of the various amino acids present in *C. reinhardtii*.

E. Lipid composition

Fatty acid	% (mol FA/mol PA)
12:0	10.42 ± 0.56
14:0	5.14 ± 0.30
16:0	47.35 ± 1.36
16:1	3.96 ± 0.09
16:2	14.78 ± 0.17
16:3	25.30 ± 0.57
18:0	4.78 ± 0.34
18:1	16.01 ± 0.11
18:2	27.63 ± 0.31
18:3	44.62 ± 1.29

In the network, lipids (PA, phosphatidic acid) were modeled as a Glycerol 3-phosphate molecule with two acetyl-ACP tails. The average acetyl-ACP chains constitute of the sum of two times the molar fractions of the various fatty acids present in *C. reinhardtii*.



CHAPTER 6

Discussion

Towards high biomass yields – a better understanding of microalgal metabolism

Abstract

To thoroughly understand the energy metabolism of microalgal cells and with that the conversion of light energy into biomass, insight into the different processes involved in O₂ production and uptake and CO₂ consumption and production is necessary. An overview of these processes that play a dominant role in the generation of metabolic energy and reductants is given. To reach high biomass yields on light (i.e. productivity) conditions at which processes such as the Mehler reaction, photoinhibition and photorespiration occur should be avoided. A number of measurement methods are proposed which could be used to determine under which cultivation conditions certain processes take place and to what extent, so that these conditions possibly can be avoided. These measurements need to be combined with flux balance analysis in order to accurately assess the real implications of these pathways for the energy budget of the microalgae. For this purpose the metabolic model for *C. reinhardtii* itself can be further improved and expanded by introducing cellular compartments and possibly adding desired product pathways. This will give more insight in the metabolism and the effect of different parameters on the conversion of light energy into biomass or useful products. If a dynamic description of the light reactions of photosynthesis is included it might ultimately be possible to make predictions on biomass and product yield based on the light regime the microalgae are exposed to.

Introduction

Maximization of microalgal product and biomass productivity in (large-scale) outdoor photobioreactors is important for commercial production of food, feed, chemicals or fuel compounds. To achieve this, insight in the metabolism of the microalgae is a valuable tool. We constructed a metabolic model to understand fundamental mechanisms behind biomass yield on light for the green microalgae *Chlamydomonas reinhardtii* (described in Chapter 4) and applied metabolic flux balancing to achieve this insight. To be able to accurately measure the inputs and outputs of the metabolism (CO_2 , O_2 , biomass, nitrogen, light) on-line during cultivation, we developed a lab-scale short light-path (SLP) photobioreactor with an on-line measurement system (described in Chapter 2 and 3). In this photobioreactor mixing was carried out independently from aeration to be able to measure the gas-exchange on-line as well as determine the effect of mixing on the biomass yield.

In this study we used the metabolic model and the SLP photobioreactor to get a better insight in the metabolism of microalgae and more specifically the O_2 metabolism. During photoautotrophic growth microalgae consume carbon dioxide (CO_2) and produce oxygen (O_2). In addition O_2 is taken up in a number of processes such as mitochondrial respiration and photorespiration. The net evolved O_2 can easily build up to high concentrations in closed photobioreactors and this can inhibit growth of the microalgae and have a negative effect on productivity (Carvalho et al. 2006; Miron et al. 1999; Wijffels et al. 2010). By cultivating microalgae under different O_2 : CO_2 ratios in this photobioreactor and measuring the oxygen production rate (OPR) and carbon dioxide uptake rate (CUR) on-line we could assess the effect of elevated O_2 concentrations on the microalgae (described in Chapter 5). The measured rates were used as input for the metabolic model to quantify the effect of higher O_2 : CO_2 ratios.

To thoroughly understand the energy metabolism of microalgal cells and with that the conversion of light energy into biomass, insight into the different processes involved in O_2 production and uptake and CO_2 consumption and production is necessary. In the next paragraphs the metabolic processes in which O_2 plays a role will be discussed as well as how they could be measured. Subsequently, ways to improve the metabolic model in order to obtain a better insight in the metabolism will be discussed.

Microalgal cultivation: mixing and oxygen

To be able to accurately measure photosynthetic activity through the on-line monitoring

of the oxygen production rate (OPR) and carbon dioxide consumption rate (CUR), the differences in O₂ and CO₂ in the ingoing and outgoing gas need to be large enough. To accomplish this we need to decrease the airflow going through the microalgal culture and as a consequence there will be less mixing in the reactor (longer light/dark cycles). To be able to measure this gas-exchange on-line and study the effect of mixing on the productivity of algal cultures independently, we designed a lab-scale photobioreactor which combines a short light-path (SLP) of 12 mm with controlled aeration and mixing by stirring, independent from the gas flow. The design and operation of this lab-scale photobioreactor is described in Chapter 2.

To reach high biomass densities and increase biomass yield at high light intensities, faster mixing could be important as was found for cultures of *Spirulina* (*Arthrospira*) (Qiang et al. 1996; Qiang and Richmond 1996). Under such conditions the cyanobacteria are only shortly exposed to over-saturating light intensities at the photobioreactor surface before traveling to darker regions of the photobioreactor, the so called L/D (light/dark) cycles. It was hypothesized that this light regime leads to higher photosynthetic efficiencies by preventing oversaturation and inducing light integration (Richmond 2000). To test whether this was the case for green microalgae we investigated the effect of mixing on cultures of *Chlorella sorokiniana* under over-saturating light in the SLP photobioreactor (Chapter 2). Batch experiments with *Chlorella sorokiniana* at different mixing speeds showed that the maximal photosynthetic efficiency occurred at relatively low biomass densities (2.3 g L⁻¹) at which light was just attenuated before reaching the rear of the culture. In our work, no real dark zone developed at the point of optimal productivity, and consequently there was no cycling between light and dark zones. Mixing only leads to movement of the microalgal cells through the light gradient within the light zone. When increasing the mixing rate twofold, we only found a small increase in biomass yield on light energy for the green microalga *Chlorella sorokiniana* in contrast to the findings for *Spirulina*.

Mixing is needed to prevent algae from settling, for supplying CO₂ and for removing O₂. But to reach higher productivities with faster mixing and thus higher energy inputs, the question arises if the increased biomass productivity is proportional to the increased energy input. Miller et al. (1964) calculated an optimum mixing speed based on the total power input for illumination and mixing. According to their calculations, there was a cut-

off between the efficiency of the algae, related to light intensity, and the optimum mixing speed. Calculations done by Norsker et al. (2010) and Weissman et al. (1988) show that high mixing velocities in closed systems are associated with high energy input costs. Even for specialty products the question is if these high costs can be justified for promoting higher productivities.

As stated above, mixing is also needed to supply CO₂ to the culture and remove the produced O₂. This produced O₂ can easily build up to high concentrations in closed photobioreactors and this can have a negative effect on productivity and inhibit growth of the microalgae (Carvalho et al. 2006; Miron et al. 1999; Wijffels et al. 2010). If mixing is decreased to reduce energy consumption, which is preferable, this effect can be even larger because even more O₂ can build up in the culture.

Thus, there are two main effects associated with mixing. First, an increase in biomass yield by faster mixing, which we found to be only small. Second, an effect on the removal of evolved O₂, which can be inhibiting for microalgal growth and have a negative effect on biomass yield.

Effect of oxygen and carbon dioxide on the metabolism of microalgae

During photoautotrophic growth there are a number of metabolic processes in which O₂ and CO₂ are involved. To be able to assess the effect of O₂ and CO₂ on the metabolism of microalgae we need to understand these processes and know when and if they occur and under which circumstances. In the following paragraphs an overview is given of the most commonly occurring processes in which O₂ and/or CO₂ are involved.

Photosynthesis, linear electron transport

Photosynthesis takes place in the chloroplasts of microalgae where the photosynthetic machinery is located on the thylakoid membranes, as shown in Figure 6.1. This machinery consists of two photosynthetic units (PSI and PSII), a Cytochrome b₆f complex and electron carriers (plastoquinone (PQ) and plastocyanin (PC)).

Per 8 photons absorbed (4 at PSII and 4 at PSI), two molecules of H₂O are split at the lumen side of PSII yielding O₂ and 4 protons. Thus, photosynthesis is the major source of O₂ production. The four electrons originating from water flow through PSII to the Cyt b₆f complex through PQ. Every second electron which arrives at the Cyt b₆f complex is cycled back to the PQ pool and additional protons are pumped to the lumen. With this Q-cycle the proton pumping stoichiometry is increased to 2 H⁺ per electron. (Cape et al. 2006)

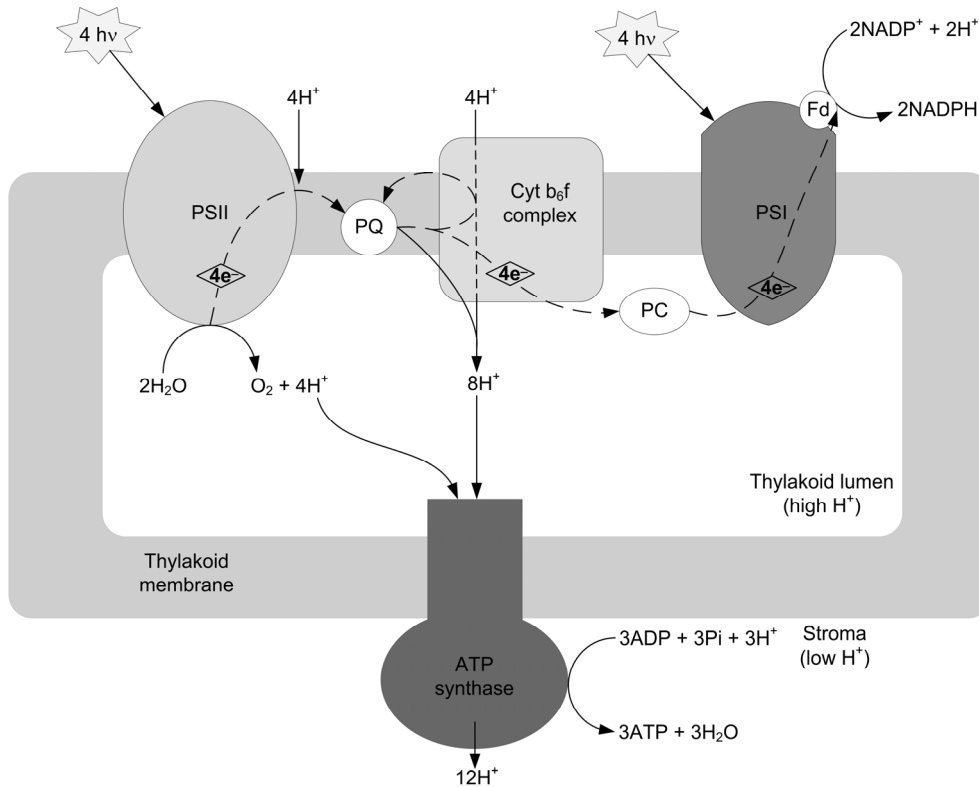
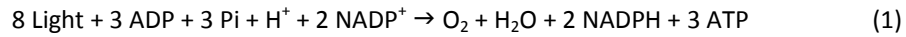


Figure 6.1 Linear electron transport in the thylakoid membranes of the chloroplast. Light is absorbed at PSII and water is split, yielding oxygen (O₂), protons (H⁺) and electrons (e⁻). Electrons move from H₂O through PSII, PQ, PSI and finally to NADP⁺. Light is also absorbed at PSI and with these electrons NADP⁺ is reduced to NADPH. Every second electron which arrives at the Cyt b₆f complex is cycled back to the PQ pool and additional protons are pumped to the lumen. This is the Q-cycle. Protons are pumped from the stroma to the lumen and this creates an electrochemical proton gradient which drives ATP synthesis through ATP synthase. *hv* = photons or quanta, PSI = photosystem I, PSII = photosystem II, PQ = plastoquinone, PC = plastocyanin, Fd = ferredoxin, Cyt b₆f complex = Cytochrome b₆f complex.

The electrons eventually flow to Ferredoxin (Fd) on PSI, through the PC pool. Here they are used to reduce two NADP⁺ to two NADPH. The electrochemical trans-membrane proton gradient that is created during this process (proton-motive force) drives ATP synthesis through ATP synthase. In this step three ATP are formed for 12 protons pumped across the thylakoid membrane. This process is represented by equation 1 and this is also how the light reaction is modeled in the metabolic network (reaction 0, Appendix

Chapter 4).



In this model we assumed a ratio between NADPH and ATP of 2 : 3 as can also be seen from this equation. However, this ratio might actually be higher since linear ET delivers less than the maximum of 3 ATP per 2 NADPH (Allen 2003), as is also discussed in Chapter 4. To fulfill the requirements of the Calvin cycle for carbon fixation the ratio of 2 : 3 needs to be restored and it is thought that cyclic ET provides the additional ATP to restore this ratio. (Allen 2003; Joliot and Joliot 2006) Perhaps the combination of linear and cyclic ET provides flexibility in the NADPH : ATP ratio to meet metabolic demands (Allen 2003). Another view is that mitochondrial respiration provides the additional ATP to restore the ratio needed for the operation of the Calvin cycle (Hoefnagel et al. 1998).

Cyclic electron transport

In cyclic electron transport (ET) electrons transported to Fd on PSI are transferred back to the PQ pool rather than to NADP⁺. These electrons then flow back to PC and are returned to PSI again. This cyclic flow of electrons induces the pumping of protons by the Cyt b₆f complex and the resulting proton gradient drives ATP synthesis by ATP synthase. In this process no NADPH is formed and also no O₂ is produced since PSII does not participate in this process. The net reaction of this process is given by equation 2:



Cyclic ET can change the ratio of ATP to NADPH in the microalgal cells and restore the ratio of NADPH : ATP to meet the demands of the Calvin cycle as discussed before (Allen 2003; Endo and Asada 2008; Joliot and Joliot 2006). In addition, cyclic ET establishes a pH gradient over the thylakoid membrane and this might help to induce pathways to dissipate excess excitation energy in PSII as heat (Allen 2003; Endo and Asada 2008; Shikanai 2010) thus preventing photoinhibition.

It is interesting to note that cyclic ET yields 1 molecule of ATP per 2 photons, where linear ET followed by the complete conversion of sugars (Glyceraldehyde 3-phosphate) produced in the chloroplast yields 1 mol of ATP per 1.5 photons. This shows that energy generation through linear photosynthetic electron transport is energetically more favor-

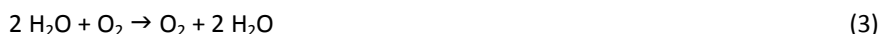
able than through cyclic electron transport. This cyclic pathway as such was not included in our model because the flux through this pathway could not be calculated from the measured rates. Nevertheless the flux through this pathway could partly explain the fact that the practically determined minimal quantum requirement of oxygen evolution is 10 instead of 8 as discussed in Chapter 4 (equivalent to $\Phi_{\text{Pmax}} = 0.8$). Considering this Φ_{Pmax} of 0.8 and the ratio of 3 ATP per 8 photons assumed for linear ET, this possible need for cyclic ET is implicitly present in our model.

Pseudocyclic electron transport, or Mehler reaction

This process is also called the Mehler reaction or sometimes the water-water cycle (Mehler 1951). In this process electrons are transferred from Fd to O_2 instead of to NADP^+ . This gives superoxide, which quickly needs to be scavenged to form hydrogen peroxide (H_2O_2). This can be converted to water in several enzymatic steps. The reactions occurring in this process are given below.

- | | | |
|----|---------------------------------|---|
| 1. | splitting of water at PSII | $2 \text{H}_2\text{O} \rightarrow 4 \text{e}^- + 4 \text{H}^+ + \text{O}_2$ |
| 2. | reduction of water at PSI | $2 \text{O}_2 + 2 \text{e}^- \rightarrow 2 \text{O}_2^-$ |
| 3. | formation of hydrogen peroxide | $2 \text{O}_2^- + 2 \text{H}^+ \rightarrow \text{O}_2 + \text{H}_2\text{O}_2$ |
| 4. | conversion of hydrogen peroxide | $\text{H}_2\text{O}_2 + 2 \text{e}^- + 2 \text{H}^+ \rightarrow 2 \text{H}_2\text{O}$ |

A more extensive overview of all reactions that occur in this process is given by Endo and Asada (2008) and Asada (1999). The net reaction of the Mehler reaction, the sum of all these steps, is given in equation 3:



In this pathway only protons are transferred over the thylakoid membrane. As in cyclic electron transport no NADPH and no O_2 are formed. The proton gradient can be used for ATP synthesis providing ADP is present (Allen 2003). Although cyclic ET around PSI and the Mehler reaction share similar physiological functions, it should be noted that cyclic ET is an energy conserving system while the Mehler reaction is an energy-dissipating system (Endo and Asada 2008). The functions of the Mehler reaction are still studied (Shikanai 2010). Possible functions are (Asada 1999; Endo and Asada 2008; Hideg 1997; Shikanai 2010):

- protecting the photosynthetic apparatus against photoinhibition at high light intensities by sustaining a pH gradient over the thylakoid membrane so that exces-

sive absorbed light can be dissipated as heat.

- to increase the ATP : NADPH ratio of the cells similar to cyclic ET. However, the quantum yield of ATP in the Mehler reaction is lower than that of cyclic ET.

The Mehler reaction takes place when the NADP⁺/NADPH pool is reduced as well as the other components of the photosynthetic electron transport chain. High light intensities can induce this situation as can CO₂ limitation and low temperatures. (Badger et al. 2000) However, over-reduction of the chloroplast can also be prevented by transporting the excess reducing equivalents out of the chloroplast through a shuttle mechanism, the Malate/Oxaloacetate shuttle. This shuttle is activated by high NADPH levels in the chloroplast after which NADPH reduces oxaloacetate to malate, which is exported from the chloroplast, yielding NADP⁺. This NADP⁺ can subsequently be used in linear ET. This shuttle seems to be preferred over the Mehler reaction, provided enough oxaloacetate is present. (Hoefnagel et al. 1998)

Chlororespiration

Chlororespiration is the process in which the PQ pool is reduced in the dark and re-oxidized via a chloroplast oxidase at the expense of O₂. In higher plants the PQ pool is reduced by a NAD(P)H-oxidoreductase but in *C. reinhardtii* the responsible complex remains to be discovered. (Bennoun 2005) A role of chlororespiration might be in regulating the redox level of the PQ pool under stress conditions and in the dark (Büchel and Gyözü 1997). However, the rate of oxygen uptake by chlororespiration is very small and hard to differentiate from mitochondrial dark respiration (Bennoun 2005).

Photorespiration

A process which occurs when high concentrations of oxygen and/or low concentrations of carbon dioxide are present is photorespiration (Badger et al. 2000; Foyer et al. 2009; Ogren 1984; Tural and Moroney 2005; Wingler et al. 2000). This process can also occur at high temperatures which will influence the kinetic properties of the Rubisco enzyme and increase its oxygenase potential (Badger et al. 2000). In this process Rubisco reacts with O₂ instead of CO₂. When Rubisco fixes carbon dioxide, two molecules of Glycerate 3-phosphate are formed (Figure 6.2a). These can be converted back to Ribulose 1,5-bisphosphate or can be used in the central carbon metabolism to form biomass components. However, if oxygen is fixed only one Glycerate 3-phosphate is formed and one

molecule of Glycolate 2-phosphate (Figure 6.2b). This compound is converted into glyoxylate through glycolate and can then be converted to Glycerate 3-phosphate at the expense of energy in the form of ATP. In addition CO_2 is 'lost' and needs to be re-fixed in the Calvin cycle. This costs additional ATP and NADPH which are formed in the light reaction (linear electron transport) of photosynthesis and thus costs additional light. Also ammonium (NH_4^+) is 'lost' and can be re-fixed into Glutamate at the expense of NADPH. Thus, in this situation less energy is available for growth, which lowers the productivity of the microalgal cells. This process and its implications on the metabolism are explained in detail in Chapter 5. Together with mitochondrial respiration this process causes net con-

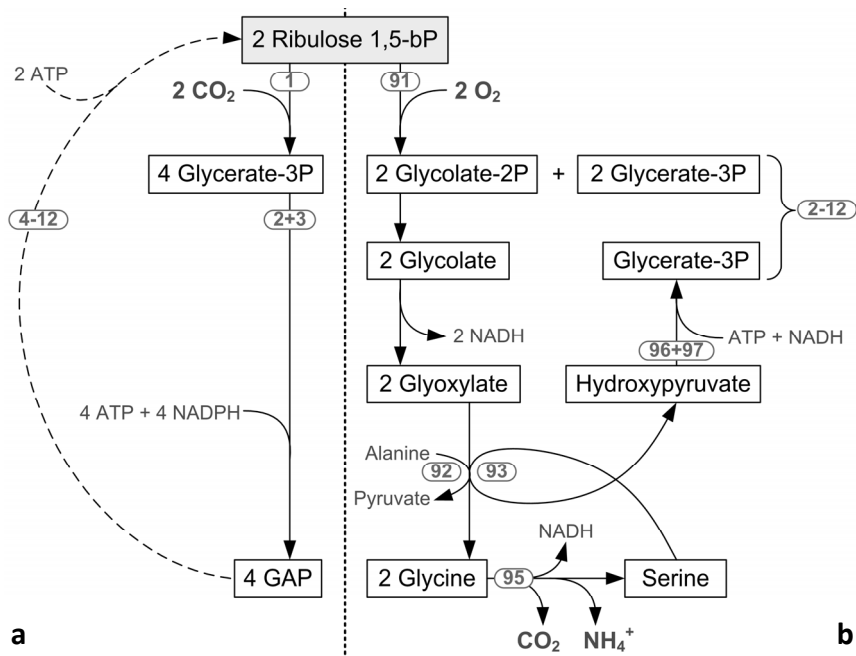
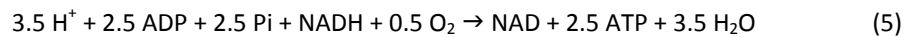
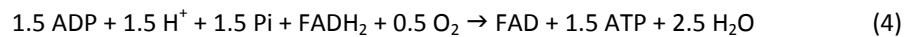


Figure 6.2 Carboxylase and oxygenase reactions of Rubisco, followed by the Calvin cycle (a) and photorespiration (b). The two processes are shown for two Ribulose 1,5-bisphosphate molecules each. The numbers correspond to the reactions in the metabolic model as shown in Appendix A, Chapter 4. When Rubisco binds CO_2 (a), per two CO_2 four Glycerate 3-phosphate are formed, which can be converted to Glyceraldehyde 3-phosphate (GAP). GAP can be regenerated into Ribulose 1,5-bP at the expense of ATP or be used in the central carbon metabolism to form building blocks for biomass. When Rubisco binds O_2 (b), per two O_2 two Glycerate 3-phosphate and two Glycolate 2-phosphate are formed. To convert these two Glycolate 2-phosphate to one Glycerate 3-phosphate, ATP is consumed, CO_2 and ammonia (NH_4^+) are lost. Re-fixing this lost CO_2 and NH_4^+ costs more ATP and NADPH elsewhere in the metabolism.

sumption of O₂ in the light. In the dark this process quickly stops due to the fact that there is no ATP and NADPH to regenerate Ribulose 1,5-bisphosphate.

Mitochondrial light respiration

This process (also named oxidative phosphorylation) mainly takes place in the mitochondria where NADH and FADH₂ are oxidized to generate extra energy in the form of ATP to support biomass formation and maintenance processes. In this process oxygen is consumed. (Geider and Osborne 1989; Graham 1980; Hoefnagel et al. 1998; Turpin et al. 1988) The respiration rate is known to be related to the growth rate and it is suggested that faster algal growth leads to a higher energy (ATP) requirement and, as such, respiratory activity increases (also observed in Chapter 3). This process is represented by equations 4 and 5 (reactions 52 and 53, Appendix Chapter 4).



Comparison of measured and calculated mitochondrial respiration rates

The rate of post-illumination O₂ uptake has been shown to provide a good measure for respiratory O₂ uptake in the light (Grande et al. 1989; Weger et al. 1989; Xue et al. 1996). A method to measure this post-illumination O₂ uptake *in situ* inside the SLP photobioreactor during cultivation is described in Chapter 3. By means of a simple extension of the cultivation system we were able to measure the respiratory O₂ uptake (OUR) using a fiber-optic oxygen micro-sensor. During the steady states at different O₂ : CO₂ ratios as described in Chapter 5 we measured the OUR for *C. reinhardtii* with this method. In addition we calculated the respiration rate with the metabolic model by adding up the fluxes through reactions 52 and 53 for each steady state (more details on the model inputs can be found in Chapter 5). Figure 6.3 shows the calculated and measured OUR for the different steady states. This graph shows a large, almost 3-fold, discrepancy between the model output and the measured values. This can be either due to the measurement method, to the model or to both.

As for the measurement method, the upside of this method is that it is fast (which is important to measure the immediate post-illumination O₂ uptake) and it enables rapid and frequent measurements without disturbing the cultivation and growth of the microalgae.

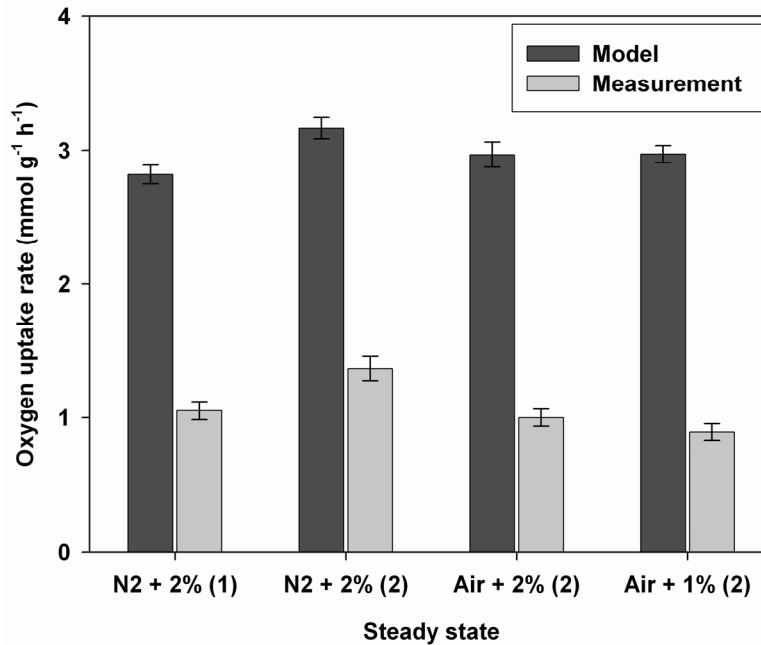


Figure 6.3 Oxygen uptake rates (in $\text{mmol g}^{-1} \text{h}^{-1}$) as calculated with the metabolic model compared to the measured rates with a fiber optic oxygen sensor for the steady states with different $\text{O}_2 : \text{CO}_2$ ratios as described before. The error bars represent the standard deviations.

The downside is that the fiber-optic sensors are not robust and can lose their optical coating easily, severely affecting the measurements.

As for the model, a number of assumptions can influence the OUR through respiration. Firstly the P/O ratio, the relationship between ATP synthesis and O_2 consumption. In the model we assumed that NADH yields 2.5 ATP and FADH_2 yields 1.5 ATP upon respiration. However, if this ratio would be lower, the O_2 uptake rate through respiration according to the model will increase (described in Chapter 4). A way to determine the P/O ratio for *E. coli* is described in Taymaz-Nikerel et al. (2010). This approach is similar to the determination of energy requirement for growth and maintenance as described in Chapter 4, with additional objective functions and chemostats using different conditions and substrates.

Secondly, the compartmentation of the model influences the energy requirement of the cell and thus the OUR through respiration. In the current model only the Calvin cycle is compartmentalized to the chloroplast. As a consequence, in the model all ATP that is used in biomass synthesis is generated in oxidative phosphorylation and is thus con-

nected with O₂ consumption. However, for example lipids are synthesized in the chloroplast *in vivo* from Glyceraldehydes 3-phosphate, the product of the Calvin cycle. For this lipid synthesis additional reducing equivalents (NADPH) and ATP are needed which can be derived directly from linear ET. Therefore less ATP needs to be generated in oxidative phosphorylation and consequently less O₂ needs to be consumed. However, for many reactions the compartment in which they occur is not known and neither are all transporters responsible for transport of compounds between compartments. Furthermore, compartmentalization requires additional measurements, like for example the composition of the chloroplast, and their contribution to the total dry weight.

Improving and expanding the metabolic flux model

Improving and expanding the metabolic model is only useful if the fluxes through the added pathways can be calculated and the improved model can be validated. Therefore some of the above described processes need to be measured during steady state conditions, like the respiration method described before. The existence of the processes explained above has been proven by measurements on either isolated chloroplasts and mitochondria or on mutants deficient in one or more enzymes, disabling these processes. However, ultimately we want to assess the effect of cultivation conditions as they occur in photobioreactors on whole microalgal cells and understand the impact on the metabolism. Thus all processes that significantly contribute to the biomass yield on light should be known and included in the model. In case the flux through some of these pathways cannot be calculated from the measurements, either additional measurements are needed (for example chloroplast composition) or conditions need to be chosen in such a way that the contribution of certain pathways can be neglected (for example Mehler reaction at low light and high growth rates). In addition to this we would like to understand and improve the metabolic pathways towards microalgal products such as lipids for biodiesel or carotenoids for food applications.

In the following paragraphs a number of measurement methods and ways to improve the metabolic model are discussed. After this some possibilities to expand the metabolic model with product pathways will be given.

Measurements

In Table 6.1 an overview is presented of several measurement methods which could be used to quantify several of the processes involving oxygen and carbon dioxide described

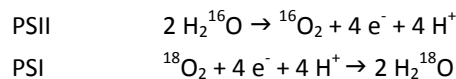
Table 6.1 Overview of measurement methods described and reviewed in literature. The processes which can be measured with these methods are also given.

Method	Process	References
$^{16}\text{O}/^{18}\text{O}$ isotope study, with NMR or MS	O_2 uptake reactions (Mehler reaction, mitochondrial respiration)	Badger et al. (2000), Bate et al. (1988), Eisenstadt et al. (2010), Endo and Asada (2008), Falkowski and Raven (2007), Kana (1993)
$^{12}\text{C}/^{13}\text{C}/^{14}\text{C}$ isotope study, with NMR or MS	CO_2 evolution (Mitochondrial respiration, photorespiration)	Grande et al. (1989), Raghavendra et al. (1994)
^{13}C labeling, with NMR or MS	Flux measurements (changes in intermediates and intracellular metabolites)	Iwatani et al. (2008), Shastri and Morgan (2007), van Winden et al. (2001a), Yang et al. (2002)
^{32}P labeling	Cyclic ET	Herzig and Dubinsky (1993)
PAM fluorescence	Φ_p and $\Phi_{p_{\max}}$ the quantum yield of PSII, PSI NADPH, ΔpH Photoinhibition	Badger et al. (2000), Häder et al. (1996), Hancke et al. (2008), Klughammer and Schreiber (2008), Kromkamp et al. (2009), Lippemeier et al. (2001), Ravenel et al. (1994), Shikanai (2010)
Dynamic fluorescence quenching	Oxygen uptake reactions (Mitochondrial respiration)	Kliphuis et al. (2010b)

before. Measuring these processes *in vivo* under relevant cultivation conditions is not easy (Badger et al. 2000). Nevertheless, some of these methods can be used to determine under which cultivation conditions certain processes take place. For example, to obtain higher yields it is beneficial to cultivate microalgae under conditions at which photorespiration or the Mehler reaction do not take place.

There are a number of different O and C isotope labeling studies that can be performed to elucidate several processes in which O₂ and CO₂ are involved. By performing ¹⁶O/¹⁸O labeling combined with a detection method such as NMR or MS insight can be obtained in the oxygen uptake reactions during photosynthesis.

For example the Mehler reaction can be observed using this method. The stoichiometry is as follows:



The O₂ evolved at PSII is derived from water, while O₂ is taken up from the dissolved O₂ in the cultivation medium. (Badger et al. 2000; Endo and Asada 2008)

Labeling of oxygen can be combined with carbon labeling to identify CO₂ evolution during photosynthesis. This is the result of mitochondrial respiration and photorespiration. The combination of these two labeling methods can shed more light on these processes. However, for these labeling studies, one has to make sure the measurement conditions are chosen in such a way that only the process which needs to be studied takes place. For example, when determining the rate of cyclic ET by ³²P labeling linear ET was blocked by DCMU (Herzig and Dubinsky 1993). The question then arises if the processes measured in such a way also occur in the exact same way under cultivation conditions.

Fluorescence techniques can be used to determine the quantum yield Φ_p of PSII and the maximum (dark-adapted) quantum yield Φ_{pmax} of PSII, giving a measure for linear ET. In addition, the quantum yield of PSI, the NADPH pool and the transmembrane pH gradient (ΔpH) can be determined with fluorescence techniques (Klughammer and Schreiber 2008; Ravenel et al. 1994).

As discussed in Chapter 4 the quantum yield is important to accurately determine how efficient linear electron transport is under certain cultivation conditions. This method is much more accurate than labeling with enriched O₂ or CO₂ to determine gross oxygen evolution or carbon fixation through linear ET (Hancke et al. 2008). The downside of this

method is that optically thin cultures without a light gradient are necessary. These can be obtained either by diluting the culture or measuring a dilute sample. The question then arises if the conditions during the measurement are the same as during large scale cultivation, where high biomass densities are required.

A tool for elucidating the intracellular fluxes in metabolic networks is ^{13}C labeling. This method relies on a number of assumptions (van Winden et al. 2001b):

- the stoichiometry of the network is complete. There are no omitted reactions that can influence the labeling state of the biomass. In addition, the reversibility of all reactions is known, since this can also have a large effect on the labeling state of the metabolites.
- there are no metabolic isotope effects, i.e. enzymes do not discriminate between molecules with various numbers of labeled C-atoms.
- all reactions take place in compartments in which all metabolites are homogeneously distributed

Almost all ^{13}C labeling techniques for algal flux balance analysis have been performed under heterotrophic or mixotrophic conditions. If enriched $1\text{-}^{13}\text{C}$ glucose is used the label is on a specific location, the first carbon atom. When measuring the isotopic steady state of the metabolism the distribution of the label over the metabolites is C-atom specific and gives information on how the metabolite was formed from glucose. However, labeling with $^{13}\text{CO}_2$ provides a challenge in this respect because the label is not location specific. Therefore measuring changes in ^{13}C labeling patterns of metabolic intermediates as a function of time is the only way to measure fluxes at steady state for photoautotrophic micro-organisms. (Shastri and Morgan 2007)

To be able to measure these changes in time, rapid sampling and quenching of the metabolism are required, which is another challenge. If flash-freezing of the whole sample is used it is, however, not possible to make a distinction between intracellular and extracellular compounds. Centrifugation is commonly used to separate the cells from the cultivation medium, but this requires handling the sample outside cultivation conditions prior to quenching. This can alter the metabolism and disturb the measurements and cannot be used for such highly dynamic experiments. A new method for quenching the metabolism of *C. reinhardtii* cells is described in Bölling and Fiehn (2005), in which the cells are injected in a cold (-25°C) solution of methanol-water supplied with Tris-acetate phosphate for osmotic conditions. However, when using this method for other algal species,

tests should be done to check whether the cells stay intact during this quenching procedure.

Model

In addition to measuring which processes occur during cultivation under different conditions, the model itself can be improved. In the next paragraphs ways to do this are discussed. However, model expansion and improvement usually has to go together with additional measurements to validate the model.

Compartmentation model

The metabolic model as introduced in Chapter 4 can be improved substantially by compartmentalizing the different reactions to the different cell organelles where they take place as described before. In this way the compounds produced in each organelle can immediately be used there as a building block as opposed to be formed in the cytosol as the model describes now. In addition, the energy generated in an organelle can immediately be used to form biomass building blocks in that organelle. The compounds can be shuttled to the different cell compartments by translocators/shuttles. An example is the photorespiratory pathway in which glycolate is formed. This is transported over the chloroplast membrane to the cytosol and the mitochondria to be converted back to Glycerate 3-phosphate, which is in turn transported back to the chloroplast to enter the Calvin cycle again. (Foyer et al. 2009; Hoefnagel et al. 1998; Wingler et al. 2000) A glycolate/glycerate translocator for the chloroplast is described by Flügge and Heldt (1991). More of these translocators for several compounds and the compartmentation of pathways have been described in literature for the chloroplast, mitochondria and cytosol (Flügge and Heldt 1991; Hoefnagel et al. 1998; Klein 1986). The chloroplast and mitochondria are closely linked through photosynthesis and carbon compound formation in the chloroplast and respiration of these compounds in the mitochondria, yielding energy and carbon intermediates for biosynthesis (Hoefnagel et al. 1998; Raghavendra et al. 1994). The interaction between these organelles and the exchange of ATP, NAD(P)H and carbon compounds are described in more detail in Hoefnagel et al. (1998).

Compartmentation of the model will describe reality more accurately. However, there are some considerations. First of all not all translocators/shuttle systems are known and it is unclear how much energy it costs to shuttle components through the cell, hence assumptions have to be made here. This might affect the energy balance of the cell.

Secondly, identical pathways may occur in different organelles. This leads to underdeterminancies and unique fluxes cannot be calculated for these pathways without further assumptions and/or measurements. Thirdly, the composition of the modeled organelles should be measured in gram per gram dry weight. By doing this, information can be obtained on which components are made and used in which organelle and which components are used elsewhere as building blocks and thus need to be transported.

Gap-filling methods

In this thesis we used a top-down approach to build our metabolic model for *C. reinhardtii*. All important pathways of primary metabolism were identified based on literature. Subsequently we checked whether these pathways were present in the genome and if they were, they were incorporated in the model. A better approach would be to use a bottom-up approach. In this approach the model would be built using a prediction of all metabolic reactions based on the complete genome, providing the genome sequence is available. This includes compartmentalization as mentioned before. Such a model would contain a number of gaps which can be filled in using gap filling methods. Network reconstructions contain gaps because our knowledge of the metabolism of any organism is incomplete. There are two types of missing information (gaps) in metabolic networks. The first type of gaps are places where a reaction is missing, creating a dead-end. The second type are reactions that are known to exist but it is not yet known which gene or genes code for their enzymes. An example of the first type is the unknown enzyme necessary in cysteine formation in our metabolic model for *Chlamydomonas reinhardtii* (Chapter 4). The computational methods to fill these gaps and improve metabolic networks are reviewed in Herrgård et al. (2006) and Orth and Palsson (2010). These algorithms use metabolic reaction databases for the organism of interest (such as KEGG) and experimental data to find gaps and add or delete reactions.

Detailed modeling of photosynthetic light reactions – dynamic effects

When modeling the metabolism of any micro-organism steady state is assumed, a situation in which the specific growth rate μ , the biomass density and all other cultivation parameters do not change over time. This steady state actually is pseudo steady state since the cells still go through cell cycles and the composition of these cells thus ‘fluctuates’. There is an added difficulty when modeling photoautotrophic micro-organisms such as green microalgae. Microalgae use light as a substrate. During cultiva-

tion a light gradient will develop in the photobioreactor and the algae will travel through this gradient due to mixing. The photosystems will be presented with different amounts of photons due to this effect and thus the rate of photosynthetic ET will fluctuate. This reaction ultimately dictates the amount of energy that can be used in the metabolism and will thus dictate the specific growth rate of the cells. However, this fluctuating light effect will dampen out when going towards biomass formation in the metabolism and thus the definition for steady state still holds for the major part of primary metabolism. Nevertheless, when changing the light regime or mixing intensity the model may not be able anymore to accurately predict the biomass yield.

Ultimately we would like to use metabolic flux models to predict biomass or product yields for microalgae in large-scale photobioreactors. In these systems the algae will continuously move through a light gradient. The dynamic light regime experienced by the microalgae depends on the depth of the photobioreactor and its hydrodynamics, the incident light intensity, the biomass concentration and its pigmentation. To be able to accurately predict the amount of energy generated in linear ET in such a system, another approach for modeling the photosystem is needed. This model has to be a dynamic model which includes the primary light and dark biochemical reactions as well as regulatory interactions and is proposed in Nedbal et al. (2007).

Metabolic flux models as discussed here cannot be used to model such processes. However, if energy generation in the photosystems can be viewed as a separate block of metabolism with only a limited number of connections to the rest of metabolism it may be possible to link a dynamic model of photosynthesis describing energy and reductant generation to a metabolic flux model describing biomass and product formation. This might be the way to go to be able to accurately predict biomass or product yields for microalgae in fluctuating light.

Towards product formation

To gain more insight in product formation and possible product yields the metabolic model can be expanded with the pathways for these products. The incorporation of these pathways depends on the microalgae of interest and on the presence of genes encoding for these pathways in the genome.

Possible pathways with which the model can be extended are:

- carotenoid formation, branching from Acetyl-CoA (Grossman et al. 2004; McCaskill

and Croteau 1993; Schwender et al. 2001). Carotenoids are compounds of interest for food, feed, cosmetics and pharmaceutical applications.

- PUFA (poly-unsaturated fatty acids) pathways, which are an extension of the fatty acid formation pathway as is incorporated in the current model. PUFA's are long-chain fatty acids which are interesting for nutraceutical purposes. (Harwood and Guschina 2009; Ward and Singh 2005)
- TAG (triacylglycerol) formation, also branching from Acetyl-CoA. TAG is a potential source of biodiesel from microalgae. (Hu et al. 2008; Radakovits et al. 2010)
- Hydrocarbon formation. Hydrocarbons are long chain lipids consisting only of carbon and hydrogen elements. These compounds can be a potential renewable energy source. (Dayananda et al. 2007; Metzger and Largeau 2005)
- EPS (exo-polysaccharide) production pathways, branching from Glucose 1-phosphate (Cogne et al. 2003). Some species of cyanobacteria and green microalgae are known to excrete EPS, which can be used as thickening or suspending agents or emulsifying compounds amongst others (De Philippis et al. 2001; Lewin 1956). Another possible role of EPS could be in bio-flocculation for downstream processing of microalgae (Lavoie and de la Noüe 1987; Salim et al. 2010).
- Carbohydrate synthesis such as starch and glucan, branching from Glucose 1-phosphate. These storage carbohydrates can be metabolized into biofuels such as ethanol and H₂. (Radakovits et al. 2010)

Conclusion

When investigating the effect of mixing we only found a small increase in productivity with increasing mixing rates. This showed that we worked at the optimal mixing rate yielding maximal photosynthetic efficiency and hence productivity at over-saturating light conditions. However, when decreasing mixing because of the associated energy input costs, O₂ will build up in the medium and this can inhibit growth of the microalgae. To investigate the effect of O₂ on the metabolism we developed and used flux balance analysis to quantify photorespiration. We found that a reduction in biomass yield of 20% was already observed at conditions common in photobioreactors (air enriched with 2% CO₂) and that this reduction was due to photorespiration. However, there are several more processes involved with O₂ as described in this discussion. These processes play a role in reaching high photosynthetic efficiencies and processes such as the Mehler reaction, photoinhibition and photorespiration should be avoided. A number of measure-

ment methods are proposed which can be used to determine under which cultivation conditions certain processes take place so that these conditions can be avoided.

During cultivation we also quantified the rate of light respiration. However, the measured rates did not agree yet with the calculated rates with the metabolic model. The method described in Chapter 3, however, is a promising method to measure this but the robustness of the method needs to be improved. Once O₂ uptake in the light can be reliably measured this can be used to further optimize the model. The metabolic model for *C. reinhardtii* can be improved and expanded by introducing cellular compartments and adding desired product pathways, for which additional measurements are needed. This will give more insight in the metabolism and the effect of different parameters on biomass yield on light. Ultimately it might be possible to make predictions on biomass and product yield based on the metabolism simulated with a predictive metabolic flux model.

Abbreviations

Φ_p	Photochemical quantum yield (-)
Φ_{pmax}	Maximum photochemical quantum yield (-)
CO ₂	Carbon dioxide
CUR	Carbon dioxide uptake rate
Cyt	Cytochrome
e ⁻	Electron or reductant
EPS	Exo-polysaccharide
ET	Electron transport
Fd	Ferredoxin
hν	Photons or quanta
H ⁺	Proton
O ₂	Oxygen
OPR	Oxygen production rate
OUR	Oxygen uptake rate
PC	Plastocyanin
PQ	Plastoquinone
PSI	Photosystem I
PSII	Photosystem II
PUFA	Poly-unsaturated fatty acid
SLP	Short light-path
TAG	Triacylglycerol



REFERENCES

A Adir N, Zer H, Shochat S, Ohad I. (2003) Photoinhibition: a historical perspective. *Photosynthesis Research* 76:343-370

Allen JF. (2003) Cyclic, pseudocyclic and noncyclic photophosphorylation: new links in the chain. *Trends in Plant Science* 8:15-19

Altschul SF, Gish W, Miller W, Myers EW, Lipman DJ. (1990) Basic local alignment search tool. *Journal of Molecular Biology* 215:403-410

Asada K. (1999) The water-water cycle in chloroplasts: scavenging of active oxygens and dissipation of excess photons. *Annual Review of Plant Physiology and Plant Molecular Biology* 50:601-639

B Baart GJE, Willemsen M, Khatami E, Haan A, Zomer B, Beuvery EC, Tramper J, Martens DE. (2008) Modeling *Neisseria meningitidis* B metabolism at different specific growth rates. *Biotechnology and Bioengineering* 101:1022-1035

Badger MR, Andrews TJ, Whitney SM, Ludwig M, Yellowlees DC, Leggat W, Price GD. (1998) The diversity and coevolution of Rubisco, plastids, pyrenoids, and chloroplast-based CO₂-concentrating mechanisms in algae. *Canadian Journal of Botany* 76:1052-1071

Badger MR, von Caemmerer S, Ruuska S, Nakano H. (2000) Electron flow to oxygen in higher plants and algae: rates and control of direct photoreduction (Mehler reaction) and Rubisco oxygenase. *Philosophical Transactions: Biological Sciences* 355:1433-1446

Baker NR, Harbinson J, Kramer DM. (2007) Determining the limitations and regulation of photosynthetic energy transduction in leaves. *Plant, Cell & Environment* 30:1107-1125

Ball SG, Dirick L, Decq A, Martiat J-C, Matagne RF. (1990) Physiology of starch storage in the unicellular alga *Chlamydomonas reinhardtii*. *Plant Science* 66:1-9

Barbosa MJ, Albrecht M, Wijffels RH. (2003) Hydrodynamic stress and lethal events in sparged microalgae cultures. *Biotechnology and Bioengineering* 83:112-120

Bate GC, Sültemeyer JDF, Fock HP. (1988) ¹⁶O₂/¹⁸O₂ analysis of oxygen exchange in *Dunaliella tertiolecta*. Evidence for the inhibition of mitochondrial respiration in the light. *Photosynthesis Research* 16:219-231

Becker EW. (2007) Microalgae as a source of protein. *Biotechnology Advances* 25:207-210

Ben-Amotz A, Katz A, Avron M. (1982) Accumulation of β-carotene in halotolerant algae: purification and characterization of β-carotene-rich globules from *Dunaliella bardawil* (Chlorophyceae). *Journal of Phycology* 18:529-537

Bennoun P. (2005) The present model for chlororespiration. In: Govindjee, Beatty JT, Gest H, Allen JF, editors. *Discoveries in Photosynthesis*. Springer Netherlands. p 905-909

Berg JM, Tymoczko JL, Stryer L. (2003) *Biochemistry*. New York: Freeman.

Bird RB, Stewart WE, Lightfoot EN. (1960) *Transport Phenomena*. New York: Wiley.

Bjorkman O, Demmig B. (1987) Photon yield of O₂ evolution and chlorophyll fluorescence charac-

- teristics at 77 K among vascular plants of diverse origins. *Planta* 170:489-504
- Bölling C, Fiehn O. (2005) Metabolite profiling of *Chlamydomonas reinhardtii* under nutrient deprivation. *Plant Physiology* 139:1995-2005
- Borodina I, Krabben P, Nielsen J. (2005) Genome-scale analysis of *Streptomyces coelicolor* A3(2) metabolism. *Genome Research* 15:820-829
- Bosma R, Miazek K, Willemsen SM, Vermuë MH, Wijffels RH. (2008) Growth inhibition of *Monodus subterraneus* by free fatty acids. *Biotechnology and Bioengineering* 101:1108-1114
- Boyd C. (1968) Fresh-water plants: a potential source of protein. *Economic Botany* 22:359-368
- Boyle NR, Morgan JA. (2009) Flux balance analysis of primary metabolism in *Chlamydomonas reinhardtii*. *BMC Systems Biology* 3 DOI: 10.1186/1752-0509-3-4
- Bozzo GG, Colman B, Matsuda Y. (2000) Active transport of CO₂ and bicarbonate is induced in response to external CO₂ concentration in the green alga *Chlorella kessleri*. *Journal of Experimental Botany* 51:1341-1348
- Büchel C, Gyöző G. (1997) Respiratory regulation of electron transport in chloroplasts: chlororespiration. In: Pessaraki M, editor. *Handbook of photosynthesis*. 1st ed. New York: Marcel Dekker, Inc. p 83-93
- Burgard AP, Vaidyaraman S, Maranas CD. (2001) Minimal reaction sets for *Escherichia coli* metabolism under different growth requirements and uptake environments. *Biotechnology Progress* 17:791-797
- Cape JL, Bowman MK, Kramer DM. (2006) Understanding the cytochrome bc complexes by what they don't do. The Q-cycle at 30. *Trends in Plant Science* 11:46-55
- Carlson R, Sreenc F. (2004) Fundamental *Escherichia coli* biochemical pathways for biomass and energy production: Creation of overall flux states. *Biotechnology and Bioengineering* 86:149-162
- Carvalho AP, Meireles LA, Malcata FX. (2006) Microalgal reactors: A review of enclosed system designs and performances. *Biotechnology Progress* 22:1490-1506
- Chisti Y. (2007) Biodiesel from microalgae. *Biotechnology Advances* 25:294-306
- Cogne G, Gros JB, Dussap CG. (2003) Identification of a metabolic network structure representative of *Arthrospira (Spirulina) platensis* metabolism. *Biotechnology and Bioengineering* 84:667-676
- Conway SL, Shinbrot T, Glasser BJ. (2004) A Taylor vortex analogy in granular flows. *Nature* 431:433-437
- Cornet JF, Dussap CG. (2009) A simple and reliable formula for assessment of maximum volumetric productivities in photobioreactors. *Biotechnology progress* 25:424-435
- Cruz JA, Avenson TJ, Kanazawa A, Takizawa K, Edwards GE, Kramer DM. (2005) Pasticity in light reactions of photosynthesis for energy production and photoprotection. *Journal of Experimental Botany* 56:395-406

-
- Cuaresma M, Janssen M, Vilchez C, Wijffels RH. (2009) Productivity of *Chlorella sorokiniana* in a short light-path (SLP) panel photobioreactor under high irradiance. *Biotechnology and Bioengineering* 104:352-359
- Curran SJ, Black RA. (2005) Oxygen transport and cell viability in an annular flow bioreactor: comparison of laminar couette and Taylor-vortex flow regimes. *Biotechnology and Bioengineering* 89:766-774
- Dayananda C, Sarada R, Usha Rani M, Shamala TR, Ravishankar GA. (2007) Autotrophic cultivation of *Botryococcus braunii* for the production of hydrocarbons and exopolysaccharides in various media. *Biomass and Bioenergy* 31:87-93
- de Gucht LPE, van der Plas LHW. (1995) Growth kinetics of glucose-limited *Petunia hybrida* cells in chemostat cultures: determination of experimental values for growth and maintenance parameters. *Biotechnology and Bioengineering* 47:42-52
- De Philippis R, Sili C, Paperi R, Vincenzini M. (2001) Exopolysaccharide-producing cyanobacteria and their possible exploitation: a review. *Journal of Applied Phycology* 13:293-299
- Delrue B, Fontaine T, Routier F, Decq A, Wieruszkeski JM, Van Den Koornhuysse N, Maddelein ML, Fournet B, Ball S. (1992) Waxy *Chlamydomonas reinhardtii*: monocellular algal mutants defective in amylose biosynthesis and granule-bound starch synthase activity accumulate a structurally modified amylopectin. *Journal of Bacteriology* 174:3612-3620
- Di Prima RC, Swinney HL. (1979) Instabilities and transition in flow between concentric rotating cylinders. In: Swinney HL, Gollub JP, editors. *Hydrodynamic Instabilities and the Transition to Turbulence*. 2nd ed. Berlin: Springer-Verlag. p 139-180
- Dubinsky Z, Falkowski PG, Wyman K. (1986) Light harvesting and utilization by phytoplankton. *Plant and Cell Physiology* 27:1335-1349
- Dubinsky Z, Stambler N. (2009) Photoacclimation processes in phytoplankton: mechanisms, consequences, and applications. *Aquatic Microbial Ecology* 56:163-176
- Duboc P, Marison I, Von Stockar U. (1999) Quantitative calorimetry and biochemical engineering. In: Kemp RB, editor. *Handbook of Thermal Analysis and Calorimetry*. Aberystwyth, Wales: Elsevier Science. p 267-365
- Dubois M, Gilles KA, Hamilton JK, Rebers PA, Smith F. (1956) Colorimetric method for determination of sugars and related substances. *Analytical Chemistry* 28:350-356
- Eisenstadt D, Barkan E, Luz B, Kaplan A. (2010) Enrichment of oxygen heavy isotopes during photosynthesis in phytoplankton. *Photosynthesis Research* 103:97-103
- Emerson R, Lewis CM. (1943) The dependence of the quantum yield of *Chlorella* on wavelength of light. *American Journal of Botany* 30:165-178
- Endo T, Asada K. (2008) Photosystem I and photoprotection: cyclic electron flow and water-water cycle. In: Demmig-Adams B, Adams WW, Mattoo AK, editors. *Photoprotection, Photoinhibi-*

- tion, *Gene Regulation, and Environment*. Dordrecht: Springer. p 205-221
- Eriksen NT, Riisgard FK, Gunther WS, Iversen JLL. (2007) On-line estimation of O₂ production, CO₂ uptake, and growth kinetics of microalgal cultures in a gas-tight photobioreactor. *Journal of Applied Phycology* 19:161-174
- Eriksen NT. (2008) The technology of microalgal culturing. *Biotechnology Letters* 30:1525-1536
- Esser A, Grossman S. (1996) Analytic expression for Taylor–Couette stability boundary. *Physics of Fluids* 8:1814-1819
- Evans JR. (1987) The dependence of quantum yield on wavelength and growth irradiance. *Australian Journal of Plant Physiology* 14:69-79
- Falkowski PG, Dubinsky Z, Wyman K. (1985) Growth-irradiance relationships in phytoplankton. *Limnology and Oceanography* 30:311-321
- Falkowski PG, Raven JA. (2007) *Aquatic photosynthesis*. Princeton: Princeton University Press.
- Flügge U, Heldt HW. (1991) Metabolite translocators of the chloroplast envelope. *Annual Review of Plant Physiology and Plant Molecular Biology* 42:129-144
- Forster J, Famili I, Fu P, Palsson BO, Nielsen J. (2003) Genome-scale reconstruction of the *Saccharomyces cerevisiae* metabolic network. *Genome Research* 13:244-253
- Foyer CH, Bloom AJ, Queval G, Noctor G. (2009) Photorespiratory metabolism: genes, mutants, energetics, and redox signaling. *Annual Review of Plant Biology* 60:455-484
- G Geider RJ, Osborne BA. (1989) Respiration and microalgal growth - a review of the quantitative relationship between dark respiration and growth. *New Phytologist* 112:327-341
- Gfeller RP, Gibbs M. (1984) Fermentative metabolism of *Chlamydomonas reinhardtii*: I. Analysis of fermentative products from starch in dark and light. *Plant physiology* 75:212-218
- Ghirardi ML, Zhang L, Lee JW, Flynn T, Seibert M, Greenbaum E, Melis A. (2000) Microalgae: a green source of renewable H₂. *Trends in Biotechnology* 18:506-511
- Ghoshal D, Goyal A. (2001) Oxygen inhibition of dissolved inorganic carbon uptake in unicellular green algae. *Phycological Research* 49:319-324
- Giordano RC, Giordano RLC. (2006) Taylor-Couette vortex flow in enzymatic reactors. In: Guisan JM, editor. *Methods in Biotechnology: Immobilization of Enzymes and Cells*. 2nd ed. Totowa, NJ: Humana Press Inc. p 321-332
- Graham D. (1980) Effects of light on "dark" respiration. In: Stumpf PK, Conn EE, editors. *The Biochemistry of Plants, Vol. 2*. Academic Press, Inc. p 525-579
- Grande KD, Marra J, Langdon C, Heinemann K, Bender ML. (1989) Rates of respiration in the light measured in marine phytoplankton using an ¹⁸O isotope-labeling technique. *Journal of Experimental Marine Biology and Ecology* 129:95-120
- Griffiths MJ, Harrison STL. (2009) Lipid productivity as a key characteristic for choosing algal species for biodiesel production. *Journal of Applied Phycology* 21:493-507

-
- Grobbelaar JU. (2000) Physiological and technological considerations for optimizing mass algal cultures. *Journal of Applied Phycology* 12:201-206
- Grossman AR, Lohr M, Im CS. (2004) *Chlamydomonas reinhardtii* in the landscape of pigments. *Annual Review of Genetics* 38:119-173
- Gurakan T, Marison IW, Stockar U, Gustafsson L, Gnaiger E. (1990) Proposals for a standardized sample handling procedure for the determination of elemental composition and enthalpy of combustion of biological material. *Thermochimica Acta* 172:251-266
- Häder DP, Lebert M, Mercado J, Aguilera J, Salles S, Flores-Moya A, Jimenez C, Figueroa FL. (1996) Photosynthetic oxygen production and PAM fluorescence in the brown alga *Padina pavonica* measured in the field under solar radiation. *Marine Biology* 127:61-66
- Hancke TB, Hancke K, Johnsen G, Sakshaug E. (2008) Rate of O₂ production derived from pulse-amplitude-modulated fluorescence: testing three biooptical approaches against measured O₂-production rate. *Journal of Phycology* 44:803-813
- Harris EH. (2009) *The Chlamydomonas sourcebook: a comprehensive guide to biology and laboratory use*. San Diego: Academic Press.
- Harwood JL, Guschina IA. (2009) The versatility of algae and their lipid metabolism. *Biochimie* 91:679-684
- Heifetz PB, Förster B, Osmond CB, Giles LJ, Boynton E. (2000) Effects of acetate on facultative autotrophy in *Chlamydomonas reinhardtii* assessed by photosynthetic measurements and stable isotope analyses. *Plant Physiology* 122:1439-1445
- Heijden RTJM van der, Heijnen JJ, Hellinga C, Romein B, Luyben KCAM. (1994) Linear constraint relations in biochemical reaction systems: I. Classification of the calculability and the balanceability of conversion rates. *Biotechnology and Bioengineering* 43:3-10
- Herbert D, Phipps PJ, Strange RE. (1971) Chemical analysis of microbial cells. In: Norris JR, Ribbons DW, editors. *Methods in Microbiology*. London and New York: Academic Press. p 209-344
- Herrgård MJ, Fong SS, Palsson BØ. (2006) Identification of genome-scale metabolic network models using experimentally measured flux profiles. *PLoS Computational Biology* 2:e72
- Herzig R, Dubinsky Z. (1993) Effect of photoacclimation on the energy partitioning between cyclic and non-cyclic photophosphorylation. *New Phytologist* 123:665-672
- Hideg E. (1997) Free radical production in photosynthesis under stress conditions. In: Pessaraki M, editor. *Handbook of Photosynthesis*. 1st ed. New York: Marcel Dekker Inc. p 911-930
- Hoefnagel MHN, Atkin OK, Wiskich JT. (1998) Interdependence between chloroplasts and mitochondria in the light and the dark. *Biochimica et Biophysica Acta* 1366:235-255
- Hondzo MM, Kapur A, Lembi CA. (1998) The effect of small-scale fluid motion on the green alga *Scenedesmus quadricauda*. *Hydrobiologia* 364:225-235
- Hu Q, Guterman H, Richmond A. (1996) A flat inclined modular photobioreactor for outdoor mass cultivation of photoautotrophs. *Biotechnology and Bioengineering* 51:51-60

References

- Hu Q, Kurano N, Kawachi M, Iwasaki I, Miyachi S. (1998) Ultrahigh-cell-density culture of a marine green alga *Chlorococcum littorale* in a flat-plate photobioreactor. *Applied Microbiology and Biotechnology* 49:655-662
- Hu Q, Sommerfeld M, Jarvis E, Ghirardi M, Posewitz M, Seibert M, Darzins A. (2008) Microalgal triacylglycerols as feedstocks for biofuel production: perspectives and advances. *Plant Journal* 54:621-639
- Hunt S. (2003) Measurements of photosynthesis and respiration in plants. *Physiologia Plantarum* 117:314-325
- Hutner SH, Provasoli L, Schatz A, Haskins CP. (1950) Some approaches to the study of the role of metals in the metabolism of micro-organisms. *Proceedings of the American Philosophical Society* 94:152-170
- Iwatani S, Yamada Y, Usuda Y. (2008) Metabolic flux analysis in biotechnology processes. *Biotechnology Letters* 30:791-799
- Janssen M, de Winter M, Tramper J, Mur LR, Snel JFH, Wijffels RH. (2000) Efficiency of light utilization of *Chlamydomonas reinhardtii* under medium-duration light/dark cycles. *Journal of Biotechnology* 78:123-137
- Janssen M, Tramper J, Mur LR, Wijffels RH. (2003) Enclosed outdoor photobioreactors: light regime, photosynthetic efficiency, scale-up and future prospects. *Biotechnology and Bioengineering* 81:193-210
- Janssen M, Wijffels R, von Stockar U. (2007) Biocalorimetric monitoring of photoautotrophic batch cultures. *Thermochimica Acta* 458:54-64
- Jensen RG, Bahr JT. (1977) Ribulose 1,5-bisphosphate carboxylase-oxygenase. *Annual Review of Plant Physiology* 28:379-400
- Joliot P, Joliot A. (2006) Cyclic electron transfer around Photosystem I. In: Goldbeck JH, editor. *Photosystem I: the light-driven plastocyanin: ferredoxin oxidoreductase*. Dordrecht: Springer. p 639-656
- Kana TM. (1993) Rapid oxygen cycling in *Trichodesmium thiebautii*. *Limnology and Oceanography* 38:18-24
- Kanehisa M, Goto S. (2000) KEGG: Kyoto Encyclopedia of Genes and Genomes. *Nucleic Acids Research* 28:27-30
- Kayser A, Weber J, Hecht V, Rinas U. (2005) Metabolic flux analysis of *Escherichia coli* in glucose-limited continuous culture: I. Growth-rate dependent metabolic efficiency at steady state. *Microbiology* 151:693-706
- Kieldsen KR, Nielsen J. (2009) *In silico* genome-scale reconstruction and validation of the *Corynebacterium glutamicum* metabolic network. *Biotechnology and Bioengineering* 102:583-597

-
- Klein U. (1986) Compartmentation of glycolysis and of the oxidative pentose-phosphate pathway in *Chlamydomonas reinhardtii*. *Planta* 167:81-86
- Kleinegris D, Janssen M, Brandenburg WA, Wijffels RH. (2010) The selectivity of milking of *Dunaliella salina*. *Marine Biotechnology* 12:14-23
- Kliphuis AMJ, de Winter L, Vejraska C, Martens DE, Janssen M, Wijffels RH. (2010a) Photosynthetic efficiency of *Chlorella sorokiniana* in a turbulently mixed short light-path photobioreactor. *Biotechnology Progress* 26:687-696
- Kliphuis AMJ, Janssen M, End EJ van den, Martens DE, Wijffels RH. (2010b) Light respiration in *Chlorella sorokiniana*. Accepted for publication in *Journal of Applied Phycology*
- Kliphuis AMJ, Klok AJK, Martens DE, Lamers PP, Janssen M, Wijffels RH. (2010c) Metabolic modeling of *Chlamydomonas reinhardtii*: energy requirements for photoautotrophic growth and maintenance. Submitted for publication
- Klughammer C, Schreiber U. (2008) Saturation Pulse method for assessment of energy conversion in PS I. *PAM Application Notes* 1:11-14
- Kok B. (1955) On the inhibition of photosynthesis by intense light. *Biochimica et Biophysica Acta* 21:234-244
- Krause GH, Weis E. (1991) Chlorophyll fluorescence and photosynthesis: the basics. *Annual Review of Plant Physiology and Plant Molecular Biology* 42:313-349
- Kromkamp JC, Beardall J, Sukenik A, Kopecký J, Masojidek J, Van Bergeijk S, Gabai S, Shaham E, Yamshon A. (2009) Short-term variations in photosynthetic parameters of *Nannochloropsis cultures* grown in two types of outdoor mass cultivation systems. *Aquatic Microbial Ecology* 56:309-322
- Kühl M, Glud RN, Ploug H, Ramsing NB. (1996) Microenvironmental control of photosynthesis and photosynthesis-coupled respiration in an epilithic cyanobacterial biofilm. *Journal of Phycology* 32:799-812
- Lamers PP, Janssen M, De Vos RCH, Bino RJ, Wijffels RH. (2008) Exploring and exploiting carotenoid accumulation in *Dunaliella salina* for cell-factory applications. *Trends in Biotechnology* 26:631-638
- Lamers PP, van de Laak CCW, Kaasenbrood PS, Lorier J, Janssen M, de Vos RCH, Bino RJ, Wijffels RH. (2010) Carotenoid and fatty acid metabolism in light-stressed *Dunaliella salina*. *Biotechnology and Bioengineering* 106:638-648
- Lathrop DP, Fineberg J, Swinney HL. (1992) Turbulent flow between concentric rotating cylinders at large Reynolds number. *Physical Review Letters* 68:1515-1518
- Lavoie A, de la Noüe J. (1987) Harvesting of *Scenedesmus obliquus* in wastewaters: auto- or bioflocculation? *Biotechnology and Bioengineering* 30:852-859
- Lee CG, Palsson BO. (1995) Continuous medium perfusion leads to long-term cell viability and oxygen production in high-density photobioreactors. *Biotechnology Letters* 17:1149-1154

References

- Lewin RA. (1956) Extracellular polysaccharides of green algae. *Canadian Journal of Microbiology* 2:665-672
- Ley AC, Mauzerall D. (1982) Absolute absorption cross-sections for photosystem II and the minimum quantum requirement for photosynthesis in *Chlorella vulgaris*. *Biochimica et Biophysica Acta* 680:95-106
- Ley AC, Mauzerall D. (1986) The extent of energy transfer among photosystem II reaction centers in *Chlorella*. *Biochimica et Biophysica Acta* 850:234-248
- Lippemeier S, Hintze R, Vanselow KH, Hartig P, Colijn F. (2001) In-line recording of PAM fluorescence of phytoplankton cultures as a new tool for studying effects of fluctuating nutrient supply on photosynthesis. *European Journal of Phycology* 36:89-100
- López-Gejo J, Haigh D, Orellana G. (2009) Relationship between the microscopic and macroscopic world in optical oxygen sensing: a luminescence lifetime microscopy study. *Langmuir* 26:2144-2150
- Lourenço SO, Barbarino E, Marquez UML, Aidar E. (1998) Distribution of intracellular nitrogen in marine microalgae: basis for the calculation of specific nitrogen-to-protein conversion factors. *Journal of Phycology* 34:798-811
- Malkin S, Fork DC. (1996) Bill Arnold and calorimetric measurements of the quantum requirement of photosynthesis - once again ahead of his time. *Photosynthesis Research* 48:41-46
- Mandalam RK, Palsson BO. (1995) *Chlorella vulgaris* (Chlorellaceae) does not secrete autoinhibitors at high cell densities. *American Journal of Botany* 82:955-963
- Mandalam RK, Palsson BO. (1998) Elemental balancing of biomass and medium composition enhances growth capacity in high-density *Chlorella vulgaris* cultures. *Biotechnology and Bioengineering* 59:605-611
- Manichaikul A, Ghamsari L, Hom EFY, Lin C, Murray RR, Chang RL, Balaji S, Hao T, Shen Y, Chavali AK and others. (2009) Metabolic network analysis integrated with transcript verification for sequenced genomes. *Nature Methods* 6:589-592
- McCaskill D, Croteau R. (1993) Procedures for the isolation and quantification of the intermediates of the mevalonic acid pathway. *Analytical Biochemistry* 215:142-149
- Mehler AH. (1951) Studies on reactions of illuminated chloroplasts. 1. Mechanism of the reduction of oxygen and other Hill reagents. *Archives of Biochemistry and Biophysics* 33:65-77
- Meiser A, Schmid-Staiger U, Trosch W. (2004) Optimization of eicosapentaenoic acid production by *Phaeodactylum tricornutum* in the flat panel airlift (FPA) reactor. *Journal of Applied Phycology* 16:215-225
- Melis A, Zhang L, Forestier M, Ghirardi ML, Seibert M. (2000) Sustained photobiological hydrogen gas production upon reversible inactivation of oxygen evolution in the green alga *Chlamydomonas reinhardtii*. *Plant Physiology* 122:127-135
- Merchant SS, Prochnik S, Vallon O, Harris EH, Karpowicz SJ, Witman GB, Terry A, Salamov A, Fritz-

-
- Laylin LK, Sanderfoot AA and others. (2007) The *Chlamydomonas* genome reveals the evolution of key animal and plant functions. *Science* 318:245-251
- Metzger P, Largeau C. (2005) *Botryococcus braunii*: a rich source for hydrocarbons and related ether lipids. *Applied Microbiology and Biotechnology* 66:486-496
- Millan-Almaraz JR, Guevara-Gonzalez RG, Romero-Troncoso RD, Osornio-Rios RA, Torres-Pacheco I. (2009) Advantages and disadvantages on photosynthesis measurement techniques: a review. *African Journal of Biotechnology* 8:7340-7349
- Miller RL, Fredrickson AG, Brown AH, Tsuchiya HM. (1964) Hydromechanical method to increase efficiency of algal photosynthesis. *I&EC Process Design and Development* 3:134-143
- Miron AS, Gomez AC, Camacho FG, Grima EM, Chisti MY. (1999) Comparative evaluation of compact photobioreactors for large-scale monoculture of microalgae. *Journal of Biotechnology* 70:249-270
- Morita M, Watanabe Y, Saiki H. (2000) High photosynthetic productivity of green microalga *Chlorella sorokiniana*. *Applied Biochemistry and Biotechnology* 87:203-218
- Moroney JV, Somanchi A. (1999) How do algae concentrate CO₂ to increase the efficiency of photosynthetic carbon fixation? *Plant Physiology* 119:9-16
- Murai Y, Oiwa H, Takeda Y. (2005) Bubble behavior in a vertical Taylor-Couette flow. *Journal of Physics: Conference Series* 14:143-156
- Nedbal L, Červený J, Rascher U, Schmidt H. (2007) E-photosynthesis: a comprehensive modeling approach to understand chlorophyll fluorescence transients and other complex dynamic features of photosynthesis in fluctuating light. *Photosynthesis Research* 93:223-234
- Norsker NH, Barbosa MJ, Vermuë MH, Wijffels RH. (2010) Microalgal production - a close look at the economics. *Biotechnology Advances*, DOI: 10.1016/j.biotechadv.2010.08.005
- Ogren WL. (1984) Photorespiration: Pathways, regulation, and modification. *Annual Review of Plant Physiology* 35:415-442
- Orth JD, Palsson BØ. (2010) Systematizing the generation of missing metabolic knowledge. *Biotechnology and Bioengineering* DOI: 10.1002/bit.22844
- Pirt SJ. (1965) The maintenance energy of bacteria in growing cultures. *Proceedings of the Royal Society of London, Series B: Biological Sciences* 163:224-231
- Pirt SJ. (1986) The thermodynamic efficiency (quantum demand) and dynamics of photosynthetic growth. *New Phytologist* 102:3-37
- Porra R. (2002) The chequered history of the development and use of simultaneous equations for the accurate determination of chlorophylls a and b. *Photosynthesis Research* 73:149-156
- Pottier L, Pruvost J, Deremetz J, Cornet JF, Legrand J, Dussap CG. (2005) A fully predictive model for one-dimensional light attenuation by *Chlamydomonas reinhardtii* in a torus photobioreac-

- tor. *Biotechnology and Bioengineering* 91:569-582
- Pramanik J, Keasling JD. (1998) Effect of *Escherichia coli* biomass composition on central metabolic fluxes predicted by a stoichiometric model. *Biotechnology and Bioengineering* 60:230-238
- Pulz O. (2001) Photobioreactors: production systems for phototrophic micro-organisms. *Applied Microbiology and Biotechnology* 57:287-293
- Qiang H, Guterman H, Richmond A. (1996) Physiological characteristics of *Spirulina platensis* (cyanobacteria) cultured at ultrahigh cell densities. *Journal of Phycology* 32:1066-1073
- Qiang H, Richmond A. (1996) Productivity and photosynthetic efficiency of *Spirulina platensis* as affected by light intensity, algal density and rate of mixing in a flat plate photobioreactor. *Journal of Applied Phycology* 8:139-145
- Qiang H, Zarmi Y, Richmond A. (1998) Combined effects of light intensity, light-path and culture density on output rate of *Spirulina platensis* (Cyanobacteria). *European Journal of Phycology* 33:165-171
- Quicker G, Schumpe A, König B, Deckwer WD. (1981) Comparison of measured and calculated oxygen solubilities in fermentation media. *Biotechnology and Bioengineering* 23:635-650
- Radakovits R, Jinkerson RE, Darzins A, Posewitz MC. (2010) Genetic engineering of algae for enhanced biofuel production. *Eukaryotic Cell* 9:486-501
- Raghavendra AS, Padmasree K, Saradadevi K. (1994) Interdependence of photosynthesis and respiration in plant cells: interactions between chloroplasts and mitochondria. *Plant Science* 97:1-14
- Ravenel J, Peltier G, Havaux M. (1994) The cyclic electron pathways around photosystem I in *Chlamydomonas reinhardtii* as determined *in vivo* by photoacoustic measurements of energy storage. *Planta* 193:251-259
- Resende MM, Tardioli PW, Fernandez VM, Ferreira ALO, Giordano RLC, Giordano RC. (2001) Distribution of suspended particles in a Taylor-Poiseuille vortex flow reactor. *Chemical Engineering Science* 56:755-761
- Richmond A, Cheng-Wu Z, Zarmi Y. (2003) Efficient use of strong light for high photosynthetic productivity: interrelationships between the optical path, the optimal population density and cell-growth inhibition. *Biomolecular engineering* 20:229-236
- Richmond A. (2000) Microalgal biotechnology at the turn of the millennium: a personal view. *Journal of Applied Phycology* 12:441-451
- Roels JA. (1983) Relaxation times and their relevance to the construction of kinetic models. In: Verachert H, de Mot R, editors. *Energetics and kinetics in Biotechnology*. Amsterdam: Elsevier Biomedical Press. p 205-221
- Royce PNC, Thornhill NF. (1991) Estimation of dissolved carbon dioxide concentrations in aerobic fermentations. *AIChE Journal* 37:1680-1686

-
- Salim S, Bosma R, Vermuë MH, Wijffels RH. (2010) Harvesting of microalgae by bio-flocculation. *Journal of Applied Phycology* DOI: 10.1007/s10811-010-9591-x
- Schmidt BJ, Lin-Schmidt X, Chamberlin A, Salehi-Ashtiani K, Papin JA. (2010) Metabolic systems analysis to advance algal biotechnology. *Biotechnology Journal* 5:660-670
- Schwender J, Gemünden C, Lichtenthaler HK. (2001) Chlorophyta exclusively use the 1-deoxyxylulose 5-phosphate/2-C-methylerythritol 4-phosphate pathway for the biosynthesis of isoprenoids. *Planta* 212:416-423
- Shastri AA, Morgan JA. (2007) A transient isotopic labeling methodology for ¹³C metabolic flux analysis of photoautotrophic micro-organisms. *Phytochemistry* 68:2302-2312
- Shelp BJ, Calvin DT. (1980) Utilization of exogenous inorganic carbon species in photosynthesis by *Chlorella pyrenoidosa*. *Plant Physiology* 65:774-779
- Shikanai T. (2010) Regulation of photosynthetic electron transport. In: Rebeiz CA, Benning C, Bohnert HJ, Daniell H, Hooper JK, Lichtenthaler HK, Portis AR, Tripathi BC, editors. *The Chloroplast: Basics and Applications*. Dordrecht: Springer Science + Business Media. p 347-361
- Sorokin C, Myers J. (1953) A high-temperature strain of *Chlorella*. *Science* 117:330-331
- Stephanopoulos GN, Aristidou A, Nielsen J. (1998) *Metabolic Engineering, principles and methodologies*. San Diego: Academic Press.
- Stouthamer AH, Bettenhausen C. (1973) Utilization of energy for growth and maintenance in continuous and batch cultures of micro-organisms - reevaluation of method for determination of ATP production by measuring molar growth yields. *Biochimica Et Biophysica Acta* 301:53-70
- Sueoka N, Chiang KS, Kates JR. (1967) Deoxyribonucleic acid replication in meiosis of *Chlamydomonas reinhardtii*: I. Isotopic transfer experiments with a strain producing eight zoospores. *Journal of Molecular Biology* 25:47-66
- Suresh S, Srivastava VC, Mishra IM. (2009) Techniques for oxygen transfer measurement in bioreactors: a review. *Journal of Chemical Technology and Biotechnology* 84:1091-1103
- Takache H, Christophe G, Cornet J-F, Pruvost J. (2010) Experimental and theoretical assessment of maximum productivities for the microalgae *Chlamydomonas reinhardtii* in two different geometries of photobioreactors. *Biotechnology Progress* 26:431-440
- Tanada T. (1951) The photosynthetic efficiency of carotenoid pigments in *Navicula minima*. *American Journal of Botany* 38:276-283
- Taymaz-Nikerel H, Borujeni AE, Verheijen PJT, Heijnen JJ, van Gulik WM. (2010) Genome-derived minimal metabolic models for *Escherichia coli* MG1655 with estimated *in vivo* respiratory ATP stoichiometry. *Biotechnology and Bioengineering* 107:369-381
- Taylor GI. (1923) Stability of a viscous liquid contained between two rotating cylinders. *Philosophi-*

- cal Transactions of the Royal Society of London, Series A* 223:289-343
- Tural BM, Moroney JV. (2005) Regulation of the expression of photorespiratory genes in *Chlamydomonas reinhardtii*. *Canadian Journal of Botany* 83:810-819
- Turpin DH, Elrifi IR, Birch DG, Weger HG, Holmes JJ. (1988) Interactions between photosynthesis, respiration, and nitrogen assimilation in microalgae. *Canadian Journal of Botany* 66:2083-2097
- Tyystjarvi E, Karunen J, Lemmetyinen H. (1998) Measurement of photosynthetic oxygen evolution with a new type of oxygen sensor. *Photosynthesis Research* 56:223-227
- Ugwu CU, Aoyagi H, Uchiyama H. (2007) Influence of irradiance, dissolved oxygen concentration, and temperature on the growth of *Chlorella sorokiniana*. *Photosynthetica* 45:309-311
- Valle O, Lien T, Knutsen G. (1981) Fluorometric determination of DNA and RNA in *Chlamydomonas* using ethidium bromide. *Journal of Biochemical and Biophysical Methods* 4:271-277
- van der Tol C, Verhoef W, Rosema A. (2009) A model for chlorophyll fluorescence and photosynthesis at leaf scale. *Agricultural and Forest Meteorology* 149:96-105
- van Winden W, Schipper D, Verheijen P, Heijnen J. (2001a) Innovations in generation and analysis of 2D [¹³C,¹H] COSY NMR spectra for metabolic flux analysis purposes. *Metabolic Engineering* 3:322-343
- van Winden W, Verheijen P, Heijnen S. (2001b) Possible pitfalls of flux calculations based on ¹³C-labeling. *Metabolic Engineering* 3:151-162
- Vona V, Di Martino Rigano V, Lobosco O, Carfagna S, Esposito S, Rigano C. (2004) Temperature responses of growth, photosynthesis, respiration and NADH:nitrate reductase in cryophilic and mesophilic algae. *New Phytologist* 163:325-331
- Vona V, Rigano VM, Esposito S, Carillo P, Carfagna S, Rigano C. (1999) Growth, photosynthesis, and respiration of *Chlorella sorokiniana* after N-starvation. Interactions between light, CO₂ and NH₄⁺ supply. *Physiologia Plantarum* 105:288-293
- Ward OP, Singh A. (2005) Omega-3/6 fatty acids: alternative sources of production. *Process Biochemistry* 40:3627-3652
- Weger HG, Herzig R, Falkowski PG, Turpin DH. (1989) Respiratory losses in the light in a marine diatom: measurements by short-term mass spectrometry. *Limnology and Oceanography* 34:1153-1161
- Weissman JC, Goebel RP, Benemann JR. (1988) Photobioreactor design: Mixing, carbon utilization, and oxygen accumulation. *Biotechnology and Bioengineering* 31:336-344
- Wijffels RH, Barbosa MJ, Eppink MHM. (2010) Microalgae for the production of bulk chemicals and biofuels. *Biofuels, Bioproducts and Biorefining* 4:287-295
- Wingler A, Lea PJ, Quick WP, Leegood RC. (2000) Photorespiration: metabolic pathways and their

role in stress protection. *Philosophical Transactions of the Royal Society B: Biological Sciences* 355:1517-1529

Xue XP, Gauthier DA, Turpin DH, Weger HG. (1996) Interactions between photosynthesis and respiration in the green alga *Chlamydomonas reinhardtii* - characterization of light-enhanced dark respiration. *Plant Physiology* 112:1005-1014

Y Yang C, Hua Q, Shimizu K. (2000) Energetics and carbon metabolism during growth of microalgal cells under photoautotrophic, mixotrophic and cyclic light-autotrophic/dark-heterotrophic conditions. *Biochemical Engineering Journal* 6:87-102

Y Yang C, Hua Q, Shimizu K. (2002) Metabolic flux analysis in *Synechocystis* using isotope distribution from ¹³C-labeled glucose. *Metabolic Engineering* 4:202-216

Y Yang L, Chu L, Chen W. (2006) Study on the flow field inside the microfiltration separator with rotary tubular membrane. *Separation Science And Technology* 41:1513-1525

Z Zijffers JW, Schippers KJ, Zheng K, Janssen M, Tramper J, Wijffels RH. (2010) Maximum photosynthetic yield of green microalgae in photobioreactors. *Marine biotechnology* DOI: 10.1007/s10126-010-9258-2





SUMMARY

Microalgae are a potential source for a wide range of products, such as carotenoids, lipids, hydrogen, protein and starch, which are of interest for food, feed and biofuel applications. Maximization of microalgal product and biomass productivity in (large-scale) outdoor photobioreactors is important for commercial production of these compounds. Microalgae are unicellular eukaryotic organisms capable of using (sun) light as an energy source through photosynthesis. During photoautotrophic growth microalgae consume CO₂ and produce O₂. In addition, O₂ is taken up in a number of processes such as mitochondrial respiration and photorespiration.

A very important objective of applied algae research is to maximize biomass (or product) yield and at the same time minimize the energy input to reduce cultivation costs. Insight in the metabolism of the microalgae is a valuable tool to optimize cultivation parameters accordingly.

To be able to study the effect of cultivation parameters such as mixing on productivity of algal cultures we designed a lab-scale photobioreactor in which a short light path (SLP) of 12 mm is combined with controlled mixing and aeration (**Chapter 2**). Mixing was provided by rotating an inner tube in the cylindrical cultivation vessel creating Taylor vortex flow and as such it could be uncoupled from aeration. Gas exchange was monitored online to gain insight in growth and productivity. The maximal productivity, hence photosynthetic efficiency, of *Chlorella sorokiniana* cultures at high light intensities (1500 μmol m⁻¹ s⁻¹) was investigated in this Taylor vortex flow SLP photobioreactor. We performed duplicate batch experiments at three different mixing rates: 70, 110 and 140 rpm, all in the turbulent Taylor vortex flow regime. For the mixing rate of 140 rpm we calculated a quantum requirement for oxygen evolution of 21.2 mol PAR photons per mol O₂ and a yield of biomass on light energy of 0.8 g mol⁻¹. The maximal photosynthetic efficiency was found at relatively low biomass densities (2.3 g L⁻¹) at which light was just attenuated before reaching the rear of the culture. Upon doubling the mixing rate we only found a small increase of 5% in productivity. Based on these results we concluded that the maximal productivity and photosynthetic efficiency for *C. sorokiniana* can be found at that biomass concentration where no significant dark zone is present and that the influence of mixing-induced light/dark fluctuations is marginal.

In addition to moving the algae through the light gradient in the photobioreactor and preventing the cells from settling, mixing is also needed to supply CO₂ to the culture and remove the O₂ produced in photosynthesis. This O₂ can easily build up to high concentra-

tions in closed photobioreactors and this can have a negative effect on productivity and inhibit growth of the microalgae. If mixing is decreased to reduce energy consumption, which is preferable, this effect can be even larger because more O₂ can build up in the culture. In illuminated microalgal cells several processes in which O₂ is involved occur simultaneously. The cultivation conditions in the experiments in **Chapter 3** were chosen in such a way that two processes dominated, photosynthesis and mitochondrial light respiration. The net O₂ exchange rate, which could be measured on-line, is the sum of the O₂ production by photosynthesis (gross OPR) and O₂ consumption through respiration in the mitochondria (OUR). To know the rates of these two processes one of these had to be measured. We measured the immediate post-illumination respiratory O₂ uptake rate (OUR) *in-situ*, using fiber-optic O₂ micro-sensors, and a small and simple extension of the cultivation system. This method enabled rapid and frequent measurements without disturbing the cultivation and growth of the microalgae. Two batch experiments were performed with *C. sorokiniana* in the SLP photobioreactor and the OUR was measured at different time points during cultivation. The net O₂ production rate (net OPR) was measured on-line. Adding the OUR and net OPR gave the gross O₂ production rate (gross OPR), which is a measure for the O₂ evolution by photosynthesis. The gross OPR was 35-40% higher than the net OPR for both experiments, showing that photosynthesis is underestimated when only looking at net OPR. The respiration rate is known to be related to the growth rate and it is suggested that faster algal growth leads to a higher energy (ATP) requirement and, as such, respiratory activity increases. This hypothesis is supported by our results, as the specific OUR was highest in the beginning of the batch culture when the specific growth rate was highest. In addition, the specific OUR decreased towards the end of the experiments until it reached a stable value of around 0.3 mmol O₂ h⁻¹ g⁻¹. This suggests that respiration could fulfill the maintenance requirements of the microalgal cells.

To obtain the desired insight in the metabolism (more specifically O₂ metabolism) and understand the mechanisms behind the allocation of light energy for microalgal growth and maintenance, we constructed a metabolic model describing the metabolism of the green microalga *Chlamydomonas reinhardtii* (**Chapter 4**). Starting from genomic information a large network with over 300 enzymatic reactions was obtained which was reduced to a smaller, more practical network by lumping linear pathways. The resulting network contained 160 reactions and 164 compounds. Seven chemostat experiments were per-

formed at different growth rates to determine the energy requirements for maintenance and biomass formation *in vivo*. The chemostats were run at low light intensities resulting in a high biomass yield on light of 1.25 g mol^{-1} . The ATP requirement for biomass formation from biopolymers was determined to be $109 \text{ mmol ATP g}^{-1}$ ($18.9 \text{ mol mol}^{-1}$) and the maintenance requirement was determined to be $2.85 \text{ mmol ATP g}^{-1} \text{ h}^{-1}$. With these energy requirements included in the metabolic network, the network described the primary metabolism of *C. reinhardtii* and can be used for modeling of *C. reinhardtii* growth and metabolism. Simulations confirmed that cultivating microalgae at low growth rates is unfavorable because of the high maintenance requirements which result in low biomass yields. At high light supply rates biomass yields will decrease due to light saturation effects. Thus, to optimize biomass yield on light energy in photobioreactors, an optimum between low and high light supply rates should be found. In addition, these simulations showed that respiration can provide both energy for maintenance and additional energy to support growth.

With this model Flux Balance Analysis (FBA) could be performed to study the effect of elevated O_2 concentrations on the metabolism and the biomass yield of *C. reinhardtii* (**Chapter 5**). High $\text{O}_2 : \text{CO}_2$ ratios can have a negative effect on growth and productivity of microalgae. To investigate the effect of O_2 and CO_2 concentrations and the ratio between these on the metabolism of *C. reinhardtii* we performed turbidostat experiments at different $\text{O}_2 : \text{CO}_2$ ratios. These experiments showed that elevated O_2 concentrations and the corresponding increase in the ratio of $\text{O}_2 : \text{CO}_2$ common in photobioreactors led to a reduction of growth and biomass yield on light with 20-30%. This was most probably related to the oxygenase activity of Rubisco and the resulting process of photorespiration. Using FBA with measured rates for each experiment we were able to quantify the ratio of the oxygenase reaction to the carboxylase reaction of Rubisco and could demonstrate that photorespiration indeed could have caused the reduction in biomass yield on light. The calculated ratio of the oxygenase reaction to the carboxylase reaction was 16.6% and 20.5% for air with 2% CO_2 and 1% CO_2 respectively. Thus, photorespiration has a significant impact on the biomass yield on light already at conditions common in photobioreactors (air with 2% CO_2).

To thoroughly understand the energy metabolism of microalgal cells and with that the conversion of light energy into biomass, insight into the different processes involved in O_2 production and uptake and CO_2 consumption and production is necessary. An over-

view of the processes that play a dominant role in the generation of metabolic energy and reductants is given in **Chapter 6**. To reach high biomass yields on light (i.e. productivity) conditions at which processes such as the Mehler reaction, photoinhibition and photorespiration occur should be avoided. A number of measurement methods are proposed which could be used to determine under which cultivation conditions certain processes take place and to what extent, so that these conditions possibly can be avoided. These measurements need to be combined with flux balance analysis in order to accurately assess the real implications of these pathways for the energy budget of the microalgae. For this purpose the metabolic model for *C. reinhardtii* itself can be further improved and expanded by introducing cellular compartments and possibly adding desired product pathways. This will give more insight in the metabolism and the effect of different parameters on the conversion of light energy into biomass or useful products. If including a dynamic description of the light reactions of photosynthesis it might ultimately be possible to make predictions on biomass and product yield based on the light regime the microalgae are exposed to.

Microalgen zijn een potentiële bron van een breed scala aan producten, zoals carotenoïden, vetten, waterstofgas, eiwitten en zetmeel, die van belang zijn voor toepassingen op het gebied van voeding, diervoeder en biobrandstoffen. Het maximaliseren van product en biomassa productiviteit in (grootschalige) buiten gelegen fotobioreactoren is belangrijk voor de commerciële productie van deze verbindingen. Microalgen zijn eencellige eukaryote organismen die door middel van fotosynthese in staat zijn zonlicht als energiebron te gebruiken voor groei. Tijdens hun fotoautotrofe groei nemen de microalgen CO₂ op en produceren ze O₂. De CO₂ wordt ingebouwd in nieuwe algenbiomassa. Verder wordt O₂ weer opgenomen, en CO₂ afgegeven, in een aantal deelprocessen, waaronder mitochondriële respiratie en fotorespiratie. Een belangrijk streven binnen het toegepaste algenonderzoek is het maximaliseren van de opbrengst aan biomassa of product en het minimaliseren van de energetische input, om zodoende de kweekkosten laag te houden. Inzicht in het metabolisme van microalgen is een belangrijk hulpmiddel om de kweekomstandigheden zodanig te optimaliseren.

Om het effect van kweekparameters zoals menging op de productiviteit van algenkweken te kunnen bepalen hebben we een labschaal fotobioreactor ontworpen, waarin een korte lichtweg (*short light path*, SLP) van 12 mm gecombineerd is met gecontroleerde menging en beluchting (**Hoofdstuk 2**). Menging vond plaats door rotatie van een buis in het cilindrische kweekvat, waardoor een Taylor-vortexstroming ontstond. Op deze manier kon de menging losgekoppeld worden van de beluchting. Online registratie van de gasuitwisseling gaf inzicht in de groei en productiviteit. In deze Taylor-vortex SLP-fotobioreactor hebben we de maximale productiviteit, en dus ook maximale fotosynthetische efficiëntie, bepaald van *Chlorella*-kweken (*C. sorokiniana*) bij een hoge lichtintensiteit (1500 μmol m⁻¹ s⁻¹). Batch-experimenten zijn in tweevoud uitgevoerd bij drie verschillende mengsnelheden: 70, 110 en 140 rpm, allemaal onder de omstandigheid van turbulente Taylor-vortexstroming. Voor de mengsnelheid van 140 rpm hebben we een quantum behoefte voor zuurstofvorming berekend van 21.2 mol PAR fotonen per mol O₂, en een opbrengst van biomassa op lichtenergie van 0.8 g mol⁻¹. We vonden deze maximale fotosynthetische efficiëntie bij relatief lage biomassa-concentraties (2.3 g L⁻¹), waarbij al het licht bijna volledig was geabsorbeerd maar het inwendige van de reactor nog niet volledig donker was. Verdubbeling van de mengsnelheid leidde slechts tot 5% toename in productiviteit. Op basis van deze

resultaten concluderen we dat de maximale productiviteit en fotosynthetische efficiëntie van *C. sorokiniana* ligt bij een biomassaconcentratie waarbij zich nog geen donkere zone ontwikkeld heeft en dat onder deze omstandigheden de invloed van door menging geïnduceerde licht-/donker cycli marginaal is.

Menging blijft echter noodzakelijk om te voorkomen dat de cellen bezinken. Verder worden algenculturen veelal gemengd door middel van beluchting die noodzakelijk is om CO₂ in de kweek te brengen en de tijdens de fotosynthese gevormde O₂ af te voeren. Als deze beluchting niet voldoende is kunnen hoge concentraties O₂ ontstaan met als gevolg een negatief effect op de productiviteit en remming van de groei van de microalgen. Als de mengsnelheid wordt verlaagd om het energieverbruik te reduceren (hetgeen de voorkeur verdient) dan kan dit negatieve effect toenemen omdat zich meer O₂ kan ophopen in de kweek. In microalgencellen vinden in het licht simultaan verschillende processen plaats waarbij O₂ is betrokken. De kweekomstandigheden van de experimenten in **Hoofdstuk 3** zijn zodanig gekozen dat twee processen dominant waren: fotosynthese en mitochondriële (licht)respiratie. De netto O₂-uitwisselingsnelheid (*oxygen production rate*, netto OPR), die on-line gemeten kon worden, is de som van de O₂-productie door fotosynthese (bruto OPR) en O₂-consumptie via respiratie in de mitochondriën (*oxygen uptake rate*, OUR). Om te kunnen weten in welke mate deze processen optraden moest één van beide worden gemeten. We bepaalden de respiratoire O₂-opnamesnelheid (OUR) *in-situ*, direct nadat een algenmonster uit het licht in het donker was geplaatst, met behulp van glasvezel O₂-microsensoren en een kleine, eenvoudige uitbreiding van het kweekstelsel. Deze methode stelde ons in staat snel en veelvuldig te meten zonder de kweek en de groei van de microalgen te verstoren. We hebben met *C. sorokiniana* twee batch-experimenten uitgevoerd in de SLP-fotobioreactor, waarbij de OUR gemeten werd op verschillende momenten tijdens de kweek. De netto O₂-productiesnelheid (netto OPR) werd on-line gemeten. Optellen van de OUR en de netto OPR gaf de bruto O₂-productiesnelheid (bruto OPR), die een maat is voor de vorming van O₂ door fotosynthese. De bruto OPR was voor beide experimenten 35-40% hoger dan de netto OPR, wat liet zien dat de fotosynthese wordt onderschat als er alleen wordt gekeken naar netto OPR. Het is bekend dat de respiratiesnelheid gerelateerd is aan de groeisnelheid en gedacht wordt dat snellere groei van algen leidt tot een hogere energetische (ATP-)behoefte en daarmee tot een hogere respiratiesnelheid. Onze resultaten ondersteunen deze hypothese, aangezien de specifieke OUR het hoogste was tijdens het begin van de batchkweek, waar ook de

specifieke groeisnelheid het hoogst was. Verder nam de specifieke OUR af naarmate het experiment vorderde, totdat een stabiele waarde werd bereikt van ongeveer $0.3 \text{ mmol O}_2 \text{ h}^{-1} \text{ g}^{-1}$. Deze waarde komt overeen met de zogenaamde onderhoudsbehoefte van deze microalg zoals deze in eerder onderzoek is gemeten op basis van de hoeveelheid geabsorbeerde lichtenergie.

Om het gewenste inzicht te verkrijgen in het metabolisme (specifieker, het O_2 -metabolisme), en om de mechanismen te begrijpen die ten grondslag liggen aan de verdeling van lichtenergie ten behoeve van groei en onderhoud van de microalgen, hebben we een metabool netwerk model gebouwd dat het metabolisme beschrijft van de groene microalg *Chlamydomonas reinhardtii* (**Hoofdstuk 4**). Op basis van genomische informatie en literatuur werd een uitgebreid netwerk van 300 enzymatische reacties geconstrueerd, waaruit door het samenvoegen van lineaire metabole routes een kleiner en praktischer netwerk gedestilleerd kon worden. Het resulterende netwerk bevatte 160 reacties en 164 verbindingen. Vervolgens werden zeven chemostaat-experimenten uitgevoerd bij verschillende groeisnelheden, om na te gaan hoeveel energie er nodig is voor onderhoud en biomassaproductie *in vivo*. De chemostaten werden uitgevoerd bij lage lichtintensiteiten om lichtverzadiging te voorkomen. Dit resulteerde in een hoge biomassaopbrengst op licht van 1.25 g mol^{-1} . De benodigde hoeveelheid ATP voor de vorming van biomassa uit biopolymeren werd vastgesteld op $109 \text{ mmol ATP g}^{-1}$ ($18.9 \text{ mol mol}^{-1}$), en de onderhoudsbehoefte werd vastgesteld op $2.85 \text{ mmol ATP g}^{-1} \text{ h}^{-1}$. Door het invoeren van deze energetische behoeften in het metabole netwerk kon het primaire metabolisme van *C. reinhardtii* beschreven worden en kan het gebruikt worden om groei en metabolisme van *C. reinhardtii* te modelleren. Simulaties bevestigden dat het kweken van microalgen bij lage groeisnelheden en hoge biomassaconcentraties (lage lichttoevoer snelheid) niet de voorkeur verdient, vanwege de hoge onderhoudsbehoefte die leiden tot een lage biomassaopbrengst. Bij hoge groeisnelheden en lage biomassaconcentraties (en de bijbehorende hoge lichttoevoer snelheid) zal de biomassaopbrengst afnemen als gevolg van lichtverzadigingseffecten. Om de biomassaopbrengst op lichtenergie in fotobioreactoren te optimaliseren moet dus een optimum gevonden worden tussen een lage en een hoge lichttoevoer snelheid. Verder lieten de simulaties ook zien dat het aannemelijk is dat respiratie zowel energie levert ten behoeve van groei als wel voor onderhoud.

Met dit model kon Flux Balans Analyse (FBA) worden uitgevoerd, om het effect te kunnen bestuderen van verhoogde O_2 -concentraties op het metabolisme en de biomassaopbrengst van *C. reinhardtii* (**Hoofdstuk 5**). Hoge $O_2 : CO_2$ -verhoudingen kunnen een negatief effect hebben op de groei en productiviteit van microalgen. Om het effect te kunnen bepalen van O_2 - en CO_2 -concentraties en hun onderlinge verhouding op het metabolisme van *C. reinhardtii* hebben we turbidostaatexperimenten uitgevoerd bij verschillende $O_2 : CO_2$ verhoudingen, door te begassen met lucht of N_2 verrijkt met 1% of 2% CO_2 . Deze experimenten lieten zien dat verhoogde O_2 -concentraties en de bijbehorende toename in de verhouding $O_2 : CO_2$ (gebruikelijk in fotobioreactoren) leidden tot een afname in groei en biomassaopbrengst op licht van 20-30%. Dit was naar alle waarschijnlijkheid te wijten aan de oxygenaseactiviteit van Rubisco en het daaruit voortvloeiende proces van fotorespiratie. Door FBA toe te passen met de gemeten snelheden uit elk experiment als randvoorwaarden konden we de verhouding kwantificeren tussen de oxygenasereactie en de carboxylasereactie van Rubisco, en konden we laten zien dat fotorespiratie inderdaad verantwoordelijk zou kunnen zijn voor de reductie in biomassaopbrengst op licht. De verhouding tussen de oxygenase- en de carboxylasereactie was 16.6% en 20.5% voor lucht met respectievelijk 2% CO_2 en 1% CO_2 . Fotorespiratie blijkt dus een significante invloed te hebben op de biomassaopbrengst op licht onder omstandigheden die gebruikelijk zijn in fotobioreactoren (lucht met 2% CO_2).

Om het metabolisme van microalגעncellen (en daarmee de omzetting van lichtenergie in biomassa) beter te begrijpen, is inzicht nodig in de verschillende processen die betrokken zijn bij de productie en opname van O_2 en de consumptie en productie van CO_2 . Een overzicht van de processen die het meest belangrijk zijn voor het genereren van metabole energie en reductanten is te vinden in **Hoofdstuk 6**. Om hoge biomassaopbrengsten op licht te kunnen bereiken dienen condities, waaronder processen zoals de Mehler-reactie, fotoinhibitie en fotorespiratie optreden, te worden vermeden. We beschrijven in dit hoofdstuk een aantal meetmethoden die kunnen worden gebruikt om te bepalen onder welke kweekomstandigheden dit soort processen plaatsvinden, en in welke mate, zodat deze omstandigheden kunnen worden vermeden. Dergelijke metingen moeten gecombineerd worden met FBA om een nauwkeurige inschatting te kunnen maken van de daadwerkelijke implicaties van processen als de Mehler-reactie op het energiebudget van de microalgen. Om dit te kunnen realiseren, moet het metabole netwerk model van *C. reinhardtii* uitgebreid worden door de introductie van cellulaire

compartimenten en eventueel ook gewenste metabole product-routes. Uiteindelijk levert dit meer inzicht op in het metabolisme en het effect van procesomstandigheden op de omzetting van lichtenergie in biomassa en/of bruikbare producten. Als verder ook een dynamische beschrijving van de fotosynthetische lichtreacties wordt ingebouwd, kan dit uiteindelijk leiden tot de mogelijkheid de biomassa- en productopbrengst te voorspellen op basis van het lichtregime waaraan de microalgen zijn blootgesteld.

Samenvatting



DANKWOOD

D

Hier ligt het dan, het eindresultaat van een hoop plezier, gepiel en gepruts in het lab, experimenten, modelleren en schrijfwerk. Wat was het leuk om met die leuke kleine algjes te werken (ooh, kijk! Ze zwemmen! Agossie!) in zo'n supermooie photobioreactor, mijn 'kindje' en mijn trots (incl. gelukbrengende kerstbal). Erg populair, ook buiten de vakgroep, heeft menig krantje gesierd en zo nu ook de omslag van mijn proefschrift! Al dat werk heb ik natuurlijk niet alleen gedaan en ik wil iedereen dan ook heel erg bedanken, zonder jullie was het niet gelukt!

René, dankjewel dat je me lang geleden op de fiets vroeg of ik al wist wat ik ging doen, ja, dat wist ik, bij jou promoveren! Dankjewel voor je begeleiding, over toppen en door dalen, en voor je input en frisse kijk op mijn resultaten en artikelen. Ik ben ook blij dat je mij wist af te remmen als ik dan toch liever weer een (in mijn ogen) niet zo fraai experiment over wilde doen, terwijl jij vond dat het prima publiceerbaar zou zijn zo (wat natuurlijk ook zo was, zie het resultaat!). Ook dankjewel voor alle avonturen, zowel boven als onder water in binnen en buitenland. Ik zal nooit onze 'infamous' duik in Ierland vergeten, daar werd pijnlijk duidelijk dat macroalgen toch behoorlijk misselijkmakend kunnen zijn..., nooit aan beginnen dus. **Marcel** en **Dirk**, ik ben blij dat jullie mijn begeleiders waren. **Marcel**, met al je kennis en geniale ideeën stimuleerde je me om het onderste uit de kan te halen. Dankzij jouw gedetailleerde commentaar werden de artikelen beter en de commentaren naar de reviewers een stuk subtieler. Fijn dat ik altijd langs kon lopen voor advies of gewoon een praatje! **Dirk**, dankjewel dat jij na een half jaartje ook bij 'de mannen' kwam horen! Met jouw input is het metabole model een feit geworden en heb ik er ook mee kunnen simuleren. Bedankt voor je geduld bij de eindeloze stroom model-vragen/problemen, voor je hulp bij de model artikelen en bovenal voor je luisterend oor.

De bioreactor en het meetsysteem kwamen niet zomaar werkend in het lab te staan, daar heeft een heleboel werk in gezeten. 'Mannen van de werkplaats', **Jan**, **Hans**, **André**, **Reinoud** en **Hans**, heel erg bedankt voor al jullie werk, het bouwen van de reactor en het aanpassen of repareren als hij keer op keer weer kuren had of als de electronica het weer eens begaf (of gewoon als ik een O-ringetje nodig had). **Fred**, dankjewel voor al je technische hulp in het lab en voor het programmeren van de DAQ (en voor al die gezellige koffie-momenten). Wat ben ik blij dat je nog een half dode zuurstofprobe met toebehoren in de kast had liggen. De basis voor een mooie meetmethode en een mooi

artikel, het was wat gepruts, maar met koffie erbij is alles mogelijk (inclusief geniale stellingen bedenken)!

Natuurlijk heb ik niet al het werk zelf gedaan, een hoop werk is verzet door mijn afstudeerstudenten. **Carsten** en **Lenneke**, jullie waren mijn eerste studenten en jullie hebben de experimenten gedaan die geleid hebben tot hoofdstuk 2, het eerste artikel. Bedankt voor al jullie werk, ook in de avonduurtjes! Blijkbaar is het toch niet té afschrikwekkend geweest, fijn dat jullie nu ook AIO zijn met algjes, succes! **Marieke**, wat een gepruts met die zuurstofprobes, maar wel helemaal alleen een chemostaat gedraaid terwijl ik in Japan was! Leuk dat je weer aan het werk bent met de STT photobioreactor, maar groen vind ik hem toch mooier.... **Yusak**, thank you for all the work in the lab. **Anne**, mijn 'partner-in-crime', dankjewel voor al je werk tijdens je afstudeervak en ook daarna, toen je ook AIO werd op een soort vervolg project van het mijne, jij ook succes! Het was toch gezellig hè, al die uren (dagen, weken) samen achter de computer om de experimenten te simuleren met het model en daarna het schrijven van ons artikel, inclusief de ups en downs (bij beiden hoort natuurlijk chocolade!). Ons artikel is 'the best', het zit hem vast in de initialen en de voornaam. Ik ga je missen!

Dan ben ik aangeland bij de vakgroep. Allereerst wil ik mijn lieve kamergenootjes, **Dorinde**, **Elsbeth**, **Thanawit** en sinds kort **Kim**, bedanken. Thank you for sharing good times (almost five years!), chatting about everything and anything, filling and emptying the 'droppot' and for making our room a happy (and green) place where I truly felt at home! **Packo** en **Dorinde**, VICI-buddies, het was fijn om met z'n drieën de *Dunaliella*-uitdaging aan te gaan. Helaas ben ik overgelopen naar zoetwater algjes (foei!) en zijn we er niet meer aan toegekomen om die superalg te creëren en een prachtig productieproces op te zetten... Dankjulliewel voor al het algen-gepraat, de besprekingen, presentaties en gezellige brainstorm-sessies! Lunchwandelaars, **Frank**, **Hylke**, **Sebas**, **Janneke**, **Dione**, **Mgeni**, **Olivier**, **Marleen**, van Unitas pannenkoeken tot Arboretum wandelingen, bedankt voor de broodnodige ontspanning iedere dag en bedankt voor een plek om vanalles te bespreken en mijn hart te luchten. Lieve **PRE-ers** en ex-**PRE-ers**, Marzia, Dominick, Marieke, Klaske, Dorinde, Elsbeth, Lieke, Mgeni, Frank, Francisco, Packo, Maartje, Marjoleine, Petra, Rouke, Sina, Pieter, Anja, Sayam, Jos, Martin, Hylke, Sebastiaan, Fred, Rik, Arjen, Miranda, Joyce, Jan, Koen, Tim, Daniël, Jan-Willem, Mathieu, Maria C, Maria B, Floor, Marian en iedereen die ik vergeten ben, allemaal super bedankt

voor alle fijne momenten bij labuitjes, AIO-reizen, borrels en koffiehoeke momenten!

Buiten het lab wil ik graag ook nog wat mensen bedanken. Lieve **Miriam**, bedankt voor de heerlijke etentjes, sushi, filmpjes, feestjes en gewoon avondjes kletsen. Hopelijk gaan we hier gewoon mee door, al dan niet over de hele wereld! **Frank**, mede-semi-bioloog, dankje voor alle libel/vlinder/vogel-excursies, foute filmavondjes, biertjes, chocolade-taart (mmmPIE!) en rare kampeermomenten. Ik ben blij dat je mijn paranimf wilt zijn! **Marcel, Floor, Tim, Marieke** en **Klaske**, bedankt voor de heerlijke reisjes en geweldige duiken. Het was fantastisch en hopelijk gaan we nog veel vaker op avontuur onder water! **Nardy** en **Joeri**, ook al zien we elkaar heel weinig, bedankt voor de gezellige avondjes en het wordt duidelijk tijd voor een reünie. **Ruben, Richard, Corjan, Frank, Wiger, Nick** en **Yvette**, bedankt voor alle fijne concerten en festivals waar we samen geweest zijn, All Hail The Mud! Lieve **Vivae**, bedankt voor alle heerlijke muziek, super weekenden en prachtige concerten die we gegeven hebben en gaan geven. Een zondag VivaVoce is goed voor weken mooie muziek in mijn hoofd! De Utrecht-clan: **Lot, Sofie** en **Sim, Mark, Noor, Luka** en **Juultje, Nicole, Frederik, Merlijntje** en **Catootje**, fijn dat jullie er altijd voor ons zijn. Hopelijk kunnen we wat vaker afspreken! **André** en **Kelly**, bedankt voor de supergezellige avondjes, dat er maar meer mogen volgen nu we een stuk dichterbij de buurt komen wonen! **Mgeni** and **Hashim**, thanks for the great evenings with good food and fun! **Annelies, Rogier** en **Isis**, drukdrukdruk maar zo nu en dan moet er tapas gegeten worden! **Stephanie**, we met at the ISAP and discovered we had a lot in common, capoeira (playing at the conference dinner, how awesome was that!), AIMS, diving and *Chlamydomonas*! Our favourite algae. Thank you for exchanging knowledge, protocols and capoeira invitations! Nu ik het toch over **capoeira** heb, bedankt trainings-maatjes, voor alle heerlijke trainingen, festivals, workshops en nieuwjaarsdinetjes: Mourão, Natureza, Espoleta, Pulginha, Poty, Marcha Lenta, Ferrugem, Espaguete, Durinho, FifiR, Betty Boop, Pé de Pau, Diamante, Duente, Modelo, Coisa, Congo, Tarzan, Paulien, Pernelle, Tartaruga, Sargento, Palma, Merel en iedereen die ik vergeten ben.

En dan last but zeker not least, mijn familie. **Pap** en **mam**, jullie staan altijd achter mij en hebben me altijd gestimuleerd. Zonder jullie zou ik niet zijn waar ik nu ben, ik hou van jullie! **Ed**, lief groot klein broertje, jou kan ik altijd bellen en andersom, dankje daarvoor. Ik vind het heel fijn dat jij aan mijn zijde staat als paranimf! Lieve **omi**, bedankt voor uw altijd luisterend oor, dat u altijd meeleeft en ook precies begrijpt waar ik mee bezig ben.

Dankwoord

‘Schoonmama’ **Tineke** en **Paul**, bedankt voor jullie steun en dat jullie er altijd zijn voor ons. **Mirjam**, schoon zusje, en **Lola**, fijn dat we in de buurt komen wonen, lufjoe!

Als allerlaatste wil ik natuurlijk **Michaël** bedanken. Lievie, zonder jou was dit niet mogelijk geweest. Dankje voor je liefde, steun, gekkigheid, plezier, muziek en alle avonturen die we hebben beleefd en gaan beleven. Samen zijn wij één en kunnen we de hele wereld aan! Ik hou van je!

Liefs,
Annette



CURRICULUM
C
VITAE

Curriculum Vitae

Anna Marguéríta Jeanetta (Annette) Kliphuis was born in Bilthoven, the Netherlands, on March 25th 1981. She went to primary school in her hometown Zeist and attended secondary school at the Christelijk College Zeist. After receiving her VWO (gymnasium) diploma in 1999 she started her studies in Bioprocess Engineering at Wageningen University. In her major thesis project at the Bioprocess Engineering group of Wageningen University she worked on cultivation and growth measurements of the marine sponge *Chondrosia reniformis*. Her two minor theses projects dealt with the role of DDM1 in DNA-methylation in roots of *Arabidopsis thaliana* (performed at the Department of Microbiology, Wageningen University) and modelling controlled release of water through biodegradable polymers (performed at the Bioprocess Engineering group of Wageningen University). For her internship Annette went to Australia where she worked on accessing marine natural products for herbicide and drug discovery by scaling up fungal fermentations and constructing DNA libraries at the Australian Institute of Marine Science (AIMS) in Townsville. During her studies she organised the international symposium "Marine Biotechnology: An Ocean Full of Prospects?". After graduating in September 2005 she started her PhD project at the Bioprocess Engineering group of Wageningen University, focusing on the metabolism of green microalgae. Currently she is working as an Associate Scientist at the DSM Biotechnology Center / Fermentation in Delft, the Netherlands.



Overview of completed training activities

Courses

Discipline specific

Biosystems Engineering, Bioreactors and Cell Factories	(2005)
Marine Biology for Divers	(2005)
LabVIEW course	(2006)
Bioreactor Design and Operation	(2006)
Basic Statistics	(2007)

General courses

VLAG PhD week	(2005)
PhD Competence Assessment	(2005)
Supervising BSc and MSc thesis work	(2006)
Project- and time management	(2006)
Techniques for writing and presenting a scientific paper	(2006)
Career Perspectives	(2009)

Conferences

NorthSea days, Vlissingen, The Netherlands	(2006)
International Marine Biotechnology Conference Eilat, Israël	(2007)
BSDL symposium, Delft, The Netherlands	(2006, 2007)
Netherlands Biotechnology Conference, Ede, The Netherlands	(2006 - 2008)
International Conference on Applied Phycology, Galway, Ireland	(2008)

Optionals

Brainstormweek Process Engineering	(2005)
Process Engineering PhD study tour to Denmark and Sweden	(2006)
Process Engineering PhD study tour to Japan	(2008)
Brainstormday Process Engineering	(2008, 2009)

Teaching

Practical Course Marine Biotechnology	(2006 - 2009)
Food Fermentation	(2007, 2008)

This research was financially supported by the technology foundation STW (www.STW.nl; project WLM.6622), which is part of the Netherlands Organization for Scientific Research (www.NWO.nl).